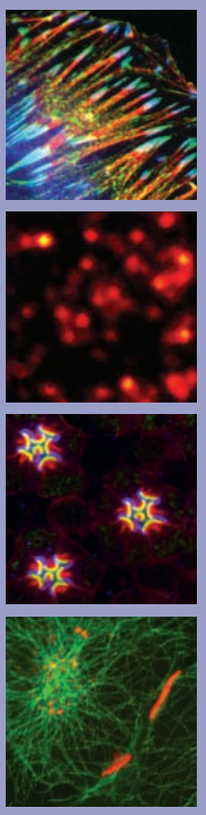

Microscopy has been a key tool for cell biologists from the outset — indeed, cell biology was literally born with microscopy. This year marks the 300th anniversary of the death of Robert Hooke, whose seminal observations under the microscope (*Micrographia*, 1665) led to the initial coining of the term 'cell' (referring to a tiny bare room, similar to a monk's cell). Since then, microscopy has revolutionized our understanding of how cells live and die. New subcellular compartments have been discovered thanks to improving microscopy techniques, and progress in cell biology still relies in great part on advances in imaging techniques.

This past decade has seen a 'rainbow' revolution in microscopy. Fluorescent proteins, such as green fluorescent protein from the jellyfish *Aequorea victoria*, have been used to visualize biological processes as they happen in living cells and whole organisms. Together with improved fluorescence microscopy and time-lapse microscopy, these impressive techniques have provided insights into the dynamics of proteins and the biological processes that they regulate. Importantly, imaging techniques are now becoming available not only to specialist biophysicists but also to cell biologists — a merger that is reflected by joint conferences and collaborations that bring these communities together. Now is therefore the perfect time to focus on this central tool in cell biology.

For this reason, *Nature Cell Biology* and *Nature Reviews Molecular Cell Biology* are pleased to present this supplement on imaging in cell biology. These journals have sole responsibility for the choice and content of the supplement and, should you wish to cite any of these articles, please refer to the citation information at the end of each article, above the reference list. The supplement consists of a series of specially commissioned articles, which were selected on the basis of feedback from the research community. The topics covered in the six Review articles span both the wavelength and the resolution scale, from magnetic resonance imaging to electron microscopy, and from single-molecule to whole-organism imaging. To conclude this supplement, Roger Y. Tsien speculates on the future of imaging and the new challenges that lie ahead. We hope that the content of these articles provides not only an essential guide to the latest techniques, their advantages and limitations, but also highlights the diverse cell-biological applications of imaging techniques.

We are pleased to acknowledge the financial support of Carl Zeiss in the production of this supplement. Thanks to this support, supplement articles are available free online for six months, where they can be found together with a Focus on imaging in cell biology (see http://www.nature.com/focus/cellbioimaging). In addition to the supplement articles, this Focus site contains key imaging articles from our past issues and from other Nature Publishing Group journals, as well as movies, images and recommended links. The latter includes a link to the ongoing *Nature Cell Biology* and *Nature Reviews Molecular Cell Biology* 'Cell of the Month' competition, and some of the winning images have been used in this supplement to emphasize that cell-biological images can be not only informative, but also visually stunning.

ALISON SCHULDT, Associate Editor, *Nature Cell Biology*
RACHEL SMALLRIDGE, Senior Editor, *Nature Reviews Molecular Cell Biology*

nature cell biology

nature REVIEWS MOLECULAR CELL BIOLOGY

REVIEW

Lighting up cells: labelling proteins with fluorophores

Atsushi Miyawaki, Asako Sawano and Takako Kogure

During the past decade, rapid improvements have been made in the tools available for labelling proteins within cells, which has increased our ability to unravel the finer details of cellular events. One significant reason for these advances has been the development of fluorescent proteins that can be incorporated into proteins by genetic fusion to produce a fluorescent label. In addition, new techniques have made it possible to label proteins with small organic fluorophores and semiconductor nanocrystals.

The conventional techniques that are used to fluorescently label proteins and image them in their native environment can be laborious. For example, reliable protein labelling requires expertise in protein chemistry, and the successful microinjection of labelled products into cells with minimal damage requires much technical experience. Moreover, it is difficult to target fluorescently labelled proteins directly to specific sites within a cell, because the distribution and targeting of most proteins is regulated by their *in vivo* translation and post-translational modifications.

By contrast, *de novo* synthesis is much more likely to result in native patterns of protein localization. Gene transfer techniques, including liposome-mediated transfection, which use various viral vectors, electroporation and the GENE GUN, make this possible and have shown significant progress in recent years. As a result, proteins can now be expressed within cells as fusions to fluorescent proteins or to small tags that can react with specialized fluorophores. Although more traditional methods such as protein microinjection are not without their advantages, these new methods for fluorescently labelling proteins by genetic fusion are opening new windows for our understanding of cellular function.

Labelling with fluorescent proteins

Expanding the colour repertoire. Green fluorescent protein (GFP) was originally isolated from the light-emitting organ of the jellyfish *Aequorea victoria*[1] by Shimomura *et al.* in 1962, although more than 30 years passed before the complementary DNA encoding the protein was subsequently characterized[2,3]. As *Aequorea* GFP is spontaneously fluorescent, chimeric GFP fusions offer the great advantage that they can be expressed *in situ* by gene transfer into cells, thereby circumventing the need for high-level heterologous production, purification, *in vitro* labelling and microinjection of recombinant proteins. In addition, these GFP fusions can be localized to particular sites within the cell by appropriate targeting signals.

Although spectral variants with blue, cyan and yellowish-green emissions have been successfully generated from the *Aequorea* GFP[4], none exhibit emission maxima longer than 529 nm[1]. Fortunately, the discovery of novel 'GFP-like proteins' from *Anthozoa* (coral animals) have significantly expanded the range of colours available for cell biological applications. As a result, the family of 'GFP-like proteins' deposited in sequence databases now includes approximately 30 significantly different members[5,6]. Despite only a modest degree of sequence similarity, these GFP-like proteins probably share a β-can fold structure that is central to the fluorescence of GFP (FIG. 1). In this review, the term 'fluorescent proteins' is used to describe those proteins that can become spontaneously fluorescent through the autocatalytic synthesis of a CHROMOPHORE. Although most GFP-like proteins fall into this category, a subset display only intense absorption without fluorescence emission, and are dubbed chromoproteins[6]. Most of the fluorescent proteins discussed in this review are summarized in FIG. 2 (also see REF. 7, which covers fluorescent proteins more broadly).

Proteins that fluoresce at red or far-red wavelengths (red fluorescent proteins or RFPs) are of specific interest, as eukaryotic cells and tissues display reduced AUTOFLUORESCENCE at these longer wavelengths. Also, RFPs can be used in combination with other fluorescent proteins that fluoresce at shorter wavelengths for both multicolour labelling and fluorescence resonance energy transfer (FRET) experiments. At present, the commercially available RFPs are derived from two wild-type GFP-like proteins. The first, DsRed (drFP583), has excitation and emission maxima at 558 nm and 583 nm, respectively[5]. It retains an impressive brightness and remains stable despite pH changes, the presence of denaturants and photobleaching[8]. The second, a far-red fluorescent protein, was generated by mutagenesis of a chromoprotein that absorbs at 571 nm[9]. The resulting protein, HcRed1 (Clontech), has excitation and emission maxima at 588 nm and 618 nm, respectively. HcRed1, however, exhibits a low MOLAR EXTINCTION COEFFICIENT (ε) at 588 nm ($\varepsilon_{588} = 20{,}000\ M^{-1}\ cm^{-1}$) and a low FLUORESCENCE QUANTUM YIELD ($\Phi = 0.015$). As the brightness of a fluorophore depends on both the ε at a certain wavelength and Φ, which define the absorption and the ratio of photons emitted to photons absorbed, respectively, HcRed1 fluoresces weakly. So far, the fluorescent protein which emits fluorescence at the longest wavelength (without any mutations being introduced) is eqFP611, cloned from the sea anemone *Entacmaea quadricolor*[10]. This protein absorbs at 559 nm and emits at 611 nm. As many spectral variants have emerged, more investigators are becoming interested in the simultaneous imaging of multiple fluorophores and/or FRET signals.

Making a successful fusion protein. There are three important points to consider when creating a functional fluorescent protein (FIG. 1a,b): the fluorescent protein must fold correctly to fluoresce, the host protein also needs to fold correctly to be functional, and the integrity of the chimeric protein must be maintained.

The length and sequence of the linker between the fluorescent protein and host protein should be optimized for each specific application. In many cases, steric hindrance or folding interference can occur between the fluorescent protein and host protein if the linker is not sufficiently long and flexible. The amino acid that confers the most flexibility to a peptide chain is glycine (Gly), which has the smallest side chain of all amino acids. A small number of glycine residues is therefore the most common method used to link two protein domains. The most widely used linker designs have sequences that primarily consist of Gly and serine (Ser) stretches, Ser residues being interspersed to improve the solubility of a poly-Gly stretch.

The decision of whether to fuse a fluorescent protein to the amino or carboxyl terminus of a protein depends on the properties of the protein. For example, a particular terminus might need to be preserved to retain proper protein function or to ensure correct localization. This decision might also be made on the basis of structural aspects of the particular fluorescent protein. For example, *Aequorea* GFP has a floppy carboxyl terminal tail of approximately ten amino acids[11], which makes its fusion to the amino terminus of other proteins possible without the addition of a linker (FIG. 1a). By contrast, DsRed is more successfully fused to the carboxyl terminus of proteins of interest (FIG. 1b), because the amino termini project fully from a tetrameric complex of DsRed (see below).

In rare cases in which neither end of a host protein can be modified, it is possible to insert the fluorescent protein into the middle of the protein. A highly flexible portion such as a β-turn should, theoretically, be tolerant to such an insertion. For example, enhanced GFP (EGFP; Clontech) has been inserted into the cytoplasmic domain of a non-conducting mutant of the Shaker K^+ channel[12] and fluorescence was visible in cells. Moreover, the intensity of fluorescence was altered only slightly by the voltage-dependent change in the domain structure.

In general, to preserve the original structure of a host protein, the resulting amino and carboxyl termini of the inserted fluorescent protein should be in close proximity; this also allows efficient folding of the fluorescent protein. A circularly permuted GFP (cpGFP), the amino and carboxyl portions of which have been interchanged and reconnected by a short spacer between the original termini[13,14], could be used for such a purpose. As the two

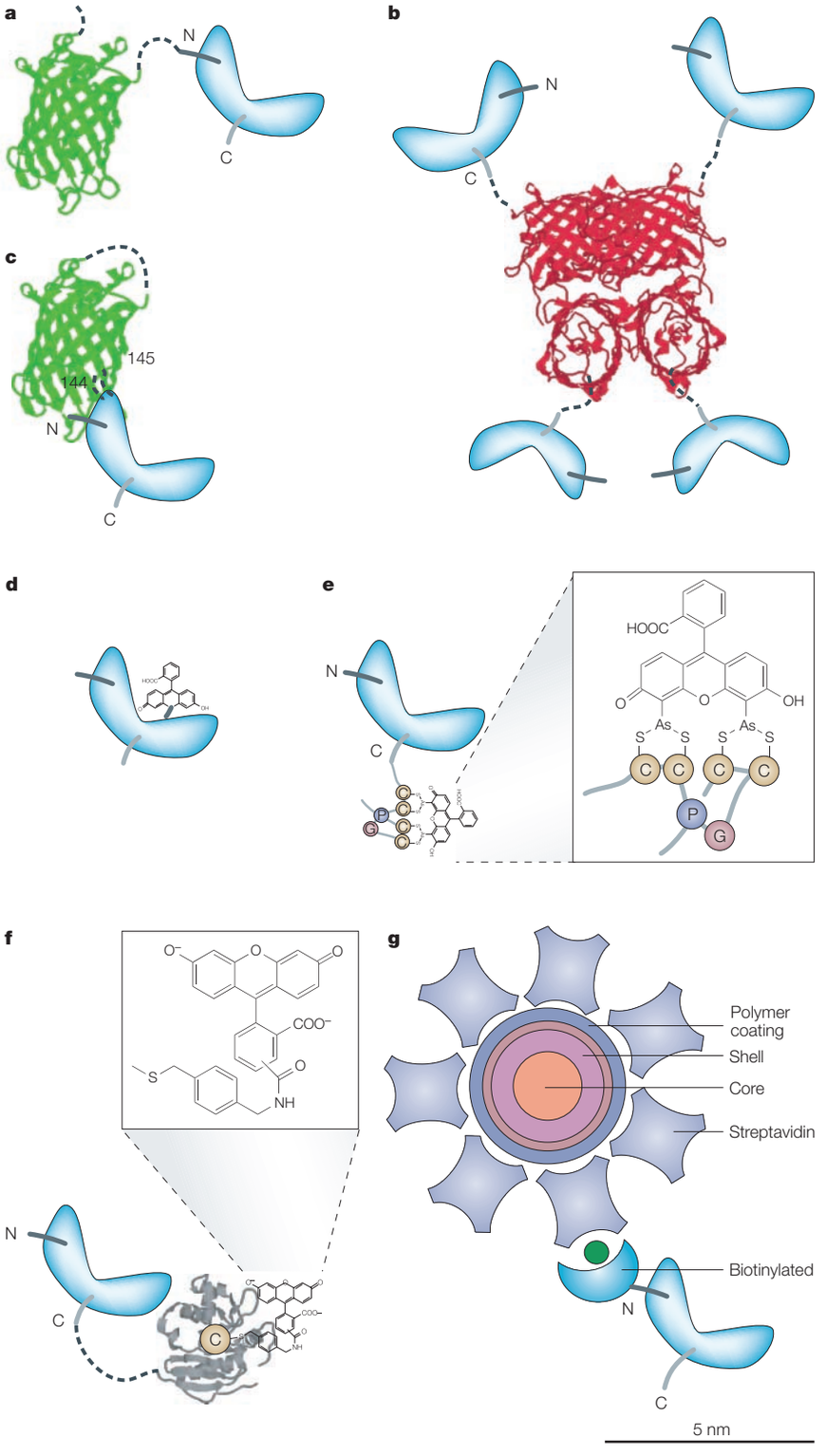

Figure 1 | **Schematic of protein labelling with a variety of fluorophores.** A host protein with a molecular mass of 10–20 kDa is shown in blue with its amino (dark grey) and carboxyl (light grey) termini. The crystal structures of the monomeric *Aequorea victoria* green fluorescent protein (GFP) (green) and tetrameric DsRed (red) were taken from the Brookhaven Protein Data Bank (PDB). **a** | The host protein is fused to the C terminus of *Aequorea* GFP through a linker (a black broken line). **b** | The host protein is fused to the N terminus of DsRed, which forms a tetrameric complex. **c** | A circularly permuted GFP, beginning with Tyr145 and ending with Asn144, is inserted into a β-turn of the host protein. **d** | Site-specific labelling of the host protein with a small organic fluorophore (fluorescein). **e** | The C terminus of the host protein is extended with the tetracysteine motif (CCPGCC), to which the FlAsH compound is covalently linked. Modified with permission from REF. 14 © (2002) Macmillan Magazines Ltd. **f** | The C terminus of the host protein is fused to ^{W160}hAGT, which becomes labelled at Cys145 following reaction with O^6-benzylguanine fluorescein (BGFL). The crystal structure of AGT was taken from the PDB. **g** | A quantum dot emitting at roughly 600 nm is conjugated to streptavidin (Qdot 605 Streptavidin Conjugate, Quantum Dot Corporation). The biotinylated host protein is then linked to the quantum dot by a streptavidin/biotin complex. The β-barrel of fluorescent proteins, fluorescein, FlAsH, ^{W160}hAGT and the quantum dot are all drawn to scale. AGT, O^6-alkylguanine-DNA alkyltransferase.

resulting termini are close to each other, it might even be possible to insert this molecule into the middle of secondary structures (FIG. 1c). However, this remains to be tested.

Maturation of fluorescent proteins. Poor folding of a fluorescent protein variant results in a non-fluorescent chimaera. Accumulation of a large amount of such a protein inside cells will decrease the fluorescent signal, and potentially perturb cellular homeostasis if the labelled host protein retains its original function. It is therefore imperative to use fluorescent protein variants that mature efficiently. In this respect, it is important to note that the folding efficiencies of both the fluorescent protein and the host protein are likely to be interdependent. Fluorescent proteins tend to fold less efficiently when fused to other proteins, although fusion to a well-folded host protein can facilitate proper fluorescent protein folding[15].

After protein synthesis, many GFP variants mature quite slowly, involving a multi-step folding process that consists of cyclization, dehydration and oxidation. However, citrine[16] and Venus[17], two bright versions of a yellow-emitting mutant of GFP (YFP) that mature efficiently, have recently been developed. These variants can also facilitate host protein folding[17]. Moreover, their rapid maturation allows the immediate detection of fluorescent signals after the introduction of genes to freshly prepared biological samples, such as brain slices[17]. Similarly to GFP variants, the red chromophore of DsRed also undergoes these maturation steps, but requires an additional autocatalytic modification of its GFP-like chromophore[18]; incomplete maturation gives rise to residual

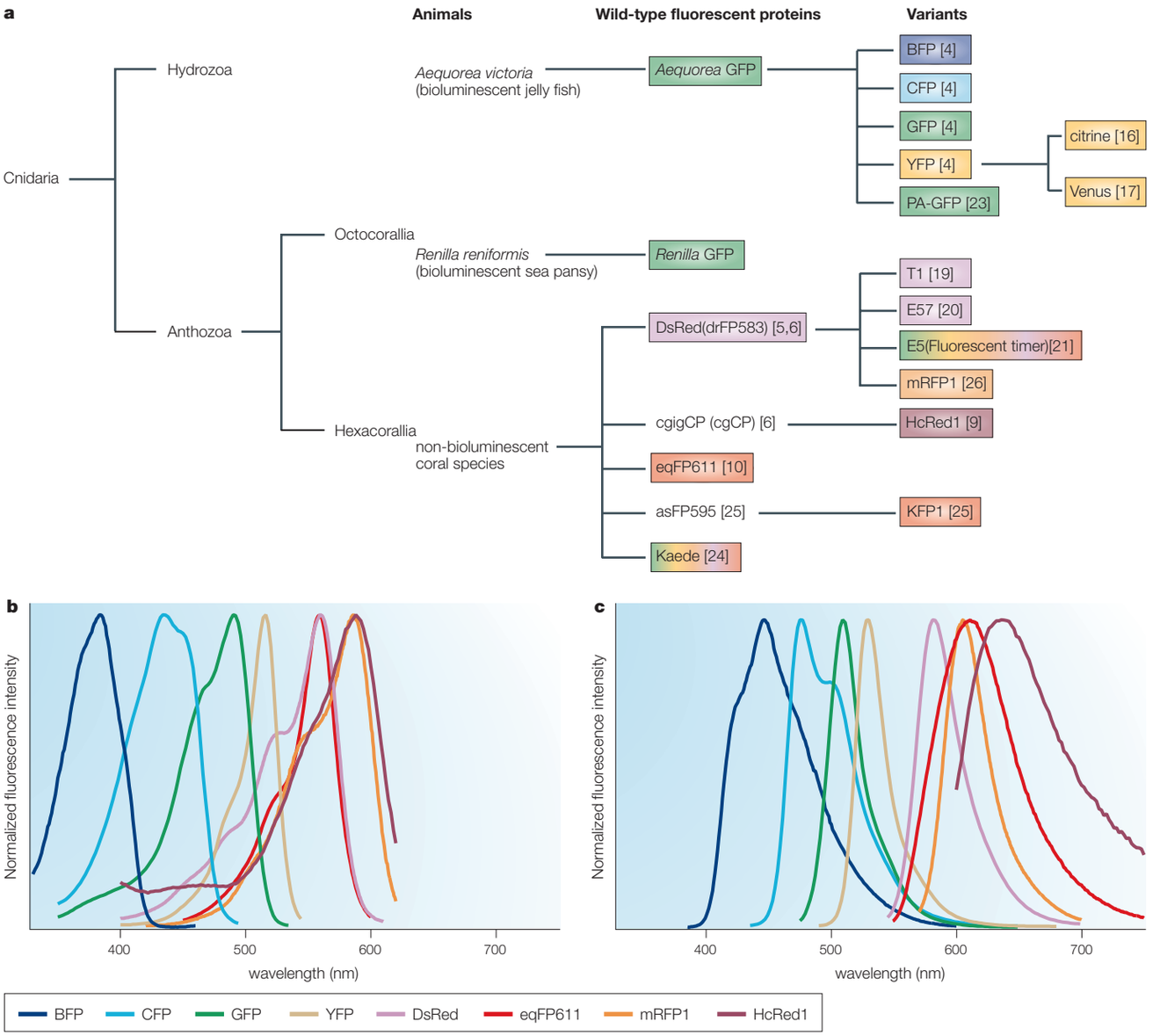

Figure 2 | **Wild-type fluorescent proteins and the spectral variants discussed in this review. a** | Phylogeny of fluorescent proteins. Colours indicate emission maxima. References are given in square brackets. Normalized excitation (**b**) and emission (**c**) spectra of representative fluorescent proteins. BFP, blue fluorescent protein; CFP, cyan fluorescent protein; GFP, green fluorescent protein; KFP1, kindling fluorescent protein; mRFP1, monomeric red fluorescent protein; PA-GFP, photoactivatable-GFP; YFP, yellow fluorescent protein.

green fluorescence, which might be a disadvantage for separation from green signals. Two recently developed varieties of DsRed, known as T1 (REF. 19) and E57 (REF. 20), display improved maturation, making them preferable for use in dual-colour experiments.

Conversely, a long-lived green state can be advantageous if the intention is to analyse the history of the synthesis of a protein in a cell. A new mutant of DsRed, E5, is particularly useful for this because it changes its colour from green to red over a predictable time course[21]. This feature makes it possible to use the ratio of green-to-red emission as a measure of the time that has elapsed since the initiation of protein synthesis. Therefore, E5 functions as a fluorescent timer that yields both temporal and spatial information about target protein age. For example, this property of E5 maturation has been applied in experiments with adrenal chromaffin cells expressing a peptide hormone fused to E5, and has been used to demonstrate that secretory vesicles are segregated functionally and spatially according to age[22].

It is emerging that the maturation and subsequent fluorescence of some GFP variants can be 'photoactivated' by specific illumination, which provides the advantage that fluorescence can be turned on at a chosen time point. During the past year, three new fluorescent proteins that undergo photochemical modification in or near the chromophore have been developed: PA-GFP[23], Kaede[24] and KFP1[25] (see also the review on page S7 of this supplement). They enable selective activation of fluorescence signals after specific illumination, and can be used to fluorescently mark individual cells, organelles or proteins[7].

The advantages and disadvantages of oligomerization. The propensity for a fluorescent protein to form oligomers is an important consideration, as such interactions can interfere with the function of the host protein to which it is fused. Unfortunately, all of the *Anthozoan* GFP-like proteins characterized so far form obligate oligomers[14]. Although oligomerization does not prevent their use for reporting gene expression or marking cells, it does preclude their use in fusion protein applications. Similarly, fusion of DsRed, which normally forms a tetramer, to host proteins often disrupts their normal behaviour, although there are some exceptions (FIG. 3A). Campbell *et al.* recently reported the successful engineering of monomeric RFP (mRFP1)[26] from DsRed. As mRFP1 matures ten times faster than its parental protein, it exhibits similar brightness to DsRed in living cells despite its lower molar extinction coefficient, fluorescence quantum yield and photostability. Because it is monomeric, mRFP1 has enabled red-fluorescence labellings that were not possible before with DsRed (FIG. 3B). Also, the excitation and emission maxima of mRFP1 are 584 nm and 607 nm, respectively (FIG. 2b,c), which gives good spectral separation from other fluorescent protein signals. This work provides hope that other oligomeric fluorescent proteins might also be converted into monomers. Indeed, the far-red variant HcRed1, which is made from a parent chromoprotein that seems to form obligate tetramers, has also been engineered to form dimers[9]. Similarly, the anemone fluorescent protein epFP611 can function as a monomer, but only at low concentrations and in the presence of detergent[10].

A further problem is the potential aggregation of fluorescent proteins, which impedes any cellular application and leads to cellular toxicity. Although the molecular mechanisms of fluorescent protein aggregation remain unclear, there are two possible explanations. First, aggregation might be due to electrostatic or hydrophobic interactions between fluorescent proteins. The possible contribution made by electrostatic interactions has been supported by recent work in which non-aggregating mutants were successfully generated by removing basic residues located near the amino termini of several fluorescent proteins[27], including DsRed. So, it might also be possible to make non-aggregating mutants by removing hydrophobic side chains on the surface of oligomeric complexes. It should be noted that *Renilla* GFP becomes soluble as a result of its dimerization; a hydrophobic patch becomes hidden at the dimerization interface and allows the surface of the dimer to become hydrophilic.

The second possibility is that aggregation might follow fluorescent protein oligomerization. So, the problem might be made worse still if host proteins are also oligomeric, as fusion to fluorescent proteins might result in crosslinking into massive aggregates. Indeed, DsRed tends to produce more serious aggregation when fused to a host protein, although, in an exception to this trend, fusion of DsRed to protein kinase C-γ (PKC-γ) retains the dynamic redistribution of the enzyme after stimulation (FIG. 3a). Overall, this aggregation problem would most easily be solved by using monomeric fluorescent proteins (FIG. 3B)[26].

In vitro labelling with organic dyes

Despite the numerous advantages afforded by *in vivo* imaging with fluorescent proteins, these approaches, as discussed above, have limitations. Another disadvantage is that the known fluorescent proteins are relatively large (~27 kDa in monomeric form) tags for protein labelling. Although there is keen interest in 'downsizing' fluorescent proteins, mutagenesis studies have not yet been successful. So far, the most promising results for smaller protein labels have come from the use of small organic fluorophores such as fluorescein and rhodamine (<1 kDa), which can be placed at specific sites in proteins using elaborate protein chemistry labelling techniques (FIG. 1d). An important benefit of using small organic fluorophores is that it minimizes possible steric hindrance problems that can interfere with protein function. In addition, site-specific attachment of the fluorophores to proteins can permit changes in the local environment, or the distances between labelled sites, to be assessed when these molecules are used for FRET[28,29]. For example, FRET was used as a spectroscopic ruler to determine the distances between protein regions labelled with small fluorophores in the Shaker K^+ channel, and demonstrated that the voltage-sensing segment of the channel twists during activation[30,31].

If membrane permeabilization or microinjection is possible, then this approach also allows fine control of the quantity of introduced fluorescently labelled proteins. Recent FRET studies have used small fluorophores as acceptors in combination with a GFP donor. For example, the combination of Cy3.5- and Cy3-labelled phospho-specific antibodies with GFP-fusion proteins has allowed the visualization of PKC-α[32] autophosphorylation and epidermal growth factor receptor (EGFR)[33] activation, respectively, in fixed and permeabilized cell samples. The EGFR studies provided the first evidence for ligand-independent lateral propagation of receptor activation in the plasma membrane, a surprising result to many who had believed that ligand binding was essential for receptor activation. In another approach used to visualize activation of the RhoGTPase Rac, cultured cells expressing a GFP–Rac fusion were injected with a fragment of p21-activated kinase labelled with an Alexa-546 dye, which selectively binds GTP-bound GFP–Rac[34]. This study revealed the spatial control of growth factor-induced Rac activation in membrane ruffles, which forms an activation gradient at the leading edge of motile cells.

In vivo labelling with organic dyes

Recently, two innovative techniques have been developed for labelling specific recombinant proteins with small organic fluorophores within live cells[35,36]: the bi-arsenic fluorophore labelling of proteins that have been genetically altered to contain tetracysteine motifs, and the labelling of proteins fused to O^6-alkylguanine-DNA alkyltransferase with enzymatic substrate derivatives.

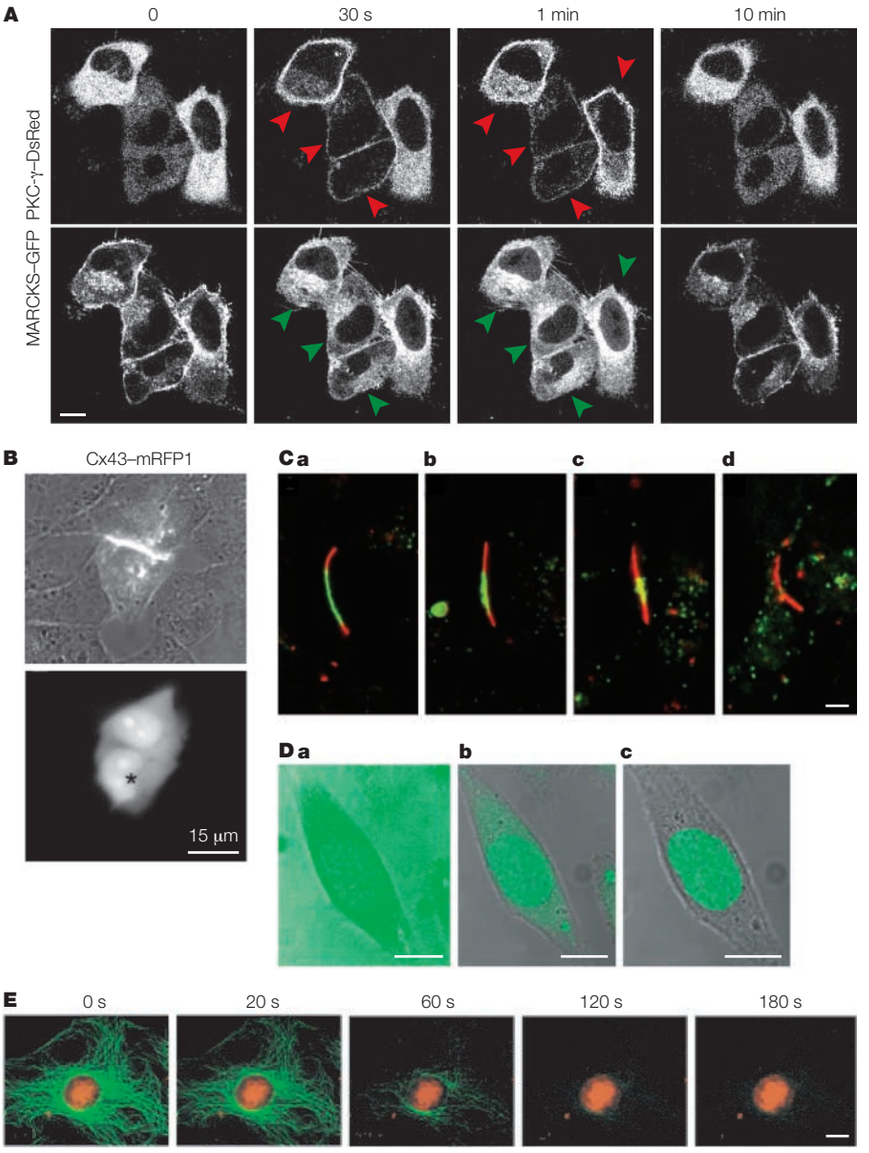

Figure 3 | **Fluorescence images of cells containing proteins labelled with fluorophores by various techniques.** **A** | Simultaneous imaging of PKC-γ–DsRed and MARCKS–GFP in HeLa cells. The images were taken at 0 s, 30 s, 1 m and 10 m after stimulation with 10 μM ATP. Green and red fluorescence signals were captured simultaneously using 488 nm and 543 nm laser lines, respectively. Remarkably, PKC-γ–DsRed preserved the original behaviour of PKC-γ despite its tetramer formation; transient redistribution of PKC-γ–DsRed from the cytosol to the plasma membrane was observed on stimulation, inducing calcium mobilization. The reciprocal translocation of MARCKS from the plasma membrane to the cytosol was visualized by fusing it to GFP. The redistribution of PKC-γ and MARCKS is indicated by arrowheads. Scale bar, 10 μm. **B** | Functional labelling of the gap junction protein Cx43 with the monomeric RFP mRFP1 (REF. 26). Transmitted light and red fluorescence. Cx43–mRFP1 was localized to the boundary between two transfected HeLa cells (top). The functionality of the gap junction formed by Cx43–mRFP1 was demonstrated by diffusion of lucifer yellow into the adjacent cell. The injection point is indicated by an asterisk (bottom). By contrast, Cx43–DsRed did not give such functional labelling of gap junction (data not shown). **C** | Gap junction dynamics revealed by sequential pulse-labelling of Cx43–tetracysteine (TC) in HeLa cells with FlAsH and ReAsH[38,39]. First, all Cx43–TC molecules were stained with FlAsH–EDT_2. After a 4- or 8-hour interval (**a** and **b**, and **c** and **d**, respectively), the newly synthesized pool of Cx43–TC was labelled with ReAsH–EDT_2. Monitoring the pools of old (green) and young (red) Cx43–TC molecules revealed that the gap junction protein moves from the periphery to the centre of the gap junction. Scale bar, 1 μm. **D** | Covalent labelling of nuclear-targeted ^{W160}hAGT with O^6-benzylguanine fluorescein (BGFL) in an AGT-deficient CHO cell[36]. A transfected cell was incubated with a membrane-permeable derivative of BGFL in the medium (**a**), and washed with phosphate buffered saline (PBS) (**b**). Successive washings reveal the localized fluorescence label within the nucleus (**c**). Scale bar, 10 μm. **E** | Photostability of quantum dot 630, which emits at 630 nm, and Alexa 488 (REF. 44). Nuclear antigens were labelled with QD 630-streptavidin (red), and microtubles were labelled with Alexa 488-conjugated to antimouse IgG (green) simultaneously in a fixed 3T3 cell. The signals of Alexa 488 faded quickly during continuous illumination at 485 nm for 3 min, whereas the signals of QD 630 were not affected. Scale bar, 10 μm. (**B**) was reproduced with permission from REF. 26 © (2002) National Academy of Sciences, (**C**) from REF. 38 © (2002) American Association for the Advancement of Science, (**D**) from REF. 36 © (2003) Macmillan Magazines Ltd, and (**E**) from REF. 44 © (2003) Macmillan Magazines Ltd. GFP, green fluorescent protein; hAGT, human O^6-alkylguanine-DNA alkyltransferase; MARCKS, myristoylated alanine-rich protein kinase C substrate; mRFP1, monomeric red fluorescent protein; PKC-γ, protein kinase C-γ; RFP, red fluorescent protein.

In the first technique, Tsien and colleagues made use of the well-known affinity of arsenoxides for closely spaced cysteine pairs[35,37]. Two arsenoxide groups were introduced into fluorescein to form FlAsH, which binds with high affinity to tetra-cysteines containing the rare sequence CCXXCC (FIG. 1e). Therefore, a host protein of interest can be genetically fused to a short peptide of 6–20 amino acids containing the CCXXCC motif, and this construct can then be produced inside cells. The FlAsH label is membrane-permeant and non-fluorescent, acquiring fluorescence only on binding to the CCXXCC motif. Importantly, this property of the compound significantly decreases the background signal generated by unbound fluorophores.

Various derivatives of FlAsH can be designed by chemical modification of the original compound[14]. For example, a red analogue of FlAsH has been synthesized using the red fluorophore resorufin, and is termed ReAsH. Using the combination of FlAsH and ReAsH, Gaietta *et al.* determined the mechanism by which connexin 43 (Cx43), a subunit of gap junction channels, is added to and removed from gap junction plaques (FIG. 3C)[38,39]. By engineering the FlAsH/ReAsH-binding motif into the Cx43 protein and then alternately labelling cells with FlAsH or ReAsH, different pools of the protein could be followed over time. This partitioning between red and green fluorescence revealed the novel characteristics of Cx43 transport, assembly into channels and turnover. This study

demonstrates the benefits of the FlAsH/ReAsH technique for studying protein ageing over any time frame, which is highly versatile compared with the green-to-red shifting E5 protein that matures in a fixed time frame.

Among the other potential applications of these fluorophores, new derivatives can be synthesized to incorporate other functionalities, such as photosensitizing groups, into recombinant proteins. In addition to its role in fluorescence labelling, a recent study of the synaptic vesicle protein synaptotagmin in *Drosophila melanogaster* neuronal synapses demonstrated that FlAsH itself is useful for the fluorophore-assisted light inactivation (FALI) of recombinant proteins[40].

More recently, there has been a report of a second technique that uses the enzymatic activity of human O^6-alkylguanine-DNA alkyltransferase (hAGT). hAGT irreversibly transfers the substrate alkyl group (an O^6-benzylguanine (BG) derivative) to one of its cysteine residues[36]. The mutant ^{W160}hAGT demonstrates increased activity against BG derivatives. Following the expression of a chimeric fusion of ^{W160}hAGT and a protein of interest, a membrane-permeable derivative of BG containing fluorescein, BGFL (O^6-benzylguanine fluorescein), is added. Once inside the cells, BGFL is acted on by the ^{W160}hAGT-containing protein, which leads to specific substrate labelling with fluorescein (FIGS 1f and 3D). Although this method seems to produce reliable labelling, there are two drawbacks. First, hAGT, at 207 amino acids in length, might be too large a fusion tag for many applications. Second, experiments on mammalian cells would need to be performed using AGT-deficient cell lines to avoid labelling of the endogenous AGT.

Other approaches have used the selective binding of a chemical ligand to its receptor protein to study pH regulation in different compartments along the secretory pathway[41,42]. For example, synthesized membrane-permeable conjugates of a hapten and fluorescent pH probes were trapped by a single-chain antibody that had been expressed in the lumen of the organelles[41]. In another approach, biotin conjugates of fluorescent pH probes were targeted to the secretory compartments by the localized expression of chicken avidin[42], which binds biotin tightly. However, further development of these chemical probes that are genetically targetable will need the exchange of more information and ideas between chemists and biologists.

Labelling with quantum dots

In addition to small organic fluorophores, semiconductor nanocrystals (quantum dots) represent a promising new fluorescent label, owing to their photostability and wide range of excitation and emission wavelengths[43]. But despite their advantages over organic fluorophores and fluorescent proteins, the use of quantum dots has so far been limited by their lack of biocompatibility. New advances in surface coating chemistry, however, have helped to overcome these problems to allow long-term, multi-colour imaging of live cells[44–46].

Quantum dots are semiconductor nanocrystalline particles, typically measuring 2–10 nm in size (roughly the size of typical proteins). They provide several important advantages over organic fluorophores and fluorescent proteins, including narrow, symmetrical and tuneable emission spectra that can be varied according to the size and material composition of the particles. This property allows flexible and close spacing of different quantum dots without substantial spectral overlap. In addition, their absorption spectra are broad, which makes it possible to excite all quantum dot colour variants simultaneously using a single excitation wavelength, thereby minimizing sample autofluorescence. Last, they have exceptional photostability.

Quantum dots are initially synthesized with hydrophobic organic ligands at their surface. For use in aqueous biological conditions, however, these organophilic species must be exchanged for ones that are more polar to prevent their aggregation and nonspecific adsorption in biological samples. Recent advances in nanomaterials have allowed quantum dots to be conjugated to biorecognition molecules[44,45], such as streptavidin (FIGS 1g and 3E) and antibodies; these conjugates have been used on both fixed cells and tissue sections. In addition, cell-surface proteins and the endocytic compartments of live cells have been labelled with quantum dot bioconjugates. More recently, quantum dots encapsulated in phospholipid micelles were injected into *Xenopus laevis* embryos, and their fluorescence was followed until the tadpole stage in a cell-autonomous manner, which illustrates that quantum dots are stable and non-toxic inside cytosolic compartments[46].

Labelling for cellular imaging

Live cell imaging has become more accessible to researchers, largely as a result of recent advances in the techniques for fluorescence labelling of proteins by gene transfer. However, general properties must be considered when developing new methods for labelling proteins. Quantitative and physiological imaging requires that cells and subcellular structures are loaded with amounts of fluorescence labelled proteins that elicit only a minimal perturbation of normal cell processes, while maintaining a favourable signal-to-noise ratio. In this context, the integrity of the labelled protein is crucial. It is also essential that the fluorophores fluoresce at a high efficiency and that the act of labelling does not disrupt the biochemical function or cellular localization of the host protein.

Each of the techniques that we have reviewed has advantages and disadvantages, which must be considered and weighed for each application. For example, the inability to control the amount of protein produced by exogenous means can be a disadvantage of gene-transfer techniques. In this regard, the more traditional introduction of fluorescence-labelled soluble proteins through a permeabilized plasma membrane or a glass pipette is superior, particularly for FRET analyses, for which a 1:1 stoichiometry between two distinct fluorescently labelled proteins is desirable. Clearly, it is imperative to evaluate the potential and limitations of each fluorescence-labelling technique so as to use them to their fullest capacity and to derive the greatest possible benefit from them. With these conditions met, the acquisition of images of cells labelled with two or more fluorophores might be a key tool to decipher the complexity of the spatial and temporal behaviour of cellular events.

Laboratory for Cell Function Dynamics, Advanced Technology Development Group, Brain Science Institute, RIKEN, 2-1 Hirosawa, Wako-city, Saitama, 351-0198, Japan.
Correspondence to A.M.
e-mail: matsushi@brain.riken.go.jp

Please cite this article as a supplement to volume 5 of Nature Cell Biology, *pages S1–S7.*
doi:10.1038/ncb1031

1. Shimomura, O., Johnson, F. H. & Saiga, Y. Extraction, purification and properties of aequorin, a bioluminescent protein from the luminous hydromedusan, *Aequorea*. *J. Cell Comp. Physiol.* **59**, 223–240 (1962).
2. Prasher, D. C., Eckenrode, V. K., Ward, W. W., Prendergast, F. G. & Cormier, M. J. Primary structure of the *Aequorea victoria* green fluorescent protein. *Gene* **111**, 229–233 (1992).
3. Chalfie, M., Tu, Y., Euskirchen, G., Ward, W. W. & Prasher, D. C. Green fluorescent protein as a marker for gene expression. *Science* **263**, 802–805 (1994).
4. Tsien, R. Y. The green fluorescent protein. *Annu. Rev. Biochem.* **67**, 509–544 (1998).
5. Matz, M. V. *et al.* Fluorescent proteins from nonbioluminescent Anthozoa species. *Nature Biotechnol.* **17**, 969–973 (1999).
6. Labas, Y. A. *et al.* Diversity and evolution of the green fluorescent protein family. *Proc. Natl Acad. Sci. USA* **99**, 4256–4261 (2002).
7. Lippincott-Schwartz, J. & Patterson, G. H. Development and use of fluorescent protein markers in living cells. *Science* **300**, 87–91 (2003).
8. Baird, G. S., Zacharias, D. A. & Tsien, R. Y. Biochemistry, mutagenesis, and oligomerization of DsRed, a red fluorescent protein from coral. *Proc. Natl Acad. Sci. USA* **99**, 11984–11989 (2000).
9. Gurskaya, N. G. *et al.* GFP-like chromoproteins as a source of far-red fluorescent proteins. *FEBS Lett.* **507**, 16–20 (2001).
10. Wiedenmann, J. S. *et al.* A far-red fluorescent protein with fast maturation and reduced oligomerization tendency from *Entacmaea quadricolor* (Anthozoa, Actinaria). *Proc. Natl Acad. Sci. USA* **99**, 11646–11651 (2002).
11. Ormö, M. *et al.* Crystal structure of the *Aequorea victoria* green fluorescent protein. *Science* **273**, 1392–1395 (1996).

12. Siegel, M. S. & Isacoff, E. Y. A genetically encoded optical probe of membrane voltage. *Neuron* **19**, 735–741 (1997).
13. Baird, G. S., Zacharias, D. A. & Tsien, R. Y. Circular permutation and receptor insertion within green fluorescent proteins. *Proc. Natl Acad. Sci. USA* **96**, 11241–11246 (1999).
14. Zhang, J., Campbell, R. E., Ting, A. Y. & Tsien, R. Y. Creating new fluorescent probes for cell biology. *Nature Rev. Mol. Cell Biol.* **3**, 906–918 (2002).
15. Sacchetti, A. & Alberti, S. Protein tags enhance GFP folding in eukaryotic cells. *Nature Biotechnol.* **17**, 1046 (1999).
16. Griesbeck, O., Baird, G. S., Campbell, R. E., Zacharias, D. A. & Tsien, R. Y. Reducing the environmental sensitivity of yellow fluorescent protein. *J. Biol. Chem.* **276**, 29188–29194 (2001).
17. Nagai, T. *et al.* A variant of yellow fluorescent protein with fast and efficient maturation for cell-biological applications. *Nature Biotechnol.* **20**, 87–90 (2002).
18. Gross, L. A., Baird, G. S., Hoffman, R. C., Baldridge, K. K. & Tsien, R. Y. The structure of the chromophore within DsRed, a red fluorescent protein from coral. *Proc. Natl Acad. Sci. USA* **97**, 11990–11995 (2000).
19. Bevis, B. J. & Glick, B. S. Rapidly maturing variants of the *Discosoma* red fluorescent protein (DsRed). *Nature Biotechnol.* **20**, 83–87 (2002).
20. Terskikh, A. V., Fradkov, A. F., Zaraisky, A. G., Kajava, A. V. & Angres, B. Analysis of DsRed mutants. Space around the fluorophore accelerates fluorescence development. *J. Biol. Chem.* **277**, 7633–7636 (2002).
21. Terskikh, A. V. *et al.* 'Fluorescent timer': protein that changes color with time. *Science* **290**, 1585–1588 (2000).
22. Duncan, R. R. *et al.* Functional and spatial segregation of secretory vesicle pools according to vesicle age. *Nature* **422**, 176–180 (2003).
23. Patterson, G. H. & Lippincott-Schwartz, J. A photoactivatable GFP for selective photolabeling of proteins and cells. *Science* **297**, 1873–1877 (2002).
24. Ando, R., Hama, H., Yamamoto-Hino, M., Mizuno, H. & Miyawaki, A. An optical marker based on the UV-induced green-to-red photoconversion of a fluorescent protein. *Proc. Natl Acad. Sci. USA* **99**, 12651–12656 (2002).
25. Chudakov, D. M. *et al.* Kindling fluorescent proteins for precise *in vivo* photolabeling. *Nature Biotechnol.* **21**, 191–194 (2003).
26. Campbell, R. E. *et al.* A monomeric red fluorescent protein. *Proc. Natl Acad. Sci. USA* **99**, 7877–7882 (2002).
27. Yanushevich, Y. G. *et al.* A strategy for the generation of non-aggregating mutants of Anthozoa fluorescent proteins. *FEBS Lett.* **511**, 11–14 (2002).
28. Stryer, L. Fluorescence energy transfer as a spectroscopic ruler. *Annu. Rev. Biochem.* **47**, 819–846 (1978).
29. Lakowicz, J. R. in *Principles of Fluorescence Spectroscopy* (ed. Lakowicz, J. R.) 368–391 (Kluwer Academic/Plenum, New York, 1999).
30. Cha, A., Snyder, G. E., Selvin, P. R. & Bezanilla, F. Atomic scale movement of the voltage-sensing region in a potassium channel measured via spectroscopy. *Nature* **402**, 809–813 (1999).
31. Glauner, K. S., Mannuzzu, L. M., Gandhi, C. S. & Isacoff, E. Y. Spectroscopic mapping of voltage sensor movement in the Shaker potassium channel. *Nature* **402**, 813–817 (1999).
32. Ng, T. *et al.* Imaging protein kinase C-α activation in cells. *Science* **183**, 2085–2089 (1999).
33. Verveer, P. J., Wouters, F. S., Reynolds, A. R. & Bastiaens, P. I. H. Quantitative imaging of lateral ErbB1 receptor signal propagation in the plasma membrane. *Science* **290**, 1567–1570 (2000).
34. Kraynov, V. S. *et al.* Localized Rac activation dynamics visualized in living cells. *Science* **290**, 333–337 (2000).
35. Griffin, B. A., Adams, S. R. & Tsien, R. Y. Specific covalent labeling of recombinant protein molecules inside live cells. *Science* **281**, 269–272 (1998).
36. Keppler, A. *et al.* A general method for the covalent labeling of fusion proteins with small molecules *in vivo*. *Nature Biotechnol.* **21**, 86–89 (2003).
37. Griffin, B. A., Adams, S. R. & Tsien, R. Y. Fluorescent labeling of recombinant proteins in living cells with FlAsH. *Methods Enzymol.* **327**, 565–578 (2000).
38. Gaietta, G. *et al.* Multicolor and electron microscopic imaging of connexin trafficking. *Science* **296**, 503–507 (2002).
39. Falk, M. M. Genetic tags for labeling live cells: gap junctions and beyond. *Trends Cell Biol.* **12**, 399–404 (2002).
40. Marek, K. W. & Davis, G. W. Transgenically encoded protein photoinactivation (FlAsH-FALI): acute inactivation of synaptotagmin I. *Neuron* **36**, 805–813 (2002).
41. Farinas, J. & Verkman, A. S. Receptor-mediated targeting of fluorescent probes in living cells. *J. Biol. Chem.* **274**, 7603–7606 (1999).
42. Wu, M. M. *et al.* Mechanisms of pH regulation in the regulated secretory pathway. *J. Biol. Chem.* **276**, 33027–33035 (2001).
43. Chan, W. C. *et al.* Luminescent quantum dots for multiplexed biological detection and imaging. *Curr. Opin. Biotechnol.* **13**, 40–46 (2002).
44. Wu, X. *et al.* Immunofluorescent labeling of cancer marker Her2 and other cellular targets with semiconductor quantum dots. *Nature Biotechnol.* **21**, 41–46 (2003).
45. Jaiswal, J. K., Mattoussi, H., Mauro, J. M. & Simon, S. M. Long-term multiple color imaging of live cells using quantum dot bioconjugates. *Nature Biotechnol.* **21**, 47–51 (2003).
46. Dubertret, B. *et al. In vivo* imaging of quantum dots encapsulated in phospholipid micelles. *Science* **298**, 1759–1762 (2002).

Acknowledgements
We thank Dr Ulrich Nienhaus for providing the spectral data of eqFP611. This work was partly supported by grants from CREST of JST (Japan Science and Technology), and the Japanese Ministry of Education, Science and Technology.

Online links

DATABASES
The following terms in this article are linked online to:
LocusLink: http://www.ncbi.nlm.nih.gov/LocusLink/
EGFR | hAGT | PCK-α | PKC-γ

FURTHER INFORMATION
Encyclopedia of Life Sciences: http://www.els.net
fluorescence microscopy | fluorescence resonance energy transfer | fluorescence spectrophotometry | fluorescent analogues in biological research
Access to this interactive links box is free online.

REVIEW

Photobleaching and photoactivation: following protein dynamics in living cells

Jennifer Lippincott-Schwartz, Nihal Altan-Bonnet and George H. Patterson

Cell biology is being transformed by the use of fluorescent proteins as fusion tags to track protein behaviour in living cells. Here, we discuss the techniques of photobleaching and photoactivation, which can reveal the location and movement of proteins. Widespread applications of these fluorescent-based methods are revealing new aspects of protein dynamics and the biological processes that they regulate.

The discovery and development of fluorescent proteins from marine organisms are revolutionizing the study of cell behaviour by providing convenient markers for gene expression and protein targeting in intact cells and organisms (see also the review on page S1 of this supplement)[1,2]. The most widely used of these fluorescent proteins — green fluorescent protein (GFP) from the jellyfish *Aequorea victoria*[3] — can be attached to virtually any protein of interest and still fold into a fluorescent molecule. The resulting GFP chimaera can be used to localize previously uncharacterized proteins[4] or to visualize and track known proteins to further understand cellular events[5].

The use of GFP as a minimally invasive tool for studying protein dynamics and function has been stimulated by the engineering of mutant GFPs with improved brightness, photostability and expression properties[2,6,7]. Cells that express proteins tagged with these GFPs can be imaged with low light intensities over many hours and so can provide useful information about changes in the steady-state distribution of a protein over time. Time-lapse imaging alone, however, cannot reveal a protein's kinetic properties (for example, whether it is freely diffusing, bound to an immobile scaffold, or undergoing binding with and dissociation from other components). Yet, it is these kinetic properties that are arguably of most interest, as they underlie protein function within cells.

In this review, we discuss two techniques — photobleaching and photoactivation — that, when combined with time-lapse imaging, can uncover the kinetic properties of a protein by making its movement observable[2,7–11]. Photobleaching — the photo-induced alteration of a fluorophore that extinguishes its fluorescence — accomplishes this through fluorescence depletion within a selected region. Photoactivation, on the other hand, works by converting molecules to a fluorescent state by using a brief pulse of high-intensity irradiation. After fluorescently highlighting specific populations of molecules by either method, the fluorescent molecules can be followed as they re-equilibrate in the cell. The extent and rate at which this occurs can be quantified and used with computer-modelling approaches to describe the kinetic parameters of a protein.

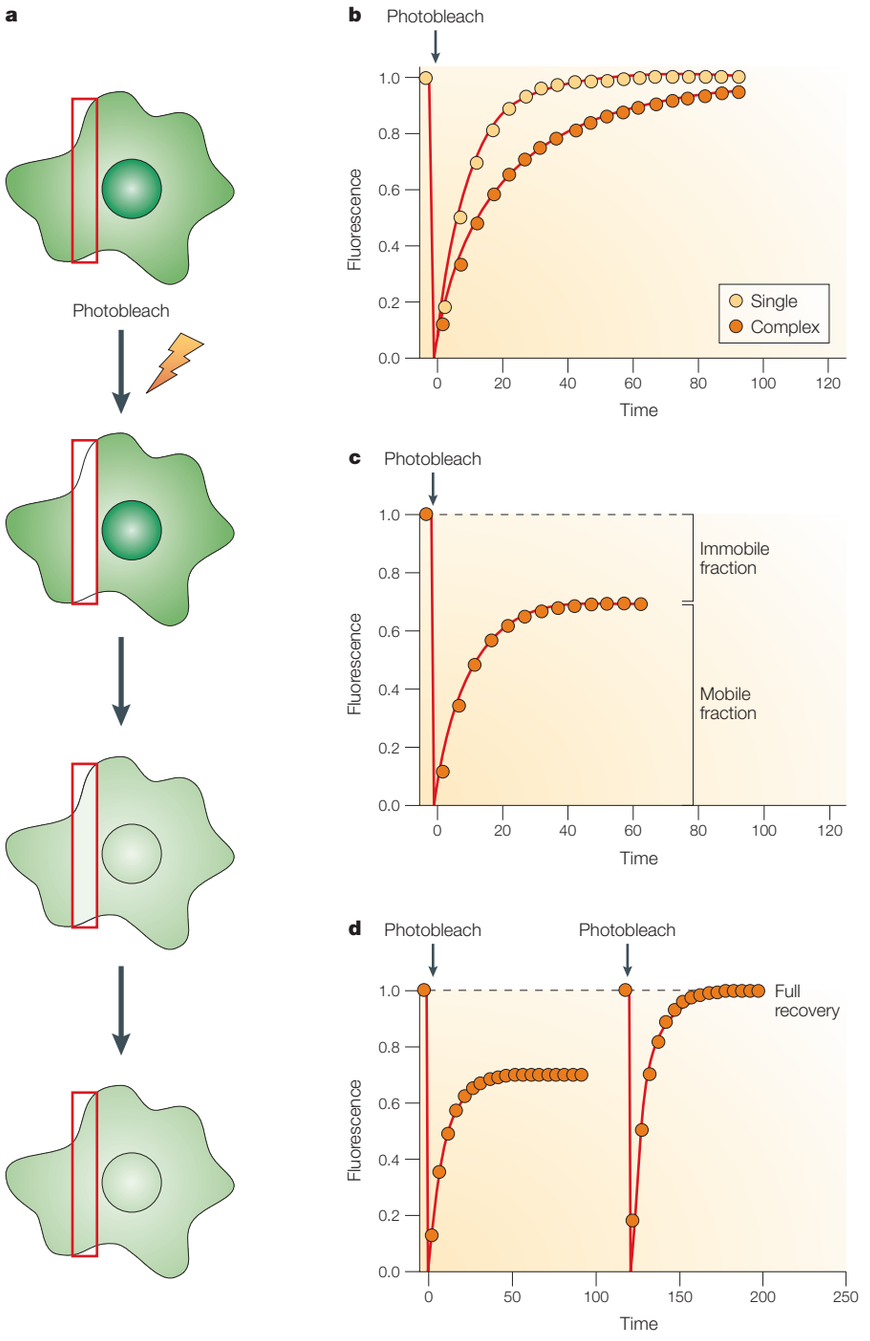

Figure 1 | **Fluorescence recovery after photobleaching. a** | A cell expressing fluorescent molecules is imaged with low light levels before and after photobleaching the strip outlined in red. Recovery of fluorescent molecules from the surrounding area into the photobleached region is monitored over time. Analysis usually includes compensation for the reduction in whole-cell fluorescence (depicted in the bottom cartoons). **b** | Fluorescence recovery into the photobleached region can be quantified in a fluorescence recovery after photobleaching (FRAP) curve. These plots depict the recovery for a single species (simulated by a single exponential curve shown in yellow circles) or the kinetics for two equal populations recovering at two different rates (simulated by a double exponential curve shown in orange circles). Note that the kinetics for recovery of the latter takes much longer to plateau. **c** | The level of fluorescence recovery in the photobleached region reveals the mobile and immobile fractions of the fluorophore in the cell (see main text for details). **d** | A simple test for photo-induced immobile fractions is to perform a second FRAP experiment in the same region of interest. In the example here, the mobile fraction of the initial FRAP experiment is ~70%. The level of recovery can be determined by normalizing the fluorescent signal in the region and repeating the FRAP experiment. In the absence of photodamage, full recovery should be observed.

Photobleaching techniques

Fluorescence recovery after photobleaching. Developed over two decades ago to study the diffusive properties of molecules in living cells[12–17], fluorescence recovery after photobleaching (FRAP) has experienced a resurgence due to the introduction of GFP and the development of commercially available confocal-microscope-based photobleaching methods[8,11,18]. In this technique, a region of interest is selectively photobleached with a high-intensity laser and the recovery that occurs as molecules move into the bleached region is monitored over time with low-intensity laser light (FIG. 1a). Depending on the protein studied, fluorescence recovery can result from protein diffusion, binding/dissociation or transport processes.

Analysis of fluorescence recovery can be used to determine the kinetic parameters of a protein, including its diffusion constant, mobile fraction, transport rate or binding/dissociation rate from other proteins. In experiments in which the protein of interest moves freely, the fluorescence will recover to the initial prebleach value and the shape of the recovery curve can be described mathematically with a single component recovery (FIG. 1b, single)[19–22]. Determining the effective diffusion coefficient (D_{eff}) and mobile fraction (M_f) of a protein from such data is relatively straightforward, given the previous analysis of FRAP kinetics[12] (for several recent reviews, see REFS 8,11,18,23). If the shape of the curve is complex (that is, it requires a multi-component diffusion equation[20,24,25]), then multiple populations of the molecule with differing diffusion rates are present (FIG. 1b, complex). This can occur when a molecule undergoes binding and release from intracellular components or exists as a monomer and multimeric forms[10]. Alternatively, the protein might not be diffusing but might be undergoing movement driven by molecular motors or membrane tension flow. A simple test for determining whether a fluorescent protein moves by diffusive movement or facilitated transport is to vary the size of the bleached area or beam radius, ω. The recovery will change with an ω^2 dependence for diffusive movement only[26]. Accurate analysis of FRAP data requires that the bleach event is much shorter than the recovery time and preferably as short as possible. Moreover, the recovery event must be monitored until a recovery plateau is achieved, which is much greater than the half-time for recovery. See TABLE 1 for other FRAP considerations.

Performing FRAP. Until recently, carrying out FRAP required custom-built systems to perform the measurements. Development of FRAP methods for use on the laser-scanning confocal microscope has made this technique widely available. Images on the confocal microscope are obtained by scanning a focused laser beam across the specimen and recording the emitted fluorescence through a pinhole that is situated in front of the light detector. One way to photobleach using this system is to define a region-of-interest at the highest possible ZOOM, set the laser power to maximum, and set the laser ATTENUATION to zero. The high zoom increases the dwell time of the laser on the bleached region per line scan (laser intensity increases proportionally to the square of the zoom factor), which therefore greatly increases the radiation per area. But a more advanced method is to use an acousto-optical tunable filter (AOTF; available on more recent commercially available confocal microscopes), which allows rapid (microsecond to millisecond) attenuation of the laser as it scans a field. By allowing rapid switching between the bleaching and normal beam, the AOTF allows accurate measurements of diffusion rates in defined areas.

Use of an AOTF also enables users to photobleach virtually any pattern or shape. This allows FRAP studies to be done on organelles of complex shapes, allowing the lateral mobility of organelle-specific membrane and lumenal proteins to be investigated. Selective photobleaching on a confocal microscope also provides a method for analysing aspects of protein dynamics other than diffusion (including assembly/disassembly of protein complexes in cells, the exchange of cytosolic proteins on and off organelles, and the lifetime and fate of membrane-bound transport intermediates[27–30] (FIG. 2a). This type of analysis often requires measuring the fluorescence signal of GFP in a specific structure or area, to compare it with fluorescent intensities of other structures or areas. Once the quantities of fluorescent molecules in different sites or states are known, computer modelling can then be used to determine the parameter values (that is, the rate constants for binding interactions and exchange times) of the processes of interest[10]. Recent applications in which kinetic modelling has been used successfully include analysing the dynamics of nuclear proteins[31–35], protein transport through membrane trafficking pathways[27,36,37] and membrane coat protein dynamics[30].

Inverse FRAP. Inverse FRAP (iFRAP) is performed as a normal FRAP experiment with the exception that the molecules outside a region of interest are photobleached and the loss of fluorescence from the non-photobleached region is monitored over time. As opposed to the rate of recovery studied using a FRAP experiment, iFRAP offers a way to monitor the rate of movement out of a region. For example, iFRAP was used to monitor the dissociation kinetics of GFP-tagged RNA polymerase I components from sites of rRNA transcription[34]. Because this method indirectly highlights a pool of molecules by decreasing the background fluorescence, it has also been used to follow Golgi to plasma membrane transport carriers as they moved from the Golgi and fused with the plasma membrane[27,37] (FIG. 2c).

Fluorescence localization after photobleaching. Fluorescence localization after photobleaching (FLAP)[38] also indirectly highlights a pool of molecules. For a FLAP experiment, the same protein-of-interest is tagged with two different fluorophores that co-localize when expressed in cells. By photobleaching one of these fluorophores, a selected pool can be highlighted and followed over time. Using cyan fluorescent protein (CFP)- and yellow fluorescent protein (YFP)-tagged β-actin, monomer versus filamentous actin dynamics was demonstrated[38], and actin transport was monitored during cell protrusion[39]. In another study, CFP- and YFP-tagged histone H2B molecules were co-expressed in cells undergoing mitosis[40]. After one pool of the YFP-containing H2B molecules was photobleached, the movement of the non-photobleached pool was used to monitor chromosome positions throughout the cell cycle.

Fluorescence loss in photobleaching. Complementary to the photobleaching techniques discussed earlier, the continuity of a cell compartment can be monitored using a technique called fluorescence loss in photobleaching (FLIP) (FIG. 2b). In a FLIP experiment, a fluorescent cell is repeatedly photobleached within a small region while the whole cell is repeatedly imaged. Any regions of the cell that are connected to the area being bleached will gradually lose fluorescence due to lateral

Table 1 | **FRAP considerations**

Problem	Potential explanations	References
Lack of recovery or partial recovery after photobleach	Possible explanations include: an immobile fraction of unbleached molecules in the cytoplasm that could not diffuse into the bleached region; an immobile fraction of molecules in the bleached area that was unable to exchange with the incoming unbleached molecules; or the bleached area is not continuous with the rest of the cell (for example, a separate membrane compartment).	8
Reversible photobleaching of GFP	The excitation might cause the GFP molecule to flicker or to be sequestered in a triplet state. Both of these situations can result in the recovery of fluorescence (in milliseconds to several seconds) of the GFP molecule in the absence of diffusion. To control for any reversible photobleaching of the GFP in a FRAP experiment, the FRAP conditions should be repeated in fixed samples in which no recovery of fluorescence should be expected. Or, alternatively, the bleach spot size could be varied and the changes in the timescale of recovery could be confirmed.	86
Non-diffusive behaviour	Measurements in FRAP studies are often complicated by the binding and dissociation of fluorescent molecules to and from intracellular components. This is usually reflected in the FRAP curves by longer recovery times, by an incomplete recovery (an immobile fraction) or by the presence of several slopes (indicating several recovery processes over different timescales). Kinetic modelling methods, along with computer simulations, have been useful tools to dissect and analyse the recovery curves obtained by FRAP. A kinetic model is characterized by biophysical parameters, such as binding and release rate constants, diffusion constants, flow rates and residence times. The model can be simulated on the computer for different parameter values. Once the parameters that best fit the experimental data have been determined, the predictions of the model can be tested experimentally.	10,30
D values of the same ROI in the same cell in two consecutive experiments are different	A potential explanation is damage to the photobleached area. Decreasing the bleach time, acquisition time or the excitation beam intensity during the recovery period could avoid damaging the cell. Using YFP rather than GFP or CFP will also make it easier to photobleach.	87

CFP, cyan fluorescent protein; FRAP, fluorescence recovery after photobleaching; GFP, green fluorescent protein; ROI, region of interest; YFP, yellow fluorescent protein.

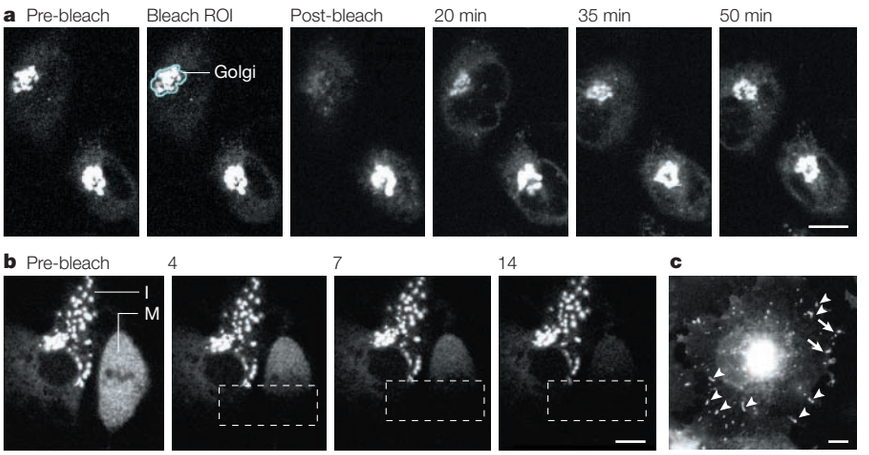

Figure 2 | **Photobleaching of GFP-tagged proteins to monitor dynamics. a** | The Golgi complex (blue outline) was photobleached in a cell expressing galtase–GFP (green fluorescent protein) in the presence of cycloheximide and the recovery was monitored over time (post-bleach image = time 0). The observed recovery indicated galtase–GFP resident in the Golgi undergoes continuous exchange with non-Golgi pools (such as those in the endoplasmic reticulum) during its lifetime. **b** | Fluorescence loss in photobleaching (FLIP) of galtase–GFP in interphase and mitotic cells. A boxed area spanning an interphase and a metaphase cell was repetitively photobleached with high-intensity laser light over time. After each photobleach, an image of the entire field was scanned with low-intensity laser light. The number of bleach cycles is indicated in each panel. Note that in a metaphase cell, unlike in interphase, the galtase–GFP fluorescence is rapidly lost after 14 cycles of photobleaching (see Movie 1 online). This indicates that it is in a continuous compartment in which it can rapidly diffuse. Images in **b** are reproduced from REF. 36 © (1999) Elsevier Science. **c** | Dimly fluorescent structures can be visualized using inverse fluorescence recovery after photobleaching (iFRAP). The transport of vesicular stomatitis virus G protein (VSV-G–GFP) in membrane-bound carriers from the Golgi to the plasma membrane was visualized by photobleaching a region of interest, which included the whole cell except the Golgi complex. After the photobleach, the export of GFP-tagged VSV-G–GFP from the Golgi complex could be imaged with low laser light (arrows) (see Movie 2 online). The images in **a** and **c** are reproduced with permission from Lippincott-Schwartz, J. *et al. Histochem. Cell Biol.* 116, 97–107 © (2001) Springer-Verlag.

movement of mobile proteins into this area. By contrast, the fluorescence in unconnected regions will not be affected. In addition to assessing continuity between areas of the cell, FLIP can be used to assess whether a protein moves uniformly across a particular cell compartment or undergoes interactions that impede its motion[28,36,41]. Furthermore, it can be used to reveal faint fluorescence in unconnected compartments that normally cannot be seen against the bright fluorescence that arises in other parts of the cell[42].

Photobleaching applications

Photobleaching techniques that are applied to live-cell imaging are transforming our understanding of cellular organization and dynamics. For the first time, the mobility of diverse molecules in the cytoplasm, nucleus, organelle lumens and membranes of living cells can be measured, and the viscosity of these environments analysed. Moreover, resident components of organelles, once thought to be stable, have been shown to continuously enter and exit these structures. These findings are defining the biophysical characteristics of cellular compartments and their components, and are illuminating regulatory features of signalling and transport pathways.

Protein dynamics in the cytoplasm. The cytoplasm contains numerous macromolecular assemblies and cytoskeletal elements (including microtubules, actin and intermediate filaments). Yet, it has only recently become clear from FRAP studies that small molecules can rapidly diffuse through this system and bind reversibly to dynamic scaffolds. Such studies have shown that molecules up to 200 kDa undergo unhindered diffusion through the cytoplasm with D_{eff} values several times lower than those found in water[43,44]. By contrast, larger molecules (>200 kDa) or macromolecular complexes have impeded diffusion, presumably due to the extensive cytoskeletal meshwork of cells[44–46].

These diffusional properties have recently been shown to participate in the spatial organization and activity of signalling pathways. One example is the mitogen-activated protein kinase (MAPK) pathway. FRAP studies[47] that examined the dynamics of the MAPK Fus3 in yeast showed that it continuously binds to and dissociates from a plasma-membrane-localized scaffold molecule, Ste5. After being activated at the plasma membrane when bound to Ste5, Fus3 rapidly relocates to the nucleus by diffusion. The spatial localization of Fus3 activation and its dynamics at the plasma membrane are thought to help control and amplify MAPK signalling. A second example from yeast is the behaviour of septins — small GTPases that recruit proteins to form a ring at the cleavage site during cell division. Using FRAP, GFP-tagged septins in yeast were shown to be mobile during most of the cell cycle but then to become immobilized at the cleavage site at the time of budding[48]. This leads to the recruitment of other proteins to this site, and thereby creates a diffusion barrier between mother and daughter cells[49]. So, by changing between mobile and immobile states, septins help to control the temporal and spatial regulation of cytokinesis.

Protein dynamics in the nucleus. FRAP measurements of GFP-labelled nuclear proteins have revealed that many compartments in the nucleus — including nucleoli, Cajal bodies and splicing-factor compartments — are not stable entities but are steady-state assemblies of proteins that undergo continuous association and dissociation[31–35]. The diffusion of proteins (including HMG17, SF2/ASF, fibrillarin, coilin and TBP) and the U7 small nuclear RNA (snRNA) in these subnuclear compartments are significantly lower (D_{eff} between 0.24–0.53 μm^2 sec^{-1}) than reported for freely diffusing peptides, GFP molecules or fluorescently labelled dextrans (≥2 μm^2 sec^{-1})[46,50]. This indicates that exchange into and out of subnuclear compartments is the rate-limiting factor for the movement of these proteins and snRNA within the nucleus. In addition to providing insights into the dynamics of subnuclear structures, FRAP studies of the nucleus have revealed the kinetics of the binding of transcription-factor machinery to DNA promoters[51,52], the intranuclear mobility of messenger RNA[53] and the geography of chromosomes[40,54].

Intra- and inter-organelle dynamics. The micro-environment within organelles and the exchange of components between organelles have also been probed using FRAP. One example is the mitochondrial matrix, which has traditionally been thought of as too dense to allow the rapid movement of its components. However, FRAP measurements of the GFP-tagged matrix enzyme cytochrome oxidase *c* revealed that this small enzyme diffuses extremely rapidly in mitochondria[55].

By contrast, components of the large macromolecular assemblies that comprise the fatty acid β-oxidation pathway were immobilized, presumably through associations with the inner mitochondrial membrane[56]. Based on these findings, it is thought that the clustered assemblies of proteins that are immobilized in the mitochondrial matrix provide a surface on which highly mobile substrates and enzymes can interact[55,56].

FRAP has also unveiled important characteristics of the ER lumen, which is enriched in molecules that are involved in protein biogenesis, folding and assembly. Under normal conditions, small soluble proteins can diffuse rapidly throughout the ER lumen with access to all areas[42,57]. However, under conditions of cell stress — such as heat shock, change in osmolarity, calcium depletion, a glycosylation block or the production of unfolded proteins[42,58–60] — there are marked changes in the mobility of proteins and lumenal continuity. So, the ER lumen is not a stable environment, but undergoes significant global changes in response to cell stress, which could affect its numerous cellular roles.

FRAP techniques have been crucial for characterizing the mobility of GFP-tagged proteins that are embedded in organelle bilayers. The measured D_{eff} for many transmembrane proteins localized in the ER, Golgi apparatus or plasma membrane have values ranging from 0.2 to 0.5 $\mu m^2\ sec^{-1}$ with little or no immobile fractions[41,42,61]. This indicates that these proteins have unhindered lateral mobility in the membranes of these compartments. By contrast, large assemblies of membrane proteins in the ER (for example, translocons, TAP transporters and nuclear pores) or plasma-membrane proteins interacting with the extracellular matrix or cortical cytoskeletal elements, diffuse more slowly or have large immobile fractions[25,60,62–65]. Studies of the diffusion properties of these molecules have important implications for understanding how proteins are retained in different membrane-bound compartments, and what mechanisms coordinate the processing and transport functions of membranes. For instance, alterations in TAP1–GFP D_{eff} under different peptide loads have provided evidence of TAP-complex conformational changes and interactions with class I major histocompatibility complex (MHC) molecules during peptide translocation[25,66]. Additionally, FRAP experiments performed on the lamin-B receptor at various points during the cell cycle show that although the receptor is immobile in the nuclear envelope during interphase, it disperses to the endoplasmic reticulum (ER) and is completely mobile during mitosis[67].

Organelles of the secretory pathway, including the Golgi apparatus, have traditionally been thought to contain relatively stable resident components. But recent studies using FRAP techniques have revealed that membrane-bound and peripherally associated Golgi-resident proteins associate only transiently with this organelle[68]. Whereas transmembrane enzymes can reside in the Golgi for up to 1–2 hours before recycling to the ER, peripherally associated coat and matrix proteins on the Golgi exchange with the soluble pools in the cytoplasm every 30–60 seconds. These results indicate that the Golgi apparatus is a highly dynamic organelle, the identity of which depends on continuous protein exchange with the cytoplasm and ongoing membrane input/output pathways.

Finally, photobleaching techniques have provided a powerful method for highlighting transport intermediates as they move along specific membrane-trafficking pathways[27,37,69,70] (FIG. 2b) and for analysing the dynamics of the protein-trafficking machinery[29,30,40,71]. Studies of GFP-tagged components of membrane-trafficking machinery that sorts cargo into membrane-bound transport intermediates have shown that they undergo continuous binding to and dissociation from membranes irrespective of vesicle budding.

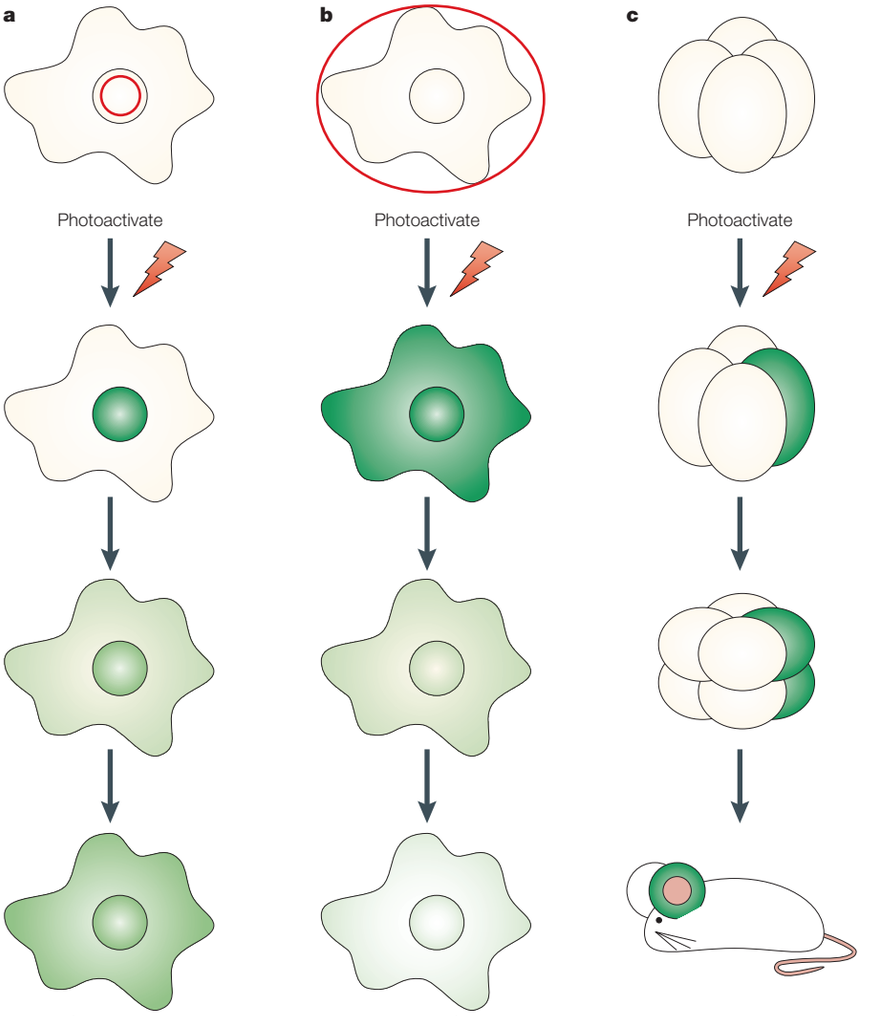

Figure 3 | **Photoactivation of fluorescent proteins. a** | Before photoactivation, cells expressing photoactivatable proteins display little fluorescence in the spectral region that is used for detecting enhanced fluorescence. After photoactivation of a selected region (indicated in red), an increase in fluorescence is observed. By directly highlighting specific populations of molecules, such as the nuclear pool of the fluorophore, the movement from this region throughout the cell can be monitored. **b** | Alternatively, the entire cell can be photoactivated and the fate of the fluorescence followed over time. Because newly synthesized proteins are not detected nor photoactivated during the imaging experiment, photoactivatable fluorescent proteins circumvent this possible artefact and might allow the fate of fluorescently tagged proteins to be monitored by 'optical pulse labelling'. **c** | Photoactivation of a single cell or population of cells can be used to monitor cell lineage within a developing organism.

These include COPII (Sec23/Sec24 and Sec13/ 31 heterodimers assembled onto ER membranes with the small GTPase, Sar1), COPI (a heptameric cytosolic protein complex recruited to Golgi membranes), Arf1 (a small GTPase) and clathrin (a major structural constituent forming the lattice around clathrin-coated vesicles). Whether this exchange represents a 'proof-reading' mechanism for ensuring proper loading of coated vesicles, or is necessary for lateral membrane differentiation into pleiomorphic transport intermediates[72], remains to be investigated. In either case, the kinetics of this exchange have major implications for models of coat protein function and of the GTP binding and hydrolysis cycles of Arf1 and Sar1.

Photoactivation

Photoactivation is the photo-induced activation of an inert molecule to an active state. It is generally associated with the ultraviolet-light-induced release of a caging group from a 'caged' compound. Photoactivation of CAGED COMPOUNDS in the study of living cells is reviewed elsewhere[73], so our discussion is limited to recent advances in the development of genetically encoded photoactivatable fluorescent proteins.

Included in the development and discovery of new fluorescent protein variants[2,6,7] (see also the review on page S1 of this supplement) were attempts to produce photoactivatable fluorescent proteins. These studies yielded several molecules or techniques for optically highlighting proteins, but each had drawbacks for use in living cells, such as modest activation[74,75], low stability[76] or a requirement for low oxygen conditions[77,78]. Recently, three photoactivatable fluorescent proteins — photoactivatable GFP (PA-GFP)[79], Kaede[80] and kindling fluorescent protein 1 (KFP1)[81] — have been reported that offer improvements over the earlier versions.

The PA-GFP[79] was developed with the aim of optimizing the photoconversion properties of *Aequorea victoria* wtGFP[74], which produces only a ~threefold increase in fluorescence under 488 nm excitation. Mutation of threonine 203 to histidine in wtGFP to produce PA-GFP decreases the initial absorbance in the minor peak region (~475 nm) and leads to ~100-fold increase after photoactivation[79]. Alternatively, for the Kaede protein, isolated from *Trachyphyllia geoffroyi*, photoactivation results in a 2,000-fold increase in its red-to-green fluorescence ratio[80]. Finally, KFP1 — an A148G mutant (where A is alanine and G is glycine) of asFP595 (asCP, where 'FP' is fluorescent protein and 'CP' is chromoprotein) from the sea anemone, *Anemonia sulcata* — gives a 30-fold increase in red fluorescence after photoactivation[81].

All of these molecules share the common characteristic of displaying low levels of fluorescence before photoactivation and higher levels after photoactivation. In a typical experiment, a cell or organism that is expressing the photoactivatable fluorescent protein is imaged at one wavelength prior to, and at various intervals after, photoactivation of a selected region with a different wavelength. However, the properties of each protein, including the wavelengths used for imaging and photoactivation, offer distinct advantages and disadvantages. For example, PA-GFP and Kaede both require ~400 nm light for photoactivation, whereas KFP1 uses green light (532 nm), which is probably better for use with living cells. Kaede displays a remarkable 2,000-fold increase in its red-to-green fluorescence ratio, but the use of both the red and green fluorescence bands could make multilabel experiments problematic. On the other hand, the green fluorescence of Kaede is bright enough to visualize the localization of the non-photoactivated proteins easily, whereas visualizing PA-GFP and KFP1 is more problematic due to their low fluorescence before photoactivation. The self-association properties of Kaede and KFP1 into tetrameric forms limit their usefulness as protein fusion tags because tetramerization might perturb parent protein localization and trafficking. The recent engineering of the DsRed protein into a monomeric form[82] is encouraging for the possibility of the eventual disruption of Kaede and KFP1 into monomers. Variants that are derived from *A. victoria*, such as PA-GFP, self-associate to a lesser degree, and even those interactions can be disrupted by one of three further point mutations[83]. Because of this, PA-GFP can be used as a reliable tag for creating fluorescent reporter molecules.

The ability to 'switch on' the fluorescence of the photoactivatable proteins makes them excellent tools for exploring protein behaviour in living cells. As the fluorescence of these proteins comes only after photoactivation, newly synthesized non-photoactivated pools are unobserved and do not complicate experimental results (FIG. 3a). This signal independence from new protein synthesis could allow the study of protein degradation of tagged molecules by 'optical pulse labelling' and monitoring of the fluorescence over time (FIG. 3b). Photoactivation of these proteins is generally rapid and gives stable fluorescence signals. Therefore, they can be used to examine various kinetic properties of tagged proteins, such as their D_{eff}, M_f, compartmental residency time and exchange. Lastly, cell lineage or movement in a developing organism can be monitored by imaging the fluorescence dispersion after photoactivation of a single cell or subpopulation of cells[81] (FIG. 3c). So, these proteins have remarkable promise to complement and extend the range of present fluorescent-protein imaging applications.

Concluding remarks

The battery of fluorescent proteins and imaging tools that allow us to monitor protein dynamics in living cells continue to provide numerous new insights into the behaviour of proteins, organelles and cells. In so doing, they have ushered in a new era of cell biology in which kinetic microscopy methods can be used to decipher pathways and mechanisms of biological processes. The microscopy techniques of photobleaching and photoactivation are perhaps the most versatile and widely used of these methods. Their ability to alter the fluorescence steady state without perturbing protein dynamics offers unprecedented opportunities for obtaining quantitative information about protein concentrations, diffusion rates, binding kinetics and protein lifetimes in single live cells, which have been indiscernible using traditional biochemical approaches. Such information is paramount to understanding how biological processes unfold, are regulated and interact in the living cell.

Looking to the future, photobleaching and photoactivation will almost certainly continue to provide important new results as their applications are extended by the development of newer instruments that push the limits of temporal and spatial detection, and by the discovery of brighter and differently coloured fluorescent proteins. For example, FRAP can be combined with other microscopic imaging approaches, including two-photon microscopy[84], (see MULTI-PHOTON MICROSCOPY) or TOTAL INTERNAL REFLECTION microscopy[85], to study events at specific sites in the cell. And, photobleaching or photoactivation can be combined with fluorescence energy-transfer techniques[2,8] to study protein interactions with greater precision. These advances will continue to require computational approaches to comprehend the plethora of quantitative experimental data[10], as well as new database tools for the analysis of specific models and their relationship to other more complex models.

Cell Biology and Metabolism Branch, National Institute of Child Health and Human Development, Building 18T/Room 101, National Institutes of Health, Bethesda, Maryland 20892, USA.
Correspondence to J.L.-S.
e-mail: jlippin@helix.nih.gov

Please cite this article as a supplement to volume 5 of Nature Cell Biology, *pages S7–S14.*
doi:10.1038/ncb1032

1. van Roessel, P. & Brand, A. H. Imaging into the future: visualizing gene expression and protein interactions with fluorescent proteins. *Nature Cell Biol.* **4**, E15–E20 (2002).
2. Zhang, J., Campbell, R. E., Ting, A. Y. & Tsien, R. Y. Creating new fluorescent probes for cell biology. *Nature Rev. Mol. Cell Biol.* **3**, 906–918 (2002).
3. Chalfie, M., Tu, Y., Euskirchen, G., Ward, W. W. & Prasher, D. C. Green fluorescent protein as a marker for gene expression. *Science* **263**, 802–805 (1994).
4. González, C. & Bejarano, L. A. Protein traps: using intracellular localization for cloning. *Trends Cell Biol.* **10**, 162–165 (2000).
5. Lippincott-Schwartz, J., Roberts, T. H. & Hirschberg, K. Secretory protein trafficking and organelle dynamics in living cells. *Annu. Rev. Cell Dev. Biol.* **16**, 557–589 (2000).
6. Tsien, R. Y. The green fluorescent protein. *Annu. Rev. Biochem.* **67**, 509–544 (1998).
7. Lippincott-Schwartz, J. & Patterson, G. H. Development and use of fluorescent protein markers in living cells. *Science* **300**, 87–91 (2003).
8. Lippincott-Schwartz, J., Snapp, E. & Kenworthy, A. Studying protein dynamics in living cells. *Nature Rev. Mol. Cell Biol.* **2**, 444–456 (2001).
9. Houtsmuller, A. B. & Vermeulen, W. Macromolecular dynamics in living cell nuclei revealed by fluorescence redistribution after photobleaching. *Histochem. Cell Biol.* **115**, 13–21 (2001).
10. Phair, R. D. & Misteli, T. Kinetic modeling approaches to *in vivo* imaging. *Nature Rev. Mol. Cell Biol.* **2**, 898–907 (2001).
11. Klonis, N. *et al.* Fluorescence photobleaching analysis for the study of cellular dynamics. *Eur. Biophys. J.* **31**, 36–51 (2002).
12. Axelrod, D., Koppel, D. E., Schlessinger, J., Elson, E. & Webb, W. W. Mobility measurement by analysis of fluorescence photobleaching recovery kinetics. *Biophys. J.* **16**, 1055–1069 (1976).
13. Elson, E. L., Schlessinger, J., Koppel, D. E., Axelrod, D. & Webb, W. W. Measurement of lateral transport on cell surfaces. *Prog. Clin. Biol. Res.* **9**, 137–147 (1976).
14. Jacobson, K., Derzko, Z., Wu, E. S., Hou, Y. & Poste, G. Measurement of the lateral mobility of cell surface components in single, living cells by fluorescence recovery after photobleaching. *J. Supramol. Struct.* **5**, 565(417)–576(428) (1976).
15. Schlessinger, J. *et al.* Lateral transport on cell membranes: mobility of concanavalin A receptors on myoblasts. *Proc. Natl Acad. Sci. USA* **73**, 2409–2013 (1976).
16. Schindler, M., Osborn, M. J. & Koppel, D. E. Lateral diffusion of lipopolysaccharide in the outer membrane of *Salmonella typhimurium*. *Nature* **285**, 261–263 (1980).
17. Sheetz, M. P., Schindler, M. & Koppel, D. E. Lateral mobility of integral membrane proteins is increased in spherocytic erythrocytes. *Nature* **285**, 510–511 (1980).
18. Reits, E. A. J. & Neefjes, J. J. From fixed to FRAP: measuring protein mobility and activity in living cells. *Nature Cell Biol.* **3**, E145–E147 (2001).
19. Kao, H. P., Abney, J. R. & Verkman, A. S. Determinants of the translational mobility of a small solute in cell cytoplasm. *J. Cell Biol.* **120**, 175–184 (1993).
20. Gordon, G. W., Chazotte, B., Wang, X. F. & Herman, B. Analysis of simulated and experimental fluorescence recovery after photobleaching. Data for two diffusing components. *Biophys. J.* **68**, 766–778 (1995).
21. Verkman, A. S. Solute and macromolecule diffusion in cellular aqueous compartments. *Trends Biochem. Sci.* **2**, 27–33 (2002).
22. Siggia, E. D., Lippincott-Schwartz, J. & Bekiranov, S. Diffusion in inhomogeneous media: theory and simulations applied to whole cell photobleach recovery. *Biophys. J.* **79**, 1761–1770 (2000).
23. Snapp, E. L., Altan, N. & Lippincott-Schwartz, J. in *Current Protocols in Cell Biology* (eds Bonifacino, J., Dasso, M., Harford, J. B., Lippincott-Schwartz, J. & Yamada, K. M.) 21.1.1–21.1.23 (John Wiley & Sons, Inc., New York, 2003).
24. Periasamy, N. & Verkman, A. S. Analysis of fluorophore diffusion by continuous distributions of diffusion coefficients: application to photobleaching measurements of multicomponent and anomalous diffusion. *Biophys. J.* **75**, 557–567 (1998).
25. Marguet, D. *et al.* Lateral diffusion of GFP-tagged H2Ld molecules and of GFP-TAP1 reports on the assembly and retention of these molecules in the endoplasmic reticulum. *Immunity* **11**, 231–240 (1999).
26. Wu, E. S., Jacobson, K., Szoka, F. & Portis, J. A. Lateral diffusion of a hydrophobic peptide, N-4-nitrobenz-2-oxa-1,3-diazole gramicidin S, in phospholipid multibilayers. *Biochemistry* **17**, 5543–5550 (1978).
27. Hirschberg, K. *et al.* Kinetic analysis of secretory protein traffic and characterization of Golgi to plasma membrane transport intermediates in living cells. *J. Cell Biol.* **143**, 1485–1503 (1998).
28. Phair, R. D. & Misteli, T. High mobility of proteins in the mammalian nucleus. *Nature* **404**, 604–609 (2000).
29. Wu, X. *et al.* Clathrin exchange during clathrin-mediated endocytosis. *J. Cell Biol.* **155**, 291–300 (2001).
30. Presley, J. F. *et al.* Dissection of COPI and Arf1 dynamics *in vivo* and role in Golgi membrane transport. *Nature* **417**, 187–193 (2002).
31. Misteli, T., Caceres, J. F. & Spector, D. L. The dynamics of a pre-mRNA splicing factor in living cells. *Nature* **387**, 523–527 (1997).
32. Snaar, S., Wiesmeijer, K., Jochemsen, A. G., Tanke, H. J. & Dirks, R. W. Mutational analysis of fibrillarin and its mobility in living human cells. *J. Cell Biol.* **151**, 653–662 (2000).
33. Chen, D., Hinkley, C. S., Henry, R. W. & Huang, S. TBP dynamics in living human cells: constitutive association of TBP with mitotic chromosomes. *Mol. Biol. Cell* **13**, 276–284 (2002).
34. Dundr, M. *et al.* A kinetic framework for a mammalian RNA polymerase *in vivo*. *Science* **298**, 1623–1626 (2002).
35. Handwerger, K. E., Murphy, C. & Gall, J. G. Steady-state dynamics of Cajal body components in the *Xenopus* germinal vesicle. *J. Cell Biol.* **160**, 495–504 (2003).
36. Zaal, K. J. M. *et al.* Golgi membranes are absorbed into and reemerge from the ER during mitosis. *Cell* **99**, 589–601 (1999).
37. Nichols, B. J. *et al.* Rapid cycling of lipid raft markers between the cell surface and Golgi complex. *J. Cell Biol.* **153**, 529–541 (2001).
38. Dunn, G. A., Dobbie, I. M., Monypenny, J., Holt, M. R. & Zicha, D. Fluorescence localization after photobleaching (FLAP): a new method for studying protein dynamics in living cells. *J. Microsc.* **205**, 109–112 (2002).
39. Zicha, D. *et al.* Rapid actin transport during cell protrusion. *Science* **300**, 142–145 (2003).
40. Gerlich, D. *et al.* Global chromosome positions are transmitted through mitosis in mammalian cells. *Cell* **112**, 751–764 (2003).
41. Cole, N. B. *et al.* Diffusional mobility of Golgi proteins in membranes of living cells. *Science* **273**, 797–801 (1996).
42. Nehls, S. *et al.* Dynamics and retention of misfolded proteins in native ER membranes. *Nature Cell Biol.* **2**, 288–295 (2000).
43. Luby-Phelps, K., Taylor, D. L. & Lanni, F. Probing the structure of cytoplasm. *J. Cell Biol.* **102**, 2015–2022 (1986).
44. Swaminathan, R., Hoang, C. P. & Verkman, A. S. Photobleaching recovery and anisotropy decay of green fluorescent protein GFP-S65T in solution and cells: cytoplasmic viscosity probed by green fluorescent protein translational and rotational diffusion. *Biophys. J.* **72**, 1900–1907 (1997).
45. Luby-Phelps, K., Castle, P. E., Taylor, D. L. & Lanni, F. Hindered diffusion of inert tracer particles in the cytoplasm of mouse 3T3 cells. *Proc. Natl Acad. Sci. USA* **84**, 4910–4913 (1987).
46. Seksek, O., Biwersi, J. & Verkman, A. S. Translational diffusion of macromolecule-sized solutes in cytoplasm and nucleus. *J. Cell Biol.* **138**, 131–142 (1997).
47. van Drogen, F., Stucke, V. M., Jorritsma, G. & Peter, M. MAP kinase dynamics in response to pheromones in budding yeast. *Nature Cell Biol.* **3**, 1051–1059 (2001).
48. Dobbelaere, J., Gentry, M. S., Hallberg, R. L. & Barral, Y. Phosphorylation-dependent regulation of septin dynamics during the cell cycle. *Dev. Cell* **4**, 345–357 (2003).
49. Faty, M., Fink, M. & Barral, Y. Septins: a ring to part mother and daughter. *Curr. Genet.* **41**, 123–131 (2002).
50. Reits, E. *et al.* Peptide diffusion, protection, and degradation in nuclear and cytoplasmic compartments before antigen presentation by MHC Class I. *Immunity* **18**, 97–108 (2003).
51. Becker, M. *et al.* Dynamic behavior of transcription factors on a natural promoter in living cells. *EMBO Rep.* **3**, 1188–1194 (2002).
52. Kimura, H., Sugaya, K. & Cook, P. R. The transcription cycle of RNA polymerase II in living cells. *J. Cell Biol.* **159**, 777–782 (2002).
53. Calapez, A. *et al.* The intranuclear mobility of messenger RNA binding proteins is ATP dependent and temperature sensitive. *J. Cell Biol.* **159**, 795–805 (2002).
54. Walter, J., Schermelleh, L., Cremer, M., Tashiro, S. & Cremer, T. Chromosome order in HeLa cells changes during mitosis and early G1, but is stably maintained during subsequent interphase stages. *J. Cell Biol.* **160**, 685–697 (2003).
55. Partikian, A., Ölveczky, B., Swaminathan, R., Li, Y. & Verkman, A. S. Rapid diffusion of green fluorescent protein in the mitochondrial matrix. *J. Cell Biol.* **140**, 821–829 (1998).
56. Haggie, P. M. & Verkman, A. S. Diffusion of tricarboxylic acid cycle enzymes in the mitochondrial matrix *in vivo*. Evidence for restricted mobility of a multienzyme complex. *J. Biol. Chem.* **277**, 40782–40788 (2002).
57. Dayel, M. J., Hom, E. F. Y. & Verkman, A. S. Diffusion of green fluorescent protein in the aequous-phase lumen of endoplasmic reticulum. *Biophys. J.* **76**, 2843–2851 (1999).
58. Subramanian, K. & Meyer, T. Calcium-induced restructuring of nuclear envelope and endoplasmic reticulum calcium stores. *Cell* **89**, 963–971 (1997).
59. Terasaki, M. Dynamics of the endoplasmic reticulum and Golgi apparatus during early sea urchin development. *Mol. Biol. Cell* **11**, 897–914 (2000).
60. Nikonov, A. V., Snapp, E. L., Lippincott-Schwartz, J. & Kreibich, G. Active translocon complexes labeled with GFP-Dad1 diffuse slowly as large polysome arrays in the endoplasmic reticulum. *J. Cell Biol.* **158**, 497–506 (2002).
61. Schmoranzer, J., Goulian, M., Axelrod, D. & Simon, S. M. Imaging constitutive exocytosis with total internal reflection fluorescence microscopy. *J. Cell Biol.* **149**, 23–32 (2000).
62. Barbour, S. & Edidin, M. Cell-specific constraints to the lateral diffusion of a membrane glycoprotein. *J. Cell Physiol.* **150**, 526–533 (1992).
63. Chakrabarti, A., Matko, J., Rahman, N. A., Barisas, B. G. & Edidin, M. Self-association of class I major histocompatibility complex molecules in liposome and cell surface membranes. *Biochemistry* **31**, 7182–7189 (1992).
64. Daigle, N. *et al.* Nuclear pore complexes form immobile networks and have a very low turnover in live mammalian cells. *J. Cell Biol.* **154**, 71–84 (2001).
65. Griffis, E. R., Altan, N., Lippincott-Schwartz, J. & Powers, M. A. Nup98 is a mobile nucleoporin with transcription-dependent dynamics. *Mol. Biol. Cell* **13**, 1282–1297 (2002).
66. Reits, E. A. J., Vos, J. C., Grommé, M. & Neefjes, J. The major substrates for TAP *in vivo* are derived from newly synthesized proteins. *Nature* **404**, 774–778 (2000).
67. Ellenberg, J. *et al.* Nuclear membrane dynamics and reassembly in living cells: targeting of an inner nuclear membrane protein in interphase and mitosis. *J. Cell Biol.* **138**, 1193–1206 (1997).
68. Ward, T. H., Polishchuk, R. S., Caplan, S., Hirschberg, K. & Lippincott-Schwartz, J. Maintenance of Golgi structure and function depends on the integrity of ER export. *J. Cell Biol.* **155**, 557–570 (2001).
69. Presley, J. F. *et al.* ER-to-Golgi transport visualized in living cells. *Nature* **389**, 81–85 (1997).
70. Nakata, T., Terada, S. & Hirokawa, N. Visualization of the dynamics of synaptic vesicle and plasma membrane proteins in living axons. *J. Cell Biol.* **140**, 659–674 (1998).
71. Stephens, D. J., Lin-Marq, N., Pagano, A., Pepperkok, R. & Paccaud, J. P. COPI-coated ER-to-Golgi transport complexes segregate from COPII in close proximity to ER exit sites. *J. Cell Sci.* **113**, 2177–2185 (2000).
72. Bonifacino, J. & Lippincott-Schwartz, J. Coat proteins: shaping membrane transport. *Nature Rev. Mol. Cell Biol.* **4**, 409–414 (2003).
73. Politz, J. C. Use of caged fluorophores to track macromolecular movement in living cells. *Trends Cell Biol.* **9**, 284–287 (1999).
74. Yokoe, H. & Meyer, T. Spatial dynamics of GFP-tagged proteins investigated by local fluorescence enhancement. *Nature Biotechnol.* **14**, 1252–1256 (1996).
75. Marchant, J. S., Stutzmann, G. E., Leissring, M. A., LaFerla, F. M. & Parker, I. Multiphoton-evoked color change of DsRed as an optical highlighter for cellular and subcellular labeling. *Nature Biotechnol.* **19**, 645–649 (2001).
76. Lukyanov, K. A. *et al.* Natural animal coloration can be determined by a nonfluorescent green fluorescent protein homolog. *J. Biol. Chem.* **275**, 25879–25882 (2000).
77. Elowitz, M. B., Surette, M. G., Wolf, P.-E., Stock, J. & Leibler, S. Photoactivation turns green fluorescent protein red. *Curr. Biol.* **7**, 809–812 (1997).
78. Sawin, K. E. & Nurse, P. Photoactivation of green fluorescent protein. *Curr. Biol.* **7**, R606–R607 (1997).
79. Patterson, G. H. & Lippincott-Schwartz, J. A photoactivatable GFP for selective photolabeling of proteins and cells. *Science* **297**, 1873–1877 (2002).
80. Ando, R., Hama, H., Yamamoto-Hino, M., Mizuno, H. & Miyawaki, A. An optical marker based on the UV-induced green-to-red photoconversion of a fluorescent protein. *Proc. Natl Acad. Sci. USA* **99**, 12651–12656 (2002).
81. Chudakov, D. M. *et al.* Kindling fluorescent proteins for precise *in vivo* photolabeling. *Nature Biotechnol.* **21**, 191–194 (2003).
82. Campbell, R. E. *et al.* A monomeric red fluorescent protein. *Proc. Natl Acad. Sci. USA* **99**, 7877–7882 (2002).
83. Zacharias, D. A., Violin, J. D., Newton, A. C. & Tsien, R. Partitioning of lipid-modified monomeric GFPs into membrane microdomains of live cells. *Science* **296**, 913–916 (2002).

84. Denk, W., Piston, D. W. & Webb, W. W. in *Handbook of Biological Confocal Microscopy* (ed. Pawley, J. B.) 445–458 (Plenum Press, New York, 1995).
85. Steyer, J. A. & Almers, W. A real-time view of life within 100 nm of the plasma membrane. *Nature Rev. Mol. Cell Biol.* **2**, 268–275 (2001).
86. Levin, M. H., Haggie, P. M., Vetrivel, L. & Verkman, A. S. Diffusion in the endoplasmic reticulum of an aquaporin-2 mutant causing human nephrogenic diabetes insipidus. *J. Biol. Chem.* **276**, 21331–21336 (2001).
87. Lippincott–Schwartz, J. *et al.* in *Green Fluorescent Proteins* (eds Sullivan, K. F. & Kay, S. A.) 261–281 (Academic Press, San Diego, 1999).

Online links

DATABASES

The following terms in this article are linked online to:

LocusLink: http://www.ncbi.nlm.nih.gov/LocusLink/
Arf1 | HMG17 | lamin-B receptor | MAPK | Sar1 | Sec13 | Sec23 | Sec24 | SF2 | TBP

Protein Data Bank: http://www.rcsb.org/pdb/
DsRed | GFP | YFP

***Saccharomyces* Genome Database:**
http://www.yeastgenome.org/
Fus3 | Ste5

Access to this interactive links box is free online.

REVIEW

4D imaging to assay complex dynamics in live specimens

Daniel Gerlich and Jan Ellenberg

A full understanding of cellular dynamics is often difficult to obtain from time-lapse microscopy of single optical sections. New microscopes and image-processing software are now making it possible to rapidly record three-dimensional images over time. This four-dimensional imaging allows precise quantitative analysis and enhances visual exploration of data by allowing cellular structures to be interactively displayed from many angles. It has become a key tool for understanding the complex organization of biological processes in live specimens.

Following the advent of indirect immunofluorescence during the 1960s, fluorescence microscopy has become an indispensable tool for localizing proteins in fixed specimens, and it often complements *in vitro* analyses of molecular mechanisms. The recent availability of a wealth of new vital markers for fluorescence microscopy[1] also allows defined molecular species to be conveniently labelled and, therefore, molecular assays to be carried out in live cells. In particular, green fluorescent protein (GFP) can be used to visualize virtually any protein in live cells[2], and a large number of GFP variants are now available, which have different spectral properties[3] and allow simultaneous detection of multiple tagged proteins[4] (see also the review on page S1 of this supplement).

When highly dynamic and spatially complex structures, such as live cells and organisms, are imaged, a more complete representation is achieved by recording the data in three spatial dimensions over time (four-dimensional (4D) imaging)[5–10]. This generates complex data, typically consisting of thousands of individual image slices, which can occupy several gigabytes of storage space per experiment. Such data require dedicated computational tools for their quantitative analysis. Here, we review typical 4D acquisition systems, important considerations for 4D experiments, and image-processing procedures for visualization and quantitation; in addition, we highlight the applications of this emerging approach in cell biology.

Acquiring 4D sequences

General considerations for 4D imaging. The fundamental consideration for any 4D live-cell imaging device is to keep the specimen alive during the acquisition of 100–10,000 images over a long period. A suitable and stable environment has to be provided, ensuring a constant temperature and a stably buffered culture medium. After this, the other significant concern in 4D imaging is the limited number of photons available to acquire fluorescence images from each cell. This is due to the limited number of fluorescent molecules that can be introduced into a cell at physiological concentrations and the limited photon yield before oxidation — which terminates fluorescence — for each fluorophore. Excessive illumination will lead to loss of signal by photobleaching and is toxic for cells (see PHOTOTOXICITY). Therefore, excitation light is typically kept to a minimum in 4D experiments, which frequently results in a suboptimal signal-to-noise ratio and a lower spatial resolution when compared with images of fixed specimens. So, for each biological application, it is crucial to find a suitable compromise between sufficient, but not toxic, illumination, spatial resolution in the x, y and z axes, temporal resolution and the signal-to-noise ratio, so that the maximum number of acceptable images can be acquired before the specimen is completely photobleached or damaged. In some cases, a single z slice (2D time-lapse recording) can yield the best results — for example, when the structure of interest is flat and when there are no marked deformations along the z axis during the experiment. In this case, the lower number of frames in 2D time-lapse imaging would yield a better signal-to-noise ratio and a better time resolution, making it favourable to 4D imaging. Furthermore, when imaging dynamic processes in 4D, each of these parameters might change during the experiment and should be adjusted interactively.

A good illustration of this is 4D imaging of chromosome dynamics in mitotic cells (FIG. 1). For such an experiment, the time lapse would need to be shortened during more dynamic phases, such as congression — the rapid movement of chromosomes to the spindle equator in prometaphase — and then prolonged during the stable metaphase orientation. The number of z slices necessary is low in prophase, when the cell is still flatly attached to the substrate, and is increased when it rounds up in metaphase (see the side view in FIG. 1d,e). In addition, 4D experiments often run for hours or days to record a biological process such as one cell cycle. Therefore, automatic 4D recording with application protocols on 4D microscopes that can autofocus, track cell movements and revisit multiple-stage locations to follow several cells in parallel can markedly increase throughput and reproducibility of 4D imaging.

Fluorescence microscopes for 4D imaging. The main difference to conventional epifluorescence microscopy is that 4D imaging requires rapid and reproducible sectioning along the optical axis (z axis). Ideally, the acquisition time for each z stack should be small compared with the time lapse between the acquisition of individual stacks to avoid movements within each 3D data set. In addition, the z positions have to be highly reproducible over time, through many stacks, to avoid drifts. Z stepping (the movement

from one optical section to the next) is achieved by either moving the specimen with a z-scanning stage, or by moving the microscope objective with a high-precision motor (piezo-stepper). To use the limited number of photons most efficiently, it is crucial to maximize efficiency of light collection and the sensitivity on 4D-imaging systems. This means that all optical components should be optimized to transmit the emission wavelengths of the desired fluorophores. Another important aspect of 4D imaging is the resolution along the z axis, which, in light microscopes, is about threefold lower than resolution along the x and y axes; this causes anisotropy in the recorded 3D image. Two alternative microscopy techniques are routinely used for the acquisition of 4D images with optimized z resolution. First, widefield fluorescence deconvolution microscopes homogeneously illuminate the whole specimen and grab the entire image simultaneously on a charge-coupled device (CCD) camera. Image stacks are then processed using iterative algorithms that assign out-of-focus light back to the fluorescent object it came from in the correct focal plane. In this manner, deconvolution can yield high-resolution 3D information from widefield images[9,11]. By contrast, confocal laser-scanning microscopes excite the fluorophore by moving a focused laser beam line-by-line over the specimen and record each image pixel sequentially on a point detector — the photomultiplier tube. A confocal aperture in front of the detector rejects out-of-focus light before it reaches the detector and confocal stacks therefore immediately yield 3D images with good axial resolution[12]. Deconvolution and confocal microscopes both have their specific advantages and disadvantages, which depend on the specific biological application (TABLE 1).

Revealing hidden structure

GFP-fusion proteins are commonly used as markers to highlight cellular structures. However, in the steady-state situation of a live cell, proteins are generally not restricted entirely to their target compartment (for example, the kinetochore, a protein complex that mediates binding of microtubules to chromosomes during mitosis) but a significant fraction can be present as an unbound pool (for example, in the cytoplasm)[13]. This might result in a diffuse background that can entirely mask the structure of interest. Alternatively, the same protein that marks a small structure of interest, such as a vesicle, can also localize predominantly to larger structures such as the Golgi apparatus, which would obscure the vesicle with its bright signal[14]. In both situations, the undesired signal can be removed specifically before the start of a time-lapse experiment on a confocal microscope by using a technique that is referred to as selective photobleaching[15]. By exposing selected sample regions to very high laser intensity, undesired background fluorescence can be removed[13,14]. This technique works only when the marker is bound stably to the structure of interest over the time course of the experiment, so that equilibration with the bleached region is prevented.

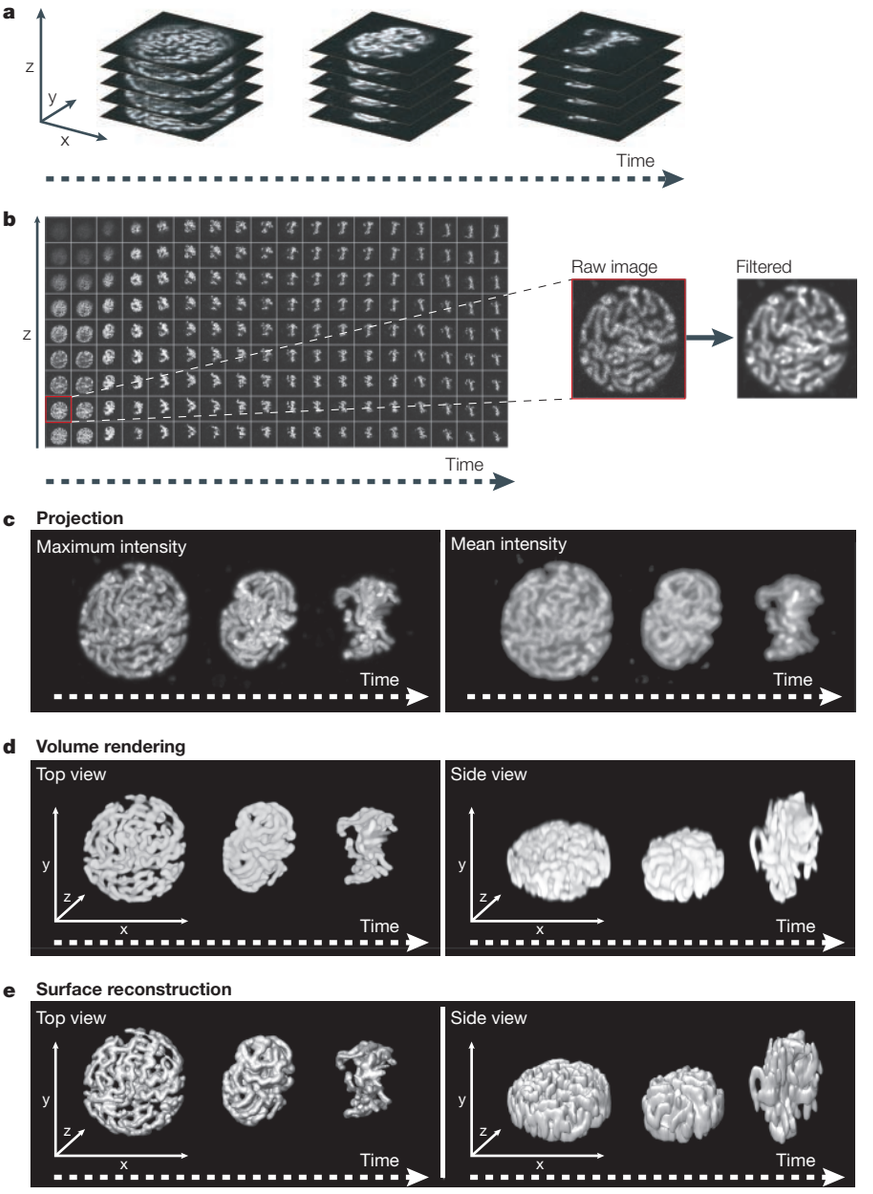

Figure 1 | **Acquisition and processing of four-dimensional image data. a** | Schematic of 4D image acquisition. A normal rat kidney (NRK) cell, which is expressing histone 2B (H2B) tagged with cyan-fluorescent protein (CFP) to allow visualization of chromatin, was imaged during mitosis. Selected stacks are shown at prophase, prometaphase and metaphase (from left to right). The original 4D image size was 512*512*18*36*3*12 (x, y, z, time, channels, bit depth; size units are in pixels), which corresponds to 764 megabytes and 1944 slices. **b** | The gallery shows a subset (8%) of all of the image slices from **a**. Raw images are filtered by using anisotropic-diffusion filtering to selectively remove background noise without degrading the image. **c** | Maximum and mean intensity projections of filtered image stacks from **a**. **d** | Volume rendering from different viewing angles. Rendering was performed on stacks with 72 z-slices, which were interpolated from the 18 z-slices of the original stacks. **e** | Rendered surface reconstructions. For animated display, see Movie 1 online.

Table 1 | **Comparison between deconvolution and confocal microscopes***

	Deconvolution microscope	Confocal microscope
Lateral (x,y) resolution	~250 nm	~250 nm
Axial (z) resolution	~700 nm	~700 nm
Acquisition speed	Dependent on fluorescence intensity; up to ~50 frames/s	Dependent on fluorescence intensity and pixel number; up to ~20 frames/s with low-resolution images
Photon efficiency	Higher than confocal microscope	Lower than deconvolution microscope
Evaluation of images during experiment	Difficult; full-resolution images only available after off-line computational image restoration	Immediate access to full-resolution images
Image-processing artefacts	Can appear with inappropriate deconvolution algorithm parameters or too low signal-to-noise ratio of raw data	Unprocessed images serve as raw data
Maximum thickness of specimen	~40 μm	~150 μm
Multi-colour imaging	Sequential acquisition of different channels by framewise filter switching	Simultaneous and pseudo-simultaneous recording in multiple channels by using linewise switching of laser wavelength
Flexibility in excitation wavelength	Full flexibility	Limited by available laser wavelengths
Selective photobleaching	Not possible except in specialized systems, in which lasers have been incorporated into the light path for this purpose	Possible in interactively defined regions
Recent applications	Cajal body movements[23], centromere dynamics[24], biogenesis of nucleoli[33], interphase chromosome dynamics[40]	Nuclear envelope breakdown[16,55] and assembly[25], mitotic chromosome dynamics[18,42]

*Values are approximate for standard applications in cell biology.

Cellular structures frequently have amorphous shapes, vary from cell to cell and undergo dynamic changes, all factors that make quantitative structural measurements extremely difficult or impossible. To circumvent this problem, spatially controlled photobleaching on a confocal microscope can also be used to introduce artificial landmarks in homogeneously fluorescent structures in an approach called PATTERN PHOTOBLEACHING. Again, this is possible when the fluorescent marker tightly binds to the structure of interest. A good example is in nuclear lamins, which dissociate from the nuclear lamina only over a time course of many hours. So, a pattern, such as a grid, can be bleached into the homogeneously fluorescent nuclear envelope that is labelled with GFP-lamin B[16]. Using high-numerical aperture objectives, the bleaching is restricted to an axial section of about 2–3 μm thickness, which even allows the bleaching of 3D patterns at different optical sections, albeit with relatively low axial resolution[16] (FIG. 2a). The resolution of the bleach can be improved by using two-photon excitation that is restricted to a smaller volume[17].

A refinement of labelling with bleachmarks involves co-expression of two different spectral variants of GFP that are fused to the same cellular marker protein. When different regions are selectively photobleached in one channel only, a combinatorial labelling scheme can discriminate up to three differently labelled structures in cellular regions that would otherwise be homogeneously labelled by these markers[18,19] (FIG. 2b). An inverse alternative to labelling with bleachmarks is photoactivation in selected regions: a recently generated variant of GFP can have its fluorescence properties altered such that it emits fluorescent light under 488 nm excitation only after previous exposure to strong 413 nm light[20]. Although labelling methods that are based on selective bleaching are not unique to 4D-imaging applications, they can markedly enhance the ability to track and quantify dynamic structural changes in time-resolved 3D data sets.

Image visualization and quantitation

The problem of noise. As for any digital fluorescence microscope image, potential error sources that might impair visualization and bias quantification of 4D images need to be considered. A first step in 4D image analysis is the removal of any signal that does not originate from the specimen ('noise'). Noise is generated by fluctuations in illumination (laser/arc-lamp intensity) and, to a lesser degree, by thermal fluctuations inside CCD cameras or photomultiplier tubes ('dark/shot noise'). Any noise source leads to increased unspecific signal and makes the identification of specific fluorescent structures more difficult. Many noise-reducing image processing filters are now available that efficiently reduce shot noise, which typically occurs in random single pixels across the image[21]. For example, ANISOTROPIC-DIFFUSION FILTERS take into account local image characteristics and therefore selectively remove shot noise without degrading the image (FIG. 1b).

In addition to noise, unspecific background signal — for example, from autofluorescence of the culture medium — impairs image analysis. So, even after noise filtering, the background of the image at regions outside the fluorescent structure is generally not zero. To quantitatively relate pixel intensity to fluorophore concentration, the background signal has to be removed from the image. This can be achieved by subtracting the mean background intensity, determined in a region outside the fluorescent structure, from all pixels.

Qualitative and quantitative visualization. The principle aim of 4D visualization is to display the full information from thousands of individual image slices in an intuitive and interactive way. Early studies visualized 4D data by arranging all image slices in an 'image gallery', which allowed the browsing and highlighting of selected structures[7] (FIG. 1b). Although this guarantees that no information is lost, it is not intuitive and requires a well-trained observer to imagine the 3D structure. Alternatively, 4D data can be projected in the x–y plane, neglecting the z dimension[22–24] (FIG. 1c). Although this allows a more intuitive access to the data by viewing it as a simple 2D movie, it sacrifices spatial information. Different algorithms are available for such PROJECTIONS: for example, maximum intensity projection produces images that have a particularly high contrast of small structures (FIG. 1c). However, it does not quantitatively represent fluorescence concentrations and cannot be used for further analysis. Instead, mean-intensity projection should be used for quantification, although it does not produce such crisp images (FIG. 1c). Mean-intensity projections can be useful to measure relative fluorophore concentrations and their

dynamic changes over time. This can be used as an approximation of the real concentration of fluorescently labelled molecules, which can only be derived from 3D analysis (see below and REF. 25). Changes of protein concentration over time are important for many cell-biological processes, and recent work has measured such changes during organelle morphogenesis[25], protein targeting[26] and transport[27,28], changes in cell shape and signal-transduction events[29].

A realistic view of animated 3D-image sequences from interactively defined viewing directions can be achieved by using computer rendering and display in virtual-reality viewers[10,25,30,31] (FIG. 1d,e). Two alternative rendering methods are VOLUME RENDERING and SURFACE RECONSTRUCTION[21]. Volume rendering is a technique for visualizing 3D images without explicitly defining the boundary of fluorescently labelled structures (FIG. 1d). In the simplest case, each optical section is expanded to its real height and these flat layers are then stacked on top of each other to generate a spatial view. As a result of the lower resolution along the optical axis in 4D live-cell recordings, side views that are rendered in this way are frequently of poor quality. Their resolution can be enhanced by insertion of virtual z-slices between subsequent optical sections based on interpolation between these two images (FIG. 1d, side view). Although volume-rendering techniques achieve a satisfactory display of biological structures, these methods are limited to pure visualization and do not deliver any quantitative information.

Surface reconstruction visualizes 3D structures after the definition of boundaries of fluorescent structures by surface polygons. The most commonly used isosurface reconstruction defines the 3D structure by thresholding the whole 4D data set. In this way, every voxel — the volume element of the 3D image — below the threshold grey value is defined as outside the structure and every voxel above the threshold value is defined as inside the structure, creating clearly defined object boundaries[32] (FIG. 1e and 2b). The drawback of this method is that the surface of many biological structures is not well represented by a single-intensity value. An example is the nuclear envelope, which is typically labelled by fluorescently tagged membrane proteins that also localize to the endoplasmic reticulum (ER). In this case, some regions of the nuclear envelope can have similar levels of brightness as the ER, making their separation by a single threshold impossible. Therefore, an alternative approach for surface reconstruction is to detect object boundaries in each 2D optical section separately and to reconstruct 3D models from these outlines. In contrast to 3D data sets, many different SEGMENTATION techniques are available for 2D images[21] that achieve better definition of biological objects than simple thresholding. After object contours have been defined in 2D, interpolation algorithms can then be used to reconstruct 3D surfaces from them with high resolution[25] (FIG. 1e).

Generally, surface reconstruction achieves a more detailed display of small structures than volume rendering, but it often requires much more user interaction during image processing to avoid artefacts. Importantly, only the object definition of reconstructed surfaces can be used to generate absolute quantitative data, such as the volume of a structure or the concentration of the fluorophore

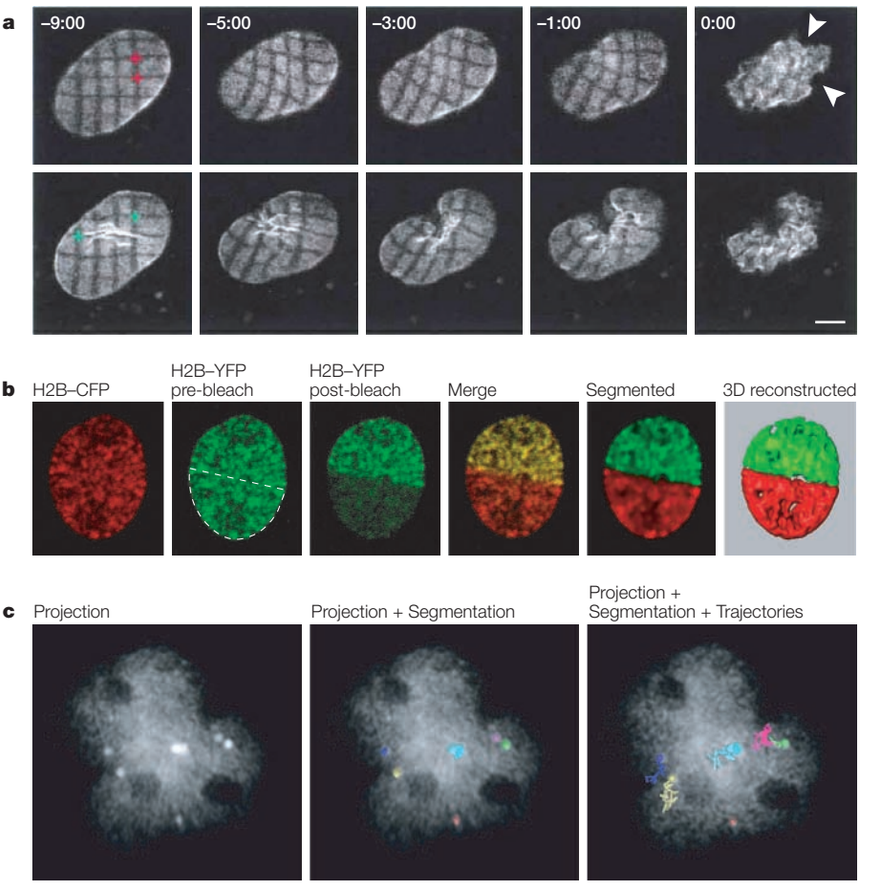

Figure 2 | **Applications of four-dimensional imaging. a** | Nuclear-envelope breakdown. Prophase was imaged in a normal rat kidney (NRK) cell expressing lamin B tagged with green-fluorescent protein (GFP) and histone 2B (H2B) expressing cyan-fluorescent protein (CFP) (not shown). Grids were bleached on the top and bottom of the lamina to provide artificial landmarks. Only the top (upper) and bottom (lower) slices from the full 4D data set are shown to demonstrate lateral deformations of the nuclear envelope during breakdown. The red crosses highlight sites of maximal stretching 2 minutes before nuclear-envelope breakdown and later hole formation (arrowheads). Stretching of the lamina occurs between the red crosses, whereas infolding occurs between the green crosses. See also Movie 2 online. Time is in minutes. Reproduced with permission from REF. 16 © (2002) Elsevier Science. **b** | Combinatorial labelling of chromatin regions in a prophase nucleus. An NRK cell coexpressing H2B fused to either yellow-fluorescent protein (YFP) or CFP was photobleached at selected regions (dashed line) in the YFP channel only. The combinatorial labelling scheme was resolved by channel subtraction[18] and was graphically reconstructed from the 3D stack. This allows chromosome subsets to be tracked through mitosis in 4D imaging experiments[18] (see Movie 3 online). **c** | Motion analysis of Cajal bodies in HeLa cells that are expressing GFP–coilin to mark Cajal bodies. 4D tracking was used to quantitatively characterize Cajal-body motion in control cells and ATP-depleted cells[23]. 3D stacks were collected on a DeltaVision Restoration microscope with a 3-minute time lapse. An intensity- and size-based segmentation was used to identify and subsequently track Cajal bodies using Volocity 2.0. Projection, an individual time point from a 90 minute time-lapse image is shown; Projection + Segmentation, objects were found using an intensity- and size-based segmentation in Volocity 2.0; Projection + Segmentation + Trajectories, as in the Projection + Segmentation, but with trajectories from all the time-points shown.

inside the structure. Such data allows changes in volume and/or concentration for specific cellular structures over time to be measured, which can be very useful to study organelle morphogenesis[25,33].

Quantitative evaluation of dynamic 3D structures: volumes and concentrations. Measuring the volume of cellular compartments and the absolute concentration of molecules within these compartments over time in live cells would be ideally suited for analysis of many biological processes by kinetic modelling. So far, the processes to which this has been applied include membrane trafficking[27], nuclear transport[34], transcription[35] and nuclear assembly[25]. Traditionally, the volume of cellular structures is often inferred from area measurements in single optical sections or in projections of image stacks. However, this does not take into account the shape or orientation of a given structure. Moreover, when movies are analysed, flattening or expansion along the optical axis during the experiment can impair volume measurements. As an example, expansion of daughter nuclei will be strongly overestimated when measured in 2D image sequences because of the significant flattening of the nuclei that occurs during attachment to the culture dish after mitotic division[25]. Volume measurements require boundary detection of cellular structures[21,36]. When combined with surface reconstruction, the volume of visualized cellular structures can be measured directly.

Grey values in digital images can be directly converted to fluorophore concentrations after appropriate calibration[27,37–39], which makes 4D imaging suitable for quantitative assays that monitor changes in molecular concentrations in live cells. In defined cellular compartments, 4D measurements of fluorescent protein concentrations are carried out by dividing the sum of the intensities by the volume of the segmented structures. Similar to volume measurements, this produces more precise results than measurements of 2D movies, particularly when there is an inhomogeneous background from a soluble fraction of the labelled protein that is outside the structure of interest. For instance, surface measurements of membrane-bound organelles, such as the nucleus or the plasma membrane, are more problematic than volume- or fluorescence-concentration measurements because light microscopes generally do not resolve small-membrane invaginations or protrusions. Therefore, surface measurements in light-microscopy images, although possible using reconstructed surface models, will generally underestimate the real surface size.

Motion analysis by single-particle tracking. Insight into many dynamic processes has been derived from tracking the movement of fluorescently labelled structures. Such studies have, for instance, measured the motion of chromosomes[18,24,40–42], nuclear bodies[23,43] (FIG. 2c), membrane vesicles along microtubules[14], dendritic spines in pyramidal neurons[44] and migrating neuronal precursor cells[45]. To quantitate the motion patterns of a set of distinct structures, single-particle tracking methods are appropriate. Tracking can be done by manually identifying and tracing moving objects in 4D data sets[46], but it is often very time-consuming to gather and analyse enough data to obtain statistically significant results in this way. Automated single-particle tracking of cellular structures involves three steps of image processing. First, objects have to be identified by using segmentation algorithms. Second, the corresponding objects are detected in successive frames by using a tracking algorithm, which produces trajectories that can be graphically visualized[23,47] (FIG. 2c). Finally, the trajectories can be further analysed to determine properties such as the mean and maximum velocities, the accelerations, and the mean square displacement or diffusion coefficients[23,47,48].

A difficulty in quantitative motion analysis of cellular structures is caused by global movements or deformations of the whole specimen during the acquisition period. Such global movements must be separated from the specific local movements of the structures of interest. This can be achieved by measuring only the relative movements of individual objects[46]. A more refined correction for global movements uses registration algorithms that can correct for translation, rotation and even global deformations[49].

Future directions

4D imaging has come of age as a powerful imaging technology for cell and developmental biology, but it is still restricted to a relatively small number of specialized labs. Historically, 4D imaging required highly specialized equipment and image-processing capabilities, but this situation is changing quite rapidly. Hardware that can acquire 4D sequences is now available 'off the shelf' and is becoming more widespread (see 4D microscope hardware in supplementary information online). In addition, some of the basic image-processing routines for 4D data are now available in several commercial software packages (see 4D software tools in supplementary information online). There remain three challenges today to make the powerful approach of 4D imaging more widely used. First, less expensive hardware is required. Fast and sensitive 4D imaging systems are still very expensive, and start at around US $125,000 for deconvolution microscopes and around US $300,000 for confocal microscopes. As a consequence, such equipment is often only available at specialized imaging facilities and not to most cell-biology labs. Second, flexible acquisition software is needed. On all existing systems, the parameter flexibility during acquisition needs to be improved. In addition, online deconvolution algorithms to, at least preliminarily, evaluate widefield data during the experiment are largely missing. Third, user-friendly and flexible 4D processing, rendering and quantification software is essentially lacking at this point. To achieve complete analysis of a 4D data sequence, users typically have to use several software packages to achieve optimal results from each of the processing steps. A single software package that integrates the full set of recurring tools that are required for typical 4D applications in a user-friendly interface and, at the same time, allows the advanced user to define his/her own processing routines, is still not available. It is worth noting here that software development for 3 or 4D images is not a domain of cell biology alone. Frequently, more advanced tools are already developed for engineering and medical applications, such as dynamic magnetic resonance imaging of organs (see review on page SS10 of this supplement), as well as for serial reconstruction and tomography by electron microscopy (see review on page SS6 of this supplement). By integrating these tools rapidly into a flexible software environment, cell-biological applications stand to benefit from developments in other disciplines.

As with traditional video microscopy, 4D imaging can be combined with other new imaging techniques to address specific questions. In addition to pattern photobleaching, these can include speckle imaging[50], fluorescence resonance energy transfer (FRET)[51] and MULTI-PHOTON MICROSCOPY[17]. Furthermore, 4D imaging will directly benefit from techniques that aim to improve the optical resolution in live specimens. Several powerful approaches, which are based on illumination through multiple objectives (Theta, 4Pi, I5M) or increased contrast by using structured illumination[52], have been developed, but most of them are not yet compatible with the speed and sensitivity that is required for live-cell imaging.

4D imaging gives us access to new worlds of dynamic function in live cells. By taking both space and time into account, processes that involve, for example, changes in structure, compartmentalization, fluxes, directed

transport and signal-mediated localization, can be studied quantitatively in real time. With appropriate fluorescent molecular reporters, quantitative and kinetic *in vivo* assays for almost any biological process of interest can be designed in the laboratory. The ultimate goal will be to make these assays sufficiently rapid and robust to use them to perform gain- and loss-of-function studies in live cells[53,54]. To understand complex living systems, we will have to get used to thinking routinely in four dimensions.

Gene Expression and Cell Biology/Biophysics Programmes, European Molecular Biology Laboratory, Meyerhofstrasse 1, D-69117 Heidelberg, Germany.
Correspondence to J.E.
e-mail: jan.ellenberg@embl-heidelberg.de

Please cite this article as a supplement to volume 5 of Nature Cell Biology, *pages S14–S19.*
doi:10.1038/ncb1033

1. Zhang, J., Campbell, R. E., Ting, A. Y. & Tsien, R. Y. Creating new fluorescent probes for cell biology. *Nature Rev. Mol. Cell Biol.* **3**, 906–918 (2002).
2. Chalfie, M., Tu, Y., Euskirchen, G., Ward, W. W. & Prasher, D. C. Green fluorescent protein as a marker for gene expression. *Science* **263**, 802–805 (1994).
3. Patterson, G., Day, R. N. & Piston, D. Fluorescent protein spectra. *J. Cell Sci.* **114**, 837–838 (2001).
4. Ellenberg, J., Lippincott-Schwartz, J. & Presley, J. F. Dual-colour imaging with GFP variants. *Trends Cell Biol.* **9**, 52–56 (1999).
5. Hiraoka, Y., Minden, J. S., Swedlow, J. R., Sedat, J. W. & Agard, D. A. Focal points for chromosome condensation and decondensation revealed by three-dimensional *in vivo* time-lapse microscopy. *Nature* **342**, 293–296 (1989).
6. Swedlow, J. R., Sedat, J. W. & Agard, D. A. Multiple chromosomal populations of topoisomerase II detected *in vivo* by time-lapse, three-dimensional wide-field microscopy. *Cell* **73**, 97–108 (1993).
7. Thomas, C., DeVries, P., Hardin, J. & White, J. Four-dimensional imaging: computer visualization of 3D movements in living specimens. *Science* **273**, 603–607 (1996).
8. Rizzuto, R., Carrington, W. & Tuft, R. A. Digital imaging microscopy of living cells. *Trends Cell Biol.* **8**, 288–292 (1998).
9. Swedlow, J. R. & Platani, M. Live cell imaging using wide-field microscopy and deconvolution. *Cell Struct. Funct.* **27**, 335–341 (2002).
10. Mohler, W. A. Visual reality: using computer reconstruction and animation to magnify the microscopist's perception. *Mol. Biol. Cell* **10**, 3061–3065 (1999).
11. McNally, J. G., Karpova, T., Cooper, J. & Conchello, J. A. Three-dimensional imaging by deconvolution microscopy. *Methods* **19**, 373–385 (1999).
12. Inoue, S. in *Handbook of Biological Confocal Microscopy* (ed. Pawley, J. B.) 1–14 (Plenum Press, New York, 1995).
13. Belgareh, N. *et al*. An evolutionarily conserved NPC subcomplex, which redistributes in part to kinetochores in mammalian cells. *J. Cell Biol.* **154**, 1147–1160 (2001).
14. Presley, J. F. *et al*. ER-to-Golgi transport visualized in living cells. *Nature* **389**, 81–85 (1997).
15. Lippincott-Schwartz, J., Snapp, E. & Kenworthy, A. Studying protein dynamics in living cells. *Nature Rev. Mol. Cell Biol.* **2**, 444–456 (2001).
16. Beaudouin, J., Gerlich, D., Daigle, N., Eils, R. & Ellenberg, J. Nuclear envelope breakdown proceeds by microtubule-induced tearing of the lamina. *Cell* **108**, 83–96 (2002).
17. Helmchen, F. & Denk, W. New developments in multiphoton microscopy. *Curr. Opin. Neurobiol.* **12**, 593–601 (2002).
18. Gerlich, D. *et al*. Global chromosome positions are transmitted through mitosis in mammalian cells. *Cell* **112**, 751–764 (2003).
19. Zicha, D. *et al*. Rapid actin transport during cell protrusion. *Science* **300**, 142–145 (2003).
20. Patterson, G. H. & Lippincott-Schwartz, J. A photo-activatable GFP for selective photolabeling of proteins and cells. *Science* **297**, 1873–1877 (2002).
21. Gerlich, D., Mattes, J. & Eils, R. Quantitative motion analysis and visualization of cellular structures. *Methods* **29**, 3–13 (2003).
22. Manders, E. M., Kimura, H. & Cook, P. R. Direct imaging of DNA in living cells reveals the dynamics of chromosome formation. *J. Cell Biol.* **144**, 813–821 (1999).
23. Platani, M., Goldberg, I., Lamond, A. I. & Swedlow, J. R. Cajal Body dynamics and association with chromatin are ATP-dependent. *Nature Cell Biol.* **4**, 502–508 (2002).
24. He, X., Asthana, S. & Sorger, P. K. Transient sister chromatid separation and elastic deformation of chromosomes during mitosis in budding yeast. *Cell* **101**, 763–775 (2000).
25. Gerlich, D., Beaudouin, J., Gebhard, M., Ellenberg, J. & Eils, R. Four-dimensional imaging and quantitative reconstruction to analyse complex spatiotemporal processes in live cells. *Nature Cell Biol.* **3**, 852–855 (2001).
26. Ellenberg, J. *et al*. Nuclear membrane dynamics and reassembly in living cells: targeting of an inner nuclear membrane protein in interphase and mitosis. *J. Cell Biol.* **138**, 1193–1206 (1997).
27. Hirschberg, K. *et al*. Kinetic analysis of secretory protein traffic and characterization of golgi to plasma membrane transport intermediates in living cells. *J. Cell Biol.* **143**, 1485–1503 (1998).
28. Ribbeck, K. & Gorlich, D. Kinetic analysis of translocation through nuclear pore complexes. *EMBO J.* **20**, 1320–1330 (2001).
29. Meyer, T. & Teruel, M. N. Fluorescence imaging of signaling networks. *Trends Cell Biol.* **13**, 101–106 (2003).
30. Thomas, C. F. & White, J. G. Four-dimensional imaging: the exploration of space and time. *Trends Biotechnol.* **16**, 175–182 (1998).
31. Marshall, W. F., Marko, J. F., Agard, D. A. & Sedat, J. W. Chromosome elasticity and mitotic polar ejection force measured in living *Drosophila* embryos by four-dimensional microscopy-based motion analysis. *Curr. Biol.* **11**, 569–578 (2001).
32. Cline, H. E., Lorensen, W. E., Ludke, S., Crawford, C. R. & Teeter, B. C. Two algorithms for the three-dimensional reconstruction of tomograms. *Med. Phys.* **15**, 320–327 (1988).
33. Savino, T. M., Gebrane-Younes, J., De Mey, J., Sibarita, J. B. & Hernandez-Verdun, D. Nucleolar assembly of the rRNA processing machinery in living cells. *J. Cell Biol.* **153**, 1097–1110 (2001).
34. Smith, A. E., Slepchenko, B. M., Schaff, J. C., Loew, L. M. & Macara, I. G. Systems analysis of Ran transport. *Science* **295**, 488–491 (2002).
35. Dundr, M. *et al*. A kinetic framework for a mammalian RNA polymerase *in vivo*. *Science* **298**, 1623–1626 (2002).
36. Monier, K., Armas, J. C., Etteldorf, S., Ghazal, P. & Sullivan, K. F. Annexation of the interchromosomal space during viral infection. *Nature Cell Biol.* **2**, 661–665 (2000).
37. Fink, C., Morgan, F. & Loew, L. M. Intracellular fluorescent probe concentrations by confocal microscopy. *Biophys. J.* **75**, 1648–1658 (1998).
38. Niswender, K. D., Blackman, S. M., Rohde, L., Magnuson, M. A. & Piston, D. W. Quantitative imaging of green fluorescent protein in cultured cells: comparison of microscopic techniques, use in fusion proteins and detection limits. *J. Microsc.* **180**, 109–116 (1995).
39. Dundr, M., McNally, J. G., Cohen, J. & Misteli, T. Quantitation of GFP-fusion proteins in single living cells. *J. Struct. Biol.* **140**, 92–99 (2002).
40. Vazquez, J., Belmont, A. S. & Sedat, J. W. Multiple regimes of constrained chromosome motion are regulated in the interphase *Drosophila* nucleus. *Curr. Biol.* **11**, 1227–1239 (2001).
41. Heun, P., Laroche, T., Shimada, K., Furrer, P. & Gasser, S. Chromosome dynamics in the yeast interphase nucleus. *Science* **7**, 2181–2186 (2001).
42. Walter, J., Schermelleh, L., Cremer, M., Tashiro, S. & Cremer, T. Chromosome order in HeLa cells changes during mitosis and early G1, but is stably maintained during subsequent interphase stages. *J. Cell Biol.* **160**, 685–697 (2003).
43. Muratani, M. *et al*. Metabolic-energy-dependent movement of PML bodies within the mammalian cell nucleus. *Nature Cell Biol.* **4**, 106–110 (2002).
44. Trachtenberg, J. T. *et al*. Long-term *in vivo* imaging of experience-dependent synaptic plasticity in adult cortex. *Nature* **420**, 788–794 (2002).
45. Koster, R. W. & Fraser, S. E. Direct imaging of *in vivo* neuronal migration in the developing cerebellum. *Curr. Biol.* **11**, 1858–1863 (2001).
46. Marshall, W. F. *et al*. Interphase chromosomes undergo constrained diffusional motion in living cells. *Curr. Biol.* **7**, 930–939 (1997).
47. Tvaruskó, W. *et al*. Time-resolved analysis and visualization of dynamic processes in living cells. *Proc. Natl Acad. Sci. USA* **96**, 7950–7955 (1999).
48. Thomann, D., Rines, D. R., Sorger, P. K. & Danuser, G. Automatic fluorescent tag detection in 3D with super-resolution: application to the analysis of chromosome movement. *J. Microsc.* **208**, 49–64 (2002).
49. Fieres, J., Mattes, J. & Eils, R. in *Pattern Recognition, Lecture Notes in Computer Science* Vol. 2191. (eds Radig, B. & Florczyk, S.) 76–83 (Springer Verlag, 2001).
50. Waterman-Storer, C. M. & Danuser, G. New directions for fluorescent speckle microscopy. *Curr. Biol.* **12**, R633–R640 (2002).
51. Wouters, F. S., Verveer, P. J. & Bastiaens, P. I. Imaging biochemistry inside cells. *Trends Cell Biol.* **11**, 203–211 (2001).
52. Gustafsson, M. G. Extended resolution fluorescence microscopy. *Curr. Opin. Struct. Biol.* **9**, 627–634 (1999).
53. Elbashir, S. M., Harborth, J., Weber, K. & Tuschl, T. Analysis of gene function in somatic mammalian cells using small interfering RNAs. *Methods* **26**, 199–213 (2002).
54. Wu, R. Z., Bailey, S. N. & Sabatini, D. M. Cell-biological applications of transfected-cell microarrays. *Trends Cell Biol.* **12**, 485–488 (2002).
55. Lenart, P. *et al*. Nuclear envelope breakdown in starfish oocytes proceeds by partial NPC disassembly followed by a rapidly spreading fenestration of nuclear membranes. *J. Cell Biol.* **160**, 1055–1068 (2003).

Acknowledgments
The authors thank J. R. Swedlow, P. Lénart, J. Beaudouin and F. Mora-Bermúdez for helpful comments on the manuscript. J. R. S. is also acknowledged for providing figure 2c. D. G. is supported by a European Molecular Biology Organization long-term fellowship. J. E. acknowledges support from the Human Frontiers Science Programme.

Online links

DATABASES

The following terms in this article are linked online to:
LocusLink: http://www.ncbi.nlm.nih.gov/LocusLink/lamins

FURTHER INFORMATION

Confocal Laser Light Microscopy: http://www.els.net/els/FDA/default.asp?id=3889ABA5-A770-41B7-851D-C5CAAA93504F
Deconvolution Fluorescence Light Microscopy: http://www.els.net/els/FDA/default.asp?id=4DDDEF12-A77D-4DCF-9F55-A0BE1A18027E
Jan Ellenberg's web site: http://www.embl-heidelberg.de/externalinfo/ellenberg/
Access to this interactive links box is free online.

MOLECULAR IMAGING OF CANCER WITH POSITRON EMISSION TOMOGRAPHY

Sanjiv Sam Gambhir

The imaging of specific molecular targets that are associated with cancer should allow earlier diagnosis and better management of oncology patients. Positron emission tomography (PET) is a highly sensitive non-invasive technology that is ideally suited for pre-clinical and clinical imaging of cancer biology, in contrast to anatomical approaches. By using radiolabelled tracers, which are injected in non-pharmacological doses, three-dimensional images can be reconstructed by a computer to show the concentration and location(s) of the tracer of interest. PET should become increasingly important in cancer imaging in the next decade.

TRACER
Also known as molecular probe or reporter probe. This molecule has a radioisotope attached to it and is injected in non-pharmacological amounts to provide imaging signal related to target(s) of interest. For PET tracers, the radioisotope is a positron emitter (e.g. ^{18}F).

POSITRON
A particle that has the same mass as an electron, but that carries a positive charge.

Crump Institute for Molecular Imaging, Department of Molecular and Medical Pharmacology, UCLA School of Medicine, 700 Westwood Boulevard, Los Angeles, California 90095-1770, USA.
e-mail: sgambhir@mednet.ucla.edu
doi:10.1038/nrc882

The fields of cancer biology, pharmacology and clinical oncology have grown rapidly over the past few years, owing to the increase in technologies that allow the study of gene and protein expression from cell extracts and intact cells in culture. The time is now ripe for technologies that can go to the next level: the study of cancer cells in their normal environment within intact living subjects.

Much of biological and medical imaging has previously been driven by anatomy-based imaging, such as computed tomography (CT). The field of nuclear medicine, by contrast, has focused on studying molecular events in living subjects through the use of technologies that can localize TRACERS. Various tracers have been discovered, by chance, to be useful, and some have been specifically designed to target molecular events. With the recent advances in molecular/cell biology that have led to target discovery, it is now possible to design specific tracers to image events non-invasively in small animals and humans with positron emission tomography (PET)[1]. PET is ideally suited for monitoring cell/molecular events early in the course of a disease, as well as during pharmacological or radiation therapy. Furthermore, it can be used for prognostic information and to image for disease recurrence.

Principles of PET

PET can be thought of as a camera that can take pictures of a subject of interest and requires an exposure time of a few seconds to several minutes. The camera does not image visible light, but images high-energy gamma-rays that are emitted from inside the subject (FIG. 1). Natural biological molecules can be labelled with an isotope that is capable of producing two gamma-rays by emitting a POSITRON from its nucleus. The positron eventually collides with a nearby electron and they annihilate each other to produce energy in the form of two 511,000 eV gamma-rays, which are emitted in directions ~180 degrees apart. Frequently used positron-emitting isotopes include ^{15}O, ^{13}N, ^{11}C and ^{18}F; the latter is often used as a substitute for hydrogen in the molecule of interest. Other less commonly used positron emitters include ^{14}O, ^{64}Cu, ^{62}Cu, ^{124}I, ^{76}Br, ^{82}Rb (rubidium) and ^{68}Ga (gallium). Most of these isotopes are produced in a CYCLOTRON[2], but some can be produced with a GENERATOR (for example, ^{68}Ga, ^{82}Rb). Labelled tracers can be introduced into the subject and then PET imaging can follow their distribution and concentration (FIG. 1). Many of the positron-emitting isotopes that are used have relatively short half-lives — the half life of ^{18}F is 110 minutes — so the chemistry leading to incorporation of the isotope into the parent molecule and its subsequent introduction into the subject must take place relatively quickly. PET radiopharmacies exist throughout the world and are capable of providing commonly used PET tracers on a daily basis.

Summary

- Positron emission tomography (PET) is a method by which cellular and molecular events can be followed. Injected radiolabelled molecular probes (tracers) are used to map out the underlying biochemistry.
- Both small-animal and clinical PET are being used to study cancer in living subjects.
- 2-^{18}F-fluoro-2-deoxy-D-glucose (FDG) is actively taken up and accumulates in cancer cells. It is useful for diagnosis, staging and monitoring the recurrence of various cancers, including lung, colorectal, melanoma, lymphoma, head and neck, as well as other malignancies.
- Many tracers already exist for PET that measure cell proliferation, bone remodelling, perfusion, oxygen metabolism, tumour-receptor density and reporter-gene expression. A new generation of tracers is being developed that should help to form libraries of molecular probes for 'customized' imaging approaches.
- Clinical PET/CT (computed tomography) scanners are now rapidly being installed, and form the basis for merging anatomical information (CT) with functional molecular information (PET) to further advance cancer management with FDG and, eventually, new-generation tracers.
- Drug and tracer research and development are rapidly evolving and should help to accelerate both the pharmaceutical and imaging industries.

Isotopes that are beta-emitters — ^{3}H, ^{14}C — are not useful for non-invasive imaging of living subjects because beta-particles (electrons) do not travel significant distances in tissue and do not lead to annhilation events, as do positrons. Gamma-emitting isotopes — ^{99m}Tc (technetium), ^{111}In (indium), ^{123}I — can also be used with tracers for imaging living subjects, but require different types of cameras ('gamma-cameras') that do not require the production of two coincident gamma-rays. Gamma-cameras are rotated around the subject in a process known as single-photon-emission computed tomography (SPECT), to produce tomographic images[3]. PET is at least tenfold more sensitive than SPECT, and positron-emitting isotopes can readily be substituted for naturally occurring atoms, producing less perturbation to the biochemical behaviour of the radiolabelled parent molecule. SPECT systems can be developed with improved spatial resolution, but not without a further loss in sensitivity. For these reasons, PET is a more robust technique for imaging most molecular events.

The spatial resolution of most clinical PET scanners is ~$(6–8)^3$ mm^3, but higher-resolution clinical brain scanners have been developed that approach resolutions of ~3^3 mm^3. The sensitivity of PET is relatively high — in the range of 10^{-11}–10^{-12} moles/litre — and is independent of the location depth of the tracer of interest. Typically, several hundred million cells in relatively close proximity must accumulate the tracer for a PET scanner to visualize them against the background. The exact number of cells that can be imaged depends on numerous factors, including the level of tracer uptake in the surrounding tissues ('background'). It is important to note that all isotopes used produce two gamma-rays of the same energy, so if two molecular probes — each with a separate isotope — are injected simultaneously, there is no way for the PET camera to distinguish them. Therefore, to perform studies that involve multiple molecular events, molecular probes are usually injected separately, which allows for the decay of the isotope. SPECT can be used with several distinctly radiolabelled tracers because of its ability to distinguish gamma-rays of different energies. The images from a PET camera, although often shown in colour, reflect gamma-ray events with the same energy — the colour scale usually reflects the concentration of isotope.

Small-animal imaging with PET

In recent years, small-animal PET cameras have been designed, which facilitate the development of molecular-imaging assays that can be used in small rodents and primates before they are tested in humans. These approaches allow the rapid testing of human cell targets that are implanted into mice, and the optimization of the imaging signal and PHARMACOKINETICS of the tracer. These systems typically have a spatial resolution of ~2^3 mm^3 (REF. 4), but newer-generation systems that are undergoing completion will have a resolution of ~1^3 mm^3 (REF. 5). Small-animal imaging requires tracers with a higher specific radioactivity, owing to the limited sensitivity of the small-animal scanners and the need to inject a smaller mass of tracer.

The development of molecular imaging assays with PET is made much easier by the ability to validate the assay in cell culture and small-animal models, and then to use the same tracer in established clinical PET sites around the world. The ability to translate from cell culture to pre-clinical models to clinical applications is an important and powerful feature of PET technology[4,6].

Molecular and cellular targets

For tracers to be successful as imaging probes for PET, they must fulfil several criteria: the positron-emitting isotope that is chemically linked to the molecule of interest must not easily dissociate. If this occurs, it is the isotope that is followed with PET, rather than the tracer. It is important that the label does not significantly alter the biological properties of the parent molecule (for example, transport, elimination or affinity of interaction with target). The tracer must also clear rapidly from sites where there is no target molecule, and from the blood, so that a high contrast can be obtained between the tumour and surrounding tissues. This is one of the

CYCLOTRON
A device that is used to accelerate charged particles to create a collision between the charged particle and a target, so that a radioactive isotope can be produced for further incorporation into a molecule of interest.

GENERATOR
A device that is used to separate and extract a radioisotope through the use of a 'parent' isotope that constantly leads to a 'daughter' isotope.

PHARMACOKINETICS
The study of the time course of absorption, distribution, metabolism and excretion of drugs and their metabolites in body tissues and fluids.

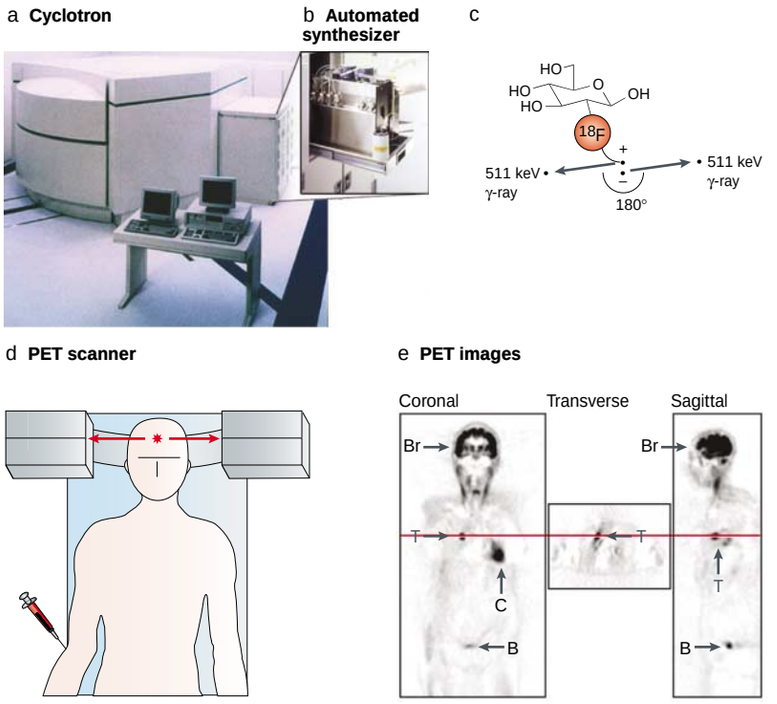

Figure 1 | **Principles of positron emission tomography (PET). a** | A cyclotron is used to accelerate charged particles to create relatively short-lived positron-emitting isotopes (for example, ^{18}F, the half-life of which is 110 minutes). **b** | Automated synthesizers can then couple the isotope to a molecule of interest to produce the molecular probe (tracer). **c** | The molecule 2-[^{18}F]fluoro-2-deoxy-D-glucose (FDG) can be synthesized and intravenously injected in non-pharmacological doses into a subject of interest. The positron emitter decays by emitting a positron from its nucleus. The positron loses energy and eventually annihilates with a nearby electron to produce two gamma-rays that are almost 180 degrees apart. **d** | The PET scanner can detect the coincident gamma-rays, and images can be reconstructed showing the location(s) and concentration of the tracer of interest. **e** | Cross-sectional FDG PET images are shown, of a patient 40 minutes after injection with FDG. Normal uptake in brain (Br) and myocardium (C), and renal excretion into the urinary bladder (B) are visible. Also seen is a tumour (T) in the lungs that takes up more FDG than the surrounding tissues.

unique features of a PET tracer compared with many existing pharmaceuticals. Without the efflux of the tracer from non-target sites, it would be impossible to image sites of specific targeting. In contrast to activatable probes or 'SMART PROBES' for optical and MRI (magnetic resonance imaging) approaches[7], which produce signal only when they interact with a target, a radiolabelled tracer constantly produces signal by decaying. This leads to areas of signal that are not related to specific targeting. For example, at early time-points, signal can often be seen in the renal and hepatobiliary systems, depending on the routes of tracer clearance. These non-specific sites of signal can sometimes cause difficulties in image interpretation, but by looking at the PET images as a function of time, or by waiting long enough — half-life of isotope permitting — to let the background signal clear by urinary and/or faecal elimination, specific and non-specific signals can usually be separated. Tracer kinetic modelling with time–activity data obtained from PET studies is a powerful way of mathematically modelling the underlying biochemical and physiological processes that govern tracer movement and metabolism within the body. Tracer metabolites must be limited in cases in which tracer kinetic modelling is used to quantify specific biochemical processes (for example, rate of phosphorylation)[8]. The importance of quantification cannot be over-emphasized, as it is crucial to the initial validation of a particular tracer, even if quantification is not usually performed in a routine clinical application.

Many approaches exist, and are being developed, that allow target cancer cells to be imaged with PET. These are reviewed in detail next.

Glucose utilization. 2-Deoxy-D-[^{14}C]glucose (DG) — formed by replacing the OH in the 2-position of D-glucose with a hydrogen — was developed in the early 1950s as a drug to block accelerated rates of glycolysis in cancer, and hence tumour growth[9]. However, it also blocked glycolysis in the brain, so it could not be used as a drug. Over 20 years later, in 1977, Sokoloff *et al.*[10] developed a new use for DG in imaging glycolysis, by labelling DG with carbon-14 and using autoradiography, which requires the animal to be killed. This use was extended when 2-[^{18}F]fluoro-2-deoxy-D-glucose (FDG) was synthesized[11] to image living subjects specifically and non-invasively with PET.

FDG was first used to study tumours in the 1980s by Di Chiro and others, who showed that the degree of malignancy of cerebral tumours was correlated with their FDG uptake[12,13]. Tumours have a higher rate of glucose use; FDG accumulation therefore also increases. In the early 1990s, FDG PET started to be used in conjunction with whole-body imaging protocols. The first applications of FDG PET outside neuro-oncology were primarily in the detection of lung cancer[14–16].

After FDG has been injected into the bloodstream, it is transported from the vascular space into the interstitial space. From here, specific glucose transporters recognize and transport it into cells. FDG is phosphorylated by hexokinase to form FDG-6-phosphate[17]. Unlike glucose, FDG lacks a hydroxyl group in the 2-position (FIG. 2a) and its first metabolite, FDG-6-phosphate, cannot act as a substrate for further glycolysis. Importantly, FDG is also eliminated via the renal system and, unlike glucose, is not reabsorbed well in the renal tubules, which leads to low levels of FDG in the blood. It is fortunate that the pharmacokinetics of glucose and FDG uptake, trapping and blood clearance are in the 30–60-minute time frame because this allows PET imaging with ^{18}F. The molecular targets of FDG are therefore glucose transporters and hexokinase[17,18]. The relative importance of each of these targets continues to be a subject of debate[19,20], and it is likely that in a given cell type, one might predominate.

Because all cells metabolize glucose, FDG is not specific for malignant transformation. This lack of specificity can be a potential problem in some cases, but it also serves to provide anatomical features in the image — by creating a low background signal in all tissues — that would otherwise not be present and would make image interpretation more difficult. Malignant transformation is often associated with increasing energy demands, a decrease in glucose-6-phosphate and the

SMART PROBES
Probes that are used in optical and magnetic resonance imaging that can be kept relatively silent until they interact with the target. After interaction, they become activated and produce a detectable signal.

MRI
(Magnetic resonance imaging). A technique to image subjects through the use of a magnetic field that aligns endogenous (for example, proton) or exogenous (for example, gadolinium) magnetic moments. Provides both anatomical imaging and functional imaging.

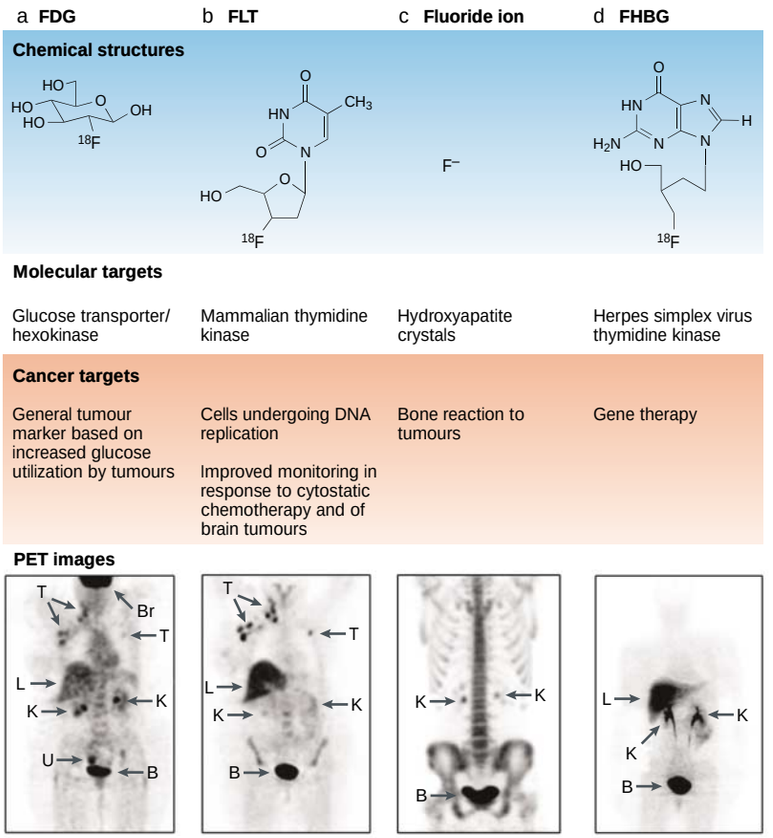

Figure 2 | **FDG, FLT, fluoride ion and FHBG PET images.** Human positron-emission tomography (PET) coronal images of four different tracers, with chemical structures of the tracers and their molecular targets. A PET image can look entirely different depending on the tracer that is injected into the subject. This is because the scanner images the distribution of the tracer, and each tracer has unique molecular targets and routes of clearance. **a**,**b** | The same patient imaged with 2-[^{18}F] fluoro-2-deoxy-D-glucose (FDG) and then with 3′-deoxy-3′-[^{18}F] fluorothymidine (FLT), a tracer that accumulates in proportion to cell-proliferative capacity. **c** | A fluoride ion scan of a different patient. **d** | A volunteer scanned with 9-(4-[^{18}F] fluoro-3-hydroxymethylbutyl)guanine (FHBG), a tracer that is expected to be useful for imaging herpes simplex virus type 1 thymidine kinase reporter-gene expression. Brain (Br), tumour (T), liver (L), kidney (K), ureter (U), bladder (B). FDG, FLT and FHBG images courtesy of UCLA Ahmanson Biological Imaging Center. Fluoride ion image courtesy of Abass Alavi, University of Pennsylvania.

upregulation of glucose transporters (especially GLUT-1) and hexokinase. It is also important to note that glucose competes with FDG at each step of uptake and trapping. In clinical practice, this is dealt with by fasting the patient for 4–6 hours before FDG injection, to minimize competition.

The current clinical applications of FDG in cancer diagnosis and management are very diverse. Because most types of cancer cell accumulate FDG, and most non-cancer cells accumulate much less, FDG PET is a very general approach to cancer imaging[21]. The overall mean sensitivity and specificity across various applications are ~85%. The primary established clinical roles for FDG PET are in the diagnosis and management of various malignancies. The assessment of solitary pulmonary nodules[22] and pre-operative staging of non-small-cell lung cancer to determine sites of metastases not seen on CT[23] are improving the management of patients. Staging in colorectal cancer, melanoma and lymphoma are all relatively well-established applications[24–27]. Imaging of brain metastases is limited because of the relatively high uptake of FDG by grey matter. Emerging roles include monitoring for recurrence and during therapy[28,29] (FIG. 3). By providing early information on the metabolic response of a tumour for a given therapy, FDG PET can aid in continuing or changing therapy to avoid potential side effects of a given therapeutic regimen. FDG PET has not been particularly effective in managing patients with prostate[30] or ovarian cancer[31], and screening high-risk patients remains to be validated. At present, the vast majority (~95%) of all clinical PET studies use FDG.

FDG is a great example of a failed drug that has become quite successful as an imaging agent. Many other such agents could be present in the databases of pharmaceutical and biotechnology companies, waiting to be exploited.

Cell proliferation. Cell proliferation is increased with malignant transformation, which consequently increases the number of cells undergoing DNA replication. The use of thymidine analogues provides a useful way of targeting DNA replication[32]. Upregulation in thymidine transport and mammalian thymidine kinases provides molecular targets for imaging. These are upregulated by cancer cells because thymidine is needed for DNA synthesis. Several agents, including [^{11}C]thymidine, have been studied, but the most promising agent so far is 3′-deoxy-3′-[^{18}F]fluorothymidine (FLT)[33,34] (FIG. 2b).

Imaging in dogs and clinical patients[34] shows the potential superiority of FLT over FDG. FLT PET imaging during therapy has the potential to be more useful than FDG for three reasons. First, there would potentially be less uptake of FLT than FDG after an inflammatory response. Second, cytostatic chemotherapeutics, which often have a greater impact on cell division than on glucose metabolism, might be better monitored with FLT. Third, brain tumours might also be better imaged with FLT: it accumulates at lower levels in most regions of the brain, because of a lack of significant neuronal cell division.

Bone remodelling. Metastasis to bone is common for several cancers, including those of prostate, breast and lung. The most common clinical procedure used to evaluate bone metastasis is [^{99m}Tc]methylenediphosphonate (MDP), which uses the gamma-camera and SPECT imaging[35]. The positron-emitting [^{18}F]fluoride ion was first described as an excellent bone-imaging tracer 40 years ago, and its use for PET imaging is still being clinically validated[35,36] (FIG. 2c).

Skeletal uptake of bone-seeking radiopharmaceuticals, such as MDP and [^{18}F]fluoride ion, is influenced by bone blood flow, the molecular size and net electric charge of the molecule, capillary surface, capillary permeability, local pH and, most importantly, metabolic activity of the bone tissue[37]. In contrast to anionic complexes, such as ^{99m}Tc-labelled diphosphonates,

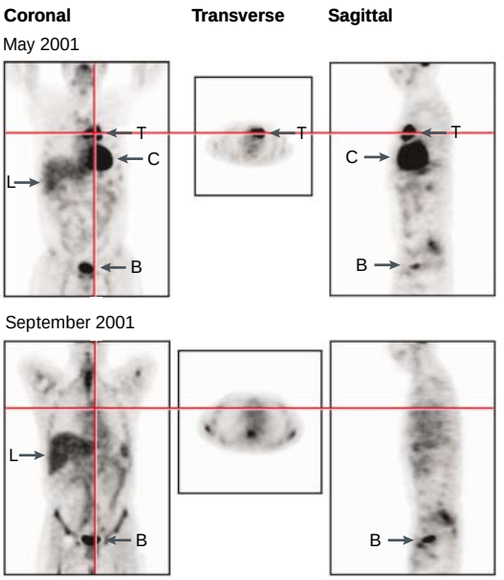

Figure 3 | **FDG PET imaging for monitoring therapy.** Shown are 2-[^{18}F]fluoro-2-deoxy-D-glucose (FDG) positron-emission tomography (PET) cross-sectional images of the same patient before and after chemotherapy for lymphoma. The tumour seen on the top image set is not well visualized in the images taken four months later. Cardiac activity is also not well visualized in the post-therapy images, and is probably related to dietary fasting differences. FDG PET is being actively investigated as an agent to monitor therapy and might show changes long before anatomical imaging, such as computed tomography, shows any response to therapy. Tumour (T), cardiac (C), bladder (B), liver (L). Images courtesy of J. Czernin, UCLA Ahmanson Biological Imaging Center.

[^{18}F]fluoride is small and is naturally incorporated into the bone matrix. After diffusion through capillaries into bone extracellular fluid, [^{18}F]fluoride exchanges slowly with hydroxyl groups in the hydroxyapatite crystal of bone to form fluoroapatite, and the activity is deposited preferentially at the surface of bone, where remodelling and turnover are greatest[38]. The relationship between bone formation and resorption is believed to determine the amount of CHEMISORPTION and incorporation of [^{18}F]fluoride into the bone matrix. The greater sensitivity and resolution of PET, as compared with SPECT, should lead to the more effective characterization of bony metastases[35], and it is likely that this technique will continue to gain more widespread acceptance as higher-throughput PET scanner technology is developed.

Perfusion. Tumours are in constant need of nutrients from the blood, and tumour neovascularization provides a crucial lifeline for rapidly dividing tumour cells[39]. Tracers that are extracted from the blood can therefore be used to assess tumour blood perfusion. The diffusion into tissues is proportional to delivery, and so is a measure of perfusion. Although a relatively non-specific assay, blood-perfusion imaging uses simple tracers and has the potential to be useful. ^{15}O-labelled water is one of the most extensively studied perfusion tracers[40] and there is a relatively good correlation between perfusion and tracer accumulation, but several other tracers for blood-perfusion assessment exist[8]. Quantitative measurements of perfusion require determination of the blood time–activity curve (input function), which can be obtained by arterial sampling or images of the left ventricle. Good studies for the validation of various tracers for specific use with tumours are still lacking. Attempts to image tumour angiogenesis specifically have also been preliminarily validated[41], and it is likely that these techniques can be extended for use with anti-angiogenesis pharmaceuticals.

Oxygen metabolism. Tumour oxygenation is a crucial factor in the successful treatment of tumours by various approaches. Hypoxia seems to be a significant prognostic variable, and it is likely that the use of tracers to monitor hypoxia before, during and after treatment will continue to increase. [^{18}F]Fluoromisonidazole (FMISO), an analogue of 2-nitroimidazole, has been used to image hypoxia in tumours[42]. FMISO diffuses into all cells and is reduced and reoxidized in normal cells; however, it continues to be reduced and binds to cell components in hypoxic cells. The use of FMISO is not optimal because of its relatively poor cellular uptake and slow clearance from normal tissues[43]. Copper bis(thiosemicarbazones), such as Cu(II)-diacetyl-bis(N^4-methylthiosemicarabaone) (Cu-ATSM), has been shown to wash out of normal tissues quickly and yet be retained in hypoxic tissues owing to its reduction by oxygen-depleted mitochondria[44]. It is probable that increasing research into the development of new hypoxia tracers, as well as the testing of existing ones, will increase over the next few years.

Tumour receptors and antigens. Although tracers for metabolism, proliferation, perfusion and hypoxia provide useful imaging of neoplasms, they are relatively non-specific and are usually less useful for imaging tumours that have very low growth rates. The development of tracers that target specific tumour antigens is therefore essential for the development and usefulness of clinical PET.

Many intracellular and cell-surface receptors are upregulated in cancer cells. To target potential receptors, it would be optimal to use tracers that have a very high affinity for the target receptor and a minimal background accumulation; this could be achieved by lowering LIPOPHILICITY. Relatively small ligands, as well as larger proteins such as antibodies, have been labelled and used as tracers to target specific receptors. Examples of small ligands include ^{11}C-labelled *N*-methylspiperone and ^{18}F-labelled spiperone for targeting the dopamine receptors on pituitary adenomas[45,46], and ^{64}Cu-labelled octreotide[47] and ^{68}Ga-labelled octreotide analogues[48] for targeting somatostatin-receptor-positive tumours. Sigma receptors are also found on many tumours, and small PET ligands to image these receptors are under investigation[49,50].

CHEMISORPTION
A chemical adsorption process in which weak chemical bonds are formed between gas or liquid molecules and a solid surface.

LIPOPHILICITY
The degree of affinity for fat.

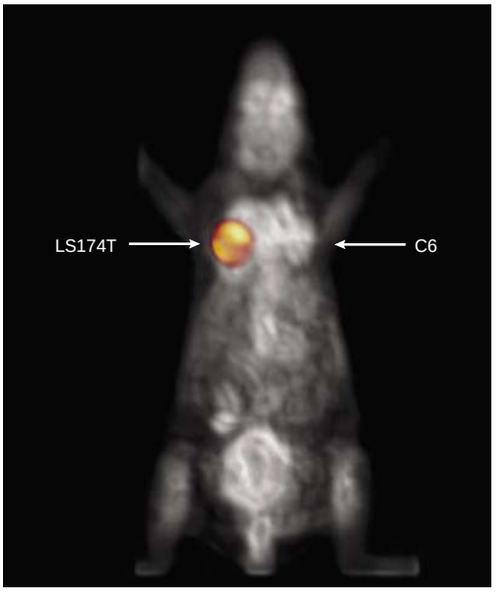

Figure 4 | **Small-animal FDG/^{124}I minibody imaging.** MicroPET (positron-emission tomography) imaging of a mouse 1 hour after tail-vein injection of 2-[^{18}F]fluoro-2-deoxy-D-glucose (FDG) (grey scale) superimposed on microPET imaging of the same mouse imaged 18 hours after injection of an ^{124}I (~4-day half-life)-labelled minibody (colour scale) targeted against carcinoembryonic antigen (CEA). The mouse carries two tumour xenografts: a C6 rat glioma as a negative control and an LS174T line that expresses CEA. The minibody signal is seen almost exclusively from the LS174T tumour only, because most background activity has already cleared 18 hours after tracer injection. Images courtesy of Anna Wu and the Crump Institute for Molecular Imaging.

Antibodies are also a potential tracer for targeting cell-surface receptors. Although primarily explored for imaging with gamma-cameras and SPECT, newer small-animal studies and clinical trials are starting with positron-labelled antibody fragments. Monoclonal antibodies developed against a specific antigen target are problematic, because their relatively slow clearance from blood leads to images with very high background signals, even at up to one week after injection of the antibody. Efforts have been made in the systematic construction of engineered antibody fragments, such as MINIBODIES and DIABODIES[51,52], against carcinoembryonic antigen (CEA). These agents show much more rapid blood clearance (owing to their smaller size) — at the expense of some affinity for CEA — in comparison with intact antibodies. Humanized versions of these engineered antibody fragments have been labelled with ^{64}Cu and ^{124}I, and mouse tumour xenograft imaging has been performed with microPET[52] (FIG. 4). Clinical PET trials with these agents are now starting. The engineered antibody fragments have the ability to be adapted for targeting other tumour-cell-surface targets (for example, ERBB2 (also known as HER2/neu)) and it remains to be seen what advantages these tracers have in the clinical setting over existing tracers such as FDG. Further reviews of antibodies and engineered antibody fragments for imaging are provided elsewhere[53].

Relatively small radioligands have been used to target intracellular receptors. One of the most extensively studied systems is radiolabelled steroids for targeting hormone-receptor-positive tumours[54]. As there are only a few thousand steroid receptors per cancer cell, there is a limited imaging signal potential from each cell. 16α[^{18}F]Fluoro-17β-oestradiol (FES), an oestrogen analogue, has good imaging characteristics in human studies and has been preliminarily studied to monitor the effectiveness of hormonal therapy with tamoxifen in breast cancer[55–57]. Tamoxifen competes with FES, so the PET signal can decrease after treatment and this can be used to gauge treatment efficacy. Androgen receptors have also been targeted by PET tracers for imaging prostate cancer. ^{18}F has been used to label several hormone analogues, including 16β-^{18}F-substituted testosterone, 5α-dihydrotestosterone and mibolerone, 16α- and 16β-[^{18}F]7α-methyl-19-nortesotsteorne, 20-[^{18}F]fluoro-R1881 (metribolone) and 20-[^{18}F]fluoromiboloerone. Some animal studies have been performed with these agents, but more detailed studies are still needed[58,59]. These tracers might eventually be used to improve the staging and monitoring of prostate cancer. More studies are still needed to determine the utility of these tracers for imaging human prostate cancer.

Gene therapy with reporter genes/probes. Imaging gene expression is important for monitoring the location(s), magnitude and time-variation of gene expression from gene-therapy vectors, and can be important in measuring the efficacy of the therapy. Without imaging methods to monitor expression, the field of gene therapy will continue to face significant obstacles for routine use. For monitoring the expression of therapeutic genes during gene therapy, several approaches to 'linking' a therapeutic gene to a 'PET reporter gene' have been studied[60]. The PET reporter gene allows an indirect method of following the expression of the linked therapeutic gene of interest. It 'reports' back on the status of expression of the gene of interest when properly linked.

The linkage can be made in one of several ways. First, an internal ribosomal entry site (IRES) can be used in a bicistronic vector that encodes both transcribed genes in one mRNA, which is translated into two proteins[61,62]. Second, an inducible bi-directional vector can be used in which doxycycline initiates the transcription of both the therapeutic gene and the reporter gene[63] (FIGS 5,6). Third, the reporter gene and therapeutic gene can be delivered by using two separate vectors[64]. Finally, fusion approaches in which a fusion protein contains both the therapeutic and reporter protein can be used[65]. All of these approaches are dependent on having a useful PET reporter gene, as described next.

Several approaches have been validated to extend the reporter-gene techniques that are normally used in cell studies to develop PET reporter genes. Although optical reporters such as green fluorescent protein (GFP) and firefly/*Renilla* luciferase offer significant advantages in cell assays, and more recently have been

MINIBODIES
An engineered antibody construct that consists of the variable-heavy- and variable-light-chain domains of a native antibody that is fused to the hinge region and to the CH3 domain of the immunogloblin molecule. Minibodies are small versions of whole antibodies, encoded in a single protein chain, that retain the antigen-binding region, the CH3 domain (to allow assembly into a bivalent molecule), and the antibody hinge (to accommodate dimerization by disulphide linkages).

DIABODIES
Engineered antibody fragments that are bivalent or bispecific molecules generated by dimerization of two variable-heavy–variable-light fragments. These molecules clear much more rapidly from the blood than do full antibodies.

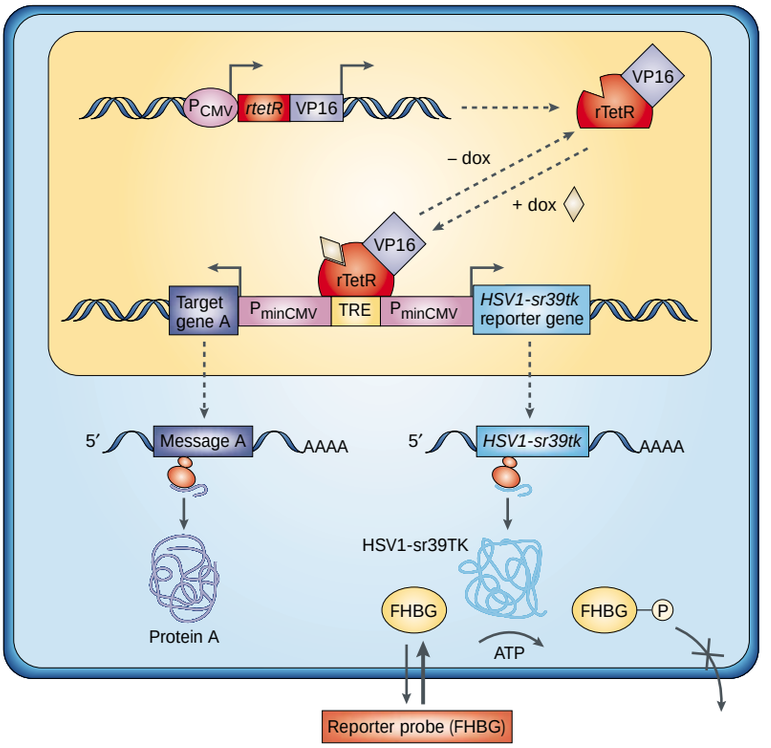

Figure 5 | **Bi-directional inducible therapeutic and reporter-gene expression.** Target (therapeutic) gene expression can be measured indirectly by imaging reporter-gene expression if expression of the two genes is 'linked'. Both genes can be simultaneously expressed from two minimal cytomegalovirus (CMV) promoters that are regulated by a single bi-directional tetracycline-responsive element (TRE). The rTetR–VP16 fusion protein is produced constitutively from a CMV promoter. When the rTetR–VP16 fusion protein binds doxycycline, the fusion protein plus doxycycline complex binds to the TRE regulatory sequence and substantially enhances expression from the two minimal CMV promoters. The target gene *A* in one coding region and a reporter gene (for example, a reporter kinase such as *HSV1-sr39tk*) in the alternative coding region are transcribed simultaneously into two mRNA molecules. Translation of the two mRNA molecules yields two distinct proteins in amounts that are directly correlated with each other. Quantitative imaging of the location(s) and magnitude of PET reporter-gene expression by trapping of a PET tracer inside the cell (for example, by phosphorylation of FHBG by the HSV1-sr39TK reporter protein) provides an indirect measure of target-gene expression.

Na/I SYMPORTER
A transporter that is found primarily in thyroid epithelial tissue that co-transports both iodide and sodium from extracellular fluid into cells.

SUICIDE GENE
A gene that can be introduced into target cells that will, under the appropriate conditions, lead to destruction of that cell. The herpes simplex virus type 1 thymidine kinase gene (*HSV1-tk*) is an example of a suicide gene. It encodes a protein that, in the presence of pro-drugs such as ganciclovir, leads to cell death. Suicide-gene-therapy approaches have been attempted as a way to destroy cancer cells.

used in small-animal models[7,60], they are not easily translated to human applications because of the limited penetration of visible light through tissues. PET reporter genes — including those that encode herpes simplex virus type 1 thymidine kinase (*HSV1-tk*)[66–68] and the dopamine type 2 receptor (*D2R*)[69] and their mutants[70,71] — have been validated in animals. Other reporter genes, including those that encode the somatostatin receptor and Na/I SYMPORTER, have also been preliminarily studied and are reviewed elsewhere[60]. The principle in using each of these PET reporter genes is to obtain sufficient PET signal primarily from those cells that express the reporter gene due to accumulation of the appropriately chosen tracer.

The *HSV1-tk* reporter gene, which encodes the HSV1-TK protein, can trap several positron-labelled tracers by phosphorylating a transported tracer. This tracer then becomes charged, so it cannot leave the cell (FIG. 5). Both acycloguanosines (for example, derivatives of ganciclovir and penciclovir) and derivatives of thymidine such as 2′-fluoro-2′-deoxy-1-β-D-arabinofuranosyl-5-iodo-uracil (FIAU) have been used as tracers for imaging *HSV1-tk* reporter-gene expression by adenovirus-mediated gene expression in the liver and stably transfected tumour cells[72]. We have also described imaging with a mutant *HSV1-sr39tk* reporter gene, which has a greater imaging sensitivity when used with acycloguanosines[70] and is less sensitive to changes in intracellular thymidine concentration.

The *D2R* reporter gene has been validated for the PET imaging of reporter-gene expression with [^{18}F]fluoroethylspiperone (FESP) as the tracer ligand[69], and, more recently, a mutant D2R has also been reported[71] that is uncoupled from signal transduction, while maintaining affinity for FESP. Although it might seem that a receptor approach might lead to less imaging sensitivity than an enzyme-based approach (for example, *HSV1-tk*), there are advantages, including no requirement for tracer transport into the cell for cell-surface receptors. Detailed comparisons of various approaches can be found elsewhere[72].

Studies in imaging reporter-gene expression in human subjects have only recently started. As might be expected, as *HSV1-tk* is both a reporter gene and a SUICIDE GENE[73], imaging its expression in humans would be a good initial proof of principle for the use of PET imaging in gene therapy. We have studied the kinetics, biodistribution, stability, dosimetry and safety of 9-(4-[^{18}F]fluoro-3-hydroxymethylbutyl)guanine (FHBG) in healthy human volunteers[74], for eventual use in human gene-therapy trials (FIG. 2d). Imaging *HSV1-tk* reporter gene expression near the gall bladder, kidneys and bladder with FHBG might be difficult owing to the background signal in these regions, which is caused by routes of tracer clearance. Furthermore, imaging within the brain would be difficult because FHBG does not significantly cross the blood–brain barrier. Clinical trials with FHBG in patients undergoing *HSV1-tk* gene therapy are now starting. In another preliminary study, Jacobs *et al.*[75] have recently shown that [^{124}I]FIAU PET imaging might be useful in patients with glioblastoma who are undergoing *HSV1-tk* suicide-gene therapy. The *HSV1-tk* gene was delivered by the intratumoral infusion of cationic liposomes. The disruption of the blood–brain barrier allows imaging in these patients. Although still in validation, it is likely that the PET reporter-gene approaches will aid various gene-therapy trials directly. Issues of aberrant gene expression in unintended sites will be particularly helpful in making safe the routine use of gene therapy.

Other applications. The use of ^{11}C- and ^{18}F-labelled choline has recently gained attention for applications in prostate cancer imaging[76–78]. This approach relies on the fact that these tracers are readily incorporated into cells through phosphorylcholine synthesis and integration in membrane phospholipids. The use of radiolabelled amino acids, including methionine and tyrosine, is also a growing area, and might prove to be useful in specific applications (for example, brain metastases);

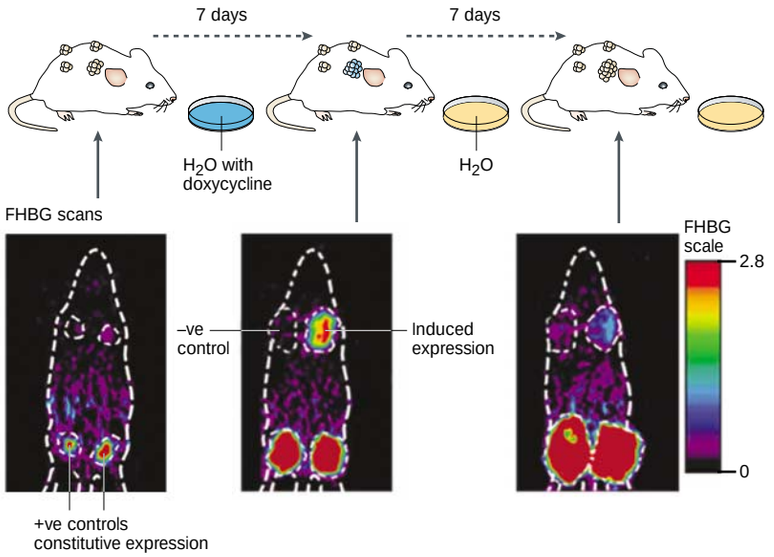

Figure 6 | **MicroPET imaging of bi-directional inducible therapeutic and reporter-gene expression.** Sequential microPET (positron-emission tomography) imaging studies of a nude mouse carrying four tumours. Four tumour cell lines — two positive controls (constitutive reporter-gene expression), one negative control and one inducible line (reporter-gene expression induced by doxycycline (see FIG.5 for expression system)) — were injected subcutaneously into four separate sites in a single mouse. When tumours reached a size of at least 5 mm, the mouse was imaged with 9-(4-[^{18}F] fluoro-3-hydroxymethylbutyl)guanine (FHBG). Doxycycline was then added to the water supply for 7 days. The mouse was then scanned again with FHBG. Doxycycline was removed from the water supply for the next 7 days, and the mouse was again scanned with FHBG. The locations of the four tumours and the mouse outline are shown by the dotted regions of interest. All images are 1–2 mm coronal sections through the four tumours. The %ID/g (% injected dose per gram tissue) scale for FHBG is shown on the right. The negative control tumours show no gene expression, and the positive control tumours show increased expression over the time course. The tumour on the top right, with inducible gene expression, initially does not accumulate FHBG, then at 7 days after addition of doxycycline, induction of reporter-gene expression traps FHBG. Seven days after withdrawal of doxycycline, there is decreased induction and minimal trapping of FHBG.The FHBG image signal correlates well with target-gene expression (not shown). Images reproduced with permission from REF. 63.© (2001) Nature Publishing Group.

this is reviewed elsewhere[79]. It remains to be determined under what circumstances radiolabelled choline and amino acids outperform FDG.

The use of antisense tracers for targeting endogenous mRNA levels would be very useful because of the ability to adapt these approaches to target the expression of almost any endogenous gene. By rearranging the base sequence of the tracer, while keeping the radiolabelling strategy the same, large libraries of such tracers could be generated. Antisense probes of high specific radioactivity have been developed, but it remains uncertain whether these approaches will be robust enough to image endogenous gene expression *in vivo*[80–82]. Problems of efficient delivery, non-specific interactions and sufficient efflux from cells that do not contain target mRNA will need to be resolved. Investigations to couple approaches with split reporter proteins[83] or trans-splicing approaches[84–86], in conjunction with HIV Tat-mediated delivery of DNA, RNA or protein[87], are being studied to image mRNA levels. These approaches might provide signal amplification by using mRNA hybridization to provide specificity for the target, and could simultaneously provide sensitivity through signal amplification from the reporter protein. Applications of PET in assessing multidrug resistance[88], and intra-operative beta-probes with FDG for guiding surgery[89], are also areas of active investigation. Other tracers for various cancer molecular targets are reviewed elsewhere[8,90,91].

Multimodality imaging

PET imaging provides unique information on tumour biochemistry and physiology, but without much anatomical information — that obtained is generally due to the non-specificity of the tracer. For example, with FDG PET, the muscles throughout the body are usually detected by their use of glucose. As more specific tracers with rapid clearance from non-specific tissues are developed, correlative anatomical imaging is crucially needed. Although software tools can be used to register data from scans obtained separately from CT and PET, this is difficult to do outside the brain as a result of many variables, including patient motion. Clinical PET/CT systems have been developed and are undergoing rapid refinement[92–94]. It is likely that most clinical PET systems around the world will be replaced with PET/CT systems during the next 5–10 years. The ability to obtain data from both modalities is already significantly improving clinical decision-making[95] (FIG. 7). Small-animal studies should also benefit from obtaining anatomical and functional images. MicroCT studies[96,97] and microPET studies can be performed separately[98], but the availability of a small-animal microPET/CT scanner will be useful, and several such instruments are in development. In addition to CT, the use of MRI[99] and even optical approaches, when coupled with PET, might prove useful in small-animal and perhaps even clinical imaging.

Drug development and PET

One of the most under-used applications of microPET and clinical PET is in the area of drug development[100,101]. For the most part, the imaging community and the pharmaceutical/biotechnology industries have remained isolated with minimal overlap, but this has started to change over the past few years, and many pharmaceutical companies are investing in research imaging programs that use microPET and PET.

Drugs that are ready to proceed to testing *in vivo* can have their pharmacokinetics analysed in small animals, as well as humans, with PET. This first requires labelling the pharmaceutical with a positron-emitting isotope, but is potentially highly cost-effective. This is because the costs of the time invested in the labelling technique(s) can be offset by a more rapid translation to human testing. Although trace levels of the drug can be introduced into humans, mass levels might need to be used to mimic the biodistribution of the drug of interest accurately. In addition, existing PET tracers can be used to monitor a new pharmaceutical. For example, a new drug that is a ligand for a receptor can be studied with PET by imaging displacement of an existing PET tracer before and after drug administration. The total radioactivity

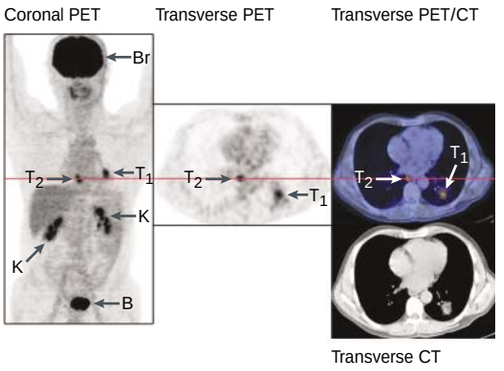

Figure 7 | **FDG PET/CT imaging for improved patient management.** Shown are images from a new generation of hybrid positron-emission tomography (PET) and computed tomography (CT) dual-modality scanner. This scanner can take both PET and CT images in the same patient, allowing registration of functional (PET) and anatomical (CT) information. The patient is a 42-year-old smoker with known non-small-cell lung cancer and referred for a PET/CT scan for staging his disease before potential surgery. 2-[^{18}F]fluoro-2-deoxy-D-glucose (FDG) PET coronal image shows the lung tumour in the left lower lobe (T1), but a second area of increased uptake is seen in the mediastinum (T2). On the FDG PET transverse images, this second lesion localizes to the middle mediastinum. FDG PET alone in this setting would indicate that this is probably a lymph node of the known lung carcinoma. However, the transverse section of the PET/CT shows that this second area is localized in the oesophageal wall and is not a distinct lymph node. This patient had an additional biopsy that proved oesophageal cancer. This case illustrates the importance of having anatomical definition for the PET study. As PET tracers further improve and localize only to the site of a tumour, it will be vital to have information on the exact anatomical location(s) of tracer uptake. Brain (Br), tumours (T1,T2), kidneys (K), bladder (B). Images provided courtesy of Gustav K. von Schulthess, University Hospital, Zurich, Switzerland.

measured by PET can contain significant amounts of radiolabelled metabolites, so that tracer kinetic modelling and blood sampling of metabolites are often needed to quantify the levels of drug.

It is also possible to start the process of merging the development of a PET tracer and a pharmaceutical from a very early stage. This can be done by developing libraries of molecules that can be conveniently radiolabelled and can also be used for screening for therapeutic efficacy against one or more targets. The advantage of being able to study a radiopharmaceutical in an animal model and then quickly move into human studies is an important area that is likely to be used for many drugs. Clinical trials might be accelerated through earlier human studies to rule out drugs that have unfavourable biodistribution and/or pharmacokinetics. This ability to translate easily from animal to human studies should help to increase the use of PET for drug development. Additionally, the development of new PET tracers should be enhanced by greater partnerships between the pharmaceutical and imaging communities[101–105].

Prospects for the future

Clinical and small-animal PET should expand significantly over the next decade, as more research groups and clinical centres acquire these technologies. In addition, small radiopharmacies with cyclotrons should continue to grow, providing for the routine availability of FDG and other existing tracers. The existing tracers could eventually give way to a newer generation of molecular probes that are more sensitive and specific. Advances in detector technology and image reconstruction techniques should help to produce a new generation of scanners that have better spatial resolution, sensitivity and significantly improved throughput time (less than 10 minutes for the entire body of a patient). PET will probably be replaced by PET/CT systems to provide anatomical and functional image information, especially as tracers become more specific and lead to minimal background signal. The use of PET/CT imaging in the diagnosis and management of cancer patients will be expanded with the development of new tracers. The use of PET/CT systems by radiation oncologists to perform more detailed therapy planning should also increase significantly.

It is likely that PET will be important in the molecular imaging of cancer; however, it will probably be part of a multimodality imaging approach. There should be continued roles for SPECT, CT, MRI, ultrasound and new optical imaging approaches (for example, optical breast-cancer imaging). PET will have an advantage in terms of its greater sensitivity at all depths, as well as the ability to use biological molecules that retain most, if not all, their properties after being radiolabelled. These advantages for PET will be coupled with significant challenges of developing relatively large libraries of useful tracers. PET assays will need to move towards generalized tracers in which the radioisotope labelling chemistry remains largely unchanged, but the underlying molecular structure can be easily modified to image a new molecular target. Alternatively, pre-targeting approaches, in which a non-radioactive molecule is administered first and followed by a tracer, might allow signal amplification and generalization to many targets.

The next decade should see applications in individualized or 'customized' imaging. Scenarios in which an individual's tumour is characterized in detail by gene and protein profiling should allow the use of tracers that are specific for the individual's tumour. This could allow better imaging during therapy and enhanced monitoring for recurrence by using tracers that are optimal for a given individual. Finally, the continued use of small-animal PET in developing new pharmaceuticals, as well as PET tracers for newly identified cancer targets, should help in significantly enhancing the fields of tumour biology, and cancer therapeutics and management. It will be important to use PET with a specific tracer in clearly defined populations of patients in which its efficacy has proved to be cost-effective. Finally, all practitioners of molecular imaging will need to work closely with engineering and biological scientists, pharmaceutical companies and clinical oncologists to build the next generation of useful tracers for PET and technologies that will some day significantly expand the capabilities of PET use in oncology.

1. Phelps, M. E., Hoffman, E. J., Mullani, N. A. & Ter-Pogossian, M. M. Application of annihilation coincidence detection to transaxial reconstruction tomography. *J. Nucl. Med.* **16**, 210–224 (1975).
2. Strijckmans, K. The isochronous cyclotron: principles and recent developments. *Comput. Med. Imaging Graph.* **25**, 69–78 (2001).
3. Rosenthal, M. S. *et al.* Quantitative SPECT imaging: a review and recommendations by the Focus Committee of the Society of Nuclear Medicine Computer and Instrumentation Council. *J. Nucl. Med.* **36**, 1489–1513 (1995).
4. Cherry, S. R. & Gambhir, S. S. Use of positron emission tomography in animal research. *Ilar J.* **42**, 219–232 (2001).
Describes the use of animal PET technology and its many applications.
5. Chatziioannou, A., Tai, Y. C., Doshi, N. & Cherry, S. R. Detector development for microPET II: a 1 micron resolution PET scanner for small animal imaging. *Phys. Med. Biol.* **46**, 2899–2910 (2001).
6. Chatziioannou, A. F. Molecular imaging of small animals with dedicated PET tomographs. *Eur. J. Nucl. Med.* **29**, 98–114 (2002).
7. Weissleder, R. Scaling down imaging: molecular mapping of cancer in mice. *Nature Rev. Cancer* **2**, 11–18 (2002).
8. Cutler, C. S., Lewis, J. S. & Anderson, C. J. Utilization of metabolic, transport and receptor-mediated processes to deliver agents for cancer diagnosis. *Adv. Drug Deliv. Rev.* **37**, 189–211 (1999).
9. Woodward, G. E. & Hudson, M. T. *Cancer Res.* **14**, 599–605 (1954).
10. Sokoloff, L. *et al.* The [^{14}C]deoxyglucose method for the measurement of local cerebral glucose utilization: theory, procedure, and normal values in the conscious and anesthetized albino rat. *J. Neurochem.* **28**, 897–916 (1977).
Describes the use of [^{14}C]deoxyglucose to measure glucose utilization, which is the basis for the eventual development of a PET-compatible tracer (FDG).
11. Ido, T. *et al.* Labeled 2-deoxy-D-glucose analogs: ^{18}F labeled 2-deoxy-2-fluoro-D-glucose, 2-deoxy-2-fluoro-D-mannose and ^{14}C-2- deoxy-2-fluoro-D-glucose. *J. Labeled Compounds Radiopharmacol.* **14**, 175–183 (1978).
12. Di Chiro, G. *et al.* in *Positron Emission Tomography* (eds Greitz, T., Ingvar, D. H. & Widen, L.) 351–361 (Raven, New York, 1985).
13. Di Chiro, G. Positron emission tomography using [^{18}F] fluorodeoxyglucose in brain tumors. A powerful diagnostic and prognostic tool. *Invest. Radiol.* **22**, 360–371 (1987).
14. Kubota, K. *et al.* Differential diagnosis of lung tumor with positron emission tomography: a prospective study. *J. Nucl. Med.* **31**, 1927–1932 (1990).
15. Gupta, N. C. *et al.* Solitary pulmonary nodules: detection of malignancy with PET with 2-[F-18]-fluoro-2-deoxy-D-glucose. *Radiology* **184**, 441–444 (1992).
16. Hoh, C. K. *et al.* Cancer detection with whole-body PET using 2-[^{18}F]fluoro-2-deoxy-D-glucose. *J. Comput. Assist. Tomogr.* **17**, 582–589 (1993).
17. Smith, T. A. Mammalian hexokinases and their abnormal expression in cancer. *Br. J. Biomed. Sci.* **57**, 170–178 (2000).
18. Smith, T. A. FDG uptake, tumour characteristics and response to therapy: a review. *Nucl. Med. Commun.* **19**, 97–105 (1998).
19. Nelson, C. A., Wang, J. Q., Leav, I. & Crane, P. D. The interaction among glucose transport, hexokinase, and glucose-6-phosphatase with respect to ^{3}H-2-deoxyglucose retention in murine tumor models. *Nucl. Med. Biol.* **23**, 533–541 (1996).
20. Smith, T. A. The rate-limiting step for tumor [^{18}F]fluoro-2-deoxy-D-glucose (FDG) incorporation. *Nucl. Med. Biol.* **28**, 1–4 (2001).
21. Gambhir, S. S. *et al.* A tabulated summary of the FDG PET literature. *J. Nucl. Med.* **42**, 1S–93S (2001).
Describes in detail the accuracy of FDG PET in many different applications, including all major cancers.
22. Gambhir, S. S. *et al.* Analytical decision model for the cost-effective management of solitary pulmonary nodules. *J. Clin. Oncol.* **16**, 2113–2125 (1998).
23. Scott, W. J., Shepherd, J. & Gambhir, S. S. Cost-effectiveness of FDG-PET for staging non-small cell lung cancer: a decision analysis. *Ann. Thorac. Surg.* **66**, 1876–1883; discussion 1883–1885 (1998).
24. Huebner, R. H. *et al.* A meta-analysis of the literature for whole-body FDG PET detection of recurrent colorectal cancer. *J. Nucl. Med.* **41**, 1177–1189 (2000).
25. Park, K. C. *et al.* Decision analysis for the cost-effective management of recurrent colorectal cancer. *Ann. Surg.* **233**, 310–319 (2001).
26. Schwimmer, J. *et al.* A review of the literature for whole-body FDG PET in the management of patients with melanoma. *Q. J. Nucl. Med.* **44**, 153–167 (2000).
27. Delbeke, D. Oncological applications of FDG PET imaging: brain tumors, colorectal cancer, lymphoma and melanoma. *J. Nucl. Med.* **40**, 591–603 (1999).
28. Lapela, M. *et al.* Experience in qualitative and quantitative FDG PET in follow-up of patients with suspected recurrence from head and neck cancer. *Eur. J. Cancer* **36**, 858–867 (2000).
29. Akhurst, T. *et al.* An initial experience with FDG-PET in the imaging of residual disease after induction therapy for lung cancer. *Ann. Thoracic Surg.* **73**, 259–264 (2002).
30. Seltzer, M. A. *et al.* Comparison of helical computerized tomography, positron emission tomography and monoclonal antibody scans for evaluation of lymph node metastases in patients with prostate specific antigen relapse after treatment for localized prostate cancer. *J. Urol.* **162**, 1322–1328 (1999).
31. Schroder, W., Zimny, M., Rudlowski, C., Bull, U. & Rath, W. The role of F-18-fluoro-deoxyglucose positron emission tomography (F-18-FDG PET) in diagnosis of ovarian cancer. *Int. J. Gynecol. Cancer* **9**, 117–122 (1999).
32. Shields, A. F., Grierson, J. R., Kozawa, S. M. & Zheng, M. Development of labeled thymidine analogues for imaging tumor proliferation. *Nucl. Med. Biol.* **23**, 17–22 (1996).
Describes tracer approaches to the imaging of DNA synthetic rates.
33. Krohn, K. A., Mankoff, D. A. & Eary, J. F. Imaging cellular proliferation as a measure of response to therapy. *J. Clin. Pharmacol. Suppl.* 96S–103S (2001).
34. Shields, A. F. *et al.* Imaging proliferation *in vivo* with [F-18]FLT and positron emission tomography. *Nature Med.* **4**, 1334–1336 (1998).
35. Blake, G. M., Park-Holohan, S. J., Cook, G. J. & Fogelman, I. Quantitative studies of bone with the use of ^{18}F-fluoride and ^{99m}Tc-methylene diphosphonate. *Semin. Nucl. Med.* **31**, 28–49 (2001).
36. Ohta, M. *et al.* Whole body PET for the evaluation of bony metastases in patients with breast cancer: comparison with Tc-99(m)-MDP bone scintigraphy. *Nucl. Med. Commun.* **22**, 875–879 (2001).
37. Piert, M. *et al.* Assessment of porcine bone metabolism by dynamic [^{18}F]fluoride ion PET. *J. Nucl. Med.* **42**, 1091–1100 (2001).
38. Narita, N. *et al.* Distribution of fluoride concentration in the rat's bone. *Calcif. Tissue Int.* **46**, 200–204 (1990).
39. Carmeliet, P. & Jain, R. K. Angiogenesis in cancer and other diseases. *Nature* **407**, 249–257 (2000).
40. Bacharach, S. L., Libutti, S. K. & Carrasquillo, J. A. Measuring tumor blood flow with $H_2{}^{15}O$: practical considerations. *Nucl. Med. Biol.* **27**, 671–676 (2000).
41. Weber, W. A. *et al.* Tumor angiogenesis targeting using imaging agents. *Q. J. Nucl. Med.* **45**, 179–182 (2001).
42. Koh, W. J. *et al.* Evaluation of oxygenation status during fractionated radiotherapy in human nonsmall cell lung cancers using [F-18]fluoromisonidazole positron emission tomography. *Int. J. Radiat. Oncol. Biol. Phys.* **33**, 391–398 (1995).
43. Nunn, A., Linder, K. & Strauss, H. W. Nitroimidazoles and imaging hypoxia. *Eur. J. Nucl. Med.* **22**, 265–280 (1995).
44. Fujibayashi, Y. *et al.* Copper-62-ATSM: a new hypoxia imaging agent with high membrane permeability and low redox potential. *J. Nucl. Med.* **38**, 1155–1160 (1997).
45. Muhr, C. *et al.* Dopamine receptors in pituitary adenomas: PET visualization with ^{11}C-*N*-methylspiperone. *J. Comput. Assist. Tomogr.* **10**, 175–180 (1986).
46. Lucignani, G. *et al.* Differentiation of clinically non-functioning pituitary adenomas from meningiomas and craniopharyngiomas by positron emission tomography with [^{18}F]fluoro-ethyl-spiperone. *Eur. J. Nucl. Med.* **24**, 1149–1155 (1997).
47. Anderson, C. J. *et al.* ^{64}Cu-TETA-octreotide as a PET imaging agent for patients with neuroendocrine tumors. *J. Nucl. Med.* **42**, 213–221 (2001).
48. Henze, M. *et al.* PET imaging of somatostatin receptors using [^{68}Ga]DOTA-D-Phe1-Tyr3-octreotide: first results in patients with meningiomas. *J. Nucl. Med.* **42**, 1053–1056 (2001).
49. Mach, R. H. *et al.* [^{18F}]N-(*4′*-fluorobenzyl)-4-(3-bromophenyl) acetamide for imaging the sigma receptor status of tumors: comparison with [^{18}F]FDG, and [^{125}I]IUDR. *Nucl. Med. Biol.* **28**, 451–458 (2001).
50. Waterhouse, R. N. & Collier, T. L. *In vivo* evaluation of [^{18}F]1-(3-fluoropropyl)-4-(4-cyanophenoxymethyl)piperidine: a selective sigma-1 receptor radioligand for PET. *Nucl. Med. Biol.* **24**, 127–134 (1997).
51. Kortt, A. A., Dolezal, O., Power, B. E. & Hudson, P. J. Dimeric and trimeric antibodies: high avidity scFvs for cancer targeting. *Biomol. Eng.* **18**, 95–108 (2001).
52. Wu, A. M. *et al.* High-resolution microPET imaging of carcinoembryonic antigen-positive xenografts by using a copper-64-labeled engineered antibody fragment. *Proc. Natl Acad. Sci. USA* **97**, 8495–8500 (2000).
Describes the use of minibodies and diabodies for imaging in small-animal models.
53. Wu, A. M. & Yazaki, P. J. Designer genes: recombinant antibody fragments for biological imaging. *Q. J. Nucl. Med.* **44**, 268–283 (2000).
54. Katzenellenbogen, J. A. Designing steriod receptor-based radiotracers to image breast and prostate cancer. *J. Nucl. Med.* **36** (Suppl.), 8–13 (1995).
55. Dehdashti, F. *et al.* Positron tomographic assessment of estrogen receptors in breast cancer: comparison with FDG-PET and *in vitro* receptor assays. *J. Nucl. Med.* **36**, 1766–1774 (1995).
56. Mortimer, J. E. *et al.* Positron emission tomography with 2-[^{18}F]Fluoro-2-deoxy-D-glucose and 16α-[^{18}F]fluoro-17β-estradiol in breast cancer: correlation with estrogen receptor status and response to systemic therapy. *Clin. Cancer Res.* **2**, 933–939 (1996).
57. Flanagan, F. L. *et al.* PET assessment of response to tamoxifen therapy in patients with metastatic breast cancer. *J. Nucl. Med.* **37**, 99P (1996).
58. Bonasera, T. A. *et al.* Preclinical evaluation of fluorine-18-labeled androgen receptor ligands in baboons. *J. Nucl. Med.* **37**, 1009–1015 (1996).
59. Downer, J. B. *et al.* Comparison of animal models for the evaluation of radiolabeled androgens. *Nucl. Med. Biol.* **28**, 613–626 (2001).
60. Ray, P. *et al.* Monitoring gene therapy with reporter gene imaging. *Semin. Nucl. Med.* **31**, 312–320 (2001).
61. Yu, Y. *et al.* Quantification of target gene expression by imaging reporter gene expression in living animals. *Nature Med.* **6**, 933–937 (2000).
Describes the imaging of a reporter gene linked to a therapeutic gene in order to quantify therapeutic gene expression indirectly.
62. Liang, Q. *et al.* Noninvasive, repetitive, quantitative measurement of gene expression from a bicistronic message by positron emission tomography, following gene transfer with adenovirus. *Mol. Ther.* **6**, 73–82 (2002).
63. Sun, X. *et al.* Quantitative imaging of gene induction in living animals. *Gene Ther.* **8**, 1572–1579 (2001).
64. Yaghoubi, S. S. *et al.* Direct correlation between positron emission tomographic images of two reporter genes delivered by two distinct adenoviral vectors. *Gene Ther.* **8**, 1072–1080 (2001).
65. Jacobs, A. *et al.* Functional coexpression of HSV-1 thymidine kinase and green fluorescent protein: implications for noninvasive imaging of transgene expression. *Neoplasia* **1**, 154–161 (1999).
66. Tjuvajev, J. G. *et al.* Imaging herpes virus thymidine kinase gene transfer and expression by positron emission tomography. *Cancer Res.* **58**, 4333–4341 (1998).
67. Gambhir, S. S. *et al.* Imaging of adenoviral-directed herpes simplex virus type 1 thymidine kinase reporter gene expression in mice with radiolabeled ganciclovir. *J. Nucl. Med.* **39**, 2003–2011 (1998).
68. Gambhir, S. S. *et al.* Imaging adenoviral-directed reporter gene expression in living animals with positron emission tomography. *Proc. Natl Acad. Sci. USA* **96**, 2333–2338 (1999).
Describes the use of a PET reporter gene carried in an adenovirus to image virus-mediated gene delivery and expression in living mice.
69. MacLaren, D. C. *et al.* Repetitive, non-invasive imaging of the dopamine D2 receptor as a reporter gene in living animals. *Gene Ther.* **6**, 785–791 (1999).
70. Gambhir, S. S. *et al.* A mutant herpes simplex virus type 1 thymidine kinase reporter gene shows improved sensitivity for imaging reporter gene expression with positron emission tomography. *Proc. Natl Acad. Sci. USA* **97**, 2785–2790 (2000).
71. Liang, Q. *et al.* Noninvasive, quantitative imaging in living animals of a mutant dopamine D2 receptor reporter gene in which ligand binding is uncoupled from signal transduction. *Gene Ther.* **8**, 1490–1498 (2001).
72. Gambhir, S. S. *et al.* Imaging transgene expression with radionuclide imaging technologies. *Neoplasia* **2**, 118–138 (2000).
73. Moolten, F. L. Suicide genes for cancer therapy. *Sci. Med.* **4**, 16–25 (1997).
74. Yaghoubi, S. *et al.* Human pharmacokinetic and dosimetry studies of [^{18}F]FHBG: a reporter probe for imaging herpes simplex virus type-1 thymidine kinase reporter gene expression. *J. Nucl. Med.* **42**, 1225–1234 (2001).
75. Jacobs, A. *et al.* Positron-emission tomography of vector-mediated gene expression in gene therapy for gliomas. *Lancet* **358**, 727–729 (2001).

76. Hara, T., Kosaka, N. & Kishi, H. PET imaging of prostate cancer using carbon-11-choline. *J. Nucl. Med.* **39**, 990–995 (1998).
77. Kotzerke, J. *et al.* Experience with carbon-11 choline positron emission tomography in prostate carcinoma. *Eur. J. Nucl. Med.* **27**, 1415–1419 (2000).
78. Price, D. T. *et al.* Comparison of [^{18}F]fluorocholine and [^{18}F]fluorodeoxyglucose for positron emission tomography of androgen dependent and androgen independent prostate cancer. *J. Urol.* **168**, 273–280 (2002).
79. Jager, P. L. *et al.* Radiolabeled amino acids: basic aspects and clinical applications in oncology. *J. Nucl. Med.* **42**, 432–445 (2001).
80. Tavitian, B. *et al. In vivo* imaging of oligonucleotides with positron emission tomography. *Nature Med.* **4**, 467–471 (1998).
81. Tavitian, B. *In vivo* antisense imaging. *Q. J. Nucl. Med.* **44**, 236–255 (2000).
82. Hnatowich, D. J. Antisense imaging: where are we now? *Cancer Biother. Radiopharm.* **15**, 447–457 2000).
83. Paulmurugan, R., Umezawa, Y. & Gambhir, S. S. Imaging protein–protein interactions in living subjects by a reporter protein reconstitution and complementation strategies. *Mol. Imaging Biol.* (in the press).
84. Liu, X. *et al.* Partial correction of endogenous ΔF508 CFTR in human cystic fibrosis airway epithelia by spliceosome-mediated RNA trans-splicing. *Nature Biotechnol.* **20**, 47–52 (2002).
85. Puttaraju, M., DiPasquale, J., Baker, C. C., Mitchell, L. G. & Garcia-Blanco, M. A. Messenger RNA repair and restoration of protein function by spliceosome-mediated RNA trans-splicing. *Mol. Ther.* **4**, 105–114 (2001).
86. Bhaumik, S., Lewis, X., Puttaraju, M., Mitchell, L. G. & Gambhir, S. S. Imaging mRNA levels in living animals through a novel RNA trans-splicing signal amplification approach. *Mol. Imaging Biol.* (in the press).
87. Becker-Hapak, M., McAllister, S. S. & Dowdy, S. F. TAT-mediated protein transduction into mammalian cells. *Methods* **24**, 247–256 (2001).
88. Lewis, J. S. *et al.* Copper bis(diphosphine) complexes: radiopharmaceuticals for the detection of multi-drug resistance in tumours by PET. *Eur. J. Nucl. Med.* **27**, 638–646 (2000).
89. Zervos, E. E., Desai, D. C., DePalatis, L. R., Soble, D. & Martin, E. W. ^{18}F-labeled fluorodeoxyglucose positron emission tomography-guided surgery for recurrent colorectal cancer: a feasibility study. *J. Surg. Res.* **97**, 9–13 (2001).
90. Silverman, D. H. *et al.* Evaluating tumor biology and oncological disease with positron-emission tomography. *Semin. Radiat. Oncol.* **8**, 183–196 (1998).
91. Krohn, K. A. Evaluation of alternative approaches for imaging cellular growth. *Q. J. Nucl. Med.* **45**, 174–178 (2001).
92. Townsend, D. W. & Cherry, S. R. Combining anatomy and function: the path to true image fusion. *Eur. Radiol.* **11**, 1968–1974 (2001).
93. Townsend, D. W. A combined PET/CT scanner: the choices. *J. Nucl. Med.* **42**, 533–534 (2001).
Describes the PET/CT technology to perform simultaneous functional and anatomical imaging in patients.
94. Ell, P. J. & Von Schulthess, G. K. PET/CT: a new road map. *Eur. J. Nucl. Med. Mol. Imaging* **29**, 719–720 (2002).
95. Kluetz, P. G. *et al.* Combined PET/CT imaging in oncology. Impact on patient management. *Clin. Positron Imaging* **3**, 223–230 (2000).
96. Paulus, M. J., Gleason, S. S., Kennel, S. J., Hunsicker, P. R. & Johnson, D. K. High resolution X-ray computed tomography: an emerging tool for small animal cancer research. *Neoplasia* **2**, 62–70 (2000).
97. Paulus, M. J., Gleason, S. S., Easterly, M. E. & Foltz, C. J. A review of high-resolution X-ray computed tomography and other imaging modalities for small animal research. *Lab. Anim.* **30**, 36–45 (2001).
98. Berger, F. *et al.* Whole body skeletal imaging in mice using MicroPET and MicroCAT: new tools for small animal bone imaging. *Eur. J. Nucl. Med.* (in the press).
99. Shao, Y. *et al.* Simultaneous PET and MR imaging. *Phys. Med. Biol.* **42**, 1965–1970 (1997).
100. Vaalburg, W., Hendrikse, N. H. & de Vries, E. F. Drug development, radiolabelled drugs and PET. *Ann. Med.* **31**, 432–437 (1999).
101. Cherry, S. R. Fundamentals of positron emission tomography and applications in preclinical drug development. *J. Clin. Pharmacol.* **41**, 482–491 (2001).
102. Price, P. Monitoring response to treatment in the development of anticancer drugs using PET. *Nucl. Med. Biol.* **27**, 691 (2000).
103. Katz, R., Wagner, H. N., Fauntleroy, M., Kuwert, T. & Frank, R. The use of imaging as biomarkers in drug development: regulatory issues worldwide. *J. Clin. Pharmacol. Suppl.* 118S (2001).
104. Paans, A. M. & Vaalburg, W. Positron emission tomography in drug development and drug evaluation. *Curr. Pharm. Des.* **6**, 1583–1591 (2000).
105. Fowler, J. S., Volkow, N. D., Wang, G. J., Ding, Y. S. & Dewey, S. L. PET and drug research and development. *J. Nucl. Med.* **40**, 1154–1163 (1999).

Acknowledgements

I thank M.E. Phelps, H.R. Herschman and J.R. Barrio for their strong mentorship over the last decade. I also thank N. Satyamurthy, M. Namavari, T. Toyokuni, J. Rao, A.Wu, L. Wu, H. Wu, M. Carey, A. Berk, O. Witte, C. Sawyers, R. Reiter, A. Beldegrun, J. Czernin, M. Seltzer, D. Silverman, C. Hoh, H.R. Schelbert, H. Kornblum, D. Smith, D. Agus, S.C. Huang, J. Braun, S. Chow, D.L. Kaufman, S.R. Cherry, A. Chatziioannou, M. Dahlbom and E. Hoffman for their enormous help over the years. Finally, I thank all the postdoctoral fellows, graduate and undergraduate students in my laboratory who have given and continue to enthusiastically give their full efforts towards building a new field of molecular imaging.

Online links

DATABASES

The following terms in this article are linked online to:

Cancer.gov: http://www.cancer.gov/cancer_information/
bone cancer | brain cancer | breast cancer | colorectal cancer | lymphoma | melanoma | non-small-cell lung cancer | ovarian cancer | prostate cancer

GenBank: http://www.ncbi.nih.gov/Genbank/
HSV1-tk

LocusLink: http://www.ncbi.nlm.nih.gov/LocusLink/
D2R | ERBB2 | somatostatin receptor

Medscape DrugInfo:
http://promini.medscape.com/drugdb/search.asp
ganciclovir | penciclovir | tamoxifen

FURTHER INFORMATION

Academy of Molecular Imaging: http://www.ami-imaging.org

FDG PET whole-body imaging atlas with over 100 oncology cases): http://www.crump.ucla.edu/web/wba.adp

General resource for the molecular imaging field:
http://www.mi-central.org

Society for Molecular Imaging:
http://www.molecularimaging.org

Society of Nuclear Medicine: http://www.snm.org

Access to this interactive links box is free online.

MOLECULAR IMAGING IN DRUG DISCOVERY AND DEVELOPMENT

Markus Rudin and Ralph Weissleder‡*

Imaging sciences have grown exponentially during the past three decades, and many techniques, such as magnetic resonance imaging, nuclear tomographic imaging and X-ray computed tomography, have become indispensable in clinical use. Advances in imaging technologies and imaging probes for humans and for small animals are now extending the applications of imaging further into drug discovery and development, and have the potential to considerably accelerate the process. This review summarizes some of the recent developments in conventional and molecular imaging, and highlights their impact on drug discovery.

MAGNETIC RESONANCE IMAGING (MRI). A powerful diagnostic imaging method that uses radiowaves in the presence of a magnetic field to extract information from certain atomic nuclei (most commonly hydrogen). It is primarily used for producing anatomical images, but also gives information on the physico-chemical state of tissues, flow, diffusion, motion and, more recently, molecular targets.

**Novartis Institute for Biomedical Research, CH-4002 Basel, Switzerland.*
‡Center for Molecular Imaging Research, Massachusetts General Hospital, Harvard Medical School, Boston,Charlestown, Massachusetts 02129, USA.
Correspondence to R.W.
e-mail: weissleder@helix. mgh.harvard.edu
doi:10.1038/nrd1007

Imagine seeing a specific molecular target in a live animal, following a drug's distribution in the same animal and quantitating the drug's direct effect on the target, all in a matter of minutes. Although this prospect might have seemed utopian a few years ago, enabling technologies, such as novel imaging modalities and molecular probes, are being developed at a rapid pace and should allow these questions to be addressed routinely in the not-too-distant future. The widespread availability of mouse imaging systems is not as far off as many researchers might think. These systems (TABLE 1) are generally cheaper than their clinical counterparts and can be housed in basic science laboratories (see REF. 1 for a review). Given the increasingly common use of mouse models of disease to validate potential drug targets, to assess therapeutic efficacy and to identify and validate biomarkers of drug efficacy and/or safety, the ability to image mouse models non-invasively would have far-reaching applications in drug discovery and development.

Historically, *in vivo* imaging methods have largely relied on imaging gross anatomy, and diseases or treatment effects were mostly detected as structural abnormalities (these methods occasionally being referred to as structural or conventional imaging). With higher spatial resolutions and the advent of imaging agents, it became possible to image at the mesoscale and therefore derive physiological parameters in live subjects (this is often called functional imaging). More recently, it has become possible to image specific molecules and targets, a field that is often referred to as molecular imaging. Indeed, molecular imaging can be used to either image the administered drug directly (for example, following its distribution and target binding) or the target itself (for example, receptor expression and modulation of downstream targets). For the newer molecular imaging tools to be useful, there are two prerequisites: first, they must have the high sensitivity that is required to monitor interactions at a molecular level and also have sufficiently high spatial resolution to image mouse models of human disease; and second, more target-specific molecular probes must become available. The goal of this paper is to briefly review the available imaging modalities, highlight some uses of anatomical and functional imaging and then focus on exciting advances in molecular imaging (FIG. 1) and how they will affect drug discovery and development. For more in-depth reading on specific imaging modalities and diseases, the reader is referred to several recent review articles[1–7].

Imaging modalities

Imaging technologies exploit the interaction of various forms of energy with tissues to non-invasively visualize the body. Some technologies, such as MAGNETIC RESONANCE IMAGING (MRI) and X-RAY COMPUTED TOMOGRAPHY (CT), rely solely on energy–tissue interactions, whereas others, such as POSITRON EMISSION TOMOGRAPHY (PET), require the

Table 1 | **Overview of high-resolution, small-animal imaging systems**

Technique	Resolution	Depth	Time	Imaging agents	Target*	Cost‡	Primary small-animal use	Clinical use
MR	10–100 μm	No limit	Minutes–hours	Gadolinium, dysprosium, iron oxide particles	A, P, M	$$$	Versatile imaging modality with high soft-tissue contrast	Yes
CT	50 μm	No limit	Minutes	Iodine	A, P	$$	Lung and bone imaging	Yes
Ultrasound	50 μm	Millimetres	Minutes	Microbubbles	A, P	$$	Vascular and interventional imaging	Yes
PET	1–2 mm	No limit	Minutes	^{18}F,^{11}C,^{15}O	P, M	$$$	Versatile imaging modality with many different tracers	Yes
SPECT	1–2 mm	No limit	Minutes	^{99m}Tc, ^{111}In chelates	P, M	$$	Commonly used to image labelled antibodies, peptides and so on	Yes
FRI	2–3 mm	<1 cm	Seconds–minutes	Photoproteins (GFP), NIR fluorochromes	P, M	$	Rapid screening of molecular events in surface-based tumours	Development
FMT	1 mm	<10 cm	Seconds–minutes	NIR fluorochromes	P, M	$$	Quantitative imaging of targeted or 'smart' fluorochrome reporters in deep tumours	Development
BLI	Several millimetres	Centimetres	Minutes	Luciferins	M	$$	Gene expression, cell and bacterial tracking	No
Intravital microscopy (confocal, multiphoton)	1 μm	<400 μm	Seconds–minutes	Photoproteins (GFP), Fluorochromes	P, M	$$$	All of the above at higher resolutions but at limited depths and coverage	Limited development (skin)

*Primary area that a given imaging modality interrogates: A, anatomical; M, molecular P, physiological. ‡Cost of system: $ <100,000; $$ 100–300,000; $$$: >300,000. BLI, bioluminescence imaging; CT, X-ray computed tomography; FMT, fluorescence-mediated molecular tomography; FRI, fluorescence reflectance imaging; GFP, green fluorescent protein; NIR; near-infrared; MR, magnetic resonance; PET, positron emission tomography; SPECT, single-photon emission computed tomography.

administration of imaging agents or reporter probes (which can be targeted to specific cells or receptors; see below).

The choice of imaging modality in drug development depends primarily on the specific question to be addressed and different imaging techniques are, in general, complementary rather than competitive. The versatility of MRI has made it a widely used tool in pharmaceutical research. Owing to its excellent soft-tissue contrast properties, MRI allows for the sensitive detection of soft-tissue pathologies and, in addition, yields valuable physiological information. Today, MRI has evolved to be the imaging modality of choice for studying diseases of the central nervous system, such as stroke, neurodegenerative disorders and multiple sclerosis, and provides qualitative diagnostic and quantitative morphometric information, as well as functional/physiological readouts (FIG. 2). The technique is also widely used to diagnose and stage visceral pathologies (for example, neoplastic structures and cardiovascular diseases) or musculoskeletal diseases (for example, rheumatoid arthritis). CT is the classical anatomical imaging modality and is particularly suited for the study of skeletal structures and of the lung. Nuclear imaging techniques such as PET offer the sensitivity required to monitor drug distribution, pharmacokinetics and pharmacodynamics, and for imaging specific molecular end points. Depending on the ligands and radionuclides used, a myriad of molecular end points can potentially be visualized. Newer optical imaging techniques, such as fluorescence and bioluminescence imaging, are of particular value for mapping specific molecular events in mice and for tracking cells. They are also cheap, fast and do not require radionuclides. Several other imaging technologies (for example, magnetic resonance spectroscopy, electron magnetic resonance and optical spectroscopy) are under development; however, these are less well established for drug development.

Many of these non-invasive technologies were originally developed for human use, but have recently been scaled down to allow the high-resolution imaging of mice. This is highly relevant, because as genomics provides us with better animal models of disease, imaging readouts can be used to evaluate novel therapeutics. In addition, some of the imaging modalities fulfil the bench-to-bedside model, that is, they can be applied to mice, other rodents and primates and can ultimately be used in clinical trials. From the perspective of drug development, such tools will be highly valuable. In the following sections, we consider the integration of non-invasive imaging methods into modern drug discovery and development (FIG. 1).

Structural and functional imaging

Characterizing disease models and evaluating efficacy. High-resolution structural and functional imaging has become increasingly important in drug development, both experimentally and clinically. Its main advantages over other biomarkers (for example, tissue sampling, excision and fluid analysis) are the direct visualization

X-RAY COMPUTED TOMOGRAPHY (CT). As generated X-rays pass through different types of tissue, they are deflected or absorbed to different degrees. CT uses X-rays to obtain three-dimensional images by rotating an X-ray source around the subject and measuring the intensity of transmitted X-rays from different angles.

POSITRON EMISSION TOMOGRAPHY (PET). A tomographic imaging technique that detects nuclides as they decay by positron emission.

of disease processes, the ability to quantitate changes over time and the non-invasive nature of the tests. As an example, FIG. 2 shows how MR can be used to image the development of pathology in a rodent model of human embolic stroke. MR techniques allow the precise localization of the site of vascular occlusion[8], the quantification of the ensuing perfusion[9] and the oxygenation deficits[10] leading to energy failure, membrane breakdown and cytotoxicoedema[11]. Later steps in the pathophysiological cascade include the breakdown of the blood–brain barrier, the formation of vasogenic oedema[12] and the infiltration of inflammatory cells, all of which are detectable by MRI[13]. The efficacy of cytoprotective therapy has been commonly assessed using structural readouts, that is, using estimates of infarct volumes coupled with the assumption that structural damage is a surrogate for clinical outcome. More recent data, however, indicate that structural integrity (that is, normal appearance in anatomical images) is a necessary but not sufficient criterion for functional integrity as revealed by functional MRI (fMRI) studies of brain function[14]. Both anatomical and functional read-outs have therefore become established in research to determine the efficacy of newer thrombolytic and cytoprotective therapies[3,12]. For clinical applications, however, some of these surrogate markers of drug development have not yet been accepted by the US FDA. Similar structural and functional imaging approaches have been used to determine the efficacy of anti-angiogenic therapies[15–19], anti-inflammatory treatments[20,21], apoptosis-inducing agents[22–24] and many other areas of drug action.

Labelling the drug

Imaging biodistribution and pharmacokinetics. Although the biodistribution and pharmacokinetics of new agents in rodents are still commonly measured by blood and tissue sampling or autoradiography, nuclear imaging techniques have gained in importance[7]. Nuclear techniques — in particular, quantitative PET imaging — can now be carried out in small rodents[25–28] and are routinely used in canine and primate models, as well as being used clinically. A particularly exciting aspect of PET is the fact that many drugs can be labelled with ^{11}C or with ^{18}F (REFS 7,29–34), which means that labelling only minimally affects, if at all, the chemical/physicochemical properties of the compound, allowing the monitoring of the drug biodistribution. As an example, a study showing the distribution of fluconazole, a fluorine-containing anti-fungal agent, is shown in FIG. 3 (REF. 35). PET imaging was used to obtain detailed quantitative information on fluconazole kinetics and dynamics in various tissues, including the human brain. Another approach frequently used in PET imaging is to analyse the inhibition of specific binding of a well-characterized PET radioligand by an unlabelled drug.

Labelling the target

Imaging target distribution and function. Advances in genomic, proteomic and chemical sciences have accelerated the development of ever-more-precise therapeutics aimed at specific molecular targets associated with disease. Examples of such therapies include inhibitors of specific kinases (for example, Glivec/Gleevec, which targets the BCR–ABL receptor tyrosine kinase[36]), receptors[15] or proteinases[37]. Ideally, we would like to monitor these directed therapies by visualizing the intended drug target and then image the functional consequences of drug–target interactions in live animals and, ultimately, in patients. Specifically, we would like to know whether a putative drug reaches the target, whether it affects target expression and/or function (up- or down-regulation, activation or inactivation) and, ultimately, whether the drug has a disease-modifying effect. Such information can potentially be provided by molecular imaging techniques[1]. The central challenge for molecular imaging is to develop specific reporter probes and amplification strategies to differentiate target information from non-specific background noise so as to be able to cope with low (sub-nanomolar) target concentrations.

The design of molecular reporter probes is variable, but typically involves either 'targeted agents' or 'activatable agents'[1]. Targeted agents are essentially small molecules, peptides, metabolites, aptamers, antibodies or other molecules labelled with a reporter moiety that can be detected by a given imaging modality (for example, ^{11}C- and ^{18}F-labelled PET ligands[7,30,33], ^{111}In- or ^{99m}Tc-labelled ligands[38], fluorochrome-labelled ligands[39–41] and magnetic ligands[42–44]). *In vivo*

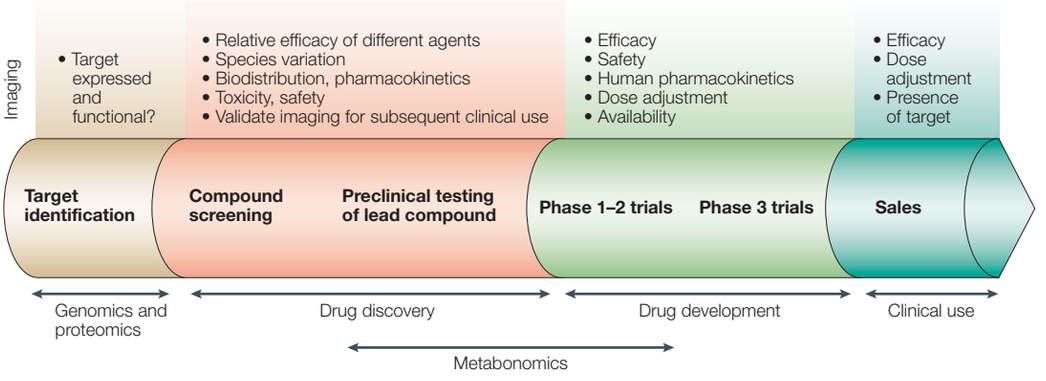

Figure 1 | **Imaging applications in the drug discovery and development process.**

visualization of a target requires specific enrichment of the reporter probe at the target site, that is, we have to wait until the non-bound fraction of the reporter probe is eliminated to minimize the background signal. Many types of targeted imaging agent have been developed for different imaging techniques (BOX 1).

During the past several years, there has been an increasing interest in PET imaging as a tool in central nervous system drug discovery and development[30,45–53]. This has been primarily due to a growing list of neuroreceptor-specific PET tracers, improvements in PET camera resolution, the availability of small-animal PET cameras[25] and improved communication between academia and drug companies. A significant number of small-molecule receptor ligands have been labelled with ^{11}C and ^{18}F, and some of these ligands readily cross the blood–brain barrier and bind to their intended targets. In particular, the dopamine and SEROTONIN (5-HT) RECEPTOR SYSTEMS have been investigated[32,50,54]. Using such specific ligands, PET studies have provided information on the

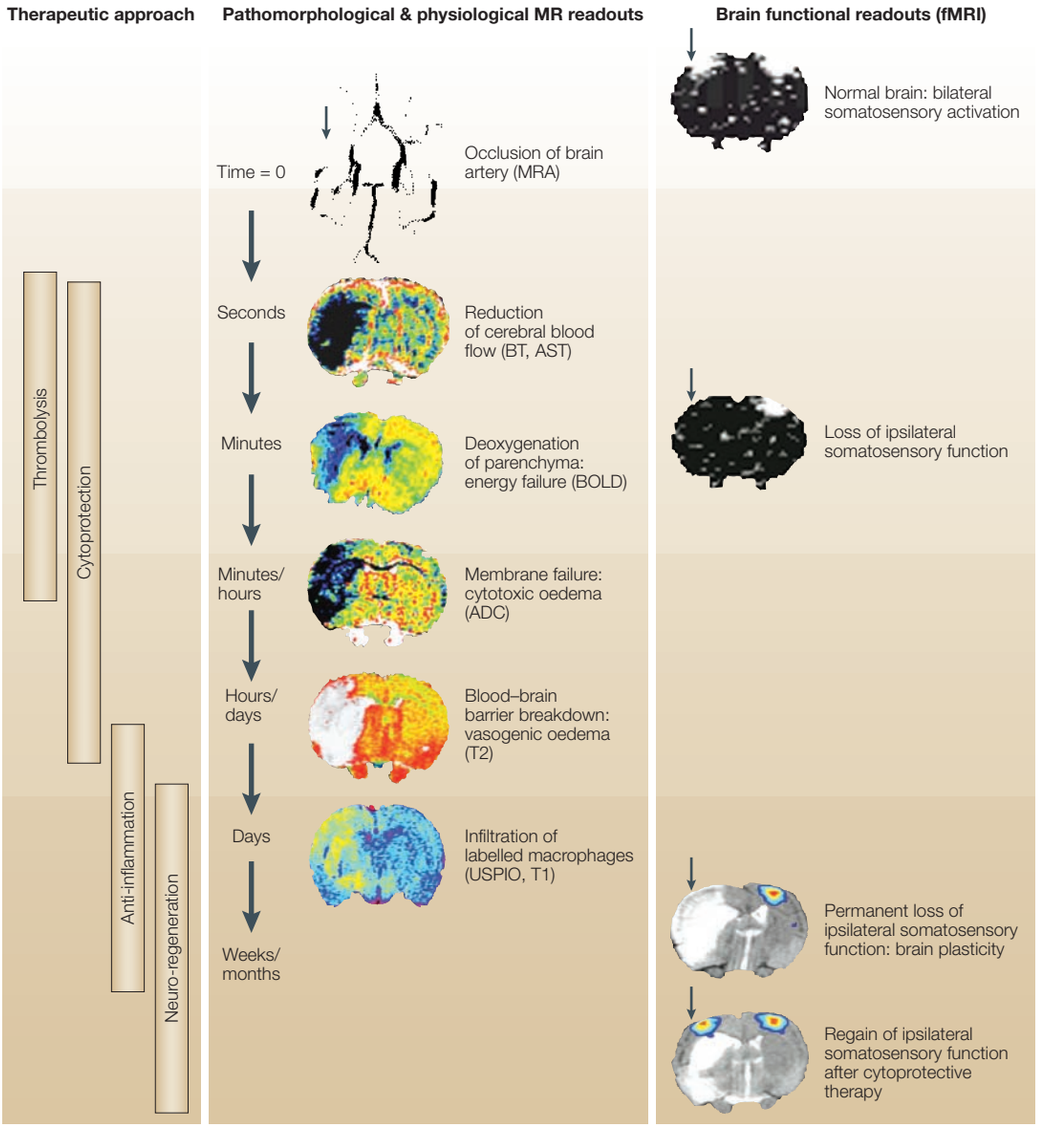

Figure 2 | **Structural and functional imaging.** Conventional structural and functional imaging has an increasingly important role in drug development. Using embolic stroke and stroke treatment, this figure summarizes the available imaging read-outs and their role in different therapeutic regimens and timing. Initially, angiographic techniques can visualize the occlusion, while other magnetic resonance imaging techniques allow the visualization of perfusion and oxygenation deficits. At later time points, diffusion and T_2 imaging can be used as surrogates for membrane failure and tissue necrosis (vasogenic oedema). Using imaging agents, cellular infiltration and repair processes can be visualized at later points. Brain function is assessed by functional magnetic resonance imaging (fMRI) methods that probe local changes in the haemodynamic parameters associated with neuronal activity. Peripheral sensory stimulation of the forepaws leads to fMRI signal in the corresponding somatosensory cortices. After middle cerebral artery (MCA) occlusion, the ipsilateral functionality is lost. The therapeutic objective is to restore function either by sparing the respective area from becoming necrotic or by enhancing plasticity (for more information, see REF. 3).

SEROTONIN SYSTEM
This is an important neurotransmission network involved in aggressive and sexual behaviour, depression, anxiety, the sleep–wake cycle, moods, thermoregulation and other functions.

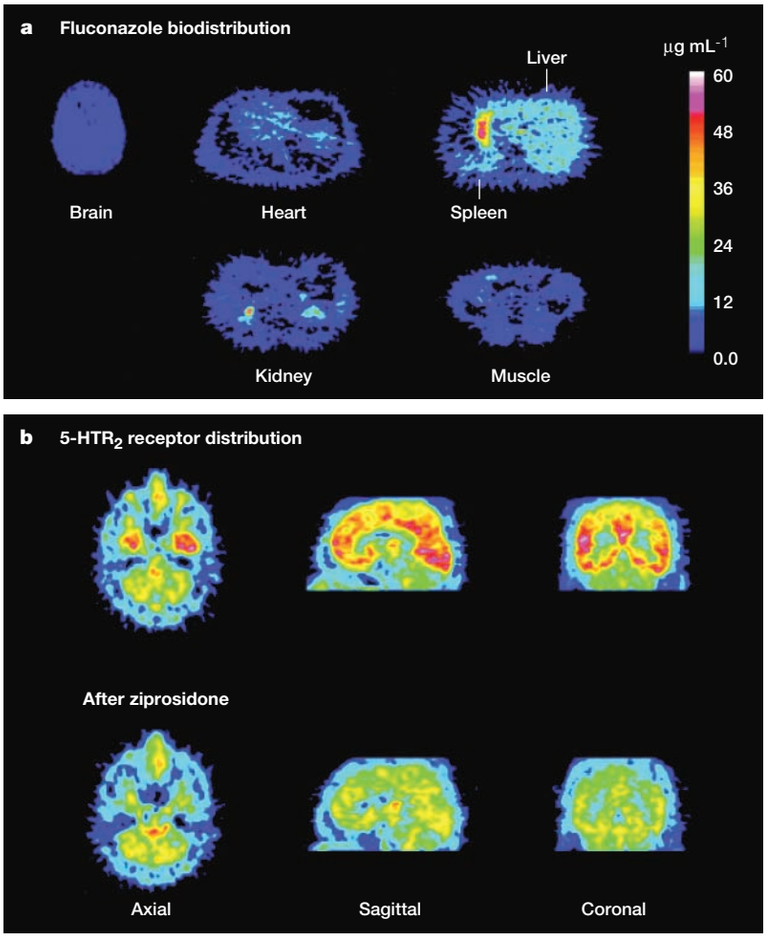

Figure 3 | **Imaging drug pharmacokinetics and pharmacodynamics. a** | Representative positron emission tomography (PET) images of human subjects injected with ^{18}F-fluconazole. Images are displayed with a common colour scale (μg ml^{-1} tissue; reprinted with permission from REF. 35 © (1993) American Society for Microbiology). **b** | Axial, sagittal and coronal images of a healthy volunteer injected with the 5HT$_2$ ligand ^{18}F-setoperone to image serotonin (5HT$_2$) receptor occupancy. The top row is before and the bottom row after administration of 40 mg of oral ziprosidone, an antipsychotic agent with high affinity for serotonin and dopamine receptors. Fitting of cortical data was used to determine binding constants and receptor occupancy. Reprinted with permission from REF. 32 © (1996) American Society for Pharmacology and Experimental Therapeutics.

amount of a therapeutic drug that gets into the brain, the minimum effective dose, the duration of action or the binding-site occupancy required to elicit a particular therapeutic or behavioural effect. FIG. 3 shows one example of how imaging of the 5-HT$_2$ receptors in the human brain can be used to evaluate the effect of an oral dose of the antipsychotic agent ziprasidone within 4 h of administration[31,32].

Activatable, or smart, probes are fundamentally different from targeted probes in that they undergo chemical or physicochemical changes on target interaction and, as such, have a built-in amplification strategy. Examples of activatable imaging agents include caged near-infrared fluorochromes (NIRF)[2], paramagnetic agents that change spin-lattice relaxivity on activation[55] or superparamagnetic sensors[56]. One example of a protease activatable agent is shown in FIG. 4, in which matrix metalloproteinase (MMP)2 expression in tumours is visualized using an activatable NIRF agent[57]. Importantly, the efficacy of the model MMP2 inhibitor AG3340 (prinomastat) could be imaged directly after the initiation of drug therapy, and the dose could be tailored accordingly[57]. Activatable NIRF agents have now been developed for several proteases (BOX 1), and the number of available imaging agents is continuously growing. A recently established NIH database — the Molecular Imaging (MOLI) database (see online link) — links the rapidly growing number of imaging agents to the respective targets.

Targeted and activatable imaging probes are key enablers for visualizing drug–target interactions. From a drug developer's point of view, this is certainly a highly attractive feature; however, additional downstream read-outs of drug efficacy are equally important. These surrogate markers might include the activation of individual signalling pathways or markers of metabolic or physiological processes. In an ideal scenario, we would like to have both a direct target-specific read-out and a downstream effector read-out, a result that could be achieved with multichannel imaging[58]. Although the recently reported armamentarium of newer imaging probes is welcome, there remain two methodological hurdles: improving intracellular delivery and developing better amplification methods. Many of the potential molecular imaging targets are located intracellularly. In general, MRI and optical imaging use large reporter moieties, and although such probes can easily target endovascular receptors, interstitial targets or the lysosomal compartment, cytoplasmic or other intracellular locations are more difficult to access. More recently, signalling peptides have been used for intracellular targeting and directing imaging agents[59,60]. An alternative solution is to use radionuclide-labelled small molecules with improved cellular permeation. Another area of potential improvement concerns the development of more efficient biocompatible amplification strategies (both chemical and biological). These include, for example, multivalency to improve affinity[61], cellular internalization and trapping of imaging ligands[59,62,63], MR imaging agents with higher relaxivity and lower detection thresholds, chemical-shift reagents[64] or fluorescent lifetime agents to reduce background noise[65].

Optical technologies for molecular imaging

Continued advances in fluorescent probe design, photoproteins and detection systems are facilitating the application of novel imaging technologies in drug discovery. The adaptation of these tools to the imaging of deep tissues in live animals is now changing the way we visualize molecular processes *in vivo* and, ultimately, in the clinic. The primary enablers have been progress in mathematically modelling photon propagation in tissue, expanding biologically compatible near-infrared (NIR) probes and the introduction of highly sensitive photon-detection technologies. Fluorescence- and bioluminescence-imaging techniques are of particular interest to the drug discovery and development process because of their low cost,

Box 1 | Some examples of existing imaging targets/probes used for *in vivo* imaging

- **Proteases: cathepsin B, cathepsin D, cathepsin K, matrix metalloproteinase (MMP)1, MMP2, MMP7, cytomegalovirus protease, human immunodeficiency virus protease, herpes simplex virus protease, hepatitis C virus protease, caspase-1, caspase-3 and thrombin.**
- **Receptors: somatostatin, bombesin, dopamine D_2 and D_1, serotonin, benzodiazepine, opioid, acetylcholine, adrenoceptor, oestrogen, cholecystokinin, epidermal growth factor receptor, vascular endothelial growth factor receptor (VEGFR), glycoprotein Ib/IIIa, folate, insulin, neurokinin, transforming growth factor, asialoglycoprotein and adenosine 2.**
- **Enzymes: herpes simplex virus thymidine kinase, farnesyl transferase, toposiomerase, cytochrome p450, hexokinase, 3-hydroxyacyl-coenzymeA dehydrogenase (HAD), choline metabolism, citrate metabolism, protein synthesis (amino acids), Akt kinase, β-galactosidase and glutamate carboxipeptidase.**
- **Angiogenesis: E-selectin, $\alpha_v\beta_3$, VEGFR, human vascular cell adhesion molecule 1, endoglin (CD105), thrombin and endostatin.**
- **Apoptosis: annexin-V, caspase-3, PtdS-binding protein, synaptotagmin and tumour necrosis factor-related apoptosis-inducing ligand.**
- **Cellular tracking: CD8, CD4, CD34, neural progenitor cells, stem cells, macrophages, dendritic cells and tumour cells.**

versatility and high-throughput capability. There are several other optical techniques being developed, such as NIR spectroscopy[66,67], *in vivo* Raman spectroscopy[68] and multiphoton imaging[5,69].

In fluorescence imaging, the energy from an external source of light is absorbed and almost immediately re-emitted at a longer wavelength of lower energy. Fluorescence imaging can be carried out at different resolutions and depth penetrations ranging from micrometres (intravital microscopy[5]) to centimetres (FLUORESCENCE-MEDIATED MOLECULAR TOMOGRAPHY; FMT[70]). One of the key strategies for imaging deeper tissues (that is, more than a few millimetres) has been to use NIR light combined with NIR fluorochromes. Imaging in the NIR region has the advantage of minimizing tissue autofluorescence, which will improve target/background ratios. FLUORESCENCE REFLECTANCE IMAGING (FRI) can be a useful technique when probing superficial structures (<5 mm deep), for example in small animals[57], during endoscopy[71,72], dermatological imaging[73], intravascular catheter-based imaging or intraoperative imaging[74]. FMT, the newest optical imaging technology, has recently been shown to three-dimensionally localize and quantify fluorescent probes in deep tissues at high sensitivity. Indeed, it has become possible to image and, importantly, quantitate fluorochrome concentrations at femtomolar levels and at a sub-millimetre spatial resolution of point sources in small animals (FIG. 4, REF. 70). In the near future, FMT techniques are expected to markedly improve in spatial resolution by using higher-density detector systems and advanced photon technologies, such as modulated-intensity light or very-short photon pulses. Clinical FMT imaging applications will ultimately require highly efficient photon-collection systems, but penetration depths of up to 10 cm are theoretically achievable depending on tissue type[75].

Bioluminescence imaging (BLI) detects luminescence generated by a biochemical reaction during which a photon is released. Firefly luciferin (a benzothiazole) and photinus luciferase are the most commonly used substrate–enzyme pairs[76], although several other luciferase–luciferin combinations can be used for image generation[77,78]. Unlike fluorescence techniques, there is no inherent background signal, which means that BLI is highly sensitive. In contrast to radionuclide imaging techniques, the interpretation of bioluminescence images can be more challenging because of the frequent positional uncertainty of the light-emitting cells. Hence, the primary applications of BLI have so far been either qualitative ("Is luciferase expressed or not?") or as a semiquantitative imaging tool to follow the same animal under identical conditions. BLI has been used to monitor the efficacy of antibiotic or chemotherapeutic agents, to identify transgenic mice that use luciferase as a reporter gene and to visualize the activation of specific pathways and cellular processes[2,76,78]. BLI is less likely to be used in human patients, owing to limitations in light penetration and the fact that stable expression of luciferase (or an analogous system) is required to generate a signal.

FLUORESCENCE-MEDIATED TOMOGRAPHY
A tomographic reconstruction method developed for *in vivo* imaging of fluorescent probes. Images of deep structures are mathematically reconstructed by solving diffusion equations, under the assumption that photons have been scattered many times.

FLUORESCENCE REFLECTANCE IMAGING
A simple method of image acquisition similar to fluorescence microscopy, except that different optics allow image acquisition of whole animals. Mostly suited for surface tumours or surgically exposed tumours.

Impact of imaging on drug discovery

The above examples illustrate the potential of established and emerging imaging technologies in drug discovery and development. When applied properly, imaging methods offer several advantages over other current practices. The use of imaging end points instead of time-consuming dissection and histology can significantly decrease the workload involved in tissue analysis and thereby speed up the evaluation of drug candidates. Imaging might provide biomarkers of a disease process and therefore help to define stratified study groups. As imaging methods are non-invasive, they allow for longitudinal studies in a single animal. This increases the statistical relevance of a study, allows for more clinically relevant study designs and decreases the number of animals required. Imaging will also provide important information on the optimal timing and dosing of drugs. Finally, emerging molecular-imaging tools can provide much earlier surrogate markers of therapy success than is at present possible.

In view of these arguments, it is reasonable to assume that imaging might reduce the development time of new drugs and provide tools for faster proof-of-concept testing in clinical studies. The latter is of key interest to the pharmaceutical industry, so why are molecular-imaging biomarkers not already being widely used as end points in clinical trials? First, regulatory agencies have historically relied on end points that require lengthy trials (for example, survival) rather than embracing new read-outs (for example, imaging vascular endothelial growth factor (VEGF)-receptor expression or a downstream target for a VEGF-receptor tyrosine kinase inhibitor). This is in part due to the fact that many of the newer imaging tools have not yet been sufficiently validated, at least for regulatory purposes. Second, molecular-imaging biomarkers, at present, exist only for a few targets and/or pathways and substantial development is still required. Third, molecular-imaging agents have to undergo lengthy approval processes (often longer than for a therapeutic agent) before their clinical use. Fourth, despite the efforts of various organizations in Europe and the United States (for example, the Society for Noninvasive Imaging in Drug Discovery (SNIDD); see online links), the interactions

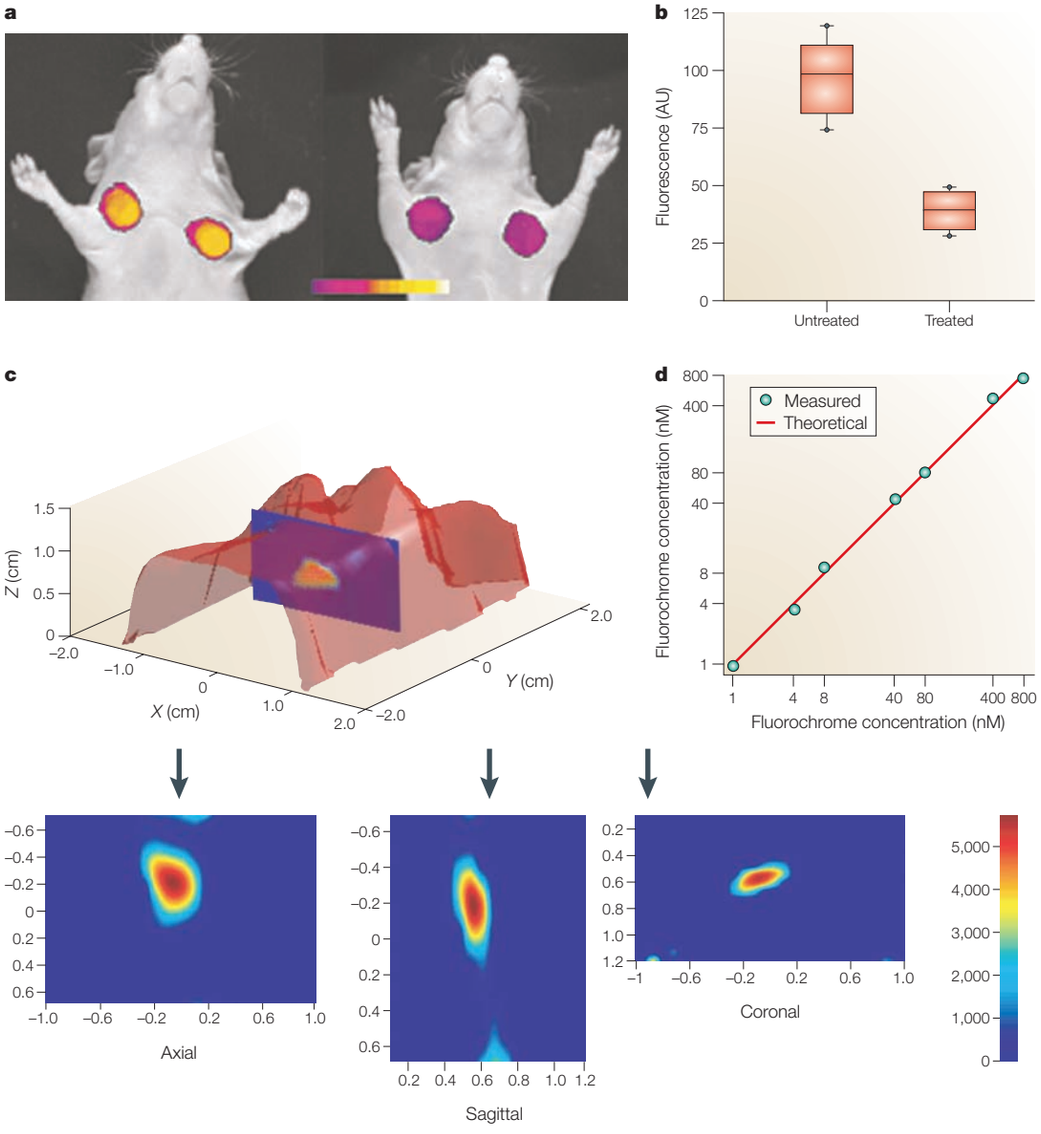

Figure 4 | **Fluorescence molecular imaging. a** | Visualization of matrix metalloproteinase (MMP)2 inhibition in a mouse tumour model using an MMP2-activatable, near-infrared (NIR) imaging probe and fluorescence reflecting imaging (FRI). Colour-coded in tumours maps of MMP2 activity are shown merged onto white-light images. **b** | Before treatment, in tumours MMP2 activity is high and decreases markedly within 48 h of an intravenous dose (150 mg kg^{-1}) of the MMP inhibitor prinomastat. Reprinted with permission from REF. 57 © (2001) Macmillan Magazines Ltd. **c** | Quantitative fluorescence-mediated tomography (FMT) imaging[70] in a mouse model of lung tumour. The animal had been treated with cisplatin and treatment efficacy is shown as binding of NIR fluorochrome-annexin V to apoptotic tumour cells. The bottom row shows reconstructions of the tumour in the three orthogonal planes. Images courtesy of V. Ntziachristos and R. Schulz. **d** | Accuracy of reconstructed fluorochrome concentrations from within tissue phantom.

between the larger imaging and drug development communities have been limited. This is partly due to intellectual property issues but also because of National Institutes of Health priorities in funding disease detection and characterization rather than the development of biomarkers. It is clear that closer and more widespread interactions between these communities would be of mutual interest. Finally, imaging competes with alternative technologies that can provide similar decision-making information; genomic and proteomic sciences detect altered expression levels associated with disease and/or therapy response, and metabonomics potentially yields biomarkers for drug efficacy or for potential safety issues[79].

Given the broad possibilities, it seems obvious that the pharmaceutical industry must invest in conventional and novel imaging technologies — indeed, we believe it should drive specific developments for its unique needs. This is particularly true for molecular-imaging applications, for which imaging and therapeutic targets are often the same. A highly specific therapy depends crucially on surveillance strategies (diagnostic kits), which allow for patient selection and close monitoring of the therapy response. Obtaining objective readouts for a patient might also help in tailoring the dosing regimen. The prerequisites for new imaging agents and approaches are clear: the techniques have to be quantitative, reproducible, specific, sensitive, applicable to clinical practice and safe. Developing novel imaging techniques and agents as part of the drug discovery process therefore seems a logical choice. Not only will this speed up drug discovery, but it will also ultimately reduce costs and result in better medicines.

1. Weissleder, R. Scaling down imaging: molecular mapping of cancer in mice. *Nature Rev. Cancer* **2**, 11–18 (2002).
Review of *in vivo* mouse imaging technologies.
2. Weissleder, R. & Ntziachristos, V. Shedding light onto live molecular targets. *Nature Med.* **9**, 123–128 (2003).
This manuscript reviews emerging novel optical *in vivo* imaging technologies.
3. Rudin, M. *et al. In vivo* magnetic resonance methods in pharmaceutical research: current status and perspectives. *NMR Biomed.* **12**, 69–97 (1999).
Review of MR technologies in drug development.
4. Beckmann, N., Mueggler, T., Allegrini, P. R., Laurent, D. & Rudin, M. From anatomy to the target: contributions of magnetic resonance imaging to preclinical pharmaceutical research. *Anat. Rec.* **265**, 85–100 (2001).
5. Jain, R. K., Munn, L. L. & Fukumura, D. Dissecting tumour pathophysiology using intravital microscopy. *Nature Rev. Cancer* **2**, 266–276 (2002).
6. Phelps, M. E. Inaugural article: positron emission tomography provides molecular imaging of biological processes. *Proc. Natl Acad. Sci. USA* **97**, 9226–9233 (2000).
Review of PET imaging applications.
7. Fischman, A. J., Alpert, N. M. & Rubin, R. H. Pharmacokinetic imaging: a noninvasive method for determining drug distribution and action. *Clin. Pharmacokinet.* **41**, 581–602 (2002).
Review of the role of PET in the study of drug pharmacokinetics.
8. Reese, T., Bochelen, D., Sauter, A., Beckmann, N. & Rudin, M. Magnetic resonance angiography of the rat cerebrovascular system without the use of contrast agents. *NMR Biomed.* **12**, 189–196 (1999).
9. Villringer, A. *et al.* Dynamic imaging with lanthanide chelates in normal brain: contrast due to magnetic susceptibility effects. *Magn. Reson. Med.* **6**, 164–174 (1988).
10. Roussel, S. A., van Bruggen, N., King, M. D. & Gadian, D. G. Identification of collaterally perfused areas following focal cerebral ischemia in the rat by comparison of gradient echo and diffusion-weighted MRI. *J. Cereb. Blood Flow Metab.* **15**, 578–586 (1995).
11. Moseley, M., Wendland, M. & Kucharczyk, J. Magnetic resonance imaging of diffusion and perfusion. *Top. Magn. Reson. Imag.* **3**, 50–67 (1991).
12. Sauter, A. & Rudin, M. Calcium antagonists reduce the extent of infarction in rat middle cerebral artery occlusion model as determined by quantitative magnetic resonance imaging. *Stroke* **17**, 1228–1234 (1986).
13. Rausch, M., Baumann, D., Neubacher, U. & Rudin, M. *In vivo* visualization of phagocytotic cells in rat brains after transient ischemia by USPIO. *NMR Biomed.* **15**, 278–283 (2002).
14. Sauter, A. *et al.* Recovery of function in cytoprotected cerebral cortex in rat stroke model assessed by functional MRI. *Magn. Reson. Med.* **47**, 759–765 (2002).
15. Cristofanilli, M., Charnsangavej, C. & Hortobagyi, G. N. Angiogenesis modulation in cancer research: novel clinical approaches. *Nature Rev. Drug Discov.* **1**, 415–426 (2002).
16. Tatum, J. L. & Hoffman, J. M. Role of imaging in clinical trials of antiangiogenesis therapy in oncology. *Acad. Radiol.* **7**, 798–799 (2000).
17. Bhujwalla, Z. M. *et al.* The physiological environment in cancer vascularization, invasion and metastasis. *Novartis Found. Symp.* **240**, 23–38; discussion 38–45, 152–153 (2001).
18. Lewin, M. *et al. In vivo* assessment of vascular endothelial growth factor-induced angiogenesis. *Int. J. Cancer* **83**, 798–802 (1999).
19. Petrovsky, A., Weissleder, W., Shalinsky, D., Hu-Lowe, D. & Bogdanov, A. Non-invasive magnetic resonance imaging (MRI) of vascular parameters affected by VEGF–receptor tyrosine kinase inhibition in a human xenograft model. *Proc. Am. Assoc. Cancer Res.* **43**, 1081 (2002).
20. Peterfy, C. G. Magnetic resonance imaging of rheumatoid arthritis: the evolution of clinical applications through clinical trials. *Semin. Arthritis Rheum.* **30**, 375–396 (2001).
21. McConnell, M. V. *et al.* MRI of rabbit atherosclerosis in response to dietary cholesterol lowering. *Arterioscler. Thromb. Vasc. Biol.* **19**, 1956–1959 (1999).
22. Chinnaiyan, A. M. *et al.* Combined effect of tumor necrosis factor-related apoptosis-inducing ligand and ionizing radiation in breast cancer therapy. *Proc. Natl Acad. Sci. USA* **97**, 1754–1759 (2000).
23. Jennings, D. *et al.* Early response of prostate carcinoma xenografts to docetaxel chemotherapy monitored with diffusion MRI. *Neoplasia* **4**, 255–262 (2002).
24. Evelhoch, J. L. *et al.* Applications of magnetic resonance in model systems: cancer therapeutics. *Neoplasia* **2**, 152–165 (2000).
25. Cherry, S. R. Fundamentals of positron emission tomography and applications in preclinical drug development. *J. Clin. Pharmacol.* **41**, 482–491 (2001).
26. Del Guerra, A. & Belcari, N. Advances in animal PET scanners. *Q. J. Nucl. Med.* **46**, 35–47 (2002).
27. Green, L. A. *et al.* Noninvasive methods for quantitating blood time–activity curves from mouse PET images obtained with fluorine-18-fluorodeoxyglucose. *J. Nucl. Med.* **39**, 729–734 (1998).
28. Chatziioannou, A., Tai, Y. C., Doshi, N. & Cherry, S. R. Detector development for microPET II: a 1 microl resolution PET scanner for small animal imaging. *Phys. Med. Biol.* **46**, 2899–2910 (2001).
29. Brady, F. *et al.* Radiolabelled tracers and anticancer drugs for assessment of therapeutic efficacy using PET. *Curr. Pharm. Des.* **7**, 1863–1892 (2001).
30. Halldin, C., Gulyas, B. & Farde, L. PET studies with carbon-11 radioligands in neuropsychopharmacological drug development. *Curr. Pharm. Des.* **7**, 1907–1929 (2001).
Review of PET in the development of drugs for mental health disorders.
31. Fischman, A. J. *et al.* Pharmacokinetics of ^{18}F fleroxacin in patients with acute exacerbations of chronic bronchitis and complicated urinary tract infection studied by positron emission tomography. *Antimicrob. Agents Chemother.* **40**, 659–664 (1996).
32. Fischman, A. J. *et al.* Positron emission tomographic analysis of central 5-hydroxytryptamine2 receptor occupancy in healthy volunteers treated with the novel antipsychotic agent, ziprasidone. *J. Pharmacol. Exp. Ther.* **279**, 939–947 (1996).
33. Aboagye, E. O. *et al.* Cancer Research UK procedures in manufacture and toxicology of radiotracers intended for pre-phase I positron emission tomography studies in cancer patients. *Br. J. Cancer* **86**, 1052–1056 (2002).
34. Gibson, R. E. *et al.* Non-invasive radiotracer imaging as a tool for drug development. *Curr. Pharm. Des.* **6**, 973–989 (2000).
35. Fischman, A. J. *et al.* Pharmacokinetics of ^{18}F-labeled fluconazole in healthy human subjects by positron emission tomography. *Antimicrob. Agents Chemother.* **37**, 1270–1277 (1993).
36. Capdeville, R., Buchdunger, E., Zimmermann, J. & Matter, A. Glivec (STI571, imatinib), a rationally developed, targeted anticancer drug. *Nature Rev. Drug Discov.* **1**, 493–502 (2002).
37. Coussens, L. M., Fingleton, B. & Matrisian, L. M. Matrix metalloproteinase inhibitors and cancer: trials and tribulations. *Science* **295**, 2387–2392 (2002).
38. Warner, R. R. & O'Dorisio T. M. Radiolabeled peptides in diagnosis and tumor imaging: clinical overview. *Semin. Nucl. Med.* **32**, 79–83 (2002).
39. Becker, A. *et al.* Receptor-targeted optical imaging of tumors with near-infrared fluorescent ligands. *Nature Biotechnol.* **19**, 327–331 (2001).
40. Bugaj, J. E., Achilefu, S., Dorshow, R. B. & Rajagopalan, R. Novel fluorescent contrast agents for optical imaging of *in vivo* tumors based on a receptor-targeted dye–peptide conjugate platform. *J. Biomed. Opt.* **6**, 122–133 (2001).
41. Tung, C. H., Lin, Y., Moon, W. K. & Weissleder, R. A receptor-targeted near-infrared fluorescence probe for *in vivo* tumor imaging. *Chembiochem* **3**, 784–786 (2002).
42. Weissleder, R. *et al. In vivo* magnetic resonance imaging of transgene expression. *Nature Med.* **6**, 351–355 (2000).
43. Hogemann, D., Ntziachristos, V., Josephson, L. & Weissleder, R. High throughput magnetic resonance imaging for evaluating targeted nanoparticle probes. *Bioconjug. Chem.* **13**, 116–121 (2002).
44. Sipkins, D. A. *et al.* Detection of tumor angiogenesis *in vivo* by αVβ3-targeted magnetic resonance imaging. *Nature Med.* **4**, 623–626 (1998).
45. Burns, H. D. *et al.* Positron emission tomography neuroreceptor imaging as a tool in drug discovery, research and development. *Curr. Opin. Chem. Biol.* **3**, 388–394 (1999).
46. Hartvig, P., Bergstrom, M., Antoni, G. & Langstrom, B. Positron emission tomography and brain monoamine neurotransmission — entries for study of drug interactions. *Curr. Pharm. Des.* **8**, 1417–1434 (2002).
47. Fowler, J. S. *et al.* Positron emission tomography studies of dopamine-enhancing drugs. *J. Clin. Pharmacol.* (Suppl.) 13–16 (1999).
48. Hietala, J. Ligand–receptor interactions as studied by PET: implications for drug development. *Ann. Med.* **31**, 438–443 (1999).
49. Laakso, A. & Hietala, J. PET studies of brain monoamine transporters. *Curr. Pharm. Des.* **6**, 1611–1623 (2000).
50. Passchier, J. & van Waarde, A. Visualisation of serotonin-1A (5-HT1A) receptors in the central nervous system. *Eur. J. Nucl. Med.* **28**, 113–129 (2001).
51. Pilowsky, L. S. Probing targets for antipsychotic drug action with PET and SPET receptor imaging. *Nucl. Med. Commun.* **22**, 829–833 (2001).
52. Volkow, N. D., Ding, Y. S., Fowler, J. S. & Gatley, S. J. Imaging brain cholinergic activity with positron emission tomography: its role in the evaluation of cholinergic treatments in Alzheimer's dementia. *Biol. Psychiatry* **49**, 211–220 (2001).
53. Waarde, A. Measuring receptor occupancy with PET. *Curr. Pharm. Des.* **6**, 1593–1610 (2000).

54. Martinez, D. *et al.* Differential occupancy of somatodendritic and postsynaptic 5HT(1A) receptors by pindolol: a dose-occupancy study with ^{11}C WAY 100635 and positron emission tomography in humans. *Neuropsychopharmacology* **24**, 209–229 (2001).
55. Louie, A. Y. *et al.* *In vivo* visualization of gene expression using magnetic resonance imaging. *Nature Biotechnol.* **18**, 321–325 (2000).
56. Perez, J. M., Josephson, L., O'Loughlin, T., Hogemann, D. & Weissleder, R. Magnetic relaxation switches capable of sensing molecular interactions. *Nature Biotechnol.* **20**, 816–820 (2002).
57. Bremer, C., Tung, C. H. & Weissleder, R. *In vivo* molecular target assessment of matrix metalloproteinase inhibition. *Nature Med.* **7**, 743–748 (2001).
58. Mahmood, U., Tung, C. H., Tang, Y. & Weissleder, R. Feasibility of *in vivo* multichannel optical imaging of gene expression: experimental study in mice. *Radiology* **224**, 446–451 (2002).
59. Lewin, M. *et al.* Tat peptide-derivatized magnetic nanoparticles allow *in vivo* tracking and recovery of progenitor cells. *Nature Biotechnol.* **18**, 410–414 (2000).
60. Sharma, V., Luker, G. D. & Piwnica-Worms, D. Molecular imaging of gene expression and protein function *in vivo* with PET and SPECT. *J. Magn. Reson. Imaging* **16**, 336–351 (2002).
61. Zhao, M., Kircher, M. F., Josephson, L. & Weissleder, R. Differential conjugation of tat peptide to superparamagnetic nanoparticles and its effect on cellular uptake. *Bioconjug. Chem.* **13**, 840–844 (2002).
62. Tjuvajev, J. G. *et al.* Imaging the expression of transfected genes *in vivo*. *Cancer Res.* **55**, 6126–6132 (1995).
63. Gambhir, S. S. *et al.* Imaging adenoviral-directed reporter gene expression in living animals with positron emission tomography. *Proc. Natl Acad. Sci. USA* **96**, 2333–2338 (1999).
64. Li, X., Zhang, S., Zhao, P., Kovacs, Z. & Sherry, A. D. Synthesis and NMR studies of new DOTP-like lanthanide(III) complexes containing a hydrophobic substituent on one phosphonate side arm. *Inorg. Chem.* **40**, 6572–6579 (2001).
65. Bornhop, D. J. *et al.* Fluorescent tissue site-selective lanthanide chelate, Tb-PCTMB for enhanced imaging of cancer. *Anal. Chem.* **71**, 2607–2615 (1999).
66. Tromberg, B. J. *et al.* Non-invasive *in vivo* characterization of breast tumors using photon migration spectroscopy. *Neoplasia* **2**, 26–40 (2000).
67. Chance, B. Near-infrared (NIR) optical spectroscopy characterizes breast tissue hormonal and age status. *Acad. Radiol.* **8**, 209–210 (2001).
68. Hanlon, E. B. *et al.* Prospects for *in vivo* Raman spectroscopy. *Phys. Med. Biol.* **45**, R1–R59 (2000).
69. Brown, E. B. *et al.* *In vivo* measurement of gene expression, angiogenesis and physiological function in tumors using multiphoton laser scanning microscopy. *Nature Med.* **7**, 864–868 (2001).
70. Ntziachristos, V., Tung, C. H., Bremer, C. & Weissleder, R. Fluorescence molecular tomography resolves protease activity *in vivo*. *Nature Med.* **8**, 757–760 (2002).
71. Marten, K. *et al.* Detection of dysplastic intestinal adenomas using enzyme-sensing molecular beacons in mice. *Gastroenterology* **122**, 406–414 (2002).
72. Ito, S. *et al.* Detection of human gastric cancer in resected specimens using a novel infrared fluorescent anti-human carcinoembryonic antigen antibody with an infrared fluorescence endoscope *in vitro*. *Endoscopy* **33**, 849–853 (2001).
73. Zonios, G., Bykowski, J. & Kollias, N. Skin melanin, hemoglobin, and light scattering properties can be quantitatively assessed *in vivo* using diffuse reflectance spectroscopy. *J. Invest. Dermatol.* **117**, 1452–1457 (2001).
74. Kuroiwa, T., Kajimoto, Y. & Ohta, T. Development and clinical application of near-infrared surgical microscope: preliminary report. *Minim. Invasive. Neurosurg.* **44**, 240–242 (2001).
75. Ntziachristos, V., Ripoll, J. & Weissleder, R. Would near-infrared fluorescence signals propagate through large human organs for clinical studies? *Opt. Lett.* **27**, 333–335 (2002).
76. Contag, C. H. *et al.* Visualizing gene expression in living mammals using a bioluminescent reporter. *Photochemistry & Photobiology* **66**, 523–531 (1997).
77. Hastings, J. W. Chemistries and colors of bioluminescent reactions: a review. *Gene* **173**, 5–11 (1996).
78. Bhaumik, S. & Gambhir, S. S. Optical imaging of Renilla luciferase reporter gene expression in living mice. *Proc. Natl Acad. Sci. USA* **99**, 377–382 (2002).
79. Nicholson, J. K., Connelly, J., Lindon, J. C. & Holmes, E. Metabonomics: a platform for studying drug toxicity and gene function. *Nature Rev. Drug Discov.* **1**, 153–161 (2002).

Online links

FURTHER INFORMATION

Academy of Molecular Imaging (AMI): http://www.ami-imaging.org
Encyclopedia of Life Sciences: http://www.els.net
computer tomography | magnetic resonance imaging
Molecular Imaging (MOLI) Database: http://207.238.28.146
Society for Magnetic Resonance in Medicine (ISMRM): http://www.ismrm.org
Society for Molecular Imaging (SMI): http://www.molecularimaging.org
Society for Non-invasive Imaging in Drug Discovery (SNIDD): http://www.snidd.org
Society of Nuclear Medicine (SNM): http://www.snm.org
Access to this interactive links box is free online.

CREATING NEW FLUORESCENT PROBES FOR CELL BIOLOGY

Jin Zhang, Robert E. Campbell*, Alice Y. Ting*‡ and Roger Y. Tsien*§*

Fluorescent probes are one of the cornerstones of real-time imaging of live cells and a powerful tool for cell biologists. They provide high sensitivity and great versatility while minimally perturbing the cell under investigation. Genetically-encoded reporter constructs that are derived from fluorescent proteins are leading a revolution in the real-time visualization and tracking of various cellular events. Recent advances include the continued development of 'passive' markers for the measurement of biomolecule expression and localization in live cells, and 'active' indicators for monitoring more complex cellular processes such as small-molecule-messenger dynamics, enzyme activation and protein–protein interactions.

PHOTOBLEACHING
The irreversible destruction, by any one of a number of different mechanisms, of a fluorophore that is under illumination.

**Department of Pharmacology and §Department of Chemistry, Massachusetts Institute of Technology, 77 Massachusetts Avenue, 18–496, Cambridge, Massachusetts 02139, USA.*
‡Department of Chemistry & Biochemistry and Howard Hughes Medical Institute, University of California, San Diego, 9500 Gilman Drive, La Jolla, California 92093–0647, USA.
Correspondence to R.Y.T
e-mail: rtsien@ucsd.edu
doi:10.1038/nrm976

Our understanding of biological systems is increasingly dependent on our ability to visualize and quantify signalling molecules and events with high spatial and temporal resolution in the cellular context. Advances in fluorescence microscopy and the engineering of the green fluorescent protein (GFP) from *Aequorea victoria* into mutants with improved properties and altered colours have provided the basic tools that allow the investigation of more complex processes in live cells. The primary advantages of fluorescent protein-based indicators over simple organic dyes are that they can be designed to respond to a much greater variety of biological events and signals, targeted to subcellular compartments, introduced into a wider variety of tissues and intact organisms, and they very rarely cause photodynamic toxicity. This review highlights recent advances in the development of fluorescent probes for cellular applications, and focuses on those that can resolve spatial and temporal patterns through targeting to subcellular compartments. As the number of successful genetically-encoded reporters increases, several design trends and considerations are becoming apparent (BOX 1). We highlight the most versatile and modular of these designs as the blueprints for the construction of new and better reporters.

Recent advances in fluorescent proteins

New variants of green fluorescent protein. There is a continuing effort to develop new GFP variants with altered excitation and emission wavelengths, enhanced brightness and an improved pH resistance relative to the original enhanced green (for example, S65T and EGFP), cyan (CFP), and yellow (YFP) variants[1–5]. From now on we refer to the entire class of *Aequorea*-derived fluorescent proteins as AFPs, whereas we use 'GFP' to denote green members of that family. The newest colour in the AFPs is 'CGFP', the Thr203Tyr mutant of CFP (where Thr is threonine and Tyr is tyrosine). CGFP has an excitation and emission wavelength that is intermediate between CFP and EGFP[2]. Despite its dimness and broad excitation and emission peaks, the remarkably pH-resistant CGFP might find a use in the labelling of acidic organelles. First-generation YFPs such as GFP–Ser65Gly/Ser72Ala/Thr203Tyr[6] (where Ser is serine, Gly is glycine and Ala is alanine) were notorious for their sensitivity to pH, chloride fluctuations and PHOTOBLEACHING. A second-generation enhanced YFP (YFP–Val68Leu/Gln69Lys; where Val is valine, Leu is leucine, Gln is glutamine and Lys is lysine) slightly improved acid resistance, but only in third-generation derivatives named 'Citrine'[3] (YFP–Val68Leu/Gln69Met; where Met is methionine) and 'Venus'[4] (YFP–Phe46Leu/Phe64Leu/Met153Thr/Val163Ala/Ser175Gly; where

Box 1 | **Considerations in designing and constructing AFP-based fluorescent reporters**

Choice of *Aequorea* fluorescent protein (AFP) variant(s)
- For intermolecular fluorescence resonance energy transfer (FRET)-based reporters (FIG. 5a), non-oligomerizing cyan fluorescent protein (CFP) and yellow fluorescent protein (YFP) variants that incorporate the Ala206Lys mutation (where Ala is alanine and Lys is lysine) are strongly recommended.
- For intramolecular FRET-based reporters (FIG. 5b), CFP should be paired with one of the latest generation YFPs such as Citrine or Venus. Further improvements to monomeric red fluorescent protein (mRFP) should provide a new FRET partner for GFP.
- For single-fluorophore conformation-sensitive reporters (FIG. 4), insertion at Tyr145 (where Tyr is tyrosine), or the use of a circularly permuted AFP or YFP is recommended.

Spectral response
- The dynamic response range of the reporter must span physiologically relevant conditions.
- A ratiometric response, as obtained from a FRET reporter, is preferable to a simple increase in fluorescence intensity.
- For most reporter constructs, optimization of polypeptide linkers between components of the reporter is crucial for the success of the construct or for maximizing the fluorescent response.

Spatio-temporal resolution
- Spatio-temporal resolution will be lost with a freely diffusing cytosolic reporter that responds slowly relative to the timescale of diffusion.
- Genetic targeting to a compartment or anchoring to a subcellular structure can improve spatio-temporal resolution.

Perturbation of intracellular conditions
- Depending on the design strategy and the expression level, the introduction of the reporter might perturb the cellular component of interest or be toxic.

Specificity
- The reporter must respond to only the stimulus of interest.
- Genetic targeting can help increase biological specificity.

Versatile molecular construction
- Consideration of the available structural data can provide a rational basis for reporter construction.
- Ideally, the design strategy should be transferable to other members of the same protein family and structural homologues.

Phe is phenylalanine) has the chloride sensitivity been eliminated and the sensitivity to pH changes and photobleaching improved greatly. Specifically, Citrine remains 50% fluorescent at the lowest pH (5.7) that has been reported so far for a YFP and shows a twofold increase in photostability relative to YFP–Val68Leu/Gln69Lys, whereas Venus is the brightest and fastest maturing (with reference to the development of fluorescence) YFP so far. Unfortunately, simply transferring the crucial Gln69Met mutation of Citrine to Venus did not confer improved photostability[4] on Venus, and so there is not yet a single YFP that is superior for all applications.

Fluorescent 'highlighters'. Fluorescent proteins that can be modulated photochemically are molecular 'highlighters' that allow specific organelles or protein subpopulations to be marked by brief, localized, intense illumination and then tracked in space and time. Early versions showed only a modest contrast[7] or could only be used under anaerobic conditions[8,9]. A new YFP mutant, 'PA–GFP' (GFP–Val163Ala/Thr203His; where His is histidine) undergoes up to a 100-fold increase in fluorescence (excitation at 488 nm) when illuminated at 413 nm[10]. An even more spectacular fluorescent protein is 'Kaede' from the stony coral *Trachyphyllia geoffroyi*, which can be converted from a green to a stable red fluorescent protein by irradiation with 350–400-nm light[11]. This colour change corresponds to a 2,000-fold increase in the red to green ratio and allows both the irradiated and unirradiated species to be visualized separately with excitation wavelengths (475 and 550 nm) that do not cause any further colour change. At present, Kaede exists as a tetramer; if it can be mutated to a monomer, it should match or surpass PA–GFP in its ability to reveal the dynamic trafficking of fusion proteins.

In addition to the photoenhancement of fluorescence described above, AFP fusions find use in fluorescence recovery after photobleaching (FRAP), fluorescence loss in photobleaching (FLIP), and fluorescence correlation spectroscopy (FCS) — other powerful techniques that can assess protein trafficking and mobility in live cells (for a review, see REF. 12).

Limiting monomer–monomer interactions. The only instance when the weak tendency of AFPs to dimerize has been documented to cause artefacts or dysfunction was in the clustering of lipid-anchored AFPs on the plasma membrane[13]. At high concentrations, AFPs might interact with each other, which results in a false-positive interaction as determined by

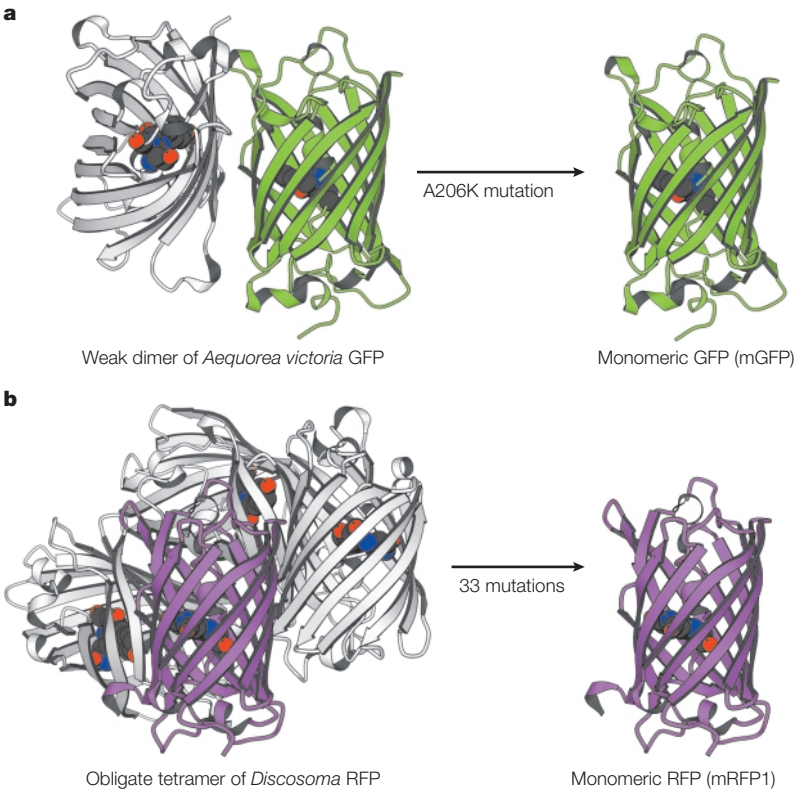

Figure 1 | **Recent advances in fluorescent proteins. a** | Introduction of the A206K mutant in *Aequorea* fluorescent proteins (AFPs) suppresses their tendency to dimerize. **b** | Several rounds of directed evolution and a total of 33 mutations were required to rescue the red fluorescence of a *Discosoma* red fluorescent protein (RFP) (DsRed or drFP583)-derived monomer following the introduction of interface-disrupting mutations.

FLUORESCENCE RESONANCE ENERGY TRANSFER (FRET). The non-radiative transfer of energy from a donor fluorophore to an acceptor fluorophore that is typically < 80 Å away. FRET will only occur between fluorophores in which the emission spectrum of the donor has a significant overlap with the excitation of the acceptor.

QUANTUM YIELD
The probability of luminescence occurring in given conditions — expressed by the ratio of the number of photons that are emitted by the luminescing species to the number of photons that are absorbed.

FLUORESCENCE RESONANCE ENERGY TRANSFER (FRET). This tendency to dimerize[14,15] can be reduced greatly or eliminated by mutating the hydrophobic amino acids that are in the dimerization interface to positively charged residues[13]. In AFPs, the effectiveness of these mutations increases in the order Phe223Arg < Leu221Lys < Ala206Lys (where Arg is arginine; FIG. 1a). It would now seem prudent to routinely use non-dimerizing mutants such as Ala206Lys when testing protein–protein interactions, or when AFP fusion proteins seem to be causing mis-targeting or dysfunction[13].

Long-wavelength red fluorescent proteins. Long-wavelength fluorescent proteins have long been sought for multicolour protein-tracking applications and for the construction of improved FRET-based reporters. Red fluorescence should provide greater tissue penetration and better spectral separation from cellular autofluorescence than either yellow or green fluorescence. The first red fluorescent protein (RFP) to be discovered was isolated from a coral of the *Discosoma* genus (this RFP is known as DsRed or drFP583)[16] and was received with much excitement, but its use has been limited severely by a number of problems. The DsRed protein requires incubation at 37°C for more than 30 h for the red fluorescence to reach a steady-state level, and a significant fraction of the protein retains the green fluorescent 490-nm excitation peak that is associated with its 'GFP-like' intermediate. In addition, DsRed is an obligate tetramer that will almost certainly tetramerize any cellular protein to which it is fused[17,18]. If the fusion partner is a monomeric protein, tetramerization might not necessarily be detrimental, but if the partner has any tendency to oligomerize by itself, gross aggregation and precipitation of the fusion is likely. If aggregation does occur, one strategy that has proven successful for both hexameric connexin-43 (REF. 19) and dimeric thymidine kinase[20] fused to DsRed, is to co-express either the unfused or EGFP-fused target protein, but this approach requires the titration of co-expression levels and dilution of the desired red signal.

A more universal solution to the problem of oligomerization is to re-engineer the RFP using a combination of targeted and random mutagenesis to minimize the oligomerization and other limitations of wild-type DsRed[21–25]. The original commercially available form of DsRed (known as DsRed1), which incorporated mammalian codon-usage preferences, was replaced by DsRed2, which showed a 2–3-fold improvement in the speed of fluorescence maturation at 37°C and a diminished 475-nm excitation peak[22,26]. DsRed2 has, in turn, been effectively superseded by T1, which reaches its full red fluorescence within tens of minutes[23]. T1 is now commercially available as DsRed-Express (Clontech, Palo Alto, USA). The first effectively non-oligomerizing RFPs came with the development of red fluorescent tandem dimers, in which two dimer-forming subunits are concatenated with a spacer that allows them to satisfy their crucial dimer interactions through intramolecular contacts[24,27]. The most recent advance is the engineering of a completely monomeric DsRed variant (mRFP1) that matures quickly, has no residual green fluorescence and excitation and emission wavelengths that are about 25 nm longer than the previous DsRed variants[24] (FIG. 1b). At present, mRFP1 is probably the best starting point for the construction of red fluorescent fusion proteins, even though it sacrifices some QUANTUM YIELD and photostability relative to the tandem dimer that is derived from DsRed (REF. 24).

Finding more fluorescent proteins. The search for new fluorescent proteins in coelenterate marine organisms has resulted in the discovery and cloning of approximately 30 distinct fluorescent proteins, although all but a handful of these remain minimally characterized[28,29]. Several of these proteins that deserve a special mention include: the dimeric *Renilla mulleri* GFP, with its exceptionally narrow excitation (498 nm) and emission (509 nm) peaks[30]; the DsRed homologues asFP595 (REF. 31) from *Anemonia sulcata* and dsFP593 (REF. 32) from *Discosoma*, which were engineered for improved red fluorescence at 595 nm and 616 nm respectively; the dimeric but dim HcRed from *Heteractis crispa*, which was derived from a tetrameric non-fluorescent chromoprotein and emits at 618 nm[26,33]; and finally eqFP611 from *Entacmaea quadricolor*, a tetrameric red fluorescent protein that emits at 611 nm and that can be dissociated to monomers at a high dilution[34].

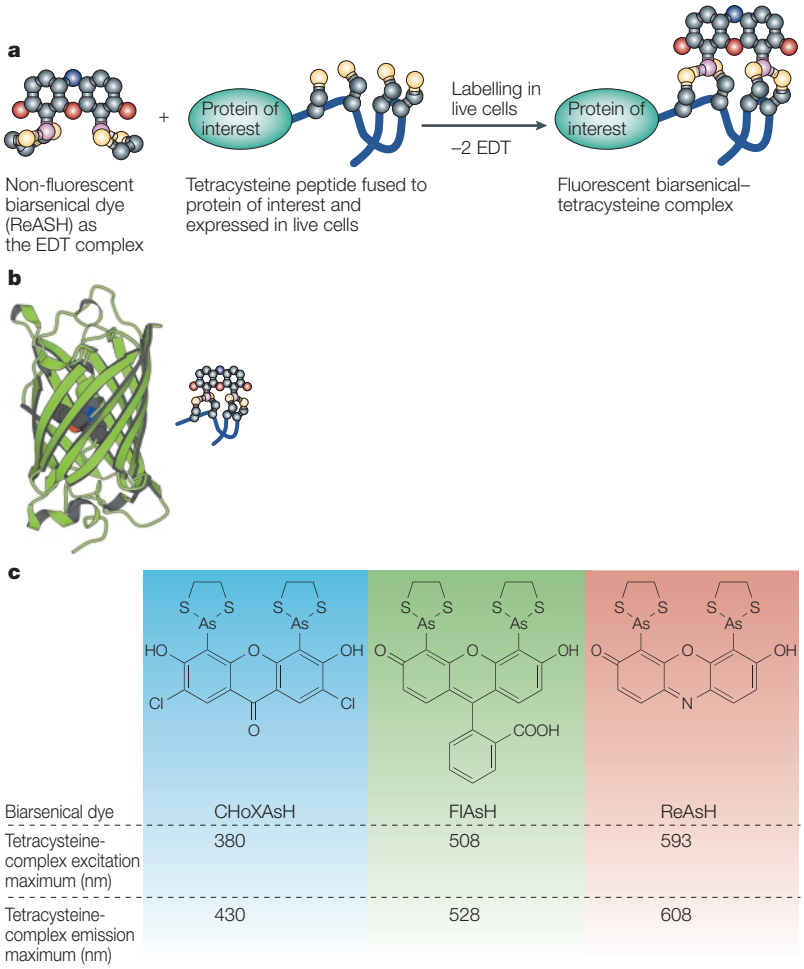

Figure 2 | **The biarsenical–tetracysteine system. a** | A non-fluorescent membrane-permeable biarsenical dye (ReAsH shown) forms specifically a fluorescent covalent complex with any intracellular protein to which a short tetracysteine-containing peptide (CCPGCC) has been genetically fused. The small size of the biarsenical dyes might be advantageous in those cases where a bulky *Aequorea* fluorescent protein (AFP) fusion disrupts normal protein function. The arsenical antidote ethanedithiol (EDT) is used to minimize the toxicity of any unbound biarsenical-dye. **b** | A comparison of the to-scale images of the green fluorescent protein (GFP) and biarsenical–tetracysteine complex. **c** | Fluorescent biarsenical labels that span the visible spectrum have been synthesized.

Recent advances in small molecule probes. Although GFP and its variants are extremely useful for tracking the expression and localization of proteins in cells, small-molecule probes with less steric bulk, faster rates of labelling and the ability to provide readouts in addition to, or other than, fluorescence are desirable.

The biarsenical–tetracysteine system. A promising alternative to GFP is the biarsenical–tetracysteine system (FIG. 2a) in which a recombinant protein that is expressed in a living cell is site-specifically labelled with a membrane-permeable biarsenical dye, which can be blue, green or red fluorescent (FIG. 2c)[35–37]. The specificity for the labelling reaction is provided by a small tetracysteine motif (at present, CCPGCC is the preferred motif) — the nucleic acid sequence of which can be fused to the gene encoding the protein of interest. The biarsenical dye and tetracysteine motif form a covalent complex in which each of the dye's arsenic atoms cooperatively binds a pair of cysteines. Toxicity is minimized by the administration of 1,2-dithiols, for example ethanedithiol (EDT) — antidotes that protect endogenous pairs of cysteines and keep the dyes largely non-fluorescent until they find their ultimate tetracysteine targets. Nevertheless, at present, background staining keeps the sensitivity and the detection limit of this method to an order of magnitude or so worse than those of GFP. The other main limitation of this method is that the target cysteines must be in their reduced form before they can bind the biarsenical dye. Although this will generally be true for cysteine residues in the reducing environment of the cytosol or nucleus, cysteines that are in the lumen of the secretory pathway or outside cells tend to oxidize spontaneously and they can only be labelled if acutely reduced.

Of the biarsenical dyes already characterized[37] (FIG. 2c), a resorufin-based red label (ReAsH) is particularly useful as it can be used for both fluorescence and electron microscopy (EM). Under intense illumination in fixed samples, ReAsH catalytically generates singlet oxygen, which oxidizes diaminobenzidine into a highly localized polymer, which is readily stained by osmium tetroxide for EM contrast. So tetracysteine tags constitute genetically targetable tags for EM that show catalytic amplification, but do not require the diffusion of large antibody molecules into fixed or frozen tissue[38].

Furthermore, sequential labelling with different biarsenical dyes can indicate the age of protein molecules. The tetracysteine motifs are labelled rapidly and saturably with one colour of a membrane-permeant biarsenical dye, such as green FlAsH (FIG. 2c), then any free dye is washed out and the live cells allowed to synthesize fresh unlabelled copies of the same tagged protein. A final exposure of the protein to a biarsenical dye of a different colour, such as red ReAsH, labels only the newly synthesized copies. This approach was used to study the life cycle of connexin-43 as it was trafficked into and out of gap junctions (FIG. 3). Newly synthesized connexins (red) enter the gap junctional plaques from their outer edges while older molecules (green) are removed by endocytosis from the plaque centres. Varying the order and timing of FlAsH versus ReAsH administration can control whether ReAsH labels exocytic vesicles that carry new connexin molecules or endocytic compartments that contain old molecules, and thereby enables each population to be visualized separately by EM[38]. The conclusion that connexins move progressively from the periphery to the centre of gap junctions agrees with the work of Lauf *et al.*[39], who photobleached gap junctions that contained GFP-tagged connexins and observed that newly synthesized connexins formed a thin fluorescent halo that thickened with time.

So, the biarsenical sequential labelling technique and photochemical marking overlap somewhat in their areas of applicability, and they can reach concordant conclusions. The biarsenical technique is unique in the small size of the tag and the ability to give EM as well as fluorescence images; the photochemically sensitive fluorescent proteins have better time-resolution, lower

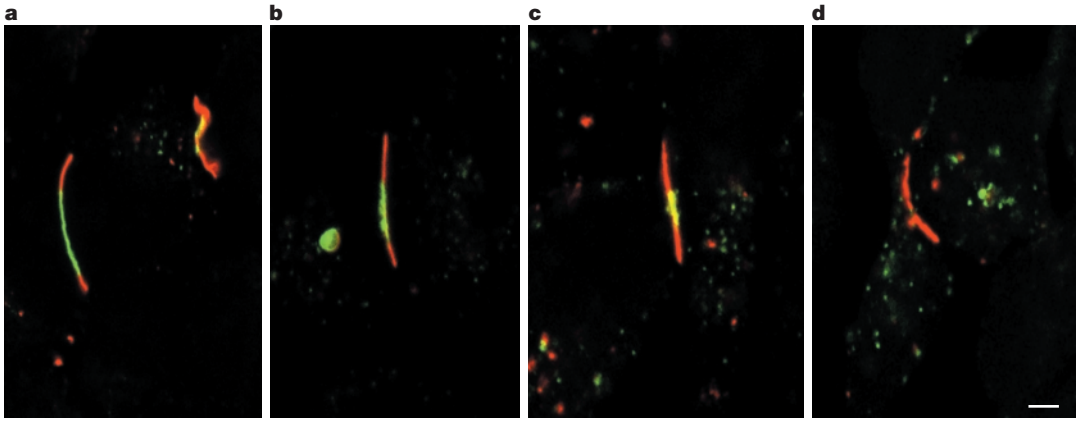

Figure 3 | **Multicolour pulse–chase biarsenical staining of gap juctions.** FlAsH and ReAsH were used to label two temporally separated pools of connexin-43 that had been fused to a tetracysteine-containing peptide (Cx43–4Cys) and then junctional plaque renewal was recorded over time[38]. HeLa cells that were expressing Cx43–4Cys were stained with FlAsH, incubated for 4 h (**a**,**b**) or 8 h (**c**,**d**), and then stained with ReAsH. Panels **a** to **d** show junctional plaques at different stages of renewal, as indicated by the different ratios of FlAsH (green) and ReAsH (red) stains. The green central zones diminish as the time interval between FlAsH and ReAsH staining increases from 4 to 8 h. Scale bar represents 1 μm. Adapted with permission from REF. 38 © 2002 American Association for the Advancement of Science.

background levels and can be marked with geometrically defined spatial patterns.

Antibody–hapten labelling. An alternative fluorescent dye-based labelling system consists of a single chain antibody which binds specifically to membrane-permeant fluorescent conjugates of its phenyloxazolinone hapten[40]. At present, because the antibody does not fold well in reducing environments, this system is best suited for use in secretory compartments and so has a complementary preference to the biarsenical–tetracysteine system. Ultimately it would be desirable to increase the affinity of the antibodies for the hapten (now an approximately 5 nM dissociation constant), and the extent to which antibody binding enhances fluorescence (~5-fold at present).

Avidin–biotin labelling. Another receptor–ligand pair that works best in the secretory compartment is the avidin–biotin pair, which is extremely popular for use *in vitro* and in histology, but has been surprisingly neglected in live cells. Chicken avidin that is expressed recombinantly in different compartments of the secretory compartment can trap biotin conjugates of fluoresceins of various pK_a values for the measurement of the pH values of those compartments, which enables the mechanism of pH regulation to be studied[41–43]. The availability of biotin conjugates and their extremely high affinity for avidin are advantages of this approach. Limitations include the tightly tetrameric nature of avidin and the essential role for biotin in the cytosol and mitochondria, such that avidin in these compartments is either toxic or biotin-saturated[44].

Phycobiliproteins. Bilin-containing proteins are important antennae for photosynthesis in cyanobacteria and photoreceptor signalling in green plants. Because they can absorb light at wavelengths that extend to the infrared, significant efforts have been made to develop biliproteins as fluorescent fusion tags — this is despite their natural oligomeric structure and their requirement for exogenous bilin cofactors or co-expression of the additional enzymes that are required for biosynthesis of the cofactor. Heterologous expression of the cyanobacterial truncated phytochrome[45], C-phycocyanin[46] and phycoerythrocyanin[47] has been achieved. The most promising class of these PHYCOBILIPROTEINS is the homodimeric phytofluors[48], which have excellent spectral properties, can be engineered as monomers and would require the co-expression of as few as three proteins[45].

Uroporphyrinogen III methylation. Another fluorescent reporter system, which seems to have been overshadowed by DsRed, is the recombinant uroporphyrinogen III methyltransferase gene (*cobA*)[49]. The cobA reporter catalyses the trimethylation of endogenous uroporphyrinogen III to generate a fluorescent small-molecule product that accumulates intracellularly. Although the cobA reporter system is not amenable to either subcellular targeting or the construction of fusion proteins, there could be certain cases in which its unique combination of a red fluorescent emission, independence from any exogenous cofactor and catalytic signal amplification will find a use.

Passive applications of fluorescent proteins

For most fluorescence imaging applications, the fluorescent label is a biologically inert participant that is used merely as a visible marker. By the very nature of their barrel-like structures (FIG. 1), which effectively shield the CHROMOPHORE from the external environment, AFPs are well suited to these more passive applications. Typical passive uses of AFPs include monitoring the appearance, degradation, location or translocation of appropriate partner proteins to which they are fused.

pK_a
The pH at which a molecule, or a particular site within a molecule, carries an ionizable H^+ 50% of the time.

PHYCOBILIPROTEINS
Proteins from blue-green algae and red algae that exhibit intense fluorescence owing to the presence of multiple bilin chromophores that are covalently attached to the protein.

CHROMOPHORE
The core portion of a molecule that is directly responsible for absorbing photons. Chromophores usually contain alternating single and double bonds.

Table 1 | **Translocating fluorescent probes**

Domains	Source proteins	Target molecules	References
PH domain	For example, Akt, ARNO, GRP1	3′ phosphoinositides including PtdIns(3,4,5)P_3 and PtdIns(3,4)P_2	55–59
PH domain	PLC	PtdIns(4,5)P_2 and InsP_3	60,61
C1 domain	PKC	DAG	62
C2 domain	PKC	Ca^{2+}	63,64
PA domain	Raf-1	PA	65

Akt, a serine/threonine kinase, also known as protein kinase B; C1 and C2, conserved domains 1 and 2 from protein kinase C; ARNO, ADP-ribosylation factor nucleotide-binding-site opener; C1, C homology-1; C2, C homology-2; DAG, Diacylglycerol; GRP1, general receptor for 3-phosphoinositides; InsP_3, inositol 1,4,5-trisphosphate; PA, phosphatidic acid; PH, pleckstrin-homology; PKC, protein kinase C; PLC, phospholipase C; PtdIns(3,4,5)P_3, phosphatidylinositol 3,4,5-triphosphate; PtdIns(4,5)P_2, phosphatidylinositol 4,5-biphosphate ; Raf 1, a serine/threonine kinase important in mitogen-activated signalling.

Fluorescence as a spatial marker

Perhaps the most popular application of fluorescent probes is to use fluorescence as a visible label to reveal either the static or dynamic spatial patterning of various cellular components. In 1995 it was still feasible to compile a nearly exhaustive list of AFP–fusion proteins[50], however, the number of published AFP–fusion proteins has since risen to many hundreds, if not thousands, and compilation of an updated list is far beyond the scope of this review.

Protein trap strategies. An interesting twist to the fluorescence imaging of intracellular localization is the identification of previously unknown protein targets on the basis of their pattern of localization[51]. In the so-called 'protein trap' strategies, a visual screen of cells that contain fusions of an AFP gene and a library of coding DNA sequences is used to identify cells that give rise to a pattern of interest. The DNA sequence that encodes the targeted fusion can then be cloned directly from the cell and the novel protein, which is presumably directing the localization, can be identified.

Fluorescent speckle microscopy. One particularly powerful technique for monitoring cytoskeletal dynamics is fluorescent speckle microscopy[52,53]. A fluorescently labelled protein is introduced into a cell at a very low level (~ 0.25%) relative to its endogenous counterpart, such that individual fluorescently labelled proteins can be detected with a sensitive imaging system. The dynamic assembly and disassembly of the actin cytoskeleton is shown by the 'flow' of the individual fluorescent speckles from regions of filament synthesis to regions of depolymerization. In order to get enough signal from a single protein it is necessary to either attach multiple small-molecule labels or to fuse the gene encoding the protein of interest to multiple AFP sequences[54].

Localizing the messenger. When fused to minimal protein domains that interact specifically with small-molecule messengers, AFPs can provide a straightforward readout of the cellular localization and transient production of such messengers[55–65]. For example, AFP that is fused to the pleckstrin-homology (PH) domain shows, through translocation from the general cytosol to the plasma membrane, the generation of 3′-phosphoinositides at the cell's leading edge on exposure to a chemoattractant[58,59]. Other messengers, such as phosphatidic acid and diacylglycerol (DAG), have been detected by similar methods (TABLE 1). In one elegant study, the comparison of the kinetics of translocation of full-length protein kinase C (PKC) versus the individual DAG-binding C1 domain and the Ca^{2+}-binding C2 domain led to a model for a sequential activation of PKC through a temporal coordination of the Ca^{2+} and DAG signals[64].

Localizing gene activity and transcripts. RNA localization can be visualized in live cells through fluorescence *in vivo* hybridization (FIVH)[66] or fusion of AFP to an RNA-binding protein or domain[67–70]. Using the latter approach, researchers have visualized the movement of endogenous bicoid messenger RNA during *Drosophila melanogaster* oogenesis through the use of AFP fused to Exu, a protein which accompanies bicoid mRNA during transport[69]. In a separate study, imaging of live neurons that were transfected with GFP-fused zipcode binding protein 1 (ZBP1) showed fast, bidirectional movements of granules in neurites, which can be inhibited by antisense oligonucleotides to the actin mRNA *zipcode* sequence[70]. Visualization of gene activity and changes in chromatin structure during transcription has also been achieved by creating large tandem arrays of DNA sequences (such as the *lac* operator or mouse mammary tumour virus promoter) that can be recognized with AFP-tagged DNA-binding proteins such as *lac* repressor or glucocorticoid receptor[71–74].

Fluorescence as a temporal marker

Analysing gene expression. AFPs are a favourable alternative to β-galactosidase (*lac*Z) as a marker of gene expression in tissue sections and transgenic organisms, because AFPs are self-sufficient and form their own chromophores[75]. The main disadvantage of AFP relative to enzymatic reporter systems is the absence of signal amplification. Whereas AFP is limited to a single FLUOROPHORE for each protein, a single copy of β-galactosidase, luciferase or β-lactamase[76] will catalyze the turnover of multiple substrate molecules, which allows much lower levels of gene expression to be detected. One approach to overcome this drawback is to target the AFP to a defined subcompartment of the cell and thereby use local contrast to distinguish its fluorescence from background autofluorescence.

FLUOROPHORE
A chromophore that can re-emit photons.

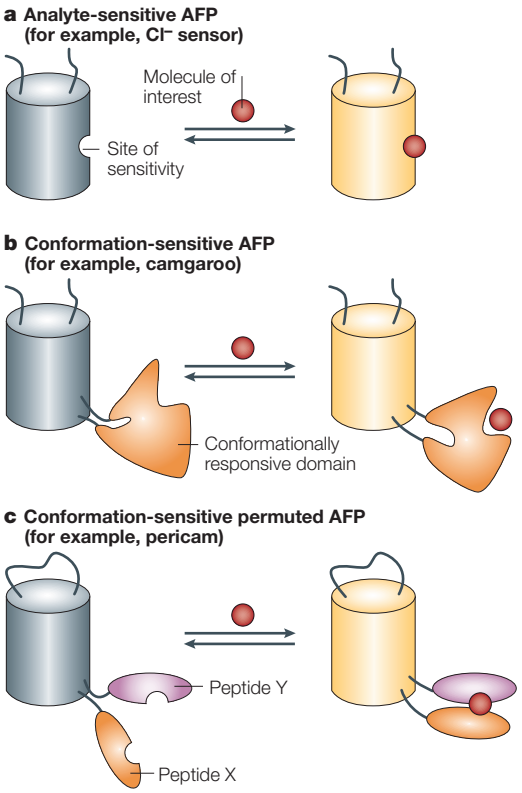

Figure 4 | **Biochemical modulation of AFP fluorescence.** **a** | *Aequorea* fluorescent protein (AFP) can be engineered to be directly sensitive to a small molecule of interest. **b** | Insertion of a conformationally responsive domain into AFP can result in a chimaera in which fluorescence is modulated by the conformational change. **c** | Alternatively, interacting proteins (or peptides) can be fused to the amino and carboxyl termini of circularly permuted AFP.

Optimizing turnover. Increasingly sophisticated reporters have been developed to monitor the temporal patterns of gene expression and protein dynamics. A limitation of AFP and similar passive markers is that the new protein cannot be distinguished from the old protein, as AFP remains fluorescent until it is degraded. Degradation can be accelerated by the fusion of AFP to degradation domains such as that of the mouse ornithine decarboxylase[77], thereby destabilizing the fluorescent protein such that it is turned over with a half-life of 2 h or less. These destabilized AFP variants minimize the accumulation of the background fluorescence that is generated by leaky, non-induced basal-level expression, which enhances their use as transcriptional reporters, albeit at the inherent cost of lower sensitivity — that is, a higher level of transcription and translation are required to produce a given level of fluorescence.

A DsRed fluorescent timer. A 'fluorescent timer' version of DsRed has been developed as a temporal marker[78]. The variant changes from green to red fluorescent over a period of ~24 h as the 'GFP-like' intermediate that accumulates is converted to the final red species owing to a further oxidative modification of the chromophore. The temporal history of the promoter activation is therefore reflected in the ratio between green and red fluorescence. Because the timescale of the fluorescent change is fixed and the resolution is restricted to several hours, this system will probably be most useful for the analysis of developmental control genes[78] in systems where the photochemically triggered green-to-red conversion of Kaede[11] or pulse–chase labelling of tetracysteine motifs[38], which were discussed previously, cannot be applied.

Analysing protein dynamics. Through the use of innovative fusion constructs, AFPs can report the temporal dynamics of cellular processes other than promoter activation. For example, the accumulation and degradation of an AFP-based substrate has been used for the quantification of ubiquitin–proteasome-dependent proteolysis in living cells[79]. Another tactic, which has found a use in the monitoring of vesicular traffic and sorting in the secretory pathway, is based on temperature-sensitive GFP mutants that fold and mature correctly only at temperatures that are non-permissive for sorting events. By growing cells at such temperatures, a cohort of fluorescently tagged proteins can accumulate in the *trans*-Golgi network. On raising the temperature, both to allow sorting and to prevent folding of the newly synthesized GFPs, the fate of the fluorescent 'bolus' can be monitored[80]. This pulse–chase-type approach has been used recently to visualize specifically the dynamics of immature secretory granules in a much larger pool of mature secretory granules[81]. So the age and fate of protein fusions can be monitored by spontaneously slow-maturing fluorescent proteins, temperature- or illumination-sensitive fluorescent proteins or pulse–chase labelling by biarsenical ligands, all of which have their own advantages and drawbacks.

Genetically encoded biochemical sensors

In the more active applications of fluorescent proteins that are described below, biochemical parameters such as metabolite concentrations, enzyme activity, or protein–protein interactions can be detected by their effects on the fluorescence properties of the designed indicators. Such indicators can be further divided into molecules with single chromophores (FIG. 4a–c) versus composites in which the emission intensity is dependent on the energy transfer between two chromophores (FIG. 5a,b).

Modulation of fluorescent protein spectra

Exploiting pH and halide-sensitive fluorescent proteins. In general, the fluorescence of AFPs is quenched reversibly by moderate acidification. This intrinsic pH sensitivity varies between different mutants and can be exploited to measure the ambient pH[82–84]. Both intensity-modulated and ratiometric pH-sensitive variants of GFP have been engineered and fused to a vesicle membrane protein to monitor vesicle exocytosis and recycling. These 'synapto-pHluorins' report synaptic neurotransmitter secretion by detecting the abrupt pH change that occurs when the acidic interior of the

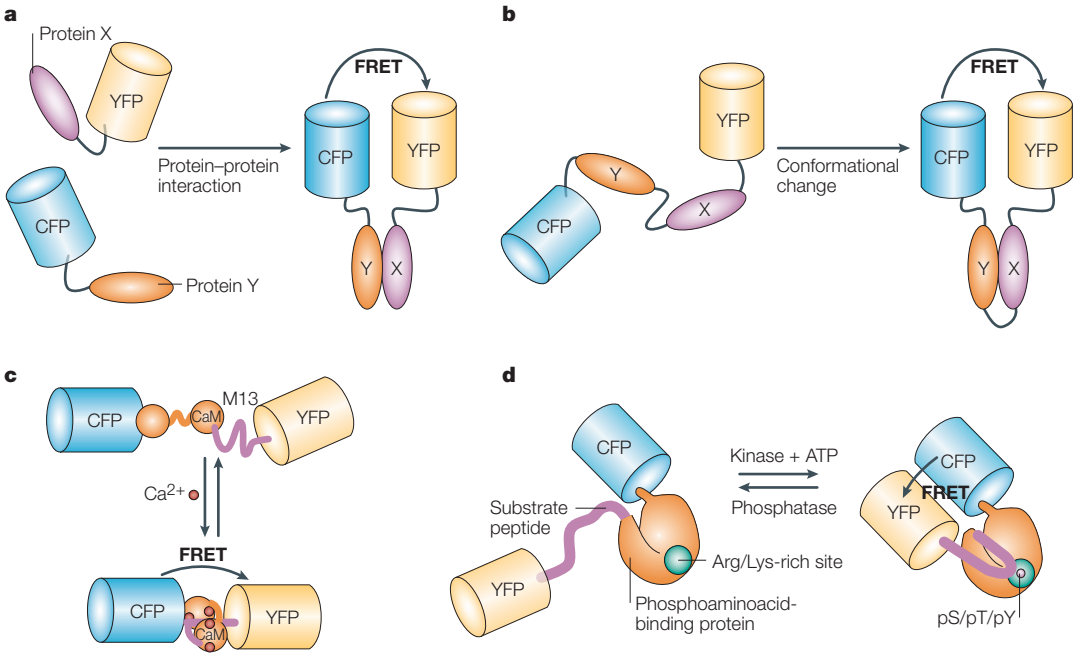

Figure 5 | **The general design of FRET-based fluorescent probes. a** | An intermolecular fluorescence resonance energy transfer (FRET)-based probe consists of two different proteins (X and Y) that are labelled with cyan fluorescent protein (CFP) and yellow fluorescent protein (YFP), respectively, which interact and bring the fluorophores into close proximity, thereby increasing the FRET efficiency. **b** | An intramolecular FRET-based probe consists of either a cleavable linker or a conformationally responsive region sandwiched between a FRET pair. **c** | Cameleon is an intramolecular FRET-based probe that is used to measure intracellular Ca^{2+}. **d** | Intramolecular phosphorylation-sensitive FRET probes have been constructed with specificities for various different kinases. Arg, arginine; CaM, calmodulin; Lys, lysine; pS, phosphoserine; pT, phosphothreonine; pY, phosphotyrosine. Figure 5, part **c** is reprinted with permission from REF. 105 *Nature* © (1997) Macmillan Magazines Ltd. Figure 5, part **d** is reproduced with permission from REFS 116,118 © 2002, National Academy of Sciences.

vesicle (pH ~5) is exposed to the outside of the cell (pH ~7) on fusion to the plasma membrane[84]. Some YFPs have particularly high pK_as in the range of 7 to 8, which makes them very useful for monitoring the pH of the cytosol and the mitochondrial matrix[85]. These same YFPs are quenched by halide ions, which bind selectively in the order $F^- > I^- > Cl^- > Br^-$ and raise the pK_a, which simulates acidification[86,87]. The halide-sensitive YFPs have been used in live cells to monitor Cl^- fluxes such as those mediated by the cystic fibrosis transmembrane conductance regulator (CFTR)[88]. Although the above indicators only change the intensity of fluorescence, examples of wavelength-shifting pH[89] and halide[90] indicators are also known. The responsiveness of YFPs to both protons and halides means that care has to be taken to disentangle the two perturbations. Sensitivity to pH and Cl^- can be a significant annoyance in applications where the YFP is to only be maximally fluorescent and inert (as in the passive applications discussed above). Fortunately, alternative YFPs with reduced pK_as, no halide sensitivity and increased brightness and photostability are now available[3,4].

Engineering fluorescent proteins to be sensitive to other parameters. The fluorescence of fluorescent proteins can be made directly sensitive to other signals by the introduction of specific mutations into the well-defined chromophore or barrel structure. A blue fluorescent protein (BFP) has been engineered, by the introduction of point mutations, to bind Zn^{2+} directly on the chromophore[91], but the modest fluorescence enhancement (twofold), low Zn^{2+} affinity (50 μM K_d) and slow association rate ($t_{1/2} > 4$ h) would need considerable improvement to become biologically useful. YFPs[92] and GFPs (G. T. Hanson, R. Aggeler, R. A. Capaldi, and S. J. Remington, unpublished observations) that are responsive to thiol-disulphide redox potentials have been engineered by placing two cysteine residues on adjacent β-strands so that they can form a reversible intramolecular disulphide bond. Such oxidation reduces the fluorescence of the YFP-based sensor by 2.2-fold[92], whereas it shifts the excitation maxima of the GFP-based sensors from 475–490 nm to 400 nm, which alters the excitation ratio by as much as 6–8-fold. Such indicators hold great promise, because, at present, the redox potentials of different compartments of cells are difficult to measure, but they are probably very important, heterogeneous and at least somewhat dynamic.

Most other biochemical parameters would require binding or sensing sites that are more complex than those created by point mutations in AFPs. Conformationally responsive elements, which range from short peptide motifs to full-length proteins, can be inserted into AFPs. The best-characterized example is the insertion of calmodulin (CaM) in place of Tyr145 of YFP, which

results in Ca^{2+} sensors (known as camgaroos) that increase fluorescence sevenfold on binding of Ca^{2+} (REFS 3,93). Camgaroos have proved to be useful for imaging Ca^{2+} inside mitochondria[94] and in MUSHROOM BODIES in the brain of *Drosophila*[95].

An important topological variation of this is to insert an AFP inside a conformationally responsive protein or pair of protein domains. An early example was a voltage sensor that consisted of AFP inserted into a non-conducting mutant of the Shaker K^+ channel[96]. More recently a smaller but faster response has been obtained by inserting wild-type GFP into a sodium channel[97]. Even larger responses might be obtained by inserting a circularly permuted AFP (cpAFP) rather than wild-type GFP[3,93]. In a cpAFP, the original amino and carboxyl termini are joined by a flexible linker, and new amino and carboxyl termini are introduced at one of several possible locations near the chromophore. Such permutation increases the flexibility and optical responsiveness to stresses that are applied on the new termini. Insertion of circularly permuted GFP (cpGFP) between CaM and M13 (a peptide which binds calmodulin in a Ca^{2+}-dependent fashion) yields Ca^{2+} indicators that are known as GCaMP[98] or pericams[99]. The inclusion of M13 increases the apparent Ca^{2+} affinity of the CaM by allowing the formation of ternary complexes, so that these molecules are more sensitive than camgaroos to small elevations in physiological levels of Ca^{2+}. Some pericam variants shift their excitation wavelengths on binding of Ca^{2+}, as opposed to just increasing fluorescence, which thereby enables ratiometric observation[99].

Intramolecular FRET-based indicators

FRET is a quantum-mechanical phenomenon that occurs when two fluorophores are in molecular proximity of each other (< 80 Å apart) (BOX 2). The emission spectrum of the donor fluorophore should overlap the excitation spectrum of the acceptor fluorophore, but both excitation spectra should be well enough separated to allow independent excitation. When the stoichiometry of the donor and the acceptor is fixed, as it is when they are fused in a single polypeptide chain, then the experimentally most convenient readout of FRET is the ratio of acceptor to donor fluorescence. Many reporters that are designed on the basis of intramolecular FRET changes (FIG. 5b) have been developed for measuring biochemical events in cells. Early applications used BFP as the donor and GFP as the acceptor, but the dimness and ability of BFP to be bleached soon led to its replacement by CFP, whereupon GFP had to be replaced by YFP to maintain spectral separation. When monomeric RFPs have been optimized sufficiently, GFP–RFP will probably become the next donor–acceptor pairing of choice.

Indicators of protease activity. The earliest FRET reporters consisted of BFP and GFP fused together with a protease-sensitive linker. Proteolysis disrupts FRET by separating the donor and acceptor units[100,101]. More recent examples have used CFP and YFP to measure caspase activity during apoptosis[102,103], which includes all-or-none activation at the single-cell level[104].

Indicators for measuring changes in calcium. Genetically encoded Ca^{2+} indicators, which are known as cameleons, were constructed by sandwiching CaM, a peptide linker and M13 between CFP and YFP[3,105–107] (FIG. 5c). Increased levels of intracellular Ca^{2+} switches on the affinity of CaM for the adjacent M13 sequence, which results in a change in orientation or distance between the two fluorescent proteins and a large increase in FRET. The replacement of glutamate by glutamine residues in the Ca^{2+}-binding sites tunes the effective affinity for Ca^{2+}. The replacement of M13 by a peptide that is derived from CaM-dependent kinase kinase produces a cameleon analogue with a larger, although somewhat slower, response than the traditional cameleons[108]. Levels of free intracellular CaM–Ca^{2+} complex can be sensed by reporters in which the donor and acceptor are connected by just a CaM-binding peptide[109,110], but in this case the binding of CaM straightens the peptide linker and so decreases FRET.

Indicators for other cellular parameters. Over the past few years, this principle of indicator design has been applied to visualize the behaviour of many other signalling molecules and proteins in cells. For example, indicators for cGMP (using cGMP-dependent protein kinase)[111,112], Ras and Rap1 activity[113], and Ran activity[114] have been constructed and applied to the study of a range of cell biological phenomena.

Reporters for the activity of tyrosine kinases[115–117] and serine/threonine kinases[118] have been made by sandwiching a substrate peptide for the kinase of interest and a phosphoaminoacid-binding domain, such as Src-homology-2 (SH2) or 14-3-3, between CFP and YFP (FIG. 5d). Phosphorylation of the substrate peptide induces the formation of an intramolecular complex with the neighbouring phosphoaminoacid-binding domain, which changes the FRET. This generic concept has been adapted to create probes for Abl, Src, the epidermal growth factor (EGF) receptor, insulin receptor, protein kinase A (PKA), and PKC, (J. D. Violin, J. Z., R. Y. T., and A. C. Newton, unpublished observations) with many more underway. The FRET change is usually reversed by phosphatases, so the fluorescent substrates report continuously the balance between kinase and phosphatase activities, with time resolution in the order of a few seconds and a spatial resolution of micrometres — far better than conventional assays with radioactive phosphorus or phospho-specific antibodies. Even finer spatial discrimination is possible if the reporters are fused to specific components of scaffolding molecules. So phosphorylation kinetics can differ significantly between sites that are indistinguishable at the resolution of the light microscope[118].

A FRET-based reporter of membrane potential exemplifies a slightly different topology, in which the voltage sensor, a truncated potassium channel, is placed amino terminal to both the CFP and YFP[119]. Voltage-dependent twists of the S4 channel helix are proposed to rotate the CFP with respect to the YFP.

MUSHROOM BODIES
Two prominent bilaterally symmetrical structures in the fly brain that are crucial for olfactory learning and memory.

Intermolecular FRET-based indicators

Indicators for cyclic AMP. The first fluorescent indicator for intracellular cAMP consisted of the PKA holoenzyme, in which the catalytic and regulatory subunits were labelled with fluorescein and rhodamine, respectively, so that cAMP-induced dissociation of the holoenzyme disrupted FRET[120]. Replacement of the dyes by BFP and GFP made this system genetically encodable and eliminated the need for *in vitro* dye conjugation and microinjection[121]. Application of this probe (with CFP and YFP replacing BFP and GFP) in cardiac myocytes showed an unusual compartmentalization of cAMP[122], whereas cAMP diffused freely in other cell types such as neurons[123,124].

Detecting protein–protein interactions. Intermolecular FRET can be used in real-time to detect interactions between two protein partners (FIG. 5a). Transcription factor homo- and heterodimerization[125,126], G-protein dissociation[127] and many other interactions[128–134] have all been visualized in live cells through the attachment of donor and acceptor fluorophores to interacting protein partners.

Protein–protein interactions can also be imaged by protein complementation assays, in which the potential partner proteins are fused not to FRET donors and acceptors but to complementary fragments of GFP[135], YFP[136], or other fluorogenic reporters[137,138], the most recent of which is β-lactamase[139,140]. The interaction of the partner proteins allows the two fragments to reconstitute the fluorescence or enzymatic activity, which is analogous to yeast two-hybrid assays in which transcriptional activation is reconstituted. Protein complementation assays generally have a much lower background and a greater dynamic range than those of FRET. When the reconstituted protein is an enzyme, its ability to catalyse the turnover of several copies of a substrate provides useful amplification, but it sacrifices subcellular spatial resolution if the reaction product is diffusible. However, FRET is instantaneous, fully reversible (that is, it monitors dissociation as well as association), has a well-characterized dependence on distance (BOX 2) and orientation, does not require the partner proteins to touch each other and contributes no attraction or repulsion of its own, provided that non-dimerizing fluorescent proteins are chosen[13]. Protein complementation takes from minutes to hours for the fragments to fold, reversibility is absent or uncertain and the requirements on the conformation and affinity of the partner proteins are quantitatively ill-defined except that they must bring the two reporter fragments into the correct juxtaposition.

Notes of caution. When the FRET donor and acceptor are in two separate molecules rather than a fused chimaera, the involvement of mixed complexes between labelled and endogenous partners becomes a greater concern, and the ratio of donor to acceptor expression is no longer fixed. FRET can no longer be assessed by exciting the donor and measuring the ratio of emissions in the donor and acceptor bands. More sophisticated methods such as the mathematical processing of three images[141–144], measuring donor dequenching on photobleaching the acceptor[13,107,126,130], or FLUORESCENCE-LIFETIME IMAGING MICROSCOPY (FLIM; see below) are required to show and quantify FRET.

Intermolecular FRET can suffer from false negatives when the donor and acceptor fluorescent proteins are: perturbing the proteins to which they are fused; in close proximity but orientated unfortunately with respect to each other; too far away from each other even when their fusion partners are interacting. Concern over false negatives has probably been the main reason why intermolecular FRET has been used mainly to obtain higher spatio-temporal resolution on known interactions rather than to screen proteomes for unknown interactions. False positives could result from the weak affinity (K_d ~ 0.1 mM) of AFPs for each other, but the only known example is when CFP and YFP were anchored to the plasma membrane by fatty acyl anchors, in which case the confinement to a surface probably raised the effective concentration considerably[13]. After the dimerization was eliminated by the monomerizing mutations described above, correlation of FRET efficiency versus YFP density showed that in living cells acyl, but not prenyl, modifications promote clustering in lipid rafts on the cytosolic face of the plasma membrane[13].

Box 2 | **FRET**

Fluorescence resonance energy transfer (FRET) is a quantum mechanical phenomenon that occurs between a fluorescence donor and a fluorescence acceptor that are in molecular proximity of each other if the emission spectrum of the donor overlaps the excitation spectrum of the acceptor. Under these conditions, energy (*E*) is transferred non-radiatively from the donor to the acceptor with an efficiency defined by the equation, where *r* is the distance between the two fluorophores and R_0 (Förster distance) is the distance at which 50% energy transfer takes place (typically 20–60 Å).

$$E = \frac{R_0^6}{R_0^6 + r^6}$$

R_0 is dependent on the extent of spectral overlap between the donor and acceptor, the quantum yield of the donor and the relative orientation of the donor and acceptor.

Excitation of a donor fluorophore in a FRET pair leads to quenching of the donor emission and to an increased, sensitized, acceptor emission. Intensity-based FRET detection methods include monitoring the donor intensity with or without acceptor photobleaching, the sensitized acceptor emission or the ratio between the donor and acceptor intensity. Methods that are based on fluorescence-decay-kinetics include determining the rate of donor photobleaching, the decrease of donor fluorescence lifetime or the appearance of new components in the acceptor decay kinetics.

FLUORESCENCE-LIFETIME IMAGING MICROSCOPY (FLIM). An imaging technique in which the lifetime, rather than the intensity, of the fluorescent signal is measured. This approach can be used to measure FRET.

FLUORESCENCE-ACTIVATED CELL SORTING
(FACS). A flow cytometry application in which live fluorescent cells are excited at a specific wavelength and then sorted into physically separated subpopulations on the basis of their fluorescence emission.

POSITRON EMISSION TOMOGRAPHY
(PET). Positron emission tomography is an imaging technique that is used to detect decaying nuclides, such as ^{15}O, ^{13}N, ^{11}C, ^{18}F, ^{124}I and ^{94m}Tc.

MAGNETIC RESONANCE IMAGING
The use of radio waves in the presence of a magnetic field to extract information from certain atomic nuclei (most commonly hydrogen, for example, in water). This technique is used to show certain types of tissue damage and the presence of tumours.

Fluorescence-lifetime imaging microscopy. Autophosphorylation of GFP-tagged PKC[145] or ErbB1 (REF. 146) has been measured by the FRET to Cy3-labelled phosphospecific antibodies, which were microinjected or applied to fixed cells and present in excess. When the acceptor is in such a large excess, FRET is best detected by the decrease in the lifetime of the donor's excited state using FLIM. FLIM and measurements of fluorescence depolarization allow the imaging of FRET between spectrally similar AFP molecules — that is, GFP–YFP or even GFP–GFP[147]. The main drawbacks of FLIM are that it sacrifices some sensitivity[134] and requires the assembly of expensive instrumentation.

Future directions

The applications of fluorescent probes will continue to expand and provide exciting new insights into the biology of living cells. Several relatively versatile reporter design strategies are now at our disposal (for example, translocation, camgaroo-, pericam- and cameleon-like strategies), but efforts to engineer new fluorophores and reporter classes must continue. For example, brighter and more red-shifted fluorescent proteins should improve the detection limits and *in vivo* applicability of AFP-based reporters. At present, all single AFP and FRET-based sensors rely on a gross structural reorganization or conformational change to produce a spectral readout. Many interesting intracellular process involve subtle conformational changes that are not amenable to the current classes of reporters, so that fluorescent protein variants with an increased sensitivity towards structural perturbations would be desirable. Another important consideration is that many of these fluorescent probes, in particular those for monitoring protein–protein interactions, function as surrogate cellular players. Visualization of their activities complement, but do not replace, measurements of endogenous components. Reporters that could assay endogenous biomolecules directly would therefore be very desirable.

Single-cell imaging with fluorescent reporters should allow the investigation of potentially interesting cell-to-cell variability that cannot be observed by the available methodologies that are based on cell population analysis[122]. Fluorescence is also an attractive readout for rapid, high-throughput approaches because of the availability of technologies such as multi-well plate readers, FLUORESCENCE-ACTIVATED CELL SORTING (FACS) and evanescent wave single-cell array technology (E-SCAT)[63].

Single-molecule spectroscopy is a young field that holds great promise. Single-molecule imaging in living cells allows the visualization of individual molecular interactions under physiological conditions and provides information that is difficult, and sometimes impossible, to obtain by conventional techniques[148]. Examples of single-molecule studies in living cells include investigations of EGF receptor dimerization[149], conformational changes in voltage-gated ion channels[150] and the mobility and aggregation of L-type Ca^{2+} channels in the plasma membrane[151].

For whole-body *in vivo* imaging, AFP has been used mainly as a visible localization marker[152] and a gene-expression marker[153]. Given the available wavelengths of excitation and emission, AFP imaging is still limited to surface structures (with a depth of penetration of approximately 1–2 mm) in experimental animals. A new generation of highly sensitive near infrared probes needs to be developed to complement existing non-optical probes for POSITRON EMISSION TOMOGRAPHY (PET) and MAGNETIC RESONANCE IMAGING (MRI).

1. Tsien, R. Y. The green fluorescent protein. *Annu. Rev. Biochem.* **67**, 509–544 (1998).
2. Sawano, A. & Miyawaki, A. Directed evolution of green fluorescent protein by a new versatile PCR strategy for site-directed and semi-random mutagenesis. *Nucleic Acids Res.* **28**, E78 (2000).
3. Griesbeck, O., Baird, G. S., Campbell, R. E., Zacharias, D. A. & Tsien, R. Y. Reducing the environmental sensitivity of yellow fluorescent protein. Mechanism and applications. *J. Biol. Chem.* **276**, 29188–29194 (2001).
4. Nagai, T. *et al.* A variant of yellow fluorescent protein with fast and efficient maturation for cell-biological applications. *Nature Biotechnol.* **20**, 87–90 (2002).
5. Scholz, O., Thiel, A., Hillen, W. & Niederweis, M. Quantitative analysis of gene expression with an improved green fluorescent protein. *Eur. J. Biochem.* **267**, 1565–1570 (2000).
6. Ormö, M. *et al.* Crystal structure of the *Aequorea victoria* green fluorescent protein. *Science* **273**, 1392–1395 (1996).
7. Yokoe, H. & Meyer, T. Spatial dynamics of GFP-tagged proteins investigated by local fluorescence enhancement. *Nature Biotechnol.* **14**, 1252–1256 (1996).
8. Sawin, K. E. & Nurse, P. Photoactivation of green fluorescent protein. *Curr. Biol.* **7**, R606–R607 (1997).
9. Elowitz, M. B., Surette, M. G., Wolf, P. E., Stock, J. & Leibler, S. Photoactivation turns green fluorescent protein red. *Curr. Biol.* **7**, 809–812 (1997).
10. Patterson, G. H. & Lippincott-Schwartz, J. A photoactivatable GFP for selective photolabeling of proteins and cells. *Science* **297**, 1873–1877 (2002).
11. Ando, R., Hama, H., Yamamoto-Hino, M., Mizuno, H. & Miyawaki, A. An optical marker based on the UV-induced green-to-red photoconversion of a fluorescent protein. *Proc. Natl Acad. Sci. USA* **99**, 12651–12656 (2002).

References 10 and 11 describe a pair of photoactivatable fluorescent proteins that can be used as fluorescent 'highlighters' to mark specific organelles or protein subpopulations.

12. Lippincott-Schwartz, J., Snapp, E. & Kenworthy, A. Studying protein dynamics in living cells. *Nature Rev. Mol. Cell Biol.* **2**, 444–456 (2001).
13. Zacharias, D. A., Violin, J. D., Newton, A. C. & Tsien, R. Y. Partitioning of lipid-modified monomeric GFPs into membrane microdomains of live cells. *Science* **296**, 913–916 (2002).
14. Ward, W. W., Prentice, H. J., Roth, A. F., Cody, C. W. & Reeves, S. C. Spectral perturbations of the *Aequorea* green-fluorescent protein. *Photochem. Photobiol.* **35**, 803–808 (1982).
15. Yang, F., Moss, L. G. & Phillips, G. N. Jr. The molecular structure of green fluorescent protein. *Nature Biotechnol.* **14**, 1246–1251 (1996).
16. Matz, M. V. *et al.* Fluorescent proteins from nonbioluminescent *Anthozoa* species. *Nature Biotechnol.* **17**, 969–973 (1999).
17. Tsien, R. Y. Rosy dawn for fluorescent proteins. *Nature Biotechnol.* **17**, 956–957 (1999).
18. Zacharias, D. A. Sticky caveats in an otherwise glowing report: oligomerizing fluorescent proteins and their use in cell biology. *Sci. STKE.* **2002**, PE23 (2002).
19. Lauf, U., Lopez, P. & Falk, M. M. Expression of fluorescently tagged connexins: a novel approach to rescue function of oligomeric DsRed-tagged proteins. *FEBS Lett.* **498**, 11–15 (2001).
20. Soling, A., Simm, A. & Rainov, N. Intracellular localization of Herpes simplex virus type 1 thymidine kinase fused to different fluorescent proteins depends on choice of fluorescent tag. *FEBS Lett.* **527**, 153 (2002).
21. Yanushevich, Y. G. *et al.* A strategy for the generation of non-aggregating mutants of *Anthozoa* fluorescent proteins. *FEBS Lett.* **511**, 11–14 (2002).
22. Terskikh, A. V., Fradkov, A. F., Zaraisky, A. G., Kajava, A. V. & Angres, B. Analysis of DsRed mutants: space around the fluorophore accelerates fluorescence development. *J. Biol. Chem.* **277**, 7633–7636 (2002).
23. Bevis, B. J. & Glick, B. S. Rapidly maturing variants of the *Discosoma* red fluorescent protein (DsRed). *Nature Biotechnol.* **20**, 83–87 (2002).
24. Campbell, R. E. *et al.* A monomeric red fluorescent protein. *Proc. Natl Acad. Sci. USA* **99**, 7877–7882 (2002).

This paper describes the directed evolution of a monomeric RFP that overcomes the problems associated with tetrameric DsRed.

25. Knop, M., Barr, F., Riedel, C. G., Heckel, T. & Reichel, C. Improved version of the red fluorescent protein (drFP583/DsRed/RFP). *BioTechniques* **33**, 592, 594, 596–598 (2002).
26. CLONTECH Laboratories Inc. *Living Colors User Manual Vol. II: Red Fluorescent Protein* 4 (Becton, Dickinson and Company, USA, 2002).
27. Fradkov, A. F. *et al.* Far-red fluorescent tag for protein labeling. *Biochem. J.* **368**, 17–21 (2002).
28. Labas, Y. A. *et al.* Diversity and evolution of the green fluorescent protein family. *Proc. Natl Acad. Sci. USA* **99**, 4256–4261 (2002).
29. Matz, M. V., Lukyanov, K. A. & Lukyanov, S. A. Family of the green fluorescent protein: journey to the end of the rainbow. *Bioessays* **24**, 953–959 (2002).
30. Peelle, B., Gururaja, T. L., Payan, D. G. & Anderson, D. C. Characterization and use of green fluorescent proteins from *Renilla mulleri* and *Ptilosarcus guernyi* for the human cell

display of functional peptides. *J. Protein Chem.* **20**, 507–519 (2001).
31. Lukyanov, K. A. *et al.* Natural animal coloration can be determined by a non-fluorescent GFP homolog. *J. Biol. Chem.* **275**, 25879–25882 (2000).
32. Fradkov, A. F. *et al.* Novel fluorescent protein from *Discosoma* coral and its mutants possesses a unique far-red fluorescence. *FEBS Lett.* **479**, 127–130 (2000).
33. Gurskaya, N. G. *et al.* GFP-like chromoproteins as a source of far-red fluorescent proteins. *FEBS Lett.* **507**, 16–20 (2001).
34. Wiedenmann, J. *et al.* A far-red fluorescent protein with fast maturation and reduced oligomerization tendency from *Entacmaea quadricolor* (*Anthozoa, Actinaria*). *Proc. Natl Acad. Sci. USA* **99**, 11646–11651 (2002).
35. Griffin, B. A., Adams, S. R. & Tsien, R. Y. Specific covalent labeling of recombinant protein molecules inside live cells. *Science* **281**, 269–272 (1998).
36. Nakanishi, J. *et al.* Imaging of conformational changes of proteins with a new environment- sensitive fluorescent probe designed for site-specific labeling of recombinant proteins in live cells. *Anal. Chem.* **73**, 2920–2928 (2001).
37. Adams, S. R. *et al.* New biarsenical ligands and tetracysteine motifs for protein labeling *in vitro* and *in vivo*: synthesis and biological applications. *J. Am. Chem. Soc.* **124**, 6063–6076 (2002).
38. Gaietta, G. *et al.* Multicolor and electron microscopic imaging of connexin trafficking. *Science* **296**, 503-507 (2002).
This paper describes the application of the tetracysteine–biarsenical system in pulse–chase labelling and electron microscopy.
39. Lauf, U. *et al.* Dynamic trafficking and delivery of connexons to the plasma membrane and accretion to gap junctions in living cells. *Proc. Natl Acad. Sci. USA* **99**, 10446–10451 (2002).
40. Farinas, J. & Verkman, A. S. Receptor-mediated targeting of fluorescent probes in living cells. *J. Biol. Chem.* **274**, 7603–7606 (1999).
41. Wu, M. M. *et al.* Organelle pH studies using targeted avidin and fluorescein-biotin. *Chem. Biol.* **7**, 197–209 (2000).
42. Wu, M. M. *et al.* Studying organelle physiology using targeted avidin and fluorescein-biotin. *Methods Enzymol.* **327**, 546–564 (2000).
43. Wu, M. M. *et al.* Mechanisms of pH regulation in the regulated secretory pathway. *J. Biol. Chem.* **276**, 33027–33035 (2001).
44. Sano, T. & Cantor, C. R. Expression of a cloned *streptavidin* gene in *Escherichia coli*. *Proc. Natl Acad. Sci. USA* **87**, 142–146 (1990).
45. Gambetta, G. A. & Lagarias, J. C. Genetic engineering of phytochrome biosynthesis in bacteria. *Proc. Natl Acad. Sci. USA* **98**, 10566–10571 (2001).
46. Tooley, A. J., Cai, Y. A. & Glazer, A. N. Biosynthesis of a fluorescent cyanobacterial C-phycocyanin holo-α subunit in a heterologous host. *Proc. Natl Acad. Sci. USA* **98**, 10560–10565 (2001).
47. Tooley, A. J. & Glazer, A. N. Biosynthesis of the cyanobacterial light-harvesting polypeptide phycoerythrocyanin holo-α subunit in a heterologous host. *J. Bacteriol.* **184**, 4666–4671 (2002).
48. Murphy, J. T. & Lagarias, J. C. The phytofluors: a new class of fluorescent protein probes. *Curr. Biol.* **7**, 870–876 (1997).
49. Wildt, S. & Deuschle, U. cobA, a red fluorescent transcriptional reporter for *Escherichia coli*, yeast, and mammalian cells. *Nature Biotechnol.* **17**, 1175–1178 (1999).
50. Cubitt, A. B. *et al.* Understanding, using and improving green fluorescent protein. *Trends Biochem. Sci.* **20**, 448–455 (1995).
51. Gonzalez, C. & Bejarano, L. A. Protein traps: using intracellular localization for cloning. *Trends Cell Biol.* **10**, 162–165 (2000).
52. Waterman-Storer, C. M., Desai, A., Bulinski, J. C. & Salmon, E. D. Fluorescent speckle microscopy, a method to visualize the dynamics of protein assemblies in living cells. *Curr. Biol.* **8**, 1227–1230 (1998).
53. Watanabe, N. & Mitchison, T. J. Single-molecule speckle analysis of actin filament turnover in lamellipodia. *Science* **295**, 1083–1086 (2002).
54. Bulinski, J. C., Odde, D. J., Howell, B. J., Salmon, T. D. & Waterman-Storer, C. M. Rapid dynamics of the microtubule binding of ensconsin *in vivo*. *J. Cell Sci.* **114**, 3885–3897 (2001).
55. Watton, S. J. & Downward, J. Akt/PKB localisation and 3′ phosphoinositide generation at sites of epithelial cell–matrix and cell–cell interaction. *Curr. Biol.* **9**, 433–436 (1999).
56. Oatey, P. B. *et al.* Confocal imaging of the subcellular distribution of phosphatidylinositol 3,4,5-trisphosphate in insulin- and PDGF-stimulated 3T3-L1 adipocytes. *Biochem. J.* **344**, 511–518 (1999).
57. Gray, A., Van Der, K. J. & Downes, C. P. The pleckstrin homology domains of protein kinase B and GRP1 (general receptor for phosphoinositides-1) are sensitive and selective probes for the cellular detection of phosphatidylinositol 3,4-bisphosphate and/or phosphatidylinositol 3,4,5-trisphosphate *in vivo*. *Biochem. J.* **344**, 929–936 (1999).
58. Servant, G. *et al.* Polarization of chemoattractant receptor signaling during neutrophil chemotaxis. *Science* **287**, 1037–1040 (2000).
59. Meili, R. *et al.* Chemoattractant-mediated transient activation and membrane localization of Akt/PKB is required for efficient chemotaxis to cAMP in *Dictyostelium*. *EMBO J.* **18**, 2092–2105 (1999).
60. Stauffer, T. P., Ahn, S. & Meyer, T. Receptor-induced transient reduction in plasma membrane PtdIns(4,5)P_2 concentration monitored in living cells. *Curr. Biol.* **8**, 343–346 (1998).
61. Hirose, K., Kadowaki, S., Tanabe, M., Takeshima, H. & Lino, M. Spatiotemporal dynamics of inositol 1,4,5-trisphosphate that underlies complex Ca^{2+} mobilization patterns. *Science* **284**, 1527–1530 (1999).
62. Oancea, E., Teruel, M. N., Quest, A. F. G. & Meyer, T. Green fluorescent protein (GFP)-tagged cysteine-rich domains from protein kinase C as fluorescent indicators for diacylglycerol signaling in living cells. *J. Cell Biol.* **140**, 485–498 (1998).
63. Teruel, M. N. & Meyer, T. Parallel single-cell monitoring of receptor-triggered membrane translocation of a calcium-sensing protein module. *Science* **295**, 1910–1912 (2002).
64. Oancea, E. & Meyer, T. Protein kinase C as a molecular machine for decoding calcium and diacylglycerol signals. *Cell* **95**, 307-318 (1998).
Reference 64 compares the kinetics of translocation of full-length PKC versus individual DAG-binding C1 domain and Ca^{2+}-binding C2 domain, which led to a model for a sequential activation of PKC through a temporal coordination between Ca^{2+} and DAG signals.
65. Rizzo, M. A., Shome, K., Watkins, S. C. & Romero, G. The recruitment of Raf-1 to membranes is mediated by direct interaction with phosphatidic acid and is independent of association with Ras. *J. Biol. Chem.* **275**, 23911–23918 (2000).
66. Dirks, R. W., Molenaar, C. & Tanke, H. J. Methods for visualizing RNA processing and transport pathways in living cells. *Histochem. Cell Biol.* **115**, 3–11 (2001).
67. Bassell, G. J., Oleynikov, Y. & Singer, R. H. The travels of mRNAs through all cells large and small. *FASEB J.* **13**, 447–454 (1999).
68. Bertrand, E. *et al.* Localization of ASH1 mRNA particles in living yeast. *Mol. Cell* **2**, 437–445 (1998).
69. Theurkauf, W. E. & Hazelrigg, T. I. *In vivo* analyses of cytoplasmic transport and cytoskeletal organization during *Drosophila* oogenesis: characterization of a multi-step anterior localization pathway. *Development* **125**, 3655–3666 (1998).
70. Zhang, H. L. *et al.* Neurotrophin-induced transport of a β-actin mRNP complex increases β-actin levels and stimulates growth cone motility. *Neuron* **31**, 261–275 (2001).
71. Muller, W. G., Walker, D., Hager, G. L. & McNally, J. G. Large-scale chromatin decondensation and recondensation regulated by transcription from a natural promoter. *J. Cell Biol.* **154**, 33–48 (2001).
72. Tsukamoto, T. *et al.* Visualization of gene activity in living cells. *Nature Cell Biol.* **2**, 871–878 (2000).
73. Straight, A. F., Marshall, W. F., Sedat, J. W. & Murray, A. W. Mitosis in living budding yeast: anaphase A but no metaphase plate. *Science* **277**, 574–578 (1997).
74. Robinett, C. C. *et al. In vivo* localization of DNA sequences and visualization of large-scale chromatin organization using lac operator/repressor recognition. *J. Cell Biol.* **135**, 1685–1700 (1996).
75. Hadjantonakis, A. K. & Nagy, A. The color of mice: in the light of GFP-variant reporters. *Histochem. Cell Biol.* **115**, 49–58 (2001).
76. Zlokarnik, G. *et al.* Quantitation of transcription and clonal selection of single living cells using β-lactamase as reporter. *Science* **279**, 84–88 (1998).
77. Li, X. *et al.* Generation of destabilized green fluorescent protein as a transcription reporter. *J. Biol. Chem.* **273**, 34970–34975 (1998).
78. Terskikh, A. *et al.* 'Fluorescent timer': protein that changes color with time. *Science* **290**, 1585-1588 (2000).
This paper describes a DsRed-derived transcriptional reporter that changes colour from green to red over a period of 24 h, thereby preserving the temporal history of promoter activation.
79. Dantuma, N. P., Lindsten, K., Glas, R., Jellne, M. & Masucci, M. G. Short-lived green fluorescent proteins for quantifying ubiquitin/proteasome-dependent proteolysis in living cells. *Nature Biotechnol.* **18**, 538–543 (2000).
80. Kaether, C. & Gerdes, H. H. Visualization of protein transport along the secretory pathway using green fluorescent protein. *FEBS Lett.* **369**, 267–271 (1995).
81. Rudolf, R., Salm, T., Rustom, A. & Gerdes, H. H. Dynamics of immature secretory granules: role of cytoskeletal elements during transport, cortical restriction, and F-actin-dependent tethering. *Mol. Biol. Cell* **12**, 1353–1365 (2001).
82. Kneen, M., Farinas, J., Li, Y. & Verkman, A. S. Green fluorescent protein as a noninvasive intracellular pH indicator. *Biophys. J.* **74**, 1591–1599 (1998).
83. Llopis, J., McCaffery, J. M., Miyawaki, A., Farquhar, M. G. & Tsien, R. Y. Measurement of cytosolic, mitochondrial and Golgi pH in single living cells with green fluorescent protein. *Proc. Natl Acad. Sci. USA* **95**, 6803–6808 (1998).
84. Miesenböck, G., De Angelis, D. A. & Rothman, J. E. Visualizing secretion and synaptic transmission with pH-sensitive green fluorescent proteins. *Nature* **394**, 192–195 (1998).
Reference 84 describes 'synapto-pHluorins' that report synaptic neurotransmitter secretion by detecting the abrupt pH change that occurs when the acidic interior of the vesicle (pH ~5) is exposed to the outside of the cell (pH ~7) on fusion to the plasma membrane.
85. Matsuyama, S., Llopis, J., Deveraux, Q. L., Tsien, R. Y. & Reed, J. C. Changes in intramitochondrial and cytosolic pH: early events that modulate caspase activation during apoptosis. *Nature Cell Biol.* **2**, 318–325 (2000).
86. Wachter, R. M. & Remington, S. J. Sensitivity of the yellow variant of green fluorescent protein to halides and nitrate. *Curr. Biol.* **9**, R628–R629 (1999).
87. Wachter, R. M., Yarbrough, D., Kallio, K. & Remington, S. J. Crystallographic and energetic analysis of binding of selected anions to the yellow variants of green fluorescent protein. *J. Mol. Biol.* **301**, 157–171 (2000).
88. Jayaraman, S., Haggie, P., Wachter, R. M., Remington, S. J. & Verkman, A. S. Mechanism and cellular applications of a green fluorescent protein-based halide sensor. *J. Biol. Chem.* **275**, 6047–6050 (2000).
89. Elsliger, M.-A., Wachter, R. M., Hanson, G. T., Kallio, K. & Remington, S. J. Structural and spectral response of green fluorescent protein variants to changes in pH. *Biochemistry* **38**, 5296–5301 (1999).
90. Kuner, T. & Augustine, G. J. A genetically encoded ratiometric neurotechnique indicator for chloride: capturing chloride transients in cultured hippocampal neurons. *Neuron* **27**, 447–459 (2000).
91. Barondeau, D. P., Kassmann, C. J., Tainer, J. A. & Getzoff, E. D. Structural chemistry of a green fluorescent protein Zn biosensor. *J. Am. Chem. Soc.* **124**, 3522–3524 (2002).
92. Ostergaard, H., Henriksen, A., Hansen, F. G. & Winther, J. R. Shedding light on disulfide bond formation: engineering a redox switch in green fluorescent protein. *EMBO J.* **20**, 5853–5862 (2001).
93. Baird, G. S., Zacharias, D. A. & Tsien, R. Y. Circular permutation and receptor insertion within green fluorescent proteins. *Proc. Natl Acad. Sci. USA* **96**, 11241–11246 (1999).
94. Rapizzi, E. *et al.* Recombinant expression of the voltage-dependent anion channel enhances the transfer of Ca^{2+} microdomains to mitochondria. *J. Cell Biol.* (in the press).
95. Yu, D., Baird, G., Tsien, R. Y. & Davis, R. L. Detection of calcium transient in *Drosophila* mushroom body neurons with camgaroo. *J. Neurosci.* (in the press).
96. Siegel, M. S. & Isacoff, E. Y. A genetically encoded optical probe of membrane voltage. *Neuron* **19**, 735–741 (1997).
97. Ataka, K. & Pieribone, V. A. A genetically targetable fluorescent probe of channel gating with rapid kinetics. *Biophys. J.* **82**, 509–516 (2002).
98. Nakai, J., Ohkura, M. & Imoto, K. A high signal-to-noise Ca^{2+} probe composed of a single green fluorescent protein. *Nature Biotechnol.* **19**, 137–141 (2001).
99. Nagai, T., Sawano, A., Park, E. & Miyawaki, A. Circularly permuted green fluorescent proteins engineered to sense Ca^{2+}. *Proc. Natl Acad. Sci. USA* **98**, 3197–3202 (2001).
References 98 and 99 describe the insertion of circularly permuted GFP between calmodulin and M13 to yield Ca^{2+} indicators that have been dubbed 'GCaMP' and 'pericams', respectively.
100. Heim, R. & Tsien, R. Y. Engineering green fluorescent protein for improved brightness, longer wavelengths and fluorescence energy transfer. *Curr. Biol.* **6**, 178–182 (1996).
101. Mitra, R. D., Silva, C. M. & Youvan, D. C. Fluorescence resonance energy transfer between blue-emitting and red-shifted excitation derivatives of the green fluorescent protein. *Gene* **173**, 13–17 (1996).
102. Mahajan, N. P., Harrison-Shostak, D. C., Michaux, J. & Herman, B. Novel mutant green fluorescent protein protease substrates reveal the activation of specific caspases during apoptosis. *Chem. Biol.* **6**, 401–409 (1999).

103. Luo, K. Q., Yu, V. C., Pu, Y. & Chang, D. C. Application of the fluorescence resonance energy transfer method for studying the dynamics of caspase-3 activation during UV-induced apoptosis in living HeLa cells. *Biochem. Biophys. Res. Commun.* **283**, 1054–1060 (2001).
104. Rehm, M. *et al.* Single-cell fluorescence resonance energy transfer analysis demonstrates that caspase activation during apoptosis is a rapid process. Role of caspase-3. *J Biol. Chem.* **277**, 24506–24514 (2002).
105. Miyawaki, A. *et al.* Fluorescent indicators for Ca^{2+} based on green fluorescent proteins and calmodulin. *Nature* **388**, 882–887 (1997).
106. Miyawaki, A., Griesbeck, O., Heim, R. & Tsien, R. Y. Dynamic and quantitative Ca^{2+} measurements using improved cameleons. *Proc. Natl Acad. Sci. USA* **96**, 2135–2140 (1999).
107. Miyawaki, A. & Tsien, R. Y. Monitoring protein conformations and interactions by fluorescence resonance energy transfer between mutants of green fluorescent protein. *Methods Enzymol.* **327**, 472–500 (2000).
108. Truong, K. *et al.* FRET-based *in vivo* Ca^{2+} imaging by a new calmodulin–GFP fusion molecule. *Nature Struct. Biol.* **8**, 1069–1073 (2001).
109. Romoser, V. A., Hinkle, P. M. & Persechini, A. Detection in living cells of Ca^{2+}-dependent changes in the fluorescence emission of an indicator composed of two green fluorescent protein variants linked by a calmodulin-binding sequence. *J. Biol. Chem.* **272**, 13270–13274 (1997).
References 105 and 109 describe the first genetically encoded indicators to be composed of conformationally responsive elements sandwiched between two fluorescent proteins that can undergo FRET — a design that has since been extended to many other systems.
110. Persechini, A. & Cronk, B. The relationship between the free concentrations of Ca^{2+} and Ca^{2+}–calmodulin in intact cells. *J. Biol. Chem.* **274**, 6827–6830 (1999).
111. Sato, M., Hida, N., Ozawa, T. & Umezawa, Y. Fluorescent indicators for cyclic GMP based on cyclic GMP-dependent protein kinase I α and green fluorescent proteins. *Anal. Chem.* **72**, 5918–5924 (2000).
112. Honda, A. *et al.* Spatiotemporal dynamics of guanosine 3′,5′-cyclic monophosphate revealed by a genetically encoded, fluorescent indicator. *Proc. Natl Acad. Sci. USA* **98**, 2437–2442 (2001).
113. Mochizuki, N. *et al.* Spatio-temporal images of growth-factor-induced activation of Ras and Rap1. *Nature* **411**, 1065–1068 (2001).
114. Kalab, P., Weis, K. & Heald, R. Visualization of a Ran-GTP gradient in interphase and mitotic *Xenopus* egg extracts. *Science* **295**, 2452–2456 (2002).
115. Kurokawa, K. *et al.* A pair of FRET–based probes for tyrosine phosphorylation of the CrkII adaptor protein *in vivo*. *J. Biol. Chem.* **276**, 31305–31310 (2001).
116. Ting, A. Y., Kain, K. H., Klemke, R. L. & Tsien, R. Y. Genetically encoded fluorescent reporters of protein tyrosine kinase activities in living cells. *Proc. Natl Acad. Sci. USA* **98**, 15003–15008 (2001).
117. Sato, M., Ozawa, T., Inukai, K., Asano, T. & Umezawa, Y. Fluorescent indicators for imaging protein phosphorylation in single living cells. *Nature Biotechnol.* **20**, 287–294 (2002).
118. Zhang, J., Ma, Y., Taylor, S. S. & Tsien, R. Y. Genetically encoded reporters of protein kinase A activity reveal impact of substrate tethering. *Proc. Natl Acad. Sci. USA* **98**, 14997–15002 (2001).
References 116 and 118 describe a general strategy for non-destructively imaging kinase activities in living cells using FRET-based reporters.
119. Sakai, R., Repunte-Canonigo, V., Raj, C. D. & Knopfel, T. Design and characterization of a DNA-encoded, voltage-sensitive fluorescent protein. *Eur. J. Neurosci.* **13**, 2314–2318 (2001).
120. Adams, S. R., Harootunian, A. T., Buechler, Y. J., Taylor, S. S. & Tsien, R. Y. Fluorescence ratio imaging of cyclic AMP in single cells. *Nature* **349**, 694–697 (1991).
121. Zaccolo, M. *et al.* A genetically encoded, fluorescent indicator for cyclic AMP in living cells. *Nature Cell Biol.* **2**, 25–29 (2000).
122. Zaccolo, M. & Pozzan, T. Discrete microdomains with high concentration of cAMP in stimulated rat neonatal cardiac myocytes. *Science* **295**, 1711–1715 (2002).
The use of a genetically encodable intermolecular FRET-based cAMP indicator in cardiac myocytes showed an unusual compartmentalization of cAMP.
123. Bacskai, B. J. *et al.* Spatially resolved dynamics of cAMP and protein kinase A subunits in *Aplysia* sensory neurons. *Science* **260**, 222–226 (1993).
124. Hempel, C. M., Vincent, P., Adams, S. R., Tsien, R. Y. & Selverston, A. I. Spatio-temporal dynamics of cAMP signals in an intact neural circuit. *Nature* **384**, 166–169 (1996).
125. Periasamy, A., Kay, S. A. & Day, R. N. in *Functional Imaging and Optical Manipulation of Living Cells.* SPIE Proc. Vol. 2983 (eds Farkas, D. L. & Tromberg, B. J.) (The International Society for Optical Engineers, USA,1997).
126. Llopis, J. *et al.* Ligand-dependent interactions of coactivators SRC-1 and PBP with nuclear hormone receptors can be imaged in live cells and are required for transcription. *Proc. Natl Acad. Sci. USA* **97**, 4363–4368 (2000).
127. Janetopoulos, C., Jin, T. & Devreotes, P. Receptor-mediated activation of heterotrimeric G proteins in living cells. *Science* **291**, 2408–2411 (2001).
128. Damelin, M. & Silver, P. A. Mapping interactions between nuclear transport factors in living cells reveals pathways through the nuclear pore complex. *Mol. Cell* **5**, 133–140 (2000).
129. Ruehr, M. L., Zakhary, D. R., Damron, D. S. & Bond, M. Cyclic AMP-dependent protein kinase binding to A-kinase anchoring proteins in living cells by fluorescence resonance energy transfer of green fluorescent protein fusion proteins. *J. Biol. Chem.* **274**, 33092–33096 (1999).
130. Siegel, R. M. *et al.* Fas preassociation required for apoptosis signaling and dominant inhibition by pathogenic mutations. *Science* **288**, 2354–2357 (2000).
131. Xia, Z., Zhou, Q., Lin, J. & Liu, Y. Stable SNARE complex prior to evoked synaptic vesicle fusion revealed by fluorescence resonance energy transfer. *J. Biol. Chem.* **276**, 1766–1771 (2001).
132. Li, H. Y. *et al.* Protein–protein interaction of FHL3 with FHL2 and visualization of their interaction by green fluorescent proteins (GFP) two-fusion fluorescence resonance energy transfer (FRET). *J. Cell. Biochem.* **80**, 293–303 (2001).
133. Mas, P., Devlin, P. F., Panda, S. & Kay, S. A. Functional interaction of phytochrome B and cryptochrome 2. *Nature* **408**, 207–211 (2000).
134. Tertoolen, L. G. *et al.* Dimerization of receptor protein-tyrosine phosphatase α in living cells. *B.M.C. Cell Biol.* **2**, 8 (2001).
135. Ghosh, I., Hamilton, A. D. & Regan, L. Antiparallel leucine zipper-directed protein reassembly: Application to the green fluorescent protein. *J. Am. Chem. Soc.* **122**, 5658–5659 (2000).
136. Hu, C.-D., Chinenov, Y. & Kerppola, T. K. Visualization of interactions among bZIP and Rel family proteins in living cells using bimolecular fluorescence complementation. *Mol. Cell* **9**, 789–798 (2002).
137. Rossi, F., Charlton, C. A. & Blau, H. M. Monitoring protein-protein interactions in intact eukaryotic cells by β-galactosidase complementation. *Proc. Natl Acad. Sci. USA* **94**, 8405–8410 (1997).
138. Michnick, S. W., Remy, I., Campbell-Valois, F. X., Vallee-Belisle, A. & Pelletier, J. N. Detection of protein–protein interactions by protein fragment complementation strategies. *Methods Enzymol.* **328**, 208–230 (2000).
139. Wehrman, T., Kleaveland, B., Her, J. H., Balint, R. F. & Blau, H. M. Protein–protein interactions monitored in mammalian cells via complementation of β-lactamase enzyme fragments. *Proc. Natl Acad. Sci. USA* **99**, 3469–3474 (2002).
140. Galarneau, A., Primeau, M., Trudeau, L. E. & Michnick, S. W. β-Lactamase protein fragment complementation assays as *in vivo* and *in vitro* sensors of protein–protein interactions. *Nature Biotechnol.* **20**, 619–622 (2002).
141. Gordon, G. W., Berry, G., Liang, X. H., Levine, B. & Herman, B. Quantitative fluorescence resonance energy transfer measurements using fluorescence microscopy. *Biophys. J.* **74**, 2702–2713 (1998).
142. Sorkin, A., McClure, M., Huang, F. & Carter, R. Interaction of EGF receptor and grb2 in living cells visualized by fluorescence resonance energy transfer (FRET) microscopy. *Curr. Biol.* **10**, 1395–1398 (2000).
143. Erickson, M. G., Alseikhan, B. A., Peterson, B. Z. & Yue, D. T. Preassociation of calmodulin with voltage-gated $Ca^{(2+)}$ channels revealed by FRET in single living cells. *Neuron* **31**, 973–985 (2001).
144. Chan, F. K. *et al.* Fluorescence resonance energy transfer analysis of cell surface receptor interactions and signaling using spectral variants of the green fluorescent protein. *Cytometry* **44**, 361–368 (2001).
145. Ng, T. *et al.* Imaging protein kinase Cα activation in cells. *Science* **283**, 2085–2089 (1999).
146. Verveer, P. J., Wouters, F. S., Reynolds, A. R. & Bastiaens, P. I. Quantitative imaging of lateral ErbB1 receptor signal propagation in the plasma membrane. *Science* **290**, 1567–1570 (2000).
147. Harpur, A. G., Wouters, F. S. & Bastiaens, P. I. Imaging FRET between spectrally similar GFP molecules in single cells. *Nature Biotechnol.* **19**, 167–169 (2001).
148. Weiss, S. Fluorescence spectroscopy of single biomolecules. *Science* **283**, 1676–1683 (1999).
149. Sako, Y., Minoguchi, S. & Yanagida, T. Single-molecule imaging of EGFR signalling on the surface of living cells. *Nature Cell Biol.* **2**, 168–172 (2000).
150. Sonnleitner, A., Mannuzzu, L. M., Terakawa, S. & Isacoff, E. Y. Structural rearrangements in single ion channels detected optically in living cells. *Proc. Natl Acad. Sci. USA* **99**, 12759–12764 (2002).
151. Harms, G. S. *et al.* Single-molecule imaging of l-type $Ca^{(2+)}$ channels in live cells. *Biophys. J.* **81**, 2639–2646 (2001).
152. Ito, S. *et al.* Real-time observation of micrometastasis formation in the living mouse liver using a green fluorescent protein gene-tagged rat tongue carcinoma cell line. *Int. J. Cancer* **93**, 212–217 (2001).
153. Brown, E. B. *et al. In vivo* measurement of gene expression, angiogenesis and physiological function in tumors using multiphoton laser scanning microscopy. *Nature Med.* **7**, 864–868 (2001).

Acknowledgements

We thank S. R. Adams and J. Babendure for their comments on the manuscript. This work was supported by a National Institutes of Health grant to R.Y.T. and postdoctoral fellowship to A.Y.T, a grant from the Alliance for Cellular Signaling (to J.Z. and R.Y.T.) and the Howard Hughes Medical Institute. J.Z. is supported in part by a postdoctoral fellowship from La Jolla Interfaces in Science and Burroughs Wellcome Fund, and R.E.C. is supported in part by a postdoctoral fellowship from the Canadian Institutes of Health Research.

Online links

DATABASES

The following terms in this article are linked online to:

Entrez: http://www.ncbi.nlm.nih.gov/Entrez/
Kaede
Swiss-Prot: http://www.expasy.ch/
CFTR | EGF | GFP | ZBP

FURTHER INFORMATION

Roger Y. Tsien's laboratory:
http://www.tsienlab.ucsd.edu
Alice Y. Ting's laboratory:
http://web.mit.edu/chemistry/Ting_Lab/
BD Biosciences Clontech (EGFP, YFP–S65G/V68L/S72A/T203Y, CFP, DsRed2, HcRed, Fluorescent Timer, and DsRed-Express):
http://www.clontech.com
NanoLight Technology (*Renilla mullerei* GFP):
http://www.nanolight.com
PanVera (FlAsH–EDT_2 and ReAsH–EDT_2 labelling kits):
http://www.panvera.com
Access to this interactive links box is free online.

REVIEW

Single-molecule visualization in cell biology

Yasushi Sako‡ and Toshio Yanagida*§*

Recent progress in single-molecule detection techniques has allowed us to visualize the dynamic behaviour and reaction kinetics of individual biological molecules inside living cells. Single-molecule visualization provides a direct way to quantify, with a high spatial and temporal resolution, biological events inside cells at the single-molecule level. In this article, we discuss how single-molecule visualization can be used in cell biology.

Single-molecule analysis is a powerful method to study purified biomolecules *in vitro*, because the data obtained are not obscured by the averaging that is inherent in conventional biochemical experiments[1–3]. Recently, this advantage has been extended to studies using living cells[4,5], in which it has been possible to quantify the dynamic and kinetic parameters of single-molecule reactions *in vivo*. It is difficult to determine kinetic parameters using multiple-molecule techniques because the reactions of individual molecules occur stochastically inside a cell. In addition, it is hard to spot local and temporal heterogeneities in the dynamic movement of molecules using multiple-molecule techniques. Single-molecule techniques can therefore be used to avoid such difficulties. In this review, we illustrate how single fluorescent molecules can be visualized in living cells. We then discuss the unique and important findings in cell biology that could only have been obtained using single-molecule visualization, as well as the recent progress in *in vitro* measurements that combine single-molecule visualization with other single-molecule techniques.

Why single-molecule visualization?

Single-molecule visualization of fluorophores in aqueous conditions — using TOTAL INTERNAL REFLECTION fluorescence microscopy (TIR-FM)[6] or epi-fluorescence microscopy[6,7] — was first performed in 1995. Since then, this technique has been applied to observe directly the motions of linear and rotational molecular motors, enzymatic reactions, the structural dynamics of proteins and DNA–protein interactions *in vitro*[1–3]. The visualization of single lipid molecules in a lipid bilayer and the simultaneous measurement of ion conductance and the movement of single ion channels in a model membrane have also been reported[2,4]. Furthermore, in 2000, the biological reactions of ligand and receptor proteins[8] and the movements of lipid molecules[9] were first visualized as single molecules on the surface of living cells (see Movie 1 online). Since then, ion channels[10], small G proteins and their effectors[11], cell-adhesion proteins[12], viral proteins[13] and components of the cytoskeleton[14] have been visualized as single molecules in living cells. The list of molecules that have been visualized is still growing rapidly, and the results of some of these studies are discussed in more detail below.

The advantages of single-molecule analyses. Proteins in living cells work as part of molecular networks that have specific functions, such as gene expression, energy transduction or membrane transport. Advances in molecular biology are rapidly uncovering the components of these molecular networks and are determining how they are constructed. One of the next objectives of cell biology is to quantify the flow of materials, information and energy through these molecular networks. To achieve this, both the dynamic and kinetic parameters of the single processes within the networks — such as the movement and translocation of proteins, the protein–protein interactions and the enzymatic reactions — must be determined in living cells. Single-molecule analysis *in vivo* will prove to be a powerful technique for this purpose. This technique has the ultimate level of sensitivity and can be used to detect and observe single reactions in living cells. In addition, it provides several other important advantages.

First, reactions do not need to be synchronized for single-molecule measurements. Statistically, each protein molecule reacts at a different time and position in a cell, so, to obtain the dynamic and kinetic parameters of a reaction using multiple-molecule measurements, specific techniques are required that synchronize the start-point of the reaction of every molecule. However, it is not possible to synchronize the intermediate steps of a reaction network, and single-molecule measurements have the advantage of bypassing these problems.

Second, single-molecule measurements provide information about the fluctuations and distributions of dynamic and kinetic parameters. Such information cannot be obtained from ensemble averages. Considering the local heterogeneity in the structure and environment of living cells, the fluctuation and distribution of the reactions of each molecule are probably important in understanding the mechanisms of cellular events.

Third, the above two points implicitly mean that single-molecule analysis allows the relationship between the inputs and outputs of single events of protein reactions to be quantified. In single-molecule experiments, each input and output event — for example, the binding and dissociation of a ligand or substrate — can be monitored individually. To understand reaction cascades in cells, the relationship between all the inputs and outputs of every step must be understood.

Single-molecule analysis requires statistical data so that the observed behaviour of minor, unusual molecules is not overestimated. However, monitoring many single molecules for statistical analysis is a laborious task. This is because automatic image processing is difficult for single-molecule experiments in living cells due to a limited signal-to-noise ratio and a non-homogeneous background. In addition, as signals cannot be obtained from invisible molecules, the appropriate controls, which depend on the purpose of the experiment, should be used. Despite these drawbacks, single-molecule studies provide unique insights in cell biology and so are extremely useful. As single-molecule studies deal with small numbers of molecules, sampling noise is an inevitable problem of these analyses compared with conventional biochemical analyses. However, this high level of sampling noise might be an essential factor in cell behaviour because the number of protein molecules per cell is usually relatively small (for example, most cell-signalling proteins are present at a concentration of 10^2–10^5 molecules per cell).

Techniques for single-molecule visualization. TIR-FM is a widely used technique for single-molecule detection both *in vitro* and *in vivo*[2,5]. TIR-FM, which was originally developed to observe the interface between two media with

different diffractive indices[15], uses an electromagnetic field called the 'evanescent field' to excite fluorophores (FIG. 1). As the evanescent field diminishes exponentially with distance from the interface, the excitation depth in TIR-FM is limited to a very narrow range — typically one hundred to several hundreds of nanometres. However, using such a narrow excitation depth is the most effective way to overcome the background noise problem, which is often the greatest problem of single-molecule imaging.

Objective-type TIR-FM[16], in which the excitation laser beam illuminates the specimen through an objective lens, is particularly useful for imaging living cells (FIG. 1). The top surface of the specimen is free in this type of TIR-FM, so it can be combined with high-resolution differential interference contrast microscopy, which requires an oil immersion condenser, and allows the cells to be easily accessed for changes of the surrounding medium, microinjection or micromanipulation. Using objective-type TIR-FM, precise morphological information about the cells can be obtained, the effect of drugs can be examined and electrophysiological experiments can be performed at the same time as single-molecule visualization.

Although TIR-FM provides superior contrast compared with other far-field microscopy techniques, its application is limited to the proximity of the cell surface — that is, to studying parameters in two dimensions. To observe single molecules deep inside cells in three dimensions, conventional epi-fluorescence microscopy using a laser for excitation[9] and real-time confocal microscopy[17] are applicable. The latter is thought to produce better results than TIR-FM for single-molecule imaging in dense solutions. Only sparsely labelled samples (<10 particles/μm^2) can be visualized as single molecules using TIR-FM, epi-fluorescence microscopy or confocal fluorescence microscopy owing to the low spatial resolution. However, the higher spatial resolution of SCANNING NEAR-FIELD OPTICAL MICROSCOPY might be able to overcome this limitation in the future[18]. Single molecules that are rapidly moving in solution cannot be visualized as fluorescent spots owing to the rapid three-dimensional Brownian diffusion that occurs. However, FLUORESCENCE CORRELATION SPECTROSCOPY[19], which allows single molecules to be analysed in solution, can be used to complement single-molecule visualization.

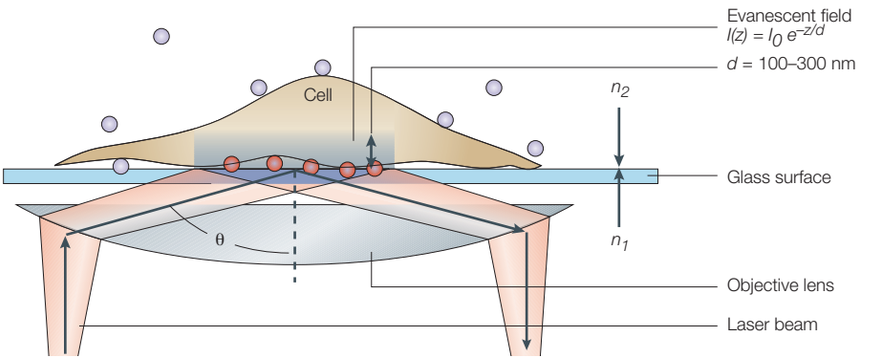

Figure 1 | **Total internal reflection fluorescence microscopy.** In total internal reflection fluorescence microscopy (TIR-FM), when a light beam illuminates the meniscus of two media obliquely from a high (n_1) to a low (n_2) diffractive index with an incident angle (θ) that is greater than the critical angle (θ_c) of total internal reflection, then an electromagnetic field called the 'evanescent field' (I) rises from the interface into the medium with a lower diffractive index. The evanescent field diminishes exponentially with distance (z) from the interface. The decay length (d) of the evanescent field is dependent on θ. In objective-type TIR-FM, a laser beam illuminates the specimen through the objective lens. As the θ_c of total internal reflection from glass (n_1 = 1.52) to water (n_2 = 1.33) is 61°, an objective lens that has a numerical aperture (NA = $n_1 \sin\theta_c$) larger than 1.33 should be used for objective-type TIR-FM. Specially designed objective lenses that have an NA of 1.45 or 1.65 are now available. Please note that this figure is not to scale. The typical decay length of an evanescent field is one hundred to several hundreds of nanometres, whereas the thickness of various regions of a typical cell is ~0.1 μm in lamellipodia to ~10 μm at the nucleus. Typical spacings between the ventral cell surface and the glass surface are ten to a few hundred nanometres. The red and purple circles represent fluorescent molecules that, in TIR-FM, are visible and invisible, respectively.

Applications in living cells

Single-molecule analyses have been effectively used both to quantify intracellular reactions and for the spatial analysis of such reactions with high resolution: for example, the kinetic analysis of receptor–ligand interactions[20]; measuring protein dynamics in the cytoplasm[21], nucleus[22] or plasma membrane[9,10,13,23]; observing the assembly and disassembly of protein oligomers[8,12] or large protein complexes[14]; and detecting the chemical reactions of proteins[8]. Examples of such studies will be discussed in more detail below.

Kinetic analysis of receptor–ligand interactions. The dissociation kinetics of a receptor–ligand interaction is an important property of cell-signalling reactions. *Dictyostelium discoideum* amoebae perform chemotaxis towards cyclic AMP, and this chemotaxis is induced through a G-protein-coupled receptor[24]. To determine how cells sense gradients of cAMP, the binding of fluorophore-labelled cAMP (Cy3–cAMP) to its receptor was observed on the surface of cells[11]. The dissociation rate constant for cAMP from its receptor was obtained by performing a statistical analysis of the time between the binding and dissociation of single molecules of Cy3–cAMP on the cells undergoing chemotactic movements[20] (FIG. 2a).

Cy3–cAMP dissociated faster from the anterior half of the cells compared to the posterior half, although the density of cAMP binding was almost uniform over the entire cell surface. This indicates that the association–dissociation cycle of cAMP is faster at the anterior end of the cell. Therefore, the reaction state of the cAMP receptors depends on the location of the chemotactic cells in relation to the concentration gradient of the cAMP signalling molecule (that is, the cAMP concentration gradient is converted to the difference in the reaction state of the cAMP receptor). This difference seems to depend on the coupling between the cAMP receptor and the trimeric G protein on the cytoplasmic side of the plasma membrane, and it is highly probable that cAMP signalling is more active in the anterior region of chemotactic amoeba than in the posterior region.

The dynamics of membrane components. It is possible to use single-molecule imaging to probe the dynamic and microscopic structures of the plasma membrane by measuring the movement of the membrane components (FIG. 2b). For example, the lateral diffusion of fluorescent lipids that were incorporated into a muscle-cell membrane has been observed for individual molecules[9]. In this study, a lipid probe with saturated acyl chains was found to be confined to small regions of the plasma membrane (spanning 0.7 μm), which indicates the presence of small lipid microdomains that are probably related to membrane rafts. In addition, the study also detected the shape and motions of the microdomains using single-molecule microscopy. As membrane rafts contain various cell-signalling molecules, the movement of the raft components are likely to be important for signal transduction from the plasma membrane.

Using a similar technique, single-molecule imaging of ion channels in the plasma membrane has been performed[10,23], and the data indicate that different types of ion channel behave in distinct ways. For example, a T-lymphocyte K^+ channel that was studied by single-molecule imaging presented as monomers and was essentially immobile[10], whereas a human cardiac Ca^{2+} channel tended to form larger aggregates and was mobile[23]. Virus entry into a living cell has also been observed by visualizing the dynamics of single viral proteins[13], and this single-molecule detection has a much higher sensitivity compared to conventional methods that require the accumulation of many viral particles in a cell. These examples highlight the potential of single-molecule techniques as new and sensitive assays in pharmacology and pathology.

Dynamics of cytoskeletal filaments. Single fluorescent tracers that are incorporated into large supramolecules can be used to monitor the dynamics of entire complexes. Watanabe and Mitchison[14] have used single molecules of actin that are tagged with green fluorescent protein (GFP–actin) as a tracer for analysing the spatial regulation of actin-filament dynamics in live fibroblast cells (FIG. 2c). The expression of GFP–actin was ingeniously controlled by truncating the enhancer region of the expression plasmid to achieve a diluted labelling of endogenous actin (1 GFP–actin molecule to 10,000–50,000 endogenous actin molecules). Incorporation into an actin filament, retrograde movement towards the cell centre and detachment from the filament was then observed for individual molecules of GFP–actin. There has been a long-standing controversy about the position of actin polymerization along an actin filament, and the appearance and duration of single fluorescent spots of GFP–actin that were incorporated into actin filaments allowed the kinetic parameters of polymerization and depolymerization to be determined. Modelling of the results indicates that basal polymerization and depolymerization are constant throughout lamellipodia — flattened, sheet-like structures that project from the surface of a cell and are composed of a meshwork of crosslinked F-actin — and that most of the actin filaments in the lamellipodia are generated by this basal polymerization. Additional polymerization within 1 μm of the tip of the cell is thought to balance the movement of actin filaments towards the centre of the cell.

Monitoring chemical reactions. Monitoring chemical reactions will be an important future goal of single-molecule analysis in living cells, and a method has been developed to detect the tyrosine phosphorylation of a membrane receptor in terms of single molecules[8] (FIG. 2d). Single-molecule analysis[8,11] has confirmed that epidermal growth factor (EGF) binding to the EGF receptor (EGFR) induces the dimerization of EGFR, which, in turn, is followed by autophosphorylation of the cytoplasmic tyrosine residues of the EGFR[25].

In these experiments[8,11], a monoclonal antibody that recognizes the cytoplasmic domain of phosphorylated EGFR was labelled with the fluorophore Cy3 and was used to detect the activation of the EGFR. EGF was conjugated to another fluorophore (Cy5). To introduce the Cy3–antibody into the cytoplasm, semi-intact cells that were perforated by streptolysin O were used[26]. After pulse stimulation of the semi-intact cells by the addition of Cy5–EGF, Cy3–antibody and ATP were added and the binding of Cy5–EGF and Cy3–antibody to the plasma membrane were simultaneously visualized as single molecules. Fluorescent spots of Cy3–antibody tended to co-localize with the clusters of Cy5–EGF, which indicates autophosphorylation of the EGFR clusters that

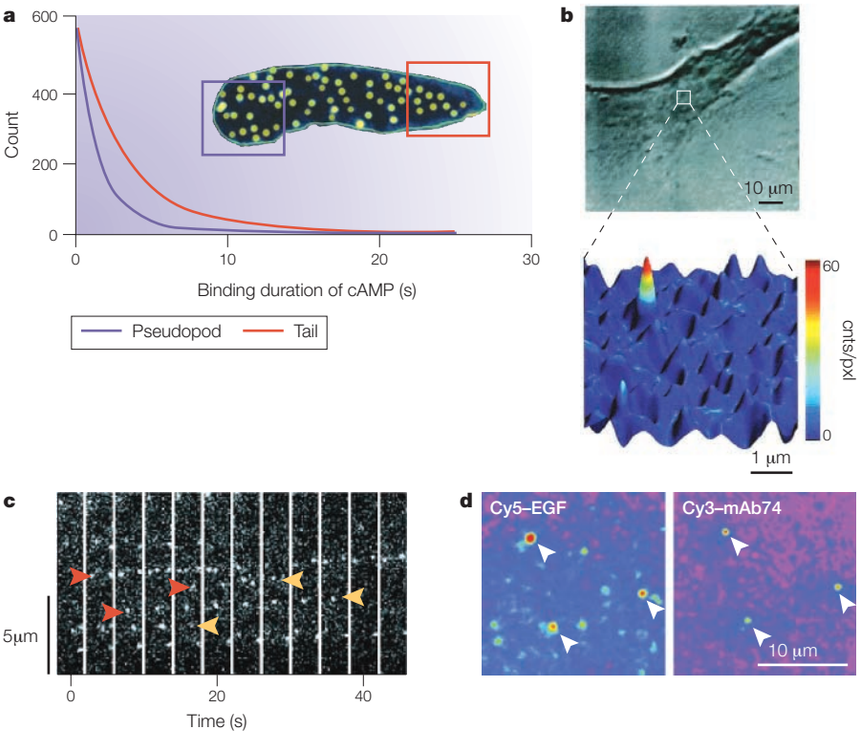

Figure 2 | **Single-molecule analysis of cellular events. a** | The binding of single molecules of Cy3-labelled cyclic AMP (Cy3–cAMP) was observed on the surface of an amoeba undergoing chemotactic movement[20]. Dissociation curves for Cy3–cAMP and its cell-surface receptor were constructed after observing many binding durations, and these curves show that the dissociation of Cy3–cAMP is faster at the anterior/pseudopod end of the cell. This figure was modified with permission from REF. 20 © (2001) American Association for the Advancement of Science. **b** | Schütz *et al.*[9] showed that Cy5-conjugated dimylistylphosphatidylethanolamine (DMPE–Cy5) became incorporated into lipid microdomains in the plasma membrane, whereas Cy5-conjugated dioleoylphosphatidylethanolamine (DOPE–Cy5) did not. The movements of membrane lipids inside and outside the microdomains could therefore be traced by the separate single-molecule visualization of DMPE–Cy5 or DOPE–Cy5, respectively. The top part of the figure shows a white light image of a cell labelled with DOPE–Cy5. The bottom part of the figure shows a magnified fluorescence image of the highlighted white box, in which a DOPE–Cy5 peak is resolved. The colour bar represents fluorescence intensity, measured in counts/pixels. This figure was reproduced with permission from REF. 9 © (2000) Oxford University Press. **c** | Watanabe and Mitchison[14] sparsely labelled cellular endogeneous actin filaments with green fluorescent protein (GFP)–actin. The polymerization, retrograde movement and depolymerization of actin filaments were analysed by single-molecule imaging of this GFP–actin. The figure shows single GFP–actins that are incorporated into a filament (red arrows), that move towards the cell centre, and that dissociate from the filament (yellow arrows) and this work showed that basal polymerization and depolymerization are constant throughout lamellipodia actin filaments. This figure was modified with permission from REF. 14 © (2002) American Association for the Advancement of Science. **d** | This image shows the activation of the epidermal growth factor (EGF) receptor (EGFR) by EGF[8]. Cells were perforated by streptolysin O and stimulated by Cy5–EGF in the presence of ATP. Activated EGFR (highlighted by arrows) was detected using the monoclonal antibody mAb74 (anti-activated EGFR), which was conjugated to the fluorophore Cy3. This figure was reproduced with permission from REF. 8 © (2000) *Nature Cell Biology*, Macmillan Magazines Ltd.

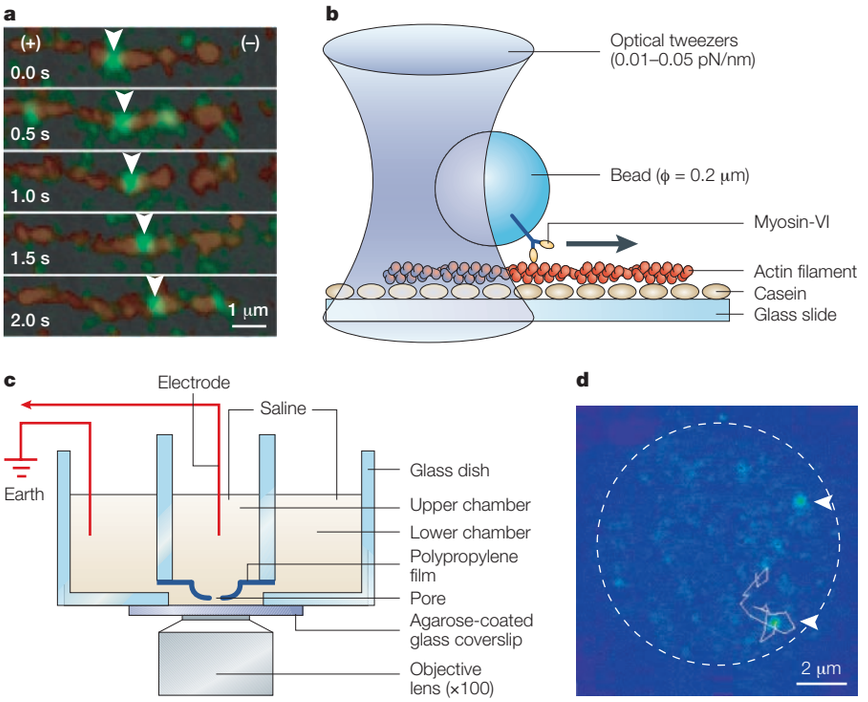

Figure 3 | **Combinations of single-molecule techniques for *in vitro* protein analysis.** Parts **a** and **b** show single-molecule imaging and manipulation of myosin-VI[39]. **a** | Myosin-VI tagged with green fluorescent protein (green) moved processively along an actin filament, which was labelled with tetramethylrhodamine (red), from the plus end to the minus end of the filament. This figure was reproduced with permission from REF. 39 © (2002) Academic Press. **b** | Beads that were conjugated to myosin-VI were trapped with optical tweezers and brought into contact with an actin filament that was bound to a glass slide. The position of the bead could be determined with subnanometre accuracy and, using this system, the step size (36 nm average) and the maximum force (~1.5 pN) of myosin-VI were measured. ϕ represents diameter. Parts **c** and **d** show simultaneous electrical and optical measurements of single ion channels[43]. **c** | The experimental set-up. Fluorescently labelled ion channels can be incorporated into a lipid bilayer at the pore of an upper chamber that is attached to an agarose-coated glass coverslip. These ion channels can then be observed by an objective-type TIR-FM at the same time as electrical measurements are taken. This figure was modified with permission from REF. 43 © (2002) Wiley-VCH. **d** | In a recent study[43], the carboxyl terminus of alamethicin was conjugated to the fluorophore Cy3, and alamethicin–Cy3 was then incorporated into a lipid bilayer (highlighted by the dashed circle). The arrows highlight alamethicin–Cy3 complexes that moved thermally in the membrane, and the path taken by one complex is shown. The ion currents from single alamethicin channels were measured simultaneously. This figure was modified with permission from REF. 43 © (2002) Wiley-VCH. pN, piconewton.

contain bound EGF. So, using this technique, a widely accepted hypothesis for the mechanism of EGFR activation — that is, that the formation of EGF–EGFR dimers is necessary for the autophosphorylation of the EGFR — was proved directly.

Single-molecule analysis *in vitro*

From the work discussed so far, it is clear that single-molecule visualization *in vivo* can be used to detect the positions and movements of individual single molecules, or to detect co-localization between two or more single molecules. SINGLE-PAIR FLUORESCENCE RESONANCE ENERGY TRANSFER[1] can be used to detect intermolecular structural change *in vitro*[8]. In addition, single-molecule FLUORESCENCE POLARIZATION and spectroscopy can be used to detect the movements and intramolecular structural changes of single molecules and the microenvironment around single molecules. However, the functions of molecules usually cannot be assessed directly by these techniques. To allow single-molecule analysis to evolve further, techniques that visualize single molecules must be combined with techniques that can detect the functions of these molecules. In fact, such combinations have already been successfully achieved in some recent experiments *in vitro*.

Combination with single-molecule manipulation: analysis of molecular motors. Biological molecules can be manipulated directly using a glass needle or the tip of a cantilever of an ATOMIC-FORCE MICROSCOPE or, less directly, using beads that are trapped by OPTICAL TWEEZERS[27]. Using these techniques, the mechanical properties of single biological molecules can be determined to nanometre and piconewton levels of accuracy for displacement and force, respectively.

For example, a molecular motor, kinesin, has been found to move processively along a microtubule with regular 8-nm steps, which indicates that kinesin 'walks' along the α–β tubulin dimer repeat[28]. In addition, the step size of muscle myosin (myosin-II) has been determined to be ~5–15 nm, although this step size has not always been consistent among all researchers (for reviews, see REFS 29–31). To understand how molecular motors work, it is crucial to know how the mechanical events are coupled to the ATP hydrolysis event. Many techniques have provided insights and, by combining the nano-manipulation technique with the single-molecule imaging technique, we have been able to observe the coupling between individual mechanical and chemical (that is, ATP hydrolysis) events of single muscle myosin molecules directly[32]. The next key question is how the power stroke of the molecular motor is developed. There is a large body of evidence that indicates conformational changes in the neck domain of myosin-II heads. Based on these findings, a lever-arm model is proposed for the movement of muscle myosin and, in this model, the neck domain acts as a lever arm, the tilting of which causes displacement of myosin[33]. This model predicts that the step size is proportional to the length of the neck domain.

Single-molecule imaging and manipulation techniques have also been used to study unconventional myosins — members of the myosin superfamily that are more amenable to movement studies than conventional myosins. However, these myosins are structurally different to conventional myosins and are not found in muscle. Their physiological roles are often unknown or unclear, although they are known to travel long distances continuously along actin filaments to transport cellular cargo (FIG. 3a,b). A class-V myosin (myosin-V) with long neck domains moves processively along actin filaments with large steps[34,35] that alter the angle of a fluorophore attached to the neck domain before and after stepping[36]. These results are consistent with a lever-arm model for myosin-V movement, although they do not prove directly that it is the tilting of the neck domain that is causing the steps. However, data have been obtained that question the lever-arm model for the movement of unconventional myosins[37–39] and, on the basis of these data, we have suggested that another mechanism, such as the biased linear diffusion of myosin heads along an actin filament, might be operating for the processive movement of these myosins[40] (see Movie 2 online).

Combination with single-molecule electrophysiology: analysis of channel proteins. The development of technology to record the current through a single ion channel allowed the functions of single proteins to be directly assessed both *in vitro* and *in vivo*[41]. This technology has shed light on the kinetic and pharmacological properties of many kinds of ion channel, although detailed mechanisms of ion-channel function are still being determined. The ability to monitor the conformation and chemical state of ion channels, combined with measurements of single-channel ion currents, would aid research in this area.

As mentioned earlier, single ion channels have been visualized in living cells[10,23] and, recently, Sonnleitner *et al*. visualized single molecules of a voltage-gated K^+ channel conjugated to tetramethylrhodamine in living cells[42]. In this study, the fluorescent intensity changed at the same time as the membrane potential, which indicates that rearrangements of the protein structure were being detected. By combining artificial-lipid-bilayer and single-molecule-imaging techniques, an experimental system has been developed that has allowed single ion-channel currents and single-molecule images of ion-channel molecules to be obtained simultaneously[43] (FIG. 3c,d). Therefore, it should not be long before simultaneous observation of the conformation and chemical states of single ion channels together with single-molecule ion currents is possible, both in artificial membranes and on the surface of living cells.

Conclusion and perspectives

Developments in single-molecule techniques in living cells have allowed us to visualize the location and movements of molecules and to determine the number of molecules that are involved in cellular reactions. Reaction kinetics of intracellular molecules have been measured and the activation of molecules has been detected. Single-molecule visualization in living cells has proven useful for quantifying cellular reactions and will be indispensable for further understanding the molecular mechanisms of cellular responses. Single-molecule techniques can be used at two levels — monitoring cellular responses in terms of the reactions of single-molecules and elucidating the mechanisms of how proteins work in terms of dynamic, kinetic and conformational changes of single molecules. Single-molecule manipulation using fine glass needles, optical tweezers or atomic-force microscopy has become widely used for protein studies *in vivo*. The manipulation of membrane proteins at the single-molecule level has already been reported in living cells[44], and 'single-channel recording'[41] is another technique that is used to assess the functions of single molecules in living cells. In the future, combining single-molecule-visualization, single-molecule-manipulation and single-molecule-electrophysiology techniques will be important to allow us to further understand the nanobiology of living cells.

**Nanobiology Laboratories, Graduate School of Frontier Biosciences, Osaka University, 2-2 Yamadaoka, Suita, Osaka 565-0871, Japan.*
‡Time's Arrow and Biosignaling, PRESTO, Japan Science and Technology Corporation, Japan.
§Soft Nanomachine Program, Japan Science and Technology Corporation, 2-2 Yamadaoka, Suita, Osaka 565-0871, Japan.
Correspondence to Y.S.
e-mail: sako@phys1.med.osaka-u.ac.jp

Please cite this article as a supplement to volume 4 of **Nature Reviews Molecular Cell Biology,** *pages SS1–SS5.*
doi:10.1038/nrm1193

1. Weiss, S. Measuring conformational dynamics of biomolecules by single molecule fluorescence spectroscopy. *Nature Struct. Biol.* **7**, 724–729 (2000).
2. Ishijima, A. & Yanagida, T. Single molecule nanobioscience. *Trends Biochem. Sci.* **26**, 438–444 (2001).
3. Xie, S. Single-molecule approach to enzymology. *Single Mol.* **2**, 229–236 (2001).
4. Hinterdorfer, P., Schütz, G., Kienberger, F. & Schindler, H. Detection and characterization of single biomolecules at surfaces. *J. Biotechnol.* **82**, 25–35 (2001).
5. Sako, Y. & Uyemura, T. Total internal reflection fluorescence microscopy for single-molecule imaging in living cells. *Cell Struct. Funct.* **27**, 205–213 (2002).
6. Funatsu, T., Harada, Y., Tokunaga, M., Saito, K. & Yanagida, T. Imaging of single fluorescent molecules and individual ATP turnover by single myosin molecules in aqueous solution. *Nature* **374**, 555–559 (1995).
7. Sase, I., Miyata, H., John, C. E. T., James, C. S. & Kinoshita, K. Jr. Real time imaging of single fluorophores on moving actin with an epifluorescence microscope. *Biophys. J.* **69**, 323–328 (1995).
8. Sako, Y., Minoguchi, S. & Yanagida, T. Single molecule imaging of EGFR signal transduction on the living cell surface. *Nature Cell Biol.* **2**, 168–172 (2000).
9. Schütz, G. J., Gerald, K., Pastuchenko, V. P. & Schindler, H. Properties of lipid microdomains in a muscle cell membrane visualized by single molecule microscopy. *EMBO J.* **19**, 892–901 (2000).
10. Schütz, G. J. *et al*. 3D imaging of individual ion channels in live cells at 40 nm resolution. *Single Mol.* **1**, 25–31 (2000).
11. Sako, Y., Hibino, K., Miyauchi, T., Miyamoto, Y., Ueda, M. & Yanagida, T. Single-molecule imaging of signaling molecules in living cells. *Single Mol.* **1**, 151–155 (2000).
12. Iino, R., Koyama, I. & Kusumi, A. Single molecule imaging of green fluorescent proteins in living cells: E-cadherin forms oligomers on the free cell surface. *Biophys. J.* **80**, 2667–2677 (2001).
13. Seisenberger, G., Ried, M. U., Müning, T. E. H., Hallek, M. & Bräuchle, C. Real-time single-molecule imaging of the infection pathway of an adeno-associated virus. *Science* **294**, 1929–1932 (2002).
14. Watanabe, N. & Mitchison, T. J. Single-molecule speckle analysis of actin filament turnover in lamellipodia. *Science* **295**, 1083–1086 (2002).
15. Axelrod, D., Burghardt, T. P. & Thompson, N. L. Total internal reflection fluorescence. *Ann. Rev. Biophys. Bioeng.* **13**, 247–268 (1984).
16. Tokunaga, M., Kitamura, K., Saito, K., Iwane, A. H. & Yanagida, T. Single molecule imaging of fluorophores and enzymatic reactions achieved by objective-type total internal reflection fluorescence microscopy. *Biochem. Biophys. Res. Commun.* **235**, 47–53 (1997).
17. Tadakuma, H., Yamaguchi, J., Ishihama, Y. & Funatsu, T. Imaging of single fluorescent molecules using video-rate confocal microscopy. *Biochem. Biophys. Res. Commun.* **287**, 323–327 (2001).
18. de Lange, F. *et al*. Cell biology beyond the diffraction limit: near-field scanning optical microscopy. *J. Cell. Sci.* **114**, 4153–4160 (2001).
19. Elson, E. L. & Magde, D. Fluorescence correlation spectroscopy. I. Conceptual basis and theory. *Biopolymers* **13**, 1–27 (1974).
20. Ueda, M., Sako, Y., Tanaka, T., Devreotes, P. & Yanagida, T. Single-molecule analysis of chemotactic signaling in *Dictyostelium* cells. *Science* **294**, 864–867 (2001).
21. Goulian, M. & Simon, S. M. Tracking single proteins within cells. *Biophys. J.* **79**, 2188–2198 (2000).
22. Kues, T., Dickmanns, A., Lührmann, R., Peters, R. & Kubitscheck, U. High intranuclear mobility and dynamic clustering of the splicing factor U1 snRNP observed by single particle tracking. *Proc. Natl Acad. Sci. USA* **98**, 12021–12026 (2001).
23. Harms, G. S. *et al*. Single-molecule imaging of L-type Ca^{2+} channels in live cells. *Biophys. J.* **81**, 2639–2646 (2001).
24. Parent, C. A. & Devreotes, P. N. A cell's sense of direction. *Science* **284**, 765–770 (1999).
25. Schlessinger, J. Cell signaling by receptor tyrosine kinases. *Cell* **103**, 211–225 (2000).
26. Kano, F., Sako, Y., Tagaya, M., Yanagida, T. & Murata, M. Reconstitution of brefeldin A-induced Golgi-tubulation and fusion with the endoplasmic reticulum in semi-intact Chinese hamster ovary cells. *Mol. Biol. Cell* **11**, 3073–3087 (2000).
27. Ashkin, A., Dziedzic, J. M., Bjorkholm, J. E. & Chu. S. Observation of a single-beam gradient force optical trap for dielectric particles. *Opt. Lett.* **11**, 288–290 (1986).
28. Svoboda, K., Schumidt, C. F., Schnapp, B. J. & Block, S. M. Direct observation of kinesin stepping by optical trapping interferometry. *Nature* **365**, 721–727 (1993).
29. Howard, J. Molecular motors: structural adaptations to cellular functions. *Nature* **389**, 561–567 (1997).
30. Yanagida, T., Kitamura, K., Tanaka, H., Iwane, A. H. & Esaki, S. Single molecule analysis of the actomyosin motor. *Curr. Opin. Cell Biol.* **12**, 20–25 (2000).
31. Spudich, J. A. The myosin swinging cross-bridge model. *Nature Rev. Mol. Cell Biol.* **2**, 387–392 (2001).
32. Ishijima, A., Kojima, H., Funatsu, T., Tokunaga, M., Higuchi, H. & Yangaida, T. Simultaneous measurement of chemical and mechanical reactions. *Cell* **92**, 161–171 (1998).
33. Spudich, J. A. How molecular motors work. *Nature* **372**, 515–518 (1994).
34. Mehta, A. D. *et al*. Myosin-V is a processive actin-based motor. *Nature* **400**, 590–593 (1999).
35. Sakamoto, T., Amitani, I., Yokota, E. & Ando, T. Direct observation of processive movement by individual myosin V molecules. *Biochem. Biophys. Res. Comm.* **272**, 586–590 (2000).
36. Forkey, J. N., Quinlan, M. E., Shaw, M. A., Corrie, J. E. T. & Goldman, Y. E. Three-dimensional structural dynamics of myosin V by single-molecule fluorescence polarization. *Nature* **422**, 399–404 (2003).
37. Tanaka, H. *et al*. The motor domain determines the large step of myosin-V. *Nature* **415**, 192–195 (2002).
38. Rock, R. S. *et al*. Myosin VI is a processive motor with a large step size. *Proc. Natl Acad. Sci. USA* **98**, 13655–13659 (2001).
39. Nishikawa, S. *et al*. Class VI myosin moves processively along actin filament backwards with large steps. *Biochem. Biophys. Res. Commun.* **290**, 311–317 (2002).
40. Kitamura, K., Tokunaga, M., Iwane, A. H. & Yanagida, T. A single myosin head moves along an actin filament with regular steps of ~5.3 nanometres. *Nature* **397**, 129–134 (1999).
41. Sakmann, B. & Neher, E. (eds) *Single-Channel Recording* (Plenum Press, New York, 1995).
42. Sonnleitner, A., Mannuzzu, L., Terakawa, S. & Isacoff, E. Y. Structural rearrangements in single ion channels detected optically in living cells. *Proc. Natl Acad. Sci. USA* **99**, 12759–12764 (2002).
43. Ide, T., Takeuchi, Y. & Yanagida, T. Development of an experimental apparatus for simultaneous observation of optical and electrical signals from single ion channels. *Single Mol.* **3**, 33–42 (2002).
44. Edidin, M., Kuo, S. C. & Sheetz, M. P. Lateral movements of membrane glycoproteins restricted by dynamic cytoplasmic barriers. *Science* **254**, 1379–1382 (1991).

Acknowledgments
We thank the former members of the Single Molecule Processes Project, Japan Science and Technology Corporation (JST), and the members of the Nanobiology Laboratories of Osaka University, Japan, for their cooperation.

Online links

DATABASES
The following terms in this article are linked online to:
LocusLink: http://www.ncbi.nlm.nih.gov/LocusLink/
actin | EGF | EGFR | myosin | tubulin
Swiss-Prot: http://www.expasy.ch/
GFP

FURTHER INFORMATION
Toshio Yanagida's laboratory:
http://www.phys1.med.osaka–u.ac.jp/
Access to this interactive links box is free online.

REVIEW

Electron microscopy in cell biology: integrating structure and function

Abraham J. Koster and Judith Klumperman‡*

Electron microscopy (EM) is at the highest-resolution limit of a spectrum of complementary morphological techniques. When combined with molecular detection methods, EM is the only technique with sufficient resolution to localize proteins to small membrane subdomains in the context of the cell. Recent procedural and technical developments have increasingly improved the power of EM as a cell-biological tool.

With the sequencing of the human genome nearly complete, characterization of the functions of the gene products will be an important next challenge in cell biology. The rapidly growing number of human disorders that are identified as an intracellular membrane-trafficking defect unequivocally shows how protein function is directly linked to intracellular localization and emphasizes the importance of understanding membrane-mediated protein-trafficking pathways. Electron microscopy (EM) is the only technique that can combine sensitive protein-detection methods with detailed information on the substructure of intracellular compartments. This combined resolution power has given EM a central position in defining intracellular protein-distribution patterns and predicts a continuing and increasing demand for EM in cell biology[1–3].

Although EM is an established technology, new methodologies have recently been developed to assess the fine-structure identity of intracellular membrane-enclosed compartments. At the same time, the methods to localize molecules of interest to within these compartments have been broadened and perfected. Furthermore, techniques are now evolving that literally add an extra dimension to EM images — electron tomography (ET) for three-dimensional (3D) imaging and CORRELATIVE MICROSCOPY for integrating the imaging of live cells and EM. Here, without the pretension of being complete, we highlight some of the most recent and developing EM techniques, which we believe will have an important role in the future of cell biology.

ImmunoEM: crucial considerations

EM is exploited to its full capacity when its power to visualize membrane compartments at high resolution is combined with methods that specifically localize the functional components of these membranes — that is, when cellular architecture is integrated with molecular information. For maximal output, we need to strive for the best possible structural preservation and to use the most sensitive protein-detection methods.

Cryofixation. The best available approach so far to immobilize and preserve cellular architecture is probably CRYOFIXATION[3–5]. HIGH-PRESSURE FREEZING is the only way to freeze biological samples of 10–200-μm thickness without generating artefacts as a result of ice-crystal formation, and is therefore the method of choice for cells and tissues[6]. In most applications, high-pressure freezing is followed by FREEZE SUBSTITUTION. These preparations are notable because of their sharp membrane delineation and the clear visibility of their cytoskeletal elements. In particular, cellular compartments that are susceptible to shrinkage as a result of chemical fixation — for example, endosomes — retain their turgid shape after high-pressure-freezing fixation (J. L. Murk, M. Kleijmeer and B. Humbel, personal communication). FIGURE 1b shows an example of a Golgi complex that was prepared using this protocol.

When freeze substitution is omitted and frozen cells are viewed directly in the electron microscope, we refer to this method as CRYOEM — a technique that was pioneered by Dubochet and colleagues (for more information, see REF. 4). CryoEM provides the exciting possibility of viewing the cell in what is probably its most natural state. The full procedure, from high-pressure freezing to visualizing slices of frozen material by EM, however, needs further development before it can be applied routinely[3,7]. CryoEM of isolated molecules is a rapidly emerging and powerful approach for obtaining structural models of macromolecular complexes in the intermediate resolution range (0.5–2.0 nm). CryoEM can be applied to those complexes that are not suitable for X-ray crystallography because of their size, instability, or the fact that they are available only in insufficient amounts (for a recent overview, see REF. 8). The resolution of cryoEM usually allows the relative positions and orientations of individual components of a macromolecular complex to be determined to within a few angströms. For example, recently, single-particle cryoEM of the ribosome-bound class I release factor RF2 indicated that binding of RF2 to a stop codon in the decoding centre of the 30S ribosomal subunit induces a conformational change in RF2 that allows it to interact simultaneously with a stop codon and the peptidyl-transferase centre of the 50S ribosomal subunit[9,10].

Chemical fixation. Although there are routine protocols for the high-pressure-freezing fixation of biological samples, precise experimental conditions must be established for each sample to prevent the formation of damaging ice crystals, and not all material is suitable for cryofixation. This is why many studies still make use of the more conventional chemical-fixation methods. Chemical fixation, however, induces structural artefacts and might cause the redistribution of particularly small soluble proteins. To weigh up the pros and cons of the two preparation methods for future EM studies, a careful analysis of the possible artefacts that are induced by chemical fixation is much needed. The more laborious high-pressure-freezing procedures might be advantageous for some, but not all, cell-biological questions.

Assessing molecular information. The most widely used approach to detect proteins in cells is IMMUNOEM. Many protein-sorting events occur in 40–60-nm, often coated, membrane subdomains, which are below the detection level of the light microscope and are distinguishable in the EM only under the most favourable conditions. The TOKUYASU CRYOSECTIONING TECHNIQUE[11], which was introduced in 1973, has been improved and perfected so that it now generally surpasses other techniques with respect to membrane visibility and labelling sensitivity[12–14]. FIGURE 2f and 2g show examples of a multivesicular endosome and small transport carriers, respectively, as they appear in ultrathin cryosections. The preferred tag for the visualization of antibodies by EM is colloidal gold (FIG. 2d–g), which can be

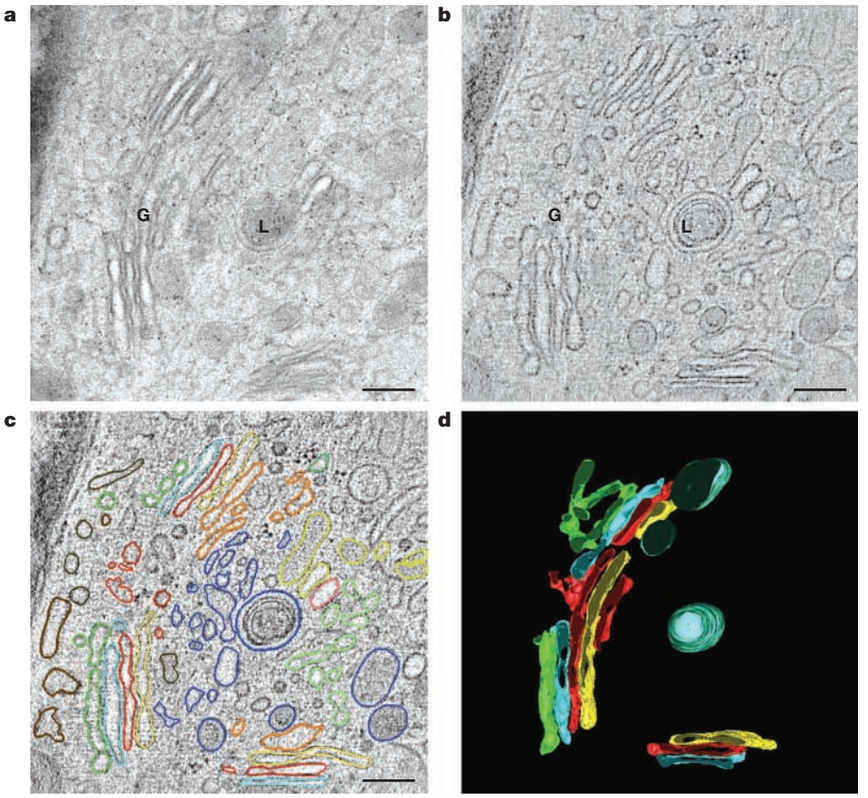

Figure 1 | **The electron-tomography process on a 250-nm thick section of a high-pressure frozen, freeze-substituted and Epon-embedded dendritic cell. a** | A digital image at 0° tilt, which was taken from a tilt series of 131 images that ranged from –65° to +65°. Because of the thickness of the section, the membranes near the Golgi complex (G) are poorly distinguished. The non-specific 10-nm colloidal gold labels (black dots) were deposited on the surface of the section to allow image alignment during the reconstruction process[27]. L, lysosome. **b** | A 3.2-nm thin digital slice from the tomogram that was computed from the above-mentioned tilt series. The limited thickness of the digital slice allows the membrane morphology to be seen more clearly. **c** | Computer-assisted contour drawing on the digital slice of the tomogram that is shown in part **b**. The scale bars in **a**, **b** and **c** represent 200 nm. **d** | A contour model of some of the structures that are visible in the tomogram shown in part **b**. This figure was kindly provided by W. J. C. Geerts (Department of Molecular Cell Biology, Faculty of Biology, Utrecht, The Netherlands) and J. L. Murk (Department of Cell Biology, University Medical Center Utrecht, The Netherlands).

made in distinct sizes for the simultaneous localization of different molecules in a single experiment. The applications are numerous. For example, transport carriers can be defined by their cargo and at the same time by the presence of specific machinery proteins[15]. Counting the individual gold particles allows the relative intracellular distributions of a protein to be assessed and, under strictly defined conditions, even absolute protein concentrations can be determined[16]. A drawback is that the gold particles do not penetrate into cells or sections. ULTRASMALL GOLD, however, does penetrate into the sample, which increases the number of labelled antigens[17,18]. The potential of ultrasmall gold to label antigens throughout the section makes it a promising candidate for the development of combined immuno-EM–ET approaches (see below).

New developments in immunoEM

Cryofixation and immunolabelling. An important development for future EM studies will be to combine cryofixation with immunoEM. The technical challenge here is that sections must be thawed before the immunolabelling procedure can be carried out. So, cryofixed cells must, at some stage, be chemically fixed as well. Several groups are developing approaches with this aim. The combination of high-pressure freezing and freeze substitution has been successfully applied, but generally gives suboptimal membrane visibility and labelling efficiency and is therefore limited in its use. One promising approach is to collect and thaw thin sections of frozen material in a mixture of membrane-stabilizing agents and fixatives. This 'section fixation' approach yields excellent images and allows determination of the subcellular localization of secretory proteins and even cholesterol[19,20]. Moreover, because section fixation occurs at low temperature and is rapid, it will probably solve at least some of the alleged penetration problems of chemical fixation. Alternatively, a combination of high-pressure freezing/freeze substitution and subsequent rehydration of the cells or tissue is presently under development. This 'rehydration' procedure will allow high-pressure-frozen material to be subjected to the Tokuyasu cryosectioning technique with a minimized chance of artefacts that are caused by chemical fixation, and therefore combines the strongest points of the two methods (J. W. Slot, unpublished observations).

Localizing lipids. Protein-trafficking events crucially depend on membranes, but remarkably little is known about the *in situ* intracellular distribution of lipids. A significant problem for lipid localization by EM is that routine fixation procedures immobilize lipids insufficiently and cause their extraction and redistribution. The best results so far were obtained with chemically fixed and freeze-substituted cells[21,22]. More recently, with some simple modifications, the Tokuyasu approach was adapted to localize cholesterol[19] and successfully provided the first EM double-labelling of two lipids — cholesterol and bis(monoacylglycero)phosphate[20]. An increasing number of lipid-binding toxins are becoming available for use in EM detection. Combined with the methodological innovations, this gives us hope that in the near future the *in situ* distribution of more types of lipids will be assessed at high resolution. Moreover, it opens up the possibility of studying protein sorting in a way that can be directly related to the lipid environment.

Adding new dimensions to EM

Electron tomography. The complexity of cellular architecture goes beyond what we can derive from two-dimensional (2D) images in the thin (~70 nm) sections that are normally viewed in the electron microscope. Our best 3D models of cell organelles are obtained by looking at their 2D appearance in a series of thin sections. This approach, however, has a resolution in the z-axis direction that is no better than the section thickness. The recently emerging technique of ET is not limited by the section thickness and can be used to generate 3D images of subcellular structures — called TOMOGRAMS — with an xyz resolution in the 2–10-nm range[23–25]. The power of ET is that it produces 3D images of cellular structures in a section that cannot be deduced from conventional 2D EM projection images in which they appear overlapped. An

example of the tomography procedure is illustrated in FIG. 1, which shows the conversion of an ET image (FIG. 1a) to a computer-based 3D model (FIG. 1d). Movies that further illustrate this procedure are available online (see Movie 1 and Movie 2 online).

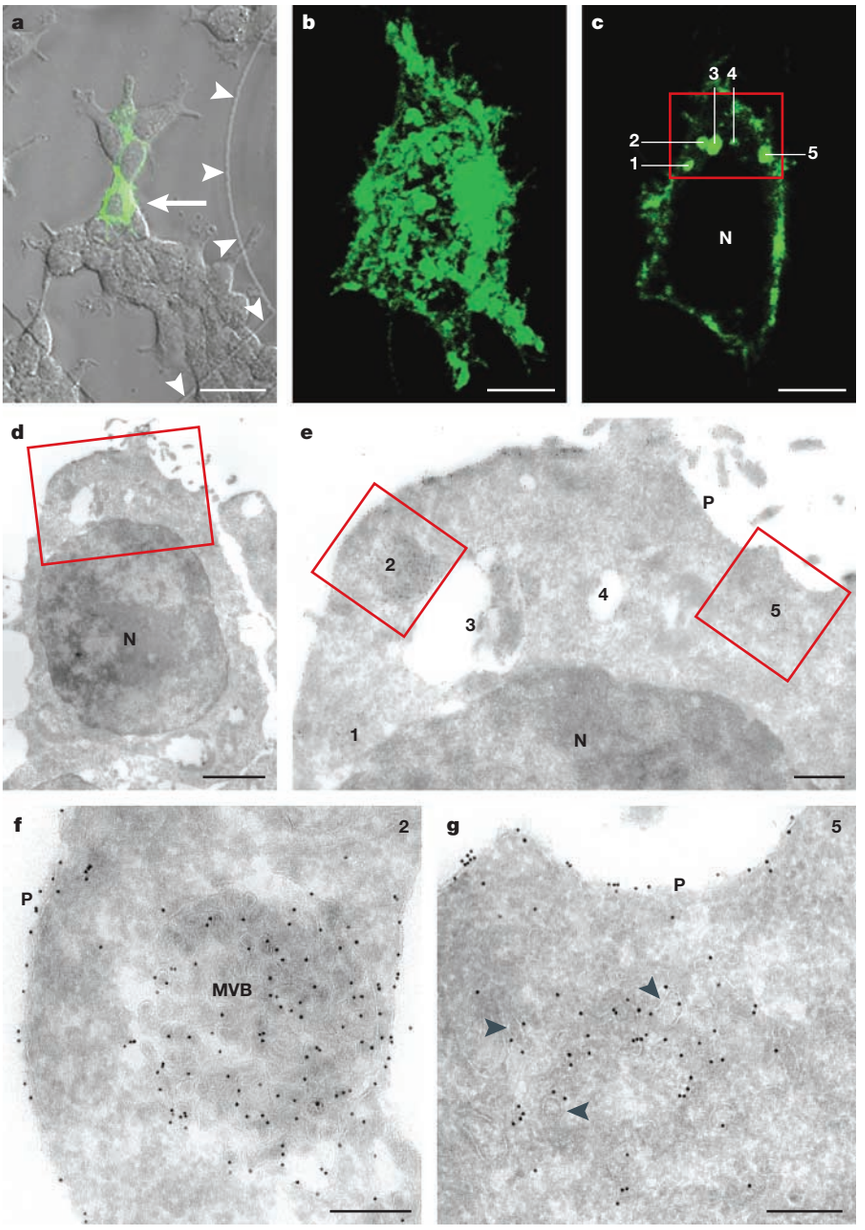

Figure 2 | **An example of correlative live-cell–electron microscopy of a single cell.** In this example, the fluorescent spots that are seen in live-cell imaging are exposed as being from distinct compartments using electron microscopy (EM). **a** | Confocal image of the selected cultured endothelial cell (arrow) that is expressing the endosomal–lysosomal protein CD63 conjugated to green fluorescent protein (GFP). Arrowheads point to marks on the coverslip (Eppendorf) that are used to relate back to these images from the cells under the electron microscope. **b** | A stacked fluorescence image of the selected cell. **c** | A confocal 370-nm slice of the selected cell that shows five distinct fluorescent spots. **d** | A correlative EM image of an ultrathin cryosection of the selected cell[39]. The boxed area is the same as in part **c**. **e** | High magnification of the boxed area that is shown in **c** and **d**. The numbers refer to the spots that are shown in **c**, which are now highlighted by the presence of 10-nm gold particles (black dots) that were obtained by immunolabelling GFP. **f** | The original fluorescent spot 2 was found to correspond to a multivesicular body (MVB). **g** | The original fluorescent spot 5 was found to correspond to a cluster of vesicular profiles (arrowheads). N, nucleus; P, plasma membrane. The scale bars represent 25 μm (**a**), 5 μm (**b**,**c**), 2 μm (**d**), 500 nm (**e**) and 200 nm (**f**,**g**). This figure was kindly provided by V. Oorschot and R. Wubbolts (Department of Cell Biology, University Medical Center Utrecht, The Netherlands).

In the membrane-traffic field, ET is especially important for mapping compartmental boundaries in cells and to reveal the structure of complex membrane systems such as the endoplasmic reticulum (ER)–Golgi interface, the Golgi region and the endosomal vacuolar system. Tomograms of cellular organelles — such as mitochondria, the Golgi complex and peroxisomes — are being published at an increasing rate[26–30] and have led to the reassessment of our understanding of some well-known cellular organelles. For example, ET has visualized a structural relationship between the ER and peroxisomes, which addressed a long-standing issue regarding peroxisome biogenesis[30]. Moreover, ET has provided support for the *cis* to *trans* movement of entire Golgi cisternae[28], and has shown that post-Golgi transport carriers bud from multiple cisternae at the *trans* side of the Golgi complex[26,27].

With the development of high-quality charge-coupled device cameras and improved computer performance[7,25], automated ET has become a reasonably fast and well-controlled approach, as far as data collection in the instrument and image processing to produce a tomogram are concerned[31]. Translation of ET data into a biological model is still, however, less straightforward. For example, the computer-assisted drawing of membranes in a tomogram often involves the selection of structures and the subjective interpretation of the image. To assure the objectivity of a constructed model, it is therefore desirable that several independent researchers interpret the data that are embedded in the original tomogram.

ET and macromolecular imaging. Evidently, the power of ET would be increased tremendously if it were combined with immunoEM — for example, by using ultrasmall gold that penetrates and labels the full thickness of the sections. In several groups — including the combined efforts of our laboratories — immunolabelling protocols for thick sections are now being developed, but alternatives for immunolabelling are also emerging. Recently, the first ET results were obtained using direct cryoEM[7,29,32]; this approach is referred to as cryoET. An important potential of cryoET is that, when the high-resolution structural template of a molecular structure is known (for example, from X-ray crystallography results) and the macromolecular structure is sufficiently large and distinct in shape, it can be identified unambiguously in the tomogram[33]. Therefore, cryoET can be used to localize large supramolecular complexes in their cellular environment without the need for further steps, such as chemical fixation, staining,

labelling or genetic modification. For example, on the basis of its shape alone, the macromolecular structure of the 26S proteasome — the cytosolic multisubunit molecular machine that is responsible for intracellular protein degradation — could be identified in the tomogram that was constructed from a frozen *Dictyostelium discoideum* cell[32]. In the long term, using cryoET, we might be able to determine the cellular location of molecular complexes of only several hundred kDa on the basis of their shape, which opens up the exciting possibility of being able to photograph molecular machineries at work in cells.

Integrating live-cell imaging and immunoEM. Imaging fluorescent proteins in living cells is a powerful technique that reveals the kinetics and direction of protein dynamics (see also the review on page S7 of this supplement). However, as with all fluorescent-microscopy methods, live-cell imaging lacks the fine-structure information against which the fluorescent signal can be interpreted. The resolution of light-microscopy-based methods is typically ~200–500 nm. Hence, a fluorescent spot can consist of many small vesicles or highlight only part of an organelle[34]. By using immunoEM, proteins can be localized at the level of the smallest vesicle, however, the static EM images give no clue as to the directionality of the membranes observed. To fill the gap between live-cell imaging and EM, several groups are developing correlative-microscopy methods[35]. In a first set of studies, green fluorescent protein (GFP) was genetically tagged to the G protein of the vesicular stomatitis virus (VSV-G)[28,36]. The individual transport intermediates were monitored by video microscopy, after which the cell under study was fixed and processed for pre-embedding immunoEM using anti-VSV-G. This approach revealed an unexpected pleiomorphic complexity of the VSV-G transport carriers. A promising alternative method, which overcomes the drawbacks of the harsh pre-embedding immunoEM procedure, makes use of a new fluorescein derivative — ReAsH[37] (see also the review on page S1 of this supplement). With respect to what is important for correlative microscopy, when the fixed cells are intensely illuminated, ReAsH catalyses the photo-oxidation of diaminobenzidine, which results in electron-dense precipitates that can be visualized by EM[37].

Recently, a new preparation method has been introduced that allows Tokuyasu cryosections to be adapted for correlative microscopy[38]. The power of this approach is shown in FIG. 2. Here, the intracellular trafficking of a GFP-conjugated construct of CD63 — a late endosomal–lysosomal protein — was imaged by both confocal microscopy and immunoEM using anti-GFP–10-nm gold on thawed cryosections. FIGURE 2 highlights an important point: seemingly similar fluorescent spots (spots 2 and 5 in FIG. 2c) are localized by immunoEM to different organelles — that is, endosomes (FIG. 2f) and Golgi-associated structures (FIG. 2g), respectively. This example shows that fluorescent patterns must be interpreted with the utmost caution and that correlative high-resolution immunoEM can provide essential information on the structures that underlie these signals.

As well as establishing the kinetics and carriers of distinct intracellular transport steps, correlative live-cell–immunoEM will be particularly useful in studying those events that involve a sudden change in the cell. For example, the conversion of a multivesicular endosome into a tubular lysosome, which is a recently discovered aspect of antigen presentation by dendritic cells, has been described in live cells[39] and using immunoEM[40]. Integrating this information would help to pinpoint the exact morphological changes and the molecular mechanisms that are involved in this intriguing process of membrane redistribution. For these correlative studies, it is important that the cells are fixed for EM at the exact moment at which the change takes place. High-pressure freezing is extremely rapid, but the time interval between cell selection under the light microscope and transfer to a high-pressure-freezing apparatus takes 15–20 seconds, which is too slow to fix rapid intracellular movements at the exact time of interest. Methods that solve this problem would provide another powerful tool for correlative live-cell–immunoEM/EM.

Finally, we would like to refer briefly to the potential of FLUORONANOGOLD complexes[41]. These probes can be used to label ultrathin cryosections and the fluorescent signal can be visualized using a sensitive light microscope. The same section can then be subjected to silver enhancement to amplify the signal for subsequent EM. At present, this technique has only been applied to fixed cells, but, when FluoroNanogold-labelled probes are designed that can be administered to living cells, it might potentially be extended to correlative live-cell–immunoEM imaging.

Final remarks

Some of the most profound insights in cell biology come from morphological analyses of subcellular structures. However, today, the appreciation of EM data is ambiguous. EM studies are often disdained as 'descriptive', as if this were a weakness. The visualization of the interior of a cell in combination with molecular topography is a continuing inspiration for conceptual thinking and for understanding molecular function. Structure is unequivocally linked to function, and EM is one of the few techniques that can resolve the structure of subcellular compartments together with their molecular make-up. EM is no more descriptive than many of the genomics or proteomics approaches, it just operates at a higher level of biological organization.

The upcoming EM technologies will allow the localization of a progressively wider spectrum of molecules against the structural background of almost perfectly preserved cellular architecture. To develop a comprehensive view on healthy and diseased cells, future EM must stand side by side with complementary light-microscopy, genetic and molecular approaches. EM equipment has become increasingly user-friendly and, with the commercialization of many of the main reagents, EM applications have come into reach of every laboratory that is willing, and able, to invest resources. However, consultation with experienced researchers who are familiar with the morphological landscapes of the cell will be invaluable to ensure that data are interpreted accurately.

**Department of Molecular Cell Biology, Faculty of Biology and Institute of Biomembranes, 3584 CH Utrecht, The Netherlands.*
‡Department of Cell Biology, Center for Electron Microscopy, University Medical Center Utrecht and Institute of Biomembranes, Heidelberglaan 100, 3584 CX Utrecht, The Netherlands.
Correspondence to J.K.
e-mail: j.klumperman@lab.azu.nl

Please cite this article as a supplement to volume 4 of **Nature Reviews Molecular Cell Biology**, *pages SS6–SS10.*
doi:10.1038/nrm1194

1. Geuze, H. J. A future for electron microscopy in cell biology? *Trends Cell Biol.* **9**, 92–93 (1999).
2. Griffiths, G. Bringing electron microscopy back into focus for cell biology. *Trends Cell Biol.* **11**, 153–154 (2001).
3. McIntosh, J. R. Electron microscopy of cells: a new beginning for a new century. *J. Cell Biol.* **153**, 25–32 (2001).
4. Steinbrecht, R. A. & Zierold, K. (eds) *Cryotechniques in Biological Electron Microscopy* (Springer, Berlin, 1987).
5. Monoghan, P., Perusinghe, N. & Müller, M. High-pressure freezing for immunocytochemistry. *J. Microsc.* **192**, 248–258 (1998).
6. Studer, D., Graber, W., Al-Amoudi, A. & Eggli, P. A new approach for cryofixation by high-pressure freezing. *J. Microsc.* **203**, 285–294 (2001).
7. Baumeister, W. Electron tomography: towards visualizing the molecular organization of the cytoplasm. *Curr. Opin. Struct. Biol.* **12**, 679–684 (2002).
8. Baumeister, W. & Steven, A. C. Macromolecular electron microscopy in the era of structural genomics. *Trends Biochem. Sci.* **25**, 624–631 (2000).
9. Klaholz, B. P. *et al.* Structure of the *Escherischia coli* ribosomal termination complex with release factor 2. *Nature* **421**, 90–94 (2003).
10. Rawat, U. B. *et al.* A cryo-electron microscopic study of ribosome-bound termination factor RF2. *Nature* **421**, 87–90 (2003).

11. Tokuyasu, K. T. A technique for ultracryotomy of cell suspensions and tissues. *J. Cell Biol.* **57**, 551–565 (1973).
12. Griffiths, G. *Fine Structure Immunocytochemistry* (Springer, Berlin, 1993).
13. Kleijmeer, M. J., Raposo, G. & Geuze, H. J. Characterization of MHC class II compartments by immunoelectron microscopy. *Methods* **10**, 191–207 (1996).
14. Liou, W., Geuze, H. J. & Slot, J. W. Improving structural integrity of cryosections for immunogold labeling. *Histochem. Cell Biol.* **106**, 41–58 (1996).
15. Martinez-Menarguez, J., Geuze, H. J., Slot, J. W. & Klumperman, J. Vesicular tubular clusters between ER and Golgi mediate concentration of soluble secretory proteins by exclusion from COPI-coated vesicles. *Cell* **98**, 81–90 (1999).
16. Slot, J. W., Posthuma, G., Chang, L. Y., Crapo, J. D. & Geuze, H. J. Quantitative aspects of immunogold labeling in embedded and in nonembedded sections. *Am. J. Anat.* **185**, 271–281 (1989).
17. Hainfeld, J. F. & Powell, R. D. New frontiers in gold labeling. *J. Histochem. Cytochem.* **48**, 471–480 (2000).
18. Humbel, B. M., Sibon, O. C., Stierhof, Y. D. & Schwarz, H. Ultra-small gold particles and silver enhancement as a detection system in immunolabeling and *in situ* hybridization experiments. *J. Histochem. Cytochem.* **43**, 735–737 (1995).
19. Möbius, W. *et al.* Immunoelectron microscopic localization of cholesterol using biotinylated and non-cytolytic perfringolysin O. *J. Histochem. Cytochem.* **50**, 43–55 (2002).
20. Möbius, W. *et al.* Recycling compartments and the internal vesicles of multivesicular bodies harbor most of the cholesterol found in the endocytic pathway. *Traffic* **4**, 222–231 (2003).
21. van Genderen, I. L., van Meer, G., Slot, J. W., Geuze, H. J. & Voorhout, W. F. Subcellular localization of Forssman glycolipid in epithelial MDCK cells by immuno-electron-microscopy after freeze-substitution. *J. Cell Biol.* **115**, 1009–1019 (1991).
22. Parton, R. G. Ultrastructural localization of gangliosides; GM1 is concentrated in caveolae. *J. Histochem. Cytochem.* **42**, 155–166 (1994).
23. Koster, A. J. *et al.* Perspectives of molecular and cellular electron tomography. *J. Struct. Biol.* **120**, 276–308 (1997).
24. Baumeister, W., Grimm, R. & Walz, J. Electron tomography of molecules and cells. *Trends Cell Biol.* **9**, 81–85 (1999).
25. Frank, J. *et al.* Three-dimensional imaging of biological complexity. *J. Struct. Biol.* **138**, 85–91 (2002).
26. Marsh, B. J., Mastronarde, D. N., Buttle, K. F., Howell, K. E. & McIntosh, J. R. Organellar relationships in the Golgi region of the pancreatic β-cell line, HIT-T15, visualized by high resolution electron tomography. *Proc. Natl Acad. Sci. USA* **98**, 2399–2406 (2001).
27. Ladinsky, M. S., Wu, C. C., McIntosh, S., McIntosh, J. R. & Howell, K. E. Structure of the Golgi and distribution of reporter molecules at 20 degrees C reveals the complexity of the exit compartments. *Mol. Biol. Cell* **13**, 2810–2825 (2002).
28. Mironov, A. A. *et al.* Small cargo proteins and large aggregates can traverse the Golgi by a common mechanism without leaving the lumen of cisternae. *J. Cell Biol.* **155**, 1225–1238 (2001).
29. Hsieh, C. E., Marko, M., Frank, J. & Mannella, C. A. Electron tomographic analysis of frozen-hydrated tissue sections. *J. Struct. Biol.* **138**, 63–73 (2002).
30. Geuze, H. J. *et al.* Involvement of the endoplasmic reticulum in peroxisome formation. *Mol. Biol. Cell* **14**, 2900–2907 (2003).
31. Ziese, U. *et al.* Automated high-throughput electron tomography by pre-calibration of image shifts. *J. Microsc.* **205**, 187–200 (2002).
32. Medalia, O. *et al.* Macromolecular architecture in eukaryotic cells visualized by cryoelectron tomography. *Science* **298**, 1209–1213 (2002).
33. Bohm, J. *et al.* Toward detecting and identifying macromolecules in a cellular context: template matching applied to electron tomograms. *Proc. Natl Acad. Sci. USA* **97**, 14245–14250 (2000).
34. Griffiths, G. *et al.* The immunofluorescent era of membrane traffic. *Trends Cell Biol.* **3**, 215–219 (1993).
35. Mironov, A. A., Polishchuk, R. S. & Luini, A. Visualizing membrane traffic *in vivo* by combined video fluorescence and 3D electron microscopy. *Trends Cell Biol.* **10**, 349–353 (2000).
36. Polishchuk, R. S. *et al.* Correlative light-electron microscopy reveals the tubular-saccular ultrastructure of carriers operating between Golgi apparatus and plasma membrane. *J. Cell Biol.* **148**, 45–58 (2000).
37. Gaietta, G. *et al.* Multicolor and electron microscopic imaging of connexin trafficking. *Science* **296**, 503–507 (2002).
38. Oorschot, V., de Wit, H., Annaert, W. G. & Klumperman, J. A novel flat-embedding method to prepare ultrathin cryosections from cultured cells in their *in situ* orientation. *J. Histochem. Cytochem.* **50**, 1067–1080 (2002).
39. Chow, A., Toomre, D., Garrett, W. & Mellman, I. Dendritic cell maturation triggers retrograde MHC class II transport from lysosomes to the plasma membrane. *Nature* **418**, 988–994 (2002).
40. Kleijmeer, M. *et al.* Reorganization of multivesicular bodies regulates MHC class II antigen presentation by dendritic cells. *J. Cell Biol.* **155**, 53–63 (2001).
41. Takizawa, T. & Robinson, J. M. FluoroNanogold is a bifunctional immunoprobe for correlative fluorescence and electron microscopy. *J. Histochem. Cytochem.* **48**, 481–486 (2000).

Acknowledgements

We thank all members of the A.J.K. and J.K. groups, especially W. Möbius, M. Kleijmeer, B. Humbel, A. Verkleij, J. Slot and H. J. Geuze for their stimulating discussions and for sharing their latest insights with us. A.J.K. is funded by a fellowship from the Royal Netherlands Academy of Arts and Sciences (KNAW), and A.J.K. and J.K. are the recipients of a grant from the Dutch Society for Scientific Research.

Online Links

DATABASES

The following terms in this article are linked online to:

Entrez: http://www.ncbi.nlm.nih.gov/Entrez/
VSV-G

Swiss-Prot: http://www.expasy.ch/
CD63 | GFP | RF2

FURTHER INFORMATION

3D Electron Microscopy at Utrecht University:
http://mcb.bio.uu.nl/3dem

UMC Utrecht University Department of Cell Biology:
http://www.med.uu.nl/celbiol/celbiol.htm

Access to this interactive links box is free online.

REVIEW

MRI: volumetric imaging for vital imaging and atlas construction

Russell E. Jacobs, Cyrus Papan, Seth Ruffins, J. Michael Tyszka and Scott E. Fraser

Magnetic resonance imaging (MRI) is well known for its ability to capture non-invasively the three-dimensional structure of complex tissues such as the human brain. The physics underlying this technique means that it can be refined to collect high-resolution images in settings that would scatter the radiation used in direct-imaging techniques. This makes microscopic MRI a powerful tool to observe events and structures deep inside otherwise opaque soft tissues.

The success of reductionistic approaches in biomedical research has yielded an unprecedented knowledge of the components that are involved in biological processes, and researchers now face the challenge of integrating this knowledge into a more complete understanding of whole systems. For example, the revolution in molecular biology has given us important new insights into the function of genes and gene products that might guide embryonic development. Many of the signalling pathways that are involved in the specification of cell types and the patterning of tissues are being defined, as are the transcription factors that are involved in controlling cell-type-specific and region-specific gene expression. To answer the basic question of how an embryo develops, we must determine how these molecular processes are assembled into an organism. The classic publications in the field of experimental embryology[1–3] illustrate the power of describing cell behaviours (in terms of cell lineages and movements) and then perturbing the development of an embryo to test hypotheses regarding the underlying mechanisms. Advanced imaging techniques offer an important stepping stone to integrate these disparate approaches[4], and allow questions about cellular and molecular signalling events to be posed in the most relevant setting of the intact embryo.

Imaging thick specimens

The focus of intravital imaging is to follow cellular and subcellular events in the context of an entire organism. This presents a significant challenge to researchers, because all but the youngest embryos are significantly thicker than can be imaged easily with light. The image collected by a camera in a wide-field light microscope is typically blurred, because light from above and below the

focal plane contributes to the image. To overcome this, computational tools, such as image deconvolution[5], can be used to minimize the blurring, but a single processed image requires the collection of several planes of image data, which is difficult in living and moving specimens. The use of laser-scanning techniques provides optical sectioning capabilities that can reject the contribution of light from above and below the plane of focus, which gives light microscopy the ability to penetrate a few hundred micrometres into the specimen[6]. However, light scattering eventually limits the performance of LASER-SCANNING MICROSCOPY, because a focused laser spot of sufficient intensity cannot be created at great depth. As a result, light-based techniques for deep imaging must obtain useful image data in the presence of a large background of scattered photons — for example, by collecting only those photons that are unscattered (ballistic photons[7]) or by collecting the photons that are scattered only once (optical coherence tomography[8]). An alternative approach is to make use of the highly scattering nature of biological tissue and to use a diffuse-imaging technique, in which light is treated as diffusing through the specimen[9]. As much promise as these techniques offer, it sometimes seems that these advances have been achieved by fighting with the underlying physics of light imaging — in short, that the field is attempting to collect a clear image in a hostile environment.

To circumvent the difficulty of collecting imaging data in a thick specimen, the field of medical imaging has adopted radiation of higher energy, which allows the collection of a significant number of unscattered photons. The use of conventional X-rays suffers from the same problem as wide-field microscopy, in that absorption or scattering by the specimen through its entire thickness contributes to the data recorded by the camera. However, computational processing of a large number of X-ray images from many angles can offer striking three-dimensional (3D) images of structures. Similar computer tomography algorithms can be used to localize radio-isotopically labelled molecules in 3D. For example, SINGLE-PHOTON EMISSION COMPUTED TOMOGRAPHY (SPECT) can be used to collect, from a number of angles, the emission of high-energy photons that occurs as a result of radioactive decay, and POSITRON EMISSION TOMOGRAPHY (PET) can be used to collect the two annihilation photons that are emitted when a positron from the decay of a radioactive label meets a nearby electron[10,11]. Central to all of these approaches is the use of ionizing radiation; therefore, the quality of the images must be balanced with the intrinsic risks of exposing biological tissues to radiation that can mutate or otherwise damage them. Magnetic resonance imaging (MRI)[12] is a powerful tool

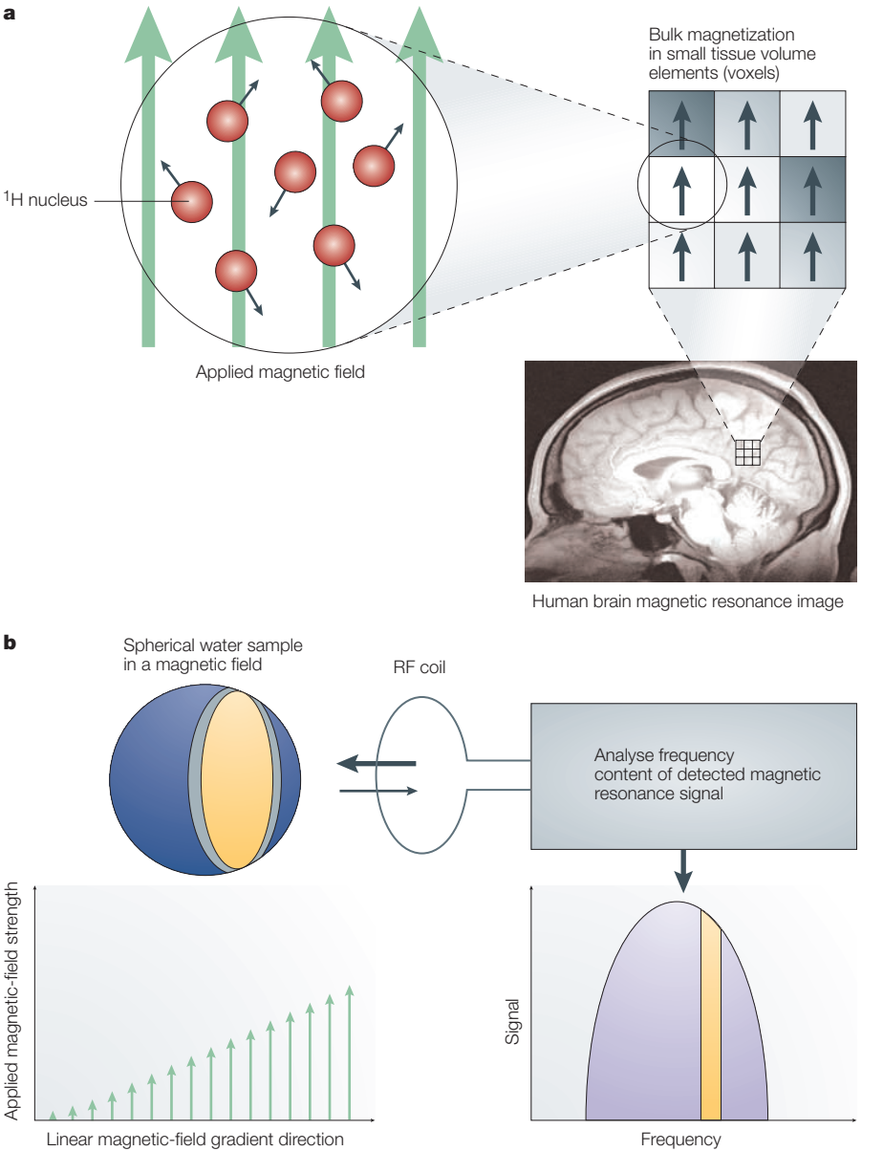

Figure 1 | **The basics of magnetic resonance imaging. a** | This panel illustrates the source of a typical magnetic resonance imaging (MRI) signal. ^{1}H nuclei (red circles) possess an intrinsic magnetism (black arrows) and align either with, or against, an applied magnetic field (green arrows). Slightly more nuclei align with the field, which leads to a small net or bulk nuclear magnetization. A typical magnetic resonance image of the human brain detects ^{1}H nuclear magnetization of water and lipids. The image of the human brain shown in the figure is composed of volume elements (voxels). These volume elements are on the order of one microlitre in size (that is, they are not to scale in the figure) and they contain perhaps 10^{19} water molecules (that is, many more than are shown in the figure), of which only a few parts per million contribute to the detectable signal. The intensity recorded from each of these voxels (shown as different shades of grey in the top right part of the figure) depends on the details of the data collection, and the local environment and chemical species in the voxel. **b** | This panel shows the use of linear magnetic-field gradients in MRI to obtain a one-dimensional (1D) projection image of a spherical water sample. When the bulk nuclear magnetization is tilted away from equilibrium by a pulse from the radio-frequency (RF) coil, the precession frequency of this magnetization is proportional to the local field strength. As a result, a linear field gradient imposed on the specimen can be used to encode the distance along the gradient direction as frequency in the detected signal. In this example, water in the yellow-shaded area of the sphere contributes signal to a narrow band of frequencies in the spectrum that forms a 1D projection image of the sphere. This approach can be extended to two-dimensional and three-dimensional MRI by using sequences of RF and field-gradient pulses and both frequency and phase analysis of the detected signal.

for imaging in otherwise difficult preparations without the use of ionizing radiation. Before discussing the present applications of MRI and its future prospects, we present a brief overview of how such images are acquired.

The basics of MRI

MRI exploits the nuclear magnetic resonance (NMR) effect, in which certain atomic nuclei can interact with radio waves when they are placed in a strong, applied magnetic field. Almost all MRI experiments observe the proton that forms the ^{1}H nucleus that is present in water, fat and other biomolecules. Individual ^{1}H nuclei have a magnetic moment, which is analogous to a subatomic bar magnet, but, practically, MRI is often described in terms of the total or bulk nuclear magnetization that arises from large groups of such nuclei — for example, a typical one microlitre volume element (or voxel) in human-brain MRI contains perhaps 10^{19} water molecules (FIG. 1a). The bulk magnetization arises from the slight excess (typically a few parts per million) of nuclei that align with, rather than against, the applied magnetic field, which is on the order of 1–12 Tesla for most MRI systems. A short pulse of radio-frequency (RF) magnetic field, which is generated by a nearby antenna (RF coil), can tilt the bulk nuclear magnetization away from its equilibrium direction. The bulk magnetization then begins to rotate or precess around the static-field direction at a frequency (the Larmor frequency) that is proportional to the strength of the static field. The same antenna that is used to tilt the magnetization can also detect the weak signal from the precessing bulk magnetization. The precessing state typically decays in tens or hundreds of milliseconds in biological tissues. Variations in the local magnetic field in tissue samples disperse the precessional frequencies in the sample, which greatly increases the decay rate of the detectable signal. However, additional RF pulses allow the signal to be 'refocused' at slightly later times in what are termed 'spin echoes'. These spin echoes — which are a well-established, basic physical phenomenon — are sufficiently large to be recorded and form the basis of many MRI collection methods[13,14].

In MRI, imaging is based on the linear relationship between the applied magnetic-field strength and the precessional frequency of the bulk magnetization. A linear-magnetic-field variation or gradient can be imposed on the sample, which results in a linear variation of the precessional frequency with distance along the gradient direction, and is known as frequency encoding (FIG. 1b). These field gradients are typically pulsed and combined with RF pulses to localize the MRI-signal source in two-dimensional (2D) and 3D space. Restrictions in the way in which the gradient and RF pulses can be combined lead to typical image-acquisition times of minutes and sometimes hours. The use of frequency encoding (and its close relation, phase encoding in 2D and 3D MRI) results in the data being acquired in an 'inverse space', which is analogous to diffraction patterns that are acquired in optics, and the final transformation to a real-space image is

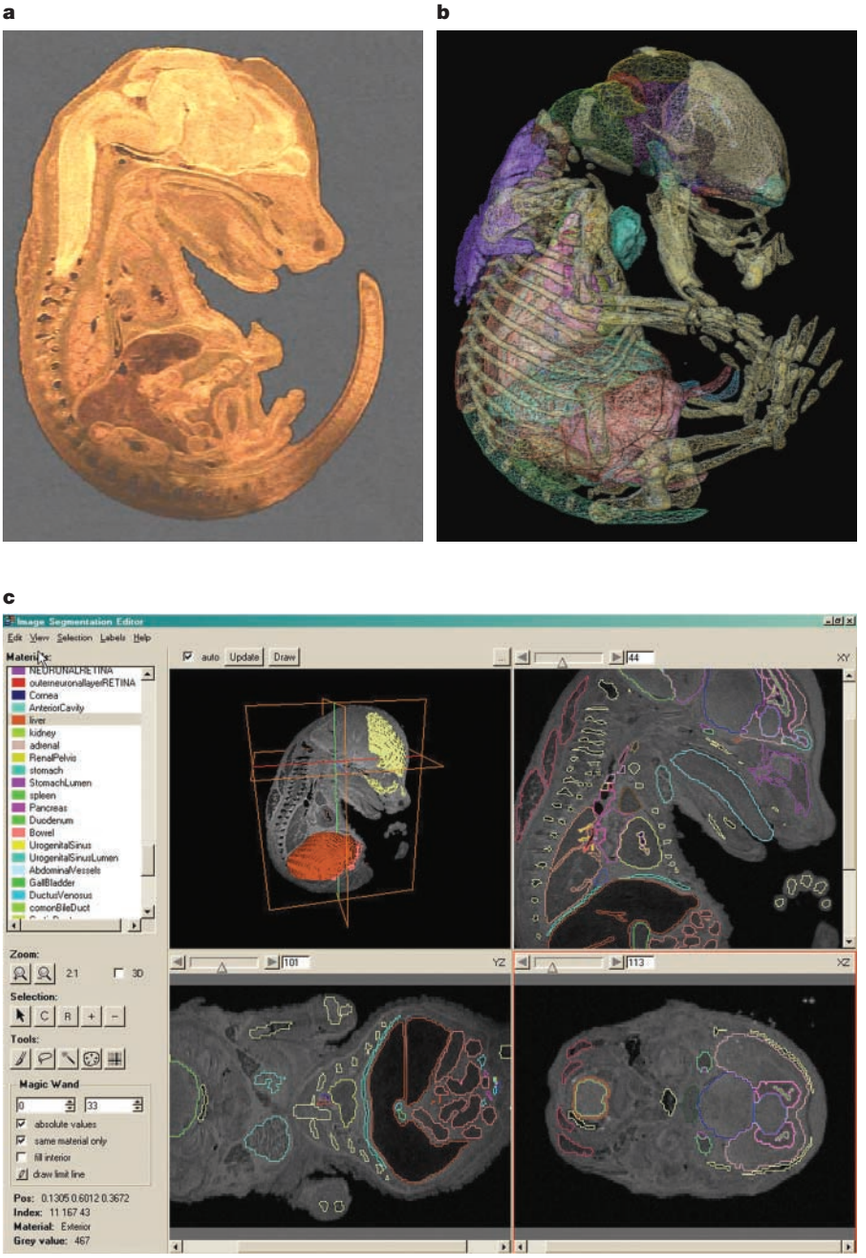

Figure 2 | **The creation of volumetric atlases from microscopic magnetic resonance imaging data.** **a** | This panel shows a single slice of a three-dimensional (3D) magnetic resonance (MR) image of a fixed mouse embryo. Images of this type must be annotated using manual segmentation. **b** | This panel depicts semi-transparent volume rendering of the surfaces of the various organ systems that were visible in the MR image and that were manually determined using the program AMIRA (TGS Software, San Diego, California, USA). **c** | This part of the figure shows a screen shot of a data set that is in the process of being segmented. Some of the primordial skeletal system and the central nervous system have been outlined. The ability to have the 3D representation (upper left image) and the three orthogonal planes in view simultaneously greatly simplifies the manual segmentation process.

obtained using computational methods. Typical spatial resolutions vary from tens of micrometres to millimetres depending on the size of the sample, the imaging time available and the limitations of the hardware.

Contrast in MRI arises from variations in the local environment and the concentration of water[15–18]. Two relaxation time constants (T_1 and T_2), which are associated with the decay of the perturbed magnetization back to equilibrium following an RF pulse, are useful when considering the intrinsic physical variations that give contrast. These two time constants vary with the local microscopic environment that is experienced by a water molecule or other detectable species. Environmental factors include, but are not limited to, viscosity, water temperature, and proximity to macromolecules or paramagnetic ions[19]. By altering the timing of the RF and gradient pulses, it is possible to sensitize the magnetic resonance image to intrinsic variations in T_1 or T_2. Other intrinsic phenomena, such as water diffusion and bulk motion, can be encoded in the image contrast, which makes MRI an incredibly flexible tool for the non-invasive imaging of biological systems. In clinical and research settings, such inherent contrast mechanisms allow the acquisition of 3D images with striking soft-tissue contrast.

Anatomical images and 3D atlases

MICROSCOPIC MAGNETIC RESONANCE IMAGING (μMRI), which is performed using large magnetic fields and field gradients, can give a resolution to ~10 μm. Such images of developing embryos contain a wealth of data and can be visually striking. As one step in transforming these data into information (and hopefully then into knowledge about embryonic development), magnetic resonance images can be used as the basis for digital atlases of development[20]. Atlases are crucial as educational and analytical tools and as tools for communicating complex information. Using μMRI, the internal structures of opaque embryos can be imaged without sectioning, which leaves the embryo in the most unperturbed state possible. Furthermore, μMRI is an excellent imaging modality for constructing 3D atlases, because small structures can be resolved and are readily identified. In addition, the data are inherently in register and are not distorted by sectioning. Perhaps the most labour-intensive and time-consuming aspect of digital atlas creation is the delineation of anatomical structures. The segmentation and annotation process is outlined in FIG. 2.

Unlike classical atlases, which often have simple pointers to anatomical features in an image, identified structures in volumetric digital atlases have defined boundaries because each element in the image volume is assigned an identifier. A typical image segmentation session involves the operator manually selecting a series of voxels in an image volume on a slice-by-slice basis, in any or all orthogonal planes, using tracing or painting tools. Selected voxels are assigned a name, colour and 'material identifier'. The assigned voxels are stored as separate image files with the same image dimensions as the original image. These 'label files' serve as the raw database input and are used to generate surface models for visualization purposes. These models are useful for visualizing the 3D geometry of specific anatomy and the spatial

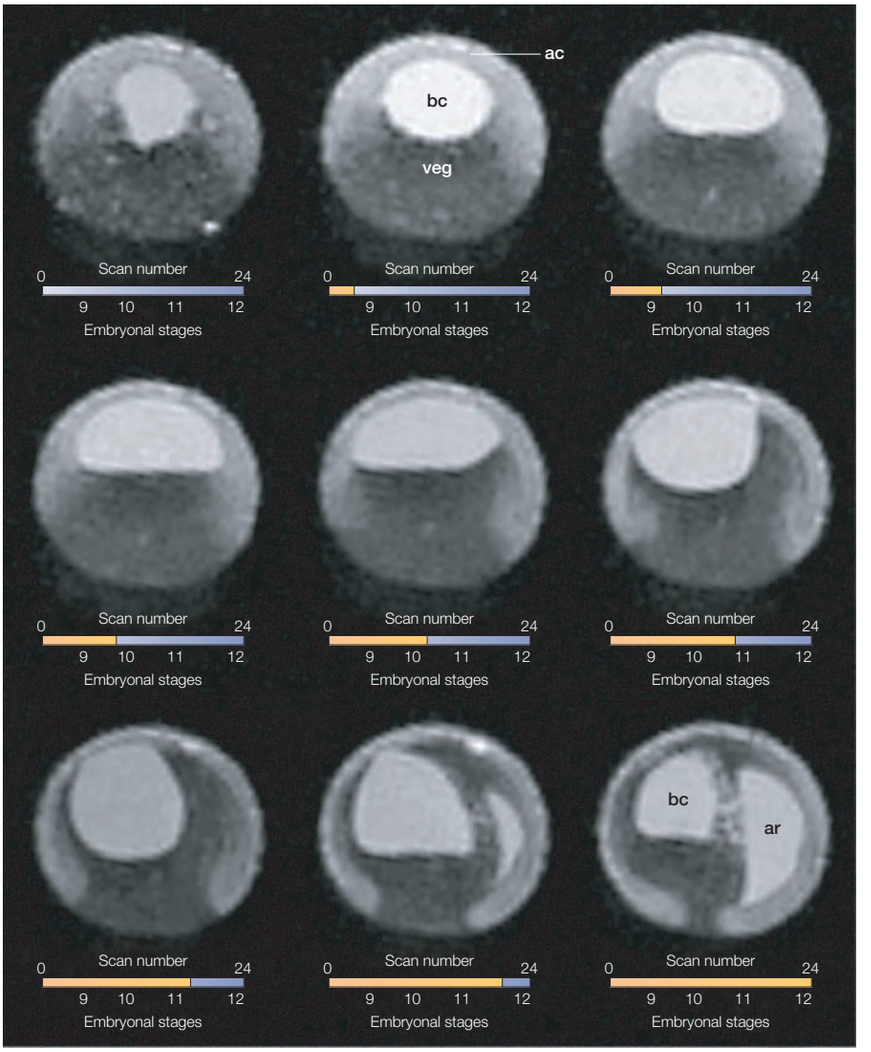

Figure 3 | **A time-lapse movie of *Xenopus laevis* gastrulation.** Each image shows a slice through a three-dimensional (3D) microscopic magnetic resonance imaging (μMRI) scan that was collected as a *Xenopus laevis* embryo developed inside the magnet (the figure shows one of every three time-points collected in the series). The animal pole is up, vegetal is down and dorsal is to the right. No contrast agent was used in this experiment; the regional differences in intensity are due to intrinsic contrast only. The fluid-filled cavities — blastocoel (bc) and archenteron (ar) — are the most intense regions in the images, the fat-filled vegetal cells (veg) are the darkest, and the animal-cap cells (ac) and their descendents are of moderate intensity. The ability to discriminate cell type by intrinsic contrast allows the convenient visualization of the thinning and spreading of the animal pole of the embryo during epiboly (the movement of the quickly dividing animal-pole cells downward to engulf the more slowly dividing vegetal cells before gastrulation) and of many of the coordinated cell movements that make up gastrulation. To collect the images, the embryo was placed in a 2-mm diameter tube in ~10 μl of rearing medium. The sample was maintained in the scanner at 15 °C throughout the course of gastrulation and was scanned hourly. At this temperature, gastrulation takes about 12 hours, which allows both sufficient time to obtain a full 3D scan without motion blur and sufficient temporal resolution to follow morphometric movements. These images were obtained using a Bruker Avance DRX500 (11.7 Tesla) system.

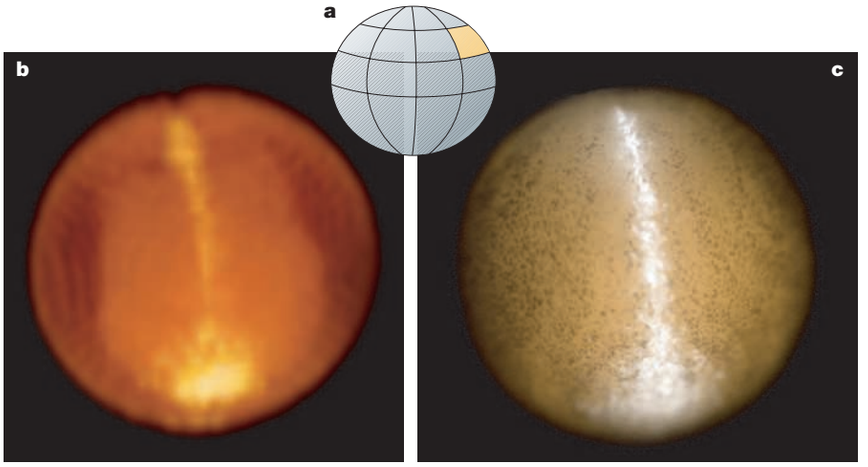

Figure 4 | **Epi-fluorescence and microscopic magnetic resonance images of a stage 13 *Xenopus laevis* embryo. a** | At the 32-cell stage, the blastomere B1 (highlighted in yellow) was injected with a bifunctional contrast agent to allow the descendants of the injected cell to be followed during development. Using both fluorescence (**b**) and magnetic resonance imaging (**c**) techniques, the labelled clone of cells is strikingly visible in the images taken at stage 13. The embryo is viewed from the dorsal side, with the anterior pole pointing downwards. The labelled clones are in the positions expected from previous fate maps, but, whereas only the surface details are visible in the fluorescence image (**b**), the three-dimensional magnetic resonance image (**c**) can show the depth of the clone and the forming primitive gut (the archenteron).

relationships between two or more structures (FIG. 2). The surface models also provide morphometric data such as the surface area and volume of the developing anatomy. In general, however, understanding developing systems goes beyond simple structural identification, so multidimensional atlases are now being created that incorporate additional information such as gene-expression, biochemistry or cell-fate data. The Edinburgh Mouse Atlas Project (see Online links) is one such digital atlas that is based on histological sections. This atlas also provides access to the anatomical ontology and Jackson Labs GDX (gene-expression database) through an image-query interface[21]. Ultimately, such higher-dimensional atlases will provide us with a convenient, compelling and intuitive way to access numerous types of information about developing organisms. For an example of MRI atlas construction, see Movie 1 online.

Live embryo imaging

As μMRI can collect images of living specimens, it offers the possibility of observing the 3D anatomy of the embryo as it develops[22]. *Xenopus laevis* embryos are ideally suited to such four-dimensional imaging, as these large (~1.2-mm diameter) embryos develop normally at room temperature in a simple medium of artificial pond water. μMRI offers an important advantage over light-based imaging technologies, because yolk inclusions in the cells of the *Xenopus* embryo scatter light and prevent the acquisition of 3D data sets using either wide-field or laser-scanning microscopes. The different regions of the embryo are distinct in μMRI owing to intrinsic contrast: the central fluid-filled cavity in the embryo (the blastocoel) is almost pure water, which results in a long T_1; the cells in the animal pole of the embryo have a much shorter T_1 and T_2 owing to the cytoplasmic components that are present in these cells and that interact with the water; and the cells in the vegetal pole of the embryo contain much less free water and more fat, which makes them distinct from the animal-pole cells[23]. In our recent experiments (C.P., S. S. Velan, S.E.F. and R.E.J., unpublished observations), we employed μMRI to record 3D time-lapse images at an isotropic resolution of 40 μm at 55 minutes per 3D image. This spatial and temporal resolution is sufficient (given the slow development of the embryos at reduced temperatures) to follow small groups of cells and, in some cases, even individual cells as the animal develops in the MR scanner (FIG. 3).

Extrinsic contrast and MRI labels

Extrinsic agents can be introduced to selectively alter the relaxation times (T_1 and T_2), which allows specific tissues, cells or fluid compartments to be rendered more distinct. T_1 agents typically involve a chelated gadolinium ion, which can speed up the return of surrounding water protons to equilibrium and thereby increase the number of spins that can absorb the next RF pulse. This selectively increases the signal in a T_1-weighted image. T_2 agents often incorporate ferromagnetic or superparamagnetic centres (for example, iron nanoparticles encapsulated in dextran) that make the local magnetic field less homogeneous and thereby speed up the phase randomization of nearby spins. This results in a decrease in the local signal in a T_2-weighted image.

Clinically, both T_1 and T_2 agents are used to label the blood pool and, in some cases, are used to enhance the visualization of a specific tissue or organ because of the affinity of a given agent. In experimental settings, such agents can be targeted more selectively by the direct microinjection of a contrast agent[22] or a bifunctional contrast agent (both fluorescence and MRI labels[24]) into single cells, by fluid-phase uptake[25] or by receptor-mediated uptake[26,27]. FIGURE 4 shows a living *Xenopus* embryo in which a single blastomere was labelled by co-injecting it with fluorescence and MRI lineage labels. This shows that it is possible to generate high-resolution images of labelled cells and their descendants throughout the development of a specimen.

Future prospects

Diffusion-tensor imaging. A basic MRI pulse sequence can be sensitized to the motion (diffusion) of water in a specific direction using additional powerful magnetic-field gradient pulses in a process known as 'diffusion weighting'. Water diffusion is restricted by cell membranes and other structures, and the diffusion rate seems to vary with direction depending on the local organization of tissues (diffusion anisotropy). By collecting sets of diffusion-weighted images that differ in sensitivity according to direction, a picture can be built up of the microscopic restrictions that are experienced by water molecules in living tissue[28]. For example, water seems to diffuse much faster along the length of white-matter nerve bundles and tracts than across their width, even in the absence of myelin[29,30]. Diffusion anisotropy is often modelled using a tissue property called the diffusion tensor[31]. Details of the tensor model are beyond the scope of this review, but it allows the average diffusion properties of tissue to be determined at every voxel of the MRI image. White-matter tracts in the human brain can therefore be traced from one region of the brain to another using the diffusion anisotropy as a guide[32,33]. Recent work from the laboratory of Susumu Mori shows the utility of high-resolution diffusion-tensor imaging (DTI) of human and mouse brains[34,35]. More sophisticated models of diffusion anisotropy that can accommodate fibre crossings and other complicated geometries

are under development[36]. DTI has confirmed many of the well-known regional connections in the normal human brain and, with further development, promises to reveal even finer neuroarchitectural detail of both normal and pathological conditions.

Magnetic resonance spectroscopy. Magnetic resonance spectroscopy (MRS) is widely used in analytical chemistry for molecular structural analysis. This powerful tool can be reapplied to living systems to extract metabolic information from a single, small volume of tissue or to create a 2D or 3D metabolic map over a larger area. Most *in vivo* applications are based on spectroscopy of the endogenous ^{1}H nucleus and reveal as many as 35 low-molecular-weight metabolites, which include intracellular *N*-acetylaspartate, creatine, choline and glutamate in the mammalian brain[37]. The diagnostic capabilities of single-voxel ^{1}H spectroscopy in the human brain are well established, and are particularly suited to diffuse neuropathologies such as Alzheimer's disease, hepatic encephalopathy, hypoxia and metabolic disorders[38].

Recent technical improvements now allow ^{1}H spectra to be acquired from hundreds and even thousands of subvolumes in the brain in a matter of minutes using a process called SPECTROSCOPIC OR CHEMICAL-SHIFT IMAGING[39,40]. The maps of metabolite concentration that are derived from these spatially resolved spectra show promise for both the diagnosis of brain tumours and planning of the subsequent therapy[41,42]. Experiments with other NMR-sensitive nuclei, such as ^{13}C and ^{31}P, both in single-voxel and imaging modes, highlight the promise of MRS for the more advanced examination of metabolic pathways, such as the tricarboxylic-acid cycle (for a recent study, see REF. 43). As more sophisticated techniques from analytical structural NMR will be reapplied *in vivo* to both human and animal brains, the future looks bright for non-invasive metabolic mapping by MRS.

Transgene detection. The spatial resolution of MRI and the chemical sensitivity of MRS mean that combining these techniques is useful for sensing transgene activity *in vivo*. The Koretsky laboratory did just this when they expressed creatine kinase (CK) as a transgene in the livers of mice. The expression of CK could be visualized in the liver by monitoring the phosphocreatine spectroscopic peak[44]. Other approaches have used a transgene for the tyrosinase gene (pcDNA3tyr) that increases melanin production and thereby renders the cells that are expressing melanin visible in a T_2-weighted image (melanin shortens the T_2 relaxation time)[45]. In addition, an MRI-detectable reporter gene has been created by engineering the transferrin receptor so that it can selectively take up transferrin-based MRI contrast agents[26,27].

In a separate approach, contrast agents have been generated that can be activated by an enzymatic activity[24,46]. The ability of such compounds to serve as a strong T_1-contrast agent is partially inhibited by the presence of a blocking moiety that prevents the direct interaction of water with the chelated gadolinium ion. In the T_1-contrast agents Egad and EgadMe, the blocking moiety is a galactose sugar, and the agent only becomes fully active after the sugar is cleaved by the enzyme β-galactosidase. EgadMe has been introduced into all of the cells of a *Xenopus* embryo by injecting it into the fertilized egg, thereby allowing the expression of the β-galactosidase marker enzyme to be observed in the living cells[46]. However, such T_1-contrast agents have yet to find widespread use in systems such as the mouse, owing to the difficulty in obtaining a uniform uptake of the contrast agent into the interior of the cells where the enzyme is localized. Our attempts to overcome this limitation by covalently attaching permeabilizing agents, such as the HIV tat peptide[47], to an otherwise impermeant contrast agent have not yet proved successful.

Conclusions

MRI provides an ideal tool for obtaining internal 3D views of optically opaque systems. Its acute sensitivity to the local physical and chemical environment provides us with knowledge about the internal structure and function of intact living systems. High-resolution μMRI is an emerging technique that is capable of imaging biological subjects *in vitro* and *in vivo* at near-cellular resolution (~10–50 μm). The capabilities of μMRI make it an ideal complement to existing technologies, as it can fill the resolution gap between PET/SPECT (~0.1–1 mm) and confocal/two-photon optical (~1 μm) imaging methodologies. Changes in tissue morphology, the progression of disease states and biochemical changes can all be visualized directly using μMRI. The principal disadvantage of MRI is its low sensitivity. This can lead to relatively long data acquisition times (seconds to days) and relatively low signal strength. Limitations in the signal strength can force users to make a difficult choice between low spatial resolution and low image contrast. Hardware improvements to increase the signal:noise ratio and new hyperpolarization techniques[48] continue to mitigate this problem. Future advancements in μMRI imaging technologies will offer views into the development, structure, function and dysfunction of the central nervous system, which will benefit basic biological research as well as provide new tools for clinical diagnostic imaging.

Biological Imaging Center, Beckman Institute and Division of Biology, California Institute of Technology, 1200 East California Boulevard, Pasadena, California 91125, USA.
Correspondence to S.E.F.
e-mail: sefraser@caltech.edu

Please cite this article as a supplement to volume 4 of **Nature Reviews Molecular Cell Biology,** *pages SS10–SS16.*

doi:10.1038/nrm1195

1. Chia, W. & Yang, X. Asymmetric division of *Drosophila* neural progenitors. *Curr. Opin. Genet. Dev.* **12**, 459–464 (2002).
2. Harland, R. & Gerhart, J. Formation and function of Spemann's organizer. *Annu. Rev. Cell Dev. Biol.* **13**, 611–667 (1997).
3. Schier, A. F. Axis formation and patterning in zebrafish. *Curr. Opin. Genet. Dev.* **11**, 393–404 (2001).
4. Lichtman, J. W. & Fraser, S. E. The neuronal naturalist: watching neurons in their native habitat. *Nature Neurosci.* **4**, S1215–S1220 (2001).
5. Jansson, P. A. *Deconvolution of Images and Spectra* (Academic Press, San Diego, California, 1997).
6. So, P. T., Dong, C. Y., Masters, B. R. & Berland, K. M. Two-photon excitation fluorescence microscopy. *Annu. Rev. Biomed. Eng.* **2**, 399–429 (2000).
7. Chance, B., Cope, M., Gratton, E., Ramanujam, N. & Tromberg, B. Phase measurement of light absorption and scatter in human tissue. *Rev. Sci. Instrum.* **69**, 3457–3481 (1998).
8. Tearney, G. J. *et al. In vivo* endoscopic optical biopsy with optical coherence tomography. *Science* **276**, 2037–2039 (1997).
9. Tromberg, B., Yodh, A., Sevick, E. & Pine, D. Diffusing photons in turbid media: introduction to the feature. *Appl. Opt.* **36**, 9 (1997).
10. Cherry, S. R. *et al.* MicroPET: a high resolution PET scanner for imaging small animals. *IEEE Trans. Nucl. Sci.* **44**, 1161–1166 (1997).
11. Chatziioannou, A., Silverman, R. W., Meadors, K., Farquhar, T. H. & Cherry, S. R. Techniques to improve the spatial sampling of microPET — a high resolution animal PET tomograph. *IEEE Trans. Nucl. Sci.* **47**, 422–427 (2000).
12. Lauterbur, P. C. Image formation by induced local interactions. Examples employing nuclear magnetic resonance. *Nature* **242**, 190–191 (1973).
13. Hahn, E. L. Spin echoes. *Phys. Rev.* **80**, 580–594 (1950).
14. Slichter, C. P. *Principles of Magnetic Resonance* (Springer–Verlag, Berlin, New York, 1990).
15. Bradley, W. G. & Bydder, G. M. *MRI Atlas of the Brain* (Raven Press, New York, London, 1990).
16. Callaghan, P. T. *Principles of Nuclear Magnetic Resonance Microscopy* (Clarendon Press, Oxford Univ. Press, Oxford, 1991).
17. Calamante, F. *et al.* Early changes in water diffusion, perfusion, T_1 and T_2 during focal cerebral ischemia in the rat studied at 8. 5 T. *Magn. Reson. Med.* **41**, 479–485 (1999).
18. Herndon, R. C., Lancaster, J. L., Toga, A. W. & Fox, P. T. Quantification of white matter and gray matter volumes from T_1 parametric images using fuzzy classifiers. *J. Magn. Reson. Imaging* **6**, 425–435 (1996).
19. Moonen, C. T., van Zijl, P. C., Frank, J. A., Le Bihan, D. & Becker, E. D. Functional magnetic resonance imaging in medicine and physiology. *Science* **250**, 53–61 (1990).
20. Dhenain, M., Ruffins, S. W. & Jacobs, R. E. Three-dimensional digital mouse atlas using high-resolution MRI. *Dev. Biol.* **232**, 458–470 (2001).
21. Davidson, D. & Baldock, R. in *Molecular Genetics of Early Human Development* (eds Strachan, T., Lindsay, S. & Wilson, D. I.) 239–260 (BIOS Scientific, Oxford, 1997).
22. Jacobs, R. E. & Fraser, S. E. Magnetic resonance microscopy of embryonic cell lineages and movements. *Science* **263**, 681–684 (1994).
23. Sehy, J. V., Ackerman, J. J. & Neil, J. J. Water and lipid MRI of the *Xenopus* oocyte. *Magn. Reson. Med.* **46**, 900–906 (2001).

24. Hüber, M. M. *et al.* Fluorescently detectable magnetic resonance imaging agents. *Bioconjug. Chem.* **9**, 242–249 (1998).
25. Dodd, S. J. *et al.* Detection of single mammalian cells by high-resolution magnetic resonance imaging. *Biophys. J.* **76**, 103–109 (1999).
26. Kayyem, J. F., Kumar, R. M., Fraser, S. E. & Meade, T. J. Receptor-targeted cotransport of DNA and magnetic-resonance contrast agents. *Chem. Biol.* **2**, 615–620 (1995).
27. Moore, A., Josephson, L., Bhorade, R. M., Basilion, J. P. & Weissleder, R. Human transferrin receptor gene as a marker gene for MR imaging. *Radiology* **221**, 244–250 (2001).
28. Basser, P. J., Mattiello, J. & LeBihan, D. Estimation of the effective self-diffusion tensor from the NMR spin echo. *J. Magn. Reson. B* **103**, 247–254 (1994).
29. Ahrens, E. T., Laidlaw, D. H., Readhead, C., Fraser, S. E. & Jacobs, R. E. Investigating white matter diffusion anisotropy using the demyelinating shiverer mutant mouse in *Proceedings of the Seventh International Society for Magnetic Resonance in Medicine* (Berkeley, California, 1999).
30. Song, S. K. *et al.* Dysmyelination revealed through MRI as increased radial (but unchanged axial) diffusion of water. *Neuroimage* **17**, 1429–1436 (2002).
31. Pierpaoli, C., Jezzard, P., Basser, P. J., Barnett, A. & Di Chiro, G. Diffusion tensor MR imaging of the human brain. *Radiology* **201**, 637–648 (1996).
32. Conturo, T. E. *et al.* Tracking neuronal fiber pathways in the living human brain. *Proc. Natl Acad. Sci. USA* **96**, 10422–10427 (1999).
33. Jones, D. K., Simmons, A., Williams, S. C. & Horsfield, M. A. Non-invasive assessment of axonal fiber connectivity in the human brain via diffusion tensor MRI. *Magn. Reson. Med.* **42**, 37–41 (1999).
34. Mori, S. & Barker, P. B. Diffusion magnetic resonance imaging: its principle and applications. *Anat. Rec.* **257**, 102–109 (1999).
35. Mori, S. *et al.* Diffusion tensor imaging of the developing mouse brain. *Magn. Reson. Med.* **46**, 18–23 (2001).
36. Frank, L. R. Characterization of anisotropy in high angular resolution diffusion-weighted MRI. *Magn. Reson. Med.* **47**, 1083–1099 (2002).
37. Govindaraju, V., Young, K. & Maudsley, A. A. Proton NMR chemical shifts and coupling constants for brain metabolites. *NMR Biomed.* **13**, 129–153 (2000).
38. Ross, B. & Bluml, S. Magnetic resonance spectroscopy of the human brain. *Anat. Rec.* **265**, 54–84 (2001).
39. Dydak, U., Weiger, M., Pruessmann, K. P., Meier, D. & Boesiger, P. Sensitivity-encoded spectroscopic imaging. *Magn. Reson. Med.* **46**, 713–722 (2001).
40. Tyszka, J. M. & Mamelak, A. N. Volumetric multishot echo-planar spectroscopic imaging. *Magn. Reson. Med.* **46**, 219–227 (2001).
41. Dowling, C. *et al.* Preoperative proton MR spectroscopic imaging of brain tumors: correlation with histopathologic analysis of resection specimens. *Am. J. Neuroradiol.* **22**, 604–612 (2001).
42. Graves, E. E. *et al.* Serial proton MR spectroscopic imaging of recurrent malignant gliomas after γ knife radiosurgery. *Am J. Neuroradiol.* **22**, 613–624 (2001).
43. Bluml, S., Moreno-Torres, A., Shic, F., Nguy, C. H. & Ross, B. D. Tricarboxylic acid cycle of glia in the *in vivo* human brain. *NMR Biomed.* **15**, 1–5 (2002).
44. Koretsky, A. P., Brosnan, M. J., Chen, L. H., Chen, J. D. & Van Dyke, T. NMR detection of creatine kinase expressed in liver of transgenic mice: determination of free ADP levels. *Proc. Natl Acad. Sci. USA* **87**, 3112–3116 (1990).
45. Weissleder, R. *et al.* MR imaging and scintigraphy of gene expression through melanin induction. *Radiology* **204**, 425–429 (1997).
46. Louie, A. Y. *et al. In vivo* visualization of gene expression using magnetic resonance imaging. *Nature Biotech.* **18**, 321–325 (2000).
47. Zhao, M., Kircher, M. F., Josephson, L. & Weissleder, R. Differential conjugation of tat peptide to superparamagnetic nanoparticles and its effect on cellular uptake. *Bioconjug. Chem.* **13**, 840–844 (2002).
48. Zook, A. L., Adhyaru, B. B. & Bowers, C. R. High capacity production of >65% spin polarized Xenon-129 for NMR spectroscopy and imaging. *J. Magn. Reson.* **159**, 175–182 (2002).

Online links

DATABASES

The following terms in this article are linked online to:

LocusLink: http://www.ncbi.nlm.nih.gov/LocusLink/
creatine kinase | β-galactosidase

FURTHER INFORMATION

Edinburgh Mouse Atlas Project: http://genex.hgu.mrc.ac.uk/

Access to this interactive links box is free online.

OPINION

Imagining imaging's future

Roger Y. Tsien

Imaging specific molecules and their interactions in space and time will be essential to understand how genomes create cells, how cells constitute organisms and how errant cells cause disease. Molecular imaging must be extended and applied from nanometre to metre scales and from milliseconds to days. This quest will require input from physics, chemistry, and the genetics and biochemistry of diverse organisms with useful talents.

Any attempt to forecast the future of a fast-moving subject is foolhardy, but at the Editors' request, I offer a few idiosyncratic extrapolations that indicate in which directions I feel imaging ought to progress.

Systematic cell and developmental biology began in the nineteenth century with morphological descriptions of visible structures, the chemical basis of which was largely unknown. Meanwhile, physiology began to describe the amazing, complex responses of living systems to real-time perturbations, but again molecular details were missing. The twentieth century witnessed explosive progress in macromolecular biochemistry and genetics, which started with the rediscovery of Mendelian genetics and the recognition of biopolymers, and culminated in the sequencing of complete genomes. However, genome sequences alone lack spatial and temporal information and are therefore as dynamic and informative as census lists or telephone directories. The challenge for the twenty-first century is to understand how these casts of molecular characters work together to make living cells and organisms, and how such understanding can be harnessed to improve health and well-being. I believe this quest will depend heavily on molecular imaging, which shows when and where genetically or biochemically defined molecules, signals or processes appear, interact and disappear, in time and space. Therefore, molecular imaging synergistically draws on physics, chemistry, anatomy, physiology, biochemistry and genetics.

Perhaps the first breakthroughs in molecular imaging were the development of fluorescent-antibody techniques in the 1940s and *in situ* hybridization techniques in the 1980s (for historical reviews, see REFS 1,2), which reveal the spatial distribution of protein and nucleotide sequences respectively, albeit only in dead fixed cells or tissue sections. Significant advances in cell physiology also came in the 1980s from the development of fluorescent organic dyes that could non-destructively image ionic signals such as pH, Ca^{2+} and membrane potential with high spatial and temporal resolution[3]. However, the range of signals for which satisfactory indicators could be devised was very limited, applications to intact organisms or non-mammalian cells were rare, and targeting to specific subcellular locations or cell types was nearly impossible. A paradigm-shifting advance that occurred in the past decade was the cloning[4] and expression[5] of the jellyfish green fluorescent protein (GFP), which enabled visible fluorescence to be genetically encoded by a single portable DNA sequence[6]. Much of the revolution wrought by GFP and its variants is reviewed in other articles in this supplement. The prevalence and success of GFP indicate that comparable revolutions might result from genetic sequences that robustly encode image contrast for other methods, such as electron microscopy (EM), NANOPROBE SCANNING, OPTICAL COHERENCE TOMOGRAPHY (OCT), magnetic resonance imaging (MRI), MAGNETOENCEPHALOGRAPHY (MEG) and near-infrared fluorescence. The spatial and temporal domains of these imaging techniques, and other techniques that are discussed in this article, are shown in FIG. 1.

One additional advantage of gene sequences is that they are easily transferred from one laboratory to another — for example, as a drop of complementary DNA on a filter or a file stating a useful mutation. Only software is as easily communicated and replicated, but high-performance imaging software often has to be highly optimized for a particular piece of hardware and its operating system, and therefore loses portability. We are lucky that the genetic code is so standardized. Advances in instrumentation hardware have the lowest rate of dissemination and all too often end up amusing only their creators unless a major manufacturer becomes a committed advocate.

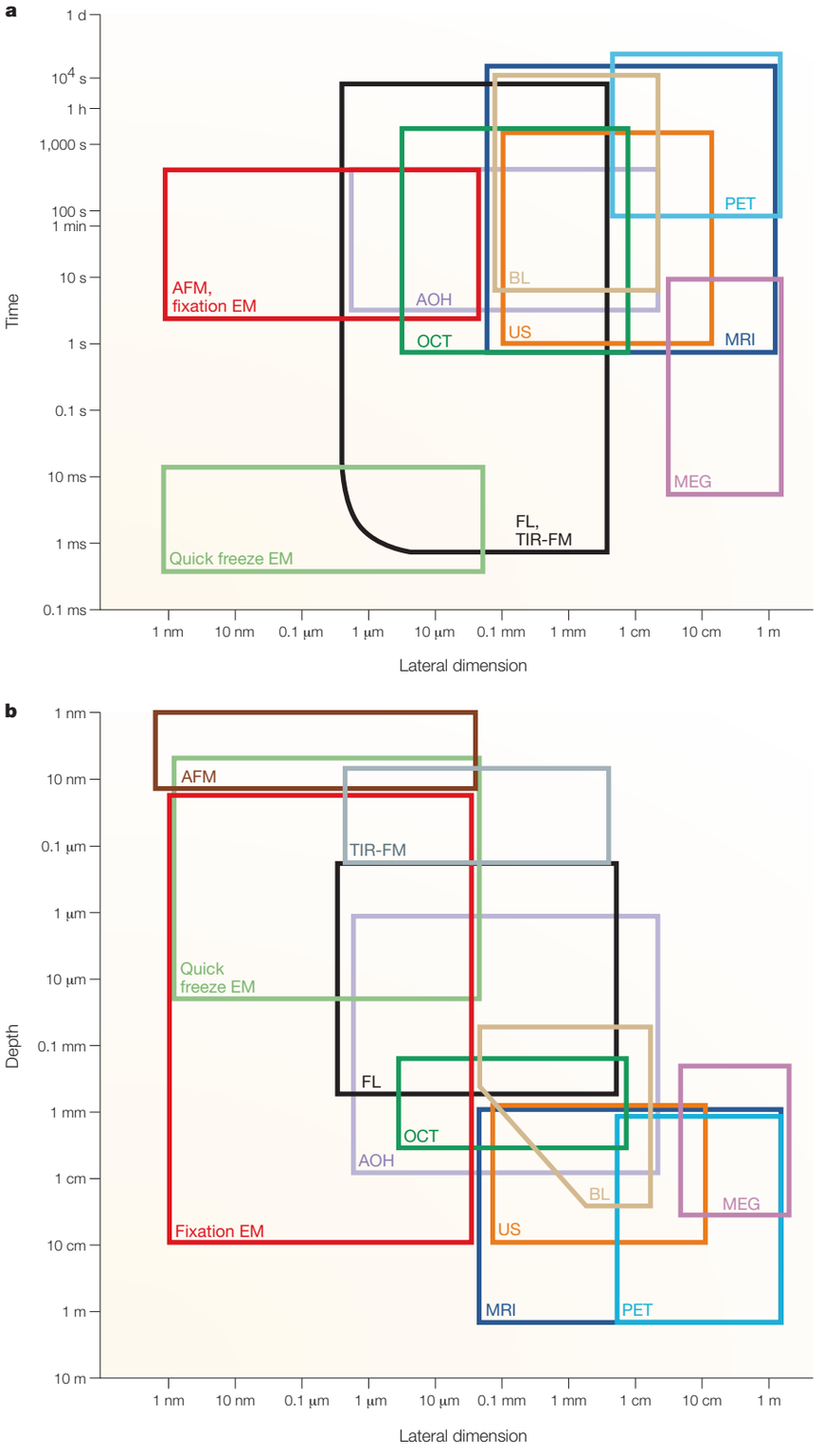

Figure 1 | **Imaging methods compared by their timescales, penetration depths and ranges of lateral dimensions.** All scales are logarithmic, and all box boundaries are estimates of typical present practices and are much fuzzier than the crisp lines shown. **a** | Each time span, except for electron microscopy (EM) techniques, indicates the range from the shortest time difference that can be comfortably resolved by a particular technique to the maximum duration of continuous observation. For EM techniques, the timescale indicates the estimated time required for freezing or fixing the tissue. Lateral dimensions range from the finest spacing over which separate objects can be discriminated up to the maximum size of a single field of view. **b** | Depth dimensions range from the minimum thickness for an adequate signal, to the maximum depth of imaging without a severe loss of sensitivity or lateral resolution. Note that far-red or near-infrared fluorescence can be comparable to bioluminescence in terms of depth resolution. Again, lateral dimensions range from the finest spacing over which separate objects can be discriminated up to the maximum size of a single field of view. AFM, atomic-force microscopy; AOH, all-optical histology; BL, bioluminescence; FL, fluorescence microscopy at visible wavelengths; MEG, magnetoencephalography; MRI, functional magnetic resonance imaging; OCT, optical coherence tomography; PET, positron emission tomography; TIR-FM, total internal reflection fluorescence microscopy; US, ultrasound.

Nanometre to micrometre imaging

Many important biological machines and signalling domains have dimensions of ~5–500 nm and therefore fall between the optimal scales for X-ray crystallography and optical microscopy. As pointed out by James Rothman, many of the most important mechanistic questions in cell biology might be rapidly answered if only we had molecular video EM — that is, the ability to non-destructively image specific molecules with the resolution of EM in real time. Fluorescence microscopy has all of these capabilities except that diffraction ordinarily limits spatial resolution to >200 nm. Finer spatial resolutions (30–100 nm) have been attained by using three innovative techniques: SCANNING NEAR-FIELD OPTICAL MICROSCOPY[7]; the coherent collection of fluorescences using a pair of diametrically opposed objectives[8]; and superlocalized depletion of the excited state by stimulated emission[9]. However, because these techniques are so new, the instrumentation

is complex, and the possible depth of imaging is limited, their widespread application has so far been prevented.

EM has the desired spatial resolution, but is inherently destructive and is normally dependent on antibody labelling for molecular selectivity. As pointed out on page SS6 of this supplement, efficient immunolabelling and fine structural preservation tend to be antithetical. Genetically encoded labels that create EM contrast in well-fixed sections without the need for antibody staining should avoid this problem, because the crucial reporter would be introduced into the live cell by transfection. The first such tag was a well-known reporter enzyme, horseradish peroxidase, that was genetically fused to targeting signals and various proteins in the secretory pathway, and was imaged by its ability to catalyse a reaction between H_2O_2 and diaminobenzidine (DAB), which results in a dense precipitate[10]. Unfortunately, however, this enzyme of 308 amino acids does not become functional when it is expressed in the cytosol, perhaps because it needs Ca^{2+} and four disulphide bonds. Re-engineering this peroxidase, or finding another that works naturally in the cytosol, would therefore be worthwhile.

Another EM-visible tag is the tetracysteine– ReAsH system, in which the protein of interest is fused to the amino-acid sequence Cys-Cys-Pro-Gly-Cys-Cys (where Cys is cysteine, Pro is proline and Gly is glycine)[11,12]. This sequence motif can be labelled in live cells or in fixed sections with ReAsH, which is a membrane-permeable biarsenical derivative of the red fluorophore resorufin. ReAsH is visible because of its red fluorescence in living cells, which survives harsh fixation. In addition, vigorous illumination of ReAsH catalyses the oxidation of DAB by O_2 to produce a precipitate that is even finer than that produced by horseradish peroxidase, DAB and H_2O_2. Dye-catalysed photodeposition of an EM-visible deposit (for the founding paper, see REF. 13) therefore becomes genetically encodable. Correlation between live-cell fluorescence movies and post-fixation EM snapshots at much higher spatial resolution provides a partial solution to the goal of molecular video EM. For an example of four-dimensional multi-photon time-lapse imaging correlated through photoconversion to three-dimensional electron microscopy, please see the Photoconversion example in the Online links. In addition, because ReAsH labelling can be performed in a pulse-chase manner, it can be used to stain young or old copies of the protein selectively and therefore to add some temporal resolution to EM. However, the technique still has scope for considerable improvements in sensitivity, selectivity and robustness.

Attempts to use GFP to catalyse the photoconversion of DAB by O_2 have generally been unsuccessful, presumably because the fluorophore inside GFP is sterically shielded from O_2 (REF. 6). A post-fixation protocol that allows GFP, or an engineered variant, to photo-oxidize DAB reliably would be valuable, because it would bypass the need for antibodies and would fit well with using GFP fusions to facilitate correlative EM.

A related challenge in EM is to image two or more distinct molecular species simultaneously — the EM equivalent of multicolour fluorescence. The nearest approximation has been double-immunoEM with different-sized gold particles. However, the size of such particles, the low percentage of antigens that get labelled and the technical difficulty of the procedures prevent routine detection of protein–protein associations or co-localization. Rather than using the size of the gold particle as the distinguishing characteristic, a spectroscopic parameter that is independent of morphology would be desirable. Perhaps the most attractive candidate is the energy loss of the electrons as they pass through the specimen and scatter inelastically off atoms of particular elements. Electron energy loss spectroscopy (EELS) is a well-established adjunct to biological EM; the challenge is therefore to devise contrast agents, preferably genetically encoded, that each cause the local deposition of elements with distinct EELS signatures[14]. An answer to this challenge could provide a powerful way to map the associations of specified pairs of proteins throughout cells and tissues.

Scanning microscopes, such as the ATOMIC-FORCE MICROSCOPE (AFM), are the only technologies that are presently capable of non-destructive continuous imaging with resolutions that are well below optical wavelengths. The AFM in TAPPING MODE can map surface topography, but it is often difficult to know which molecule corresponds to which bump on a complex biological surface. Perhaps molecular specificity might be derived from the distinctive sizes and shapes of fluorescent proteins or NANOPARTICLES, or from the detection of electron tunnelling between an AFM tip and electrochemical contrast agents, such as a redox protein in contact with a redox reagent in solution. Such tunnelling would be an extension of scanning electrochemical microscopy[15,16].

Micrometre to millimetre imaging

Cell biology from Hooke and Leeuwenhoek onward has relied on light microscopy for observations at the micrometre to millimetre length scale. GFP improvements, different colours (including the cloning of fluorescent proteins from numerous organisms)[17], and targetable dynamic indicators for physiological signals have been well covered in recent reviews[18], including several in this supplement. I therefore focus on a few unsolved problems.

How far can multi-photon excitation take us? Multi-photon excitation has been well established as the best way to recover fluorescence signals from endogenous or exogenous fluorophores that are relatively deep inside a scattering tissue such as the brain. This superiority is because the excitation is near-infrared, to which tissues are relatively transparent, and because the emitted light can be collected in a non-imaging mode (which includes photons that have undergone scattering)[19]. Nevertheless, multi-photon excitation still cannot reach much deeper than ~0.6 mm. Moreover, there are some hints that the ratio of quantum yields for fluorescence versus photobleaching — that is, the total number of photons that can be obtained before photodestruction — might be less favourable for multi-photon excitation than for conventional single-photon excitation[20].

How to get bigger spectral responses to biochemical signals? Despite the plethora of genetically encoded indicators for various biochemical signals, such as Ca^{2+}, cyclic nucleotides, phosphorylation or protein–protein associations, the maximal optical changes are often modest — that is, typically 10–50% changes in the ratio of intensities at two wavelengths. Larger responses are often obtainable from indicators in which fluorescent proteins have been split into two fragments and shuffled together with sensor domains[21–23]. However, these chimaeras are generally subject to pH interference and change their intensity in a wavelength-independent manner. Such wavelength-independent responses are subject to many more artefacts than responses in which signals at two wavelengths respond in opposite directions. The 'glass ceiling' on the dynamic range of the response might, in part, be because ratio changes of 10–20% are enough to enable biological experiments to be carried out in cultured cells. Once this threshold is attained, junior scientists find themselves under pressure to switch from improving the molecules to demonstrating biological applications. In a few cases, unusually patient investigators have made tens of constructs to optimize the response amplitude, and these seem to be the cases in which responses of twofold or greater were eventually obtained[24]. The logical extension

should be the high-throughput generation of thousands to millions of variants, coupled to automated screening for the best responders — a cycle that would probably need to be iterated many times.

Monitoring long-distance protein–protein interactions. One of the main tasks of proteomic analysis is to find and quantify protein–protein interactions, and imaging must have a crucial role whenever such interactions are to be monitored dynamically in space and time. The best established ways to image protein–protein interactions are resonance energy transfer (RET; of fluorescence (FRET) or bioluminescence (BRET)) and protein fragment complementation assays (PCA)[25,26]. Both approaches require the attachment of reporters to both putative interacting partners. In FRET and BRET, one reporter is a donor fluorophore or bioluminescent protein, the other reporter is a longer wavelength acceptor fluorophore, and the readout is energy transfer from the donor to the acceptor. The absolute efficiency of FRET can be measured *in situ* by several methods. The simplest method is to observe how much the donor brightens when the acceptor is selectively photobleached[24]. A non-destructive alternative is to measure the fluorescence at three sets of excitation and emission wavelengths and to apply correction factors for spectral overlaps and relative quantum yields[27–29]. Perhaps the most elegant, but expensive, method is to use fluorescence lifetime imaging to detect the effect of FRET on donor excited-state lifetime[30,31]. In PCA, the reporters are complementary halves of an enzyme, which can only function when the two fragments are brought together and fold around each other. The readout is the conversion of the enzyme's substrate to product. RET has a better-defined physical basis, better spatial and temporal resolution, better reversibility and less intrinsic perturbation of the interacting partners, whereas PCA has the benefits of enzymatic amplification and a much greater dynamic range over the background.

Both RET and PCA have distance ranges that are limited to single digits of nanometres, which is much less than the dimensions of known supramolecular machines, such as transcription complexes, ribosomes, chaperone assemblies, proteasomes and signal-transduction assemblies. Therefore, techniques that detect associations over tens of nanometres would be very desirable. Two-colour fluorescence correlation spectroscopy[32] monitors whether pairs of labelled macromolecules consistently diffuse, in unison, into and out of a femtolitre volume on which a laser is focused. If the partners are within the right concentration range and diffusion rate, their correlated migration strongly indicates their association. Another intriguing pair of reporters would be a generator and a detector of singlet oxygen, the diffusion range of which is ~10–50 nm through cells[33]. Clinical immunoassays that are based on singlet-oxygen proximity detection have been devised and commercialized[34], but extension to cell-biological imaging and proteomics seems to be unexplored. Placement of such reporters on antibodies might allow the proximities of unfused endogenous proteins to be assessed in fixed cells.

Imaging specific nucleic acids in living cells. So far, proteins are the only macromolecules that can be made fluorescent under genetic control. A few DNA and RNA sequences, lipids and carbohydrates can be visualized indirectly because of their ability to bind a protein that can be fused to GFP, but this strategy introduces considerable complexity and molecular bulk. For example, present ways to image RNA in living cells involve using six tandem repeats of a 19-nucleotide stem-loop sequence, each of which can bind a phage capsid protein (MS2) that is fused to GFP, which adds on a total bulk of ~270 kDa[35]. Is there any prospect of bypassing fluorescent proteins? RNA sequences of 38–90 nucleotides have been developed that can bind various fluorescent and non-fluorescent dyes with submicromolar dissociation constants[36,37], but they have not yet been optimized enough to be used for imaging in live cells. Ideally, these short RNA sequences could be genetically fused to RNAs of biological interest and would bind a non-fluorescent, non-toxic, membrane-permeable dye tightly and make it fluorescent. The many important roles and locations of various RNAs call for a range of techniques to image RNAs directly in living cells.

Imaging at millimetre scales and above

Imaging at this scale is required for non-invasive visualization inside intact organs and opaque organisms such as mammals.

The main readouts are transcriptional. At present, the most popular genetically encoded reporters for imaging at depths of more than about a millimetre in opaque organisms are firefly luciferase[38] and herpes simplex thymidine kinase[39]. The yellow–green bioluminescence from luciferase (which is fuelled by ATP, O_2 and exogenous luciferin) has a substantial component that is >600 nm, which can escape from several millimetres deep in an organism[38]. However, the deeper the source, the more scattering the photons undergo, which attenuates and blurs the image. Nevertheless, luciferase bioluminescence from just tens of cells is readily detectable in mice.

Viral thymidine kinase phosphorylates and traps ^{18}fluorine-labelled antiviral drugs inside cells and can therefore be imaged by POSITRON EMISSION TOMOGRAPHY (PET). PET requires much higher numbers of reporter-expressing cells and more expensive reagents and instrumentation compared with bioluminescence. However, PET gives true tomographic resolution at any depth of practical interest.

Genetically encoded contrast agents are largely missing (but might be developed) for several other *in vivo* imaging techniques on this scale, such as MRI, MEG, near-infrared fluorescence and OCT. MRI of β-galactosidase expression has been carried out with a gadolinium chelate that, after it is cleaved by β-galactosidase, becomes better able to relax the spins of water protons[40]. This contrast agent was only an early-stage proof-of-principle agent, because it required intracellular microinjection and was a very sluggish substrate for the enzyme. Substrates with better kinetics and larger changes in relaxivity would be highly desirable. An alternative is indicated by the well-established use of artificial SUPERPARAMAGNETIC MAGNETITE NANOPARTICLES as contrast agents in MRI. Many organisms, from microaerophilic bacteria to birds, create analogous nanoparticles ('MAGNETOSOMES') for navigation purposes[41]. Efforts are underway to clone the relevant proteins from bacterial magnetosomes. If magnetosomes can be heterologously expressed, they might be powerful focusing agents for all magnetic imaging techniques, including MRI and MEG.

Can red (600–700 nm) or, even better, infrared (>700 nm) emission be genetically encoded? Deep-ocean dragonfish were reported to luminesce with a peak at 705 nm (REF. 42), but the isolated protein was very photobleachable and showed its longest wavelength emission maximum at only 626 nm. Furthermore, this luminescence probably depends on a tetrapyrrole chromophore, which is not genetically encoded and would have to be supplied exogenously if this protein were ever to be used as a genetic fusion. Meanwhile, coral-derived fluorescent proteins with self-generated chromophores now exist with excitation peaks above 600 nm and emission maxima beyond 630 nm (REF. 17). infrared wavelengths would have been better,

but not by a huge factor, so it would be worth trying to use these coral proteins for *in vivo* imaging. An interesting alternative reporter would be *cobA*, a bacterial methyltransferase, which converts ubiquitous, endogenous, non-fluorescent uroporphyrinogen III into red fluorescent porphyrins that have emission peaks at 605 nm (REF. 44). Yet another possibility relies on exogenous polymeric substrates that are labelled with numerous infrared fluorophores that quench each other. Proteases that attack the polymer split the fluorophores apart and allow them to fluoresce[45].

OCT is a radar-like echo-ranging technique that uses ultrashort infrared pulses of $\sim 10^{-13}$ seconds duration[46]. Reflections are detected from interfaces that are up to a few millimetres deep, with a resolution as fine as tens of micrometres. OCT detects reflecting or back-scattering interfaces but not fluorophores, so how could contrast be genetically encoded? Many organisms make reflectors, including fish scales, scallop eyes and the tapetum that is responsible for the reflectivity of cats'eyes[47]. However, the system that might be most convenient for this genetic dissection and reconstitution is the reflective stack of membranes behind the eyespot of green algae such as *Chlamydomonas*[48], because the genome of this single-cell organism has been sequenced.

Can other readouts be devised? The above *in vivo* reporters — present and projected — are essentially transcriptional. Although almost any biochemical signal can be coupled to some transcriptional response element, we would often like to bypass the complexity and slow kinetics of such networks. The fastest general mechanism to sense protein conformation or proximity would probably be RET from a bioluminescent protein to a red or near-infrared fluorescent protein. For somewhat slower events, the *in vivo* reporter proteins, such as luciferase or thymidine kinase, have already been split into fragments for *in vivo* PCA[49].

Pulse-chase techniques. When continuous high-resolution imaging at a significant depth is impossible, sometimes we might have to sacrifice continuous recording and be content with a snapshot that can be read post-mortem. EM and autoradiography already work in this way. Fluorescence microscopy with a submicron spatial resolution can now be performed in fixed tissue over several millimetres of both depth and lateral extent. This can be done by imaging the top ~0.1 mm with two-photon excitation and a scanning stage, and then using a much higher-power laser to ablate that layer and expose the next underlying layer, which can then be imaged in perfect registration. This iterative cycle of imaging and vapourization ('all-optical histology') could convert a mouse brain to two terabytes of volumetric image data in <1 day (REF. 50). There are many other untapped possibilities for reporters that can be triggered, by a pulse of photons or small molecules, to memorize transient biochemical events in a form that can be imaged with high spatial resolution after fixation and sectioning.

Circumventing the limitation to transgenic animals/xenografts. The obsessive focus above on genetically encoded contrast agents for molecular imaging leaves an important gap — will such agents ever be applicable to humans? Although the co-administration of GFP genes has been used to monitor the effectiveness of gene-therapy vectors[51], the practical and ethical challenges of gene delivery into humans argue for a longer-term focus on how to image life-threatening events such as tumour metastasis. Our growing understanding of fundamental oncogenic mechanisms and differential-expression profiles in tumour versus normal tissues[52] are providing lists of messenger RNAs and proteins that are causally related to, and highly indicative of, tumour formation, metastasis and angiogenesis. Important funding agencies have recognized that non-invasive imaging of endogenous mRNA is conceptually possible and very desirable, so many laboratories are pursuing complementary strategies towards this enormous, but worthwhile, goal.

Conclusion

The growing synergy between biochemistry, genetics, physiology, anatomy and medicine will be accelerated by new modes of molecular imaging and new genetically targetable contrast agents. The latter are particularly cost-effective and portable. However, to become optimal, they will require interdisciplinary cooperation, and the transplantion and optimization of many of the unusual talents of obscure organisms.

Howard Hughes Medical Institute, Departments of Pharmacology and of Chemistry and Biochemistry, University of California, San Diego, La Jolla, California 92093-0647, USA.
e-mail: rtsien@ucsd.edu

Please cite this article as a supplement to volume 4 of Nature Reviews Molecular Cell Biology, *pages SS16–SS21.*
doi:10.1038/nrm1196

1. Goldman, M. *Fluorescent Antibody Methods* (Academic Press, New York, 1968).
2. Trask, B. J. Human cytogenetics: 46 chromosomes, 46 years and counting. *Nature Rev. Genet.* **3**, 769–778 (2002).
3. Tsien, R. Y. Fluorescent probes of cell signaling. *Annu. Rev. Neurosci.* **12**, 227–253 (1989).
4. Prasher, D. C., Eckenrode, V. K., Ward, W. W., Prendergast, F. G. & Cormier, M. J. Primary structure of the *Aequorea victoria* green-fluorescent protein. *Gene* **111**, 229–233 (1992).
5. Chalfie, M., Tu, Y., Euskirchen, G., Ward, W. W. & Prasher, D. C. Green fluorescent protein as a marker for gene expression. *Science* **263**, 802–805 (1994).
6. Tsien, R. Y. The green fluorescent protein. *Ann. Rev. Biochem.* **67**, 509–544 (1998).
7. Edidin, M. Near-field scanning optical microscopy, a siren call to biology. *Traffic* **2**, 797–803 (2001).
8. Gustafsson, M. G., Agard, D. A. & Sedat, J. W. I5M: 3D widefield light microscopy with better than 100 nm axial resolution. *J. Microsc.* **195**, 10-16 (1999).
9. Dyba, M. & Hell, S. W. Focal spots of size λ/23 open up far-field fluorescence microscopy at 33 nm axial resolution. *Phys. Rev. Lett.* **88**, 163901–163904 (2002).
10. Hopkins, C., Gibson, A., Stinchcombe, J. & Futter, C. Chimeric molecules employing horseradish peroxidase as reporter enzyme for protein localization in the electron microscope. *Methods Enzymol.* **327**, 35–45 (2000).
11. Adams, S. R. *et al.* New biarsenical ligands and tetracysteine motifs for protein labeling *in vitro* and *in vivo*: synthesis and biological applications. *J. Am. Chem. Soc.* **124**, 6063–6076 (2002).
12. Gaietta, G. *et al.* Multicolor and electron microscopic imaging of connexin trafficking. *Science* **296**, 503–507 (2002).
13. Maranto, A. R. Neuronal mapping: a photooxidation reaction makes Lucifer yellow useful for electron microscopy. *Science* **217**, 953–955 (1982).
14. Radcke, C., Stroh, T., Dworkowski, F. & Veh, R. W. Specific visualization of precipitated cerium by energy-filtered transmission electron microscopy for detection of alkaline phosphatase in immunoenzymatic double labeling of tyrosine hydroxylase and serotonin in the rat olfactory bulb. *Histochem. Cell Biol.* **118**, 459–472 (2002).
15. Liebetrau, J. M., Miller, H. M. & Baur, J. E. Scanning electrochemical microscopy of model neurons: imaging and real-time detection of morphological changes. *Anal. Chem.* **75**, 563–571 (2003).
16. Macpherson, J. V., Jones, C. E., Barker, A. L. & Unwin, P. R. Electrochemical imaging of diffusion through single nanoscale pores. *Anal. Chem.* **74**, 1841–1848 (2002).
17. Matz, M. V., Lukyanov, K. A. & Lukyanov, S. A. Family of the green fluorescent protein: journey to the end of the rainbow. *Bioessays* **24**, 953–959 (2002).
18. Zhang, J., Campbell, R. E., Ting, A. Y. & Tsien, R. Y. Creating new fluorescent probes for cell biology. *Nature Rev. Mol. Cell Biol.* **3**, 906–918 (2002).
19. Denk, W. & Svoboda, K. Photon upmanship: why multiphoton imaging is more than a gimmick. *Neuron* **18**, 351–357 (1997).
20. Patterson, G. H. & Piston, D. W. Photobleaching in two-photon excitation microscopy. *Biophys. J.* **78**, 2159–2162 (2000).
21. Baird, G. S., Zacharias, D. A. & Tsien, R. Y. Circular permutation and receptor insertion within green fluorescent proteins. *Proc. Natl Acad. Sci. USA* **96**, 11241–11246 (1999).
22. Nakai, J., Ohkura, M. & Imoto, K. A high signal-to-noise Ca^{2+} probe composed of a single green fluorescent protein. *Nature Biotechnol.* **19**, 137–141 (2001).
23. Nagai, T., Sawano, A., Park, E. & Miyawaki, A. Circularly permuted green fluorescent proteins engineered to sense Ca^{2+}. *Proc. Natl Acad. Sci. USA* **98**, 3197–3202 (2001).
24. Miyawaki, A. & Tsien, R. Y. Monitoring protein conformations and interactions by fluorescence resonance energy transfer between mutants of green fluorescent protein. *Methods Enzymol.* **327**, 472–500 (2000).
25. Michnick, S. W., Remy, I., Campbell-Valois, F. X., Vallee-Belisle, A. & Pelletier, J. N. Detection of protein–protein interactions by protein fragment complementation strategies. *Methods Enzymol.* **328**, 208–230 (2000).
26. Wehrman, T., Kleaveland, B., Her, J. H., Balint, R. F. & Blau, H. M. Protein–protein interactions monitored in mammalian cells via complementation of β-lactamase enzyme fragments. *Proc. Natl Acad. Sci. USA* **99**, 3469–3474 (2002).
27. Gordon, G. W., Berry, G., Liang, X. H., Levine, B. & Herman, B. Quantitative fluorescence resonance energy transfer measurements using fluorescence microscopy. *Biophys. J.* **74**, 2702–2713 (1998).
28. Sorkin, A., McClure, M., Huang, F. & Carter, R. Interaction of EGF receptor and grb2 in living cells visualized by fluorescence resonance energy transfer (FRET) microscopy. *Curr. Biol.* **10**, 1395–1398 (2000).

29. Erickson, M. G., Alseikhan, B. A., Peterson, B. Z. & Yue, D. T. Preassociation of calmodulin with voltage-gated Ca^{2+} channels revealed by FRET in single living cells. *Neuron* **31**, 973–985 (2001).
30. Wouters, F. S., Verveer, P. J. & Bastiaens, P. I. Imaging biochemistry inside cells. *Trends Cell Biol.* **11**, 203–211 (2001).
31. Elangovan, M., Day, R. N. & Periasamy, A. Nanosecond fluorescence resonance energy transfer-fluorescence lifetime imaging microscopy to localize the protein interactions in a single living cell. *J. Microsc.* **205**, 3–14 (2002).
32. Medina, M. A. & Schwille, P. Fluorescence correlation spectroscopy for the detection and study of single molecules in biology. *Bioessays* **24**, 758–764 (2002).
33. Moan, J. On the diffusion length of singlet oxygen in cells and tissues. *J. Photochem. Photobiol. B* **6**, 343–347 (1990).
34. Ullman, E. F. *et al.* Luminescent oxygen channeling assay (LOCI™): sensitive, broadly applicable homogeneous immunoassay method. *Clin. Chem.* **42**, 1518–1526 (1996).
35. Bertrand, E. *et al.* Localization of ASH1 mRNA particles in living yeast. *Mol. Cell* **2**, 437–445 (1998).
36. Baugh, C., Grate, D. & Wilson, C. 2.8 Å crystal structure of the malachite green aptamer. *J. Mol. Biol.* **301**, 117–128 (2000).
37. Holeman, L. A., Robinson, S. L., Szostak, J. W. & Wilson, C. Isolation and characterization of fluorophore-binding RNA aptamers. *Fold. Des.* **3**, 423–431 (1998).
38. Contag, C. H. & Bachmann, M. H. Advances in *in vivo* bioluminescence imaging of gene expression. *Annu. Rev. Biomed. Eng.* **4**, 235–260 (2002).
39. Gambhir, S. S. Molecular imaging of cancer with positron emission tomography. *Nature Rev. Cancer* **2**, 683–693 (2002).
40. Louie, A. Y. *et al. In vivo* visualization of gene expression using magnetic resonance imaging. *Nature Biotechnol.* **18**, 321–325 (2000).
41. Schuller, D. The biomineralization of magnetosomes in *Magnetospirillum gryphiswaldense*. *Int. Microbiol.* **5**, 209–214 (2002).
42. Douglas, R. H., Mullineaux, C. W. & Partridge, J. C. Long-wave sensitivity in deep-sea stomiid dragonfish with far-red bioluminescence: evidence for a dietary origin of the chlorophyll-derived retinal photosensitizer of *Malacosteus niger*. *Phil. Trans. R. Soc. Lond. B* **355**, 1269–1272 (2000).
43. Campbell, A. K. & Herring, P. J. A novel red fluorescent protein from the deep-sea luminous fish *Malacosteus niger*. *Comp. Biochem. Physiol.* **86B**, 411–417 (1987).
44. Wildt, S. & Deuschle, U. *cobA*, a red fluorescent transcriptional reporter for *Escherichia coli*, yeast, and mammalian cells. *Nature Biotechnol.* **17**, 1175–1178 (1999).
45. Ntziachristos, V., Bremer, C. & Weissleder, R. Fluorescence imaging with near-infrared light: new technological advances that enable *in vivo* molecular imaging. *Eur. Radiol.* **13**, 195–208 (2003).
46. Tadrous, P. J. Methods for imaging the structure and function of living tissues and cells: 1. Optical coherence tomography. *J. Pathol.* **191**, 115–119 (2000).
47. Land, M. F. The physics and biology of animal reflectors. *Prog. Biophys. Mol. Biol.* **24**, 75–106 (1972).
48. Roberts, D. G. W., Lamb, M. R. & Dieckmann, C. L. Characterization of the EYE2 gene required for eyespot assembly in *Chlamydomonas reinhardtii*. *Genetics* **158**, 1037–1049 (2001).
49. Paulmurugan, R., Umezawa, Y. & Gambhir, S. S. Noninvasive imaging of protein–protein interactions in living subjects by using reporter protein complementation and reconstitution strategies. *Proc. Natl Acad. Sci. USA* **99**, 15608–15613 (2002).
50. Tsai, P. S. *et al.* All-optical histology using ultrashort laser pulses. *Neuron* **39**, 27–41 (2003).
51. Wahlfors, J., Loimas, S., Pasanen, T. & Hakkarainen, T. Green fluorescent protein (GFP) fusion constructs in gene therapy research. *Histochem. Cell Biol.* **115**, 59–65 (2001).
52. Boon, K. *et al.* An anatomy of normal and malignant gene expression. *Proc. Natl Acad. Sci. USA* **99**, 11287–11292 (2002).

Online links

DATABASES

The following terms in this article are linked online to:

Entrez: http://www.ncbi.nlm.nih.gov/Entrez/
horseradish peroxidase
Swiss-Prot: http://www.expasy.ch/
β-galactosidase | GFP | luciferase | MS2 | thymidine kinase

FURTHER INFORMATION

National Center for Imaging and Microscopy Research:
http://ncmir.ucsd.edu
Photoconversion example:
http://ncmir.ucsd.edu/biology/photoconversion
Roger Tsien's laboratory: http://tsienlab.ucsd.edu
Access to this interactive links box is free online.

KINETIC MODELLING APPROACHES TO *IN VIVO* IMAGING

Robert D. Phair and Tom Misteli‡*

The ability to visualize protein dynamics and biological processes by *in vivo* microscopy is revolutionizing many areas of biology. These methods generate large, kinetically complex data sets, which often cannot be intuitively interpreted. The combination of dynamic imaging and computational modelling is emerging as a powerful tool for the quantitation of biophysical properties of molecules and processes. The new discipline of computational cell biology will be essential in uncovering the pathways, mechanisms and controls of biological processes and systems as they occur *in vivo*.

> Science is built up of facts just as a house is built up of stones, but a collection of facts is no more a science than a heap of stones is a house.
>
> *H. Poincaré*

Ever since the first microscope was built in the seventeenth century, morphological observations by microscopy have driven the course of biology. Microscopes allowed the discovery of the cell as the structural unit of tissues and organisms, and they provided the tools to uncover the interior structure and organization of cells. Later, fluorescence-labelling methods with antibodies allowed the visualization of specific proteins within cells, and the development of microscopy systems with increasingly better spatial and temporal resolution — such as CONFOCAL and MULTI-PHOTON MICROSCOPY — has resulted in a detailed description of cellular architecture. Despite their success, conventional microscopy methods suffer serious limitations. They require chemical fixation and involve the observation of biological samples under non-physiological conditions. Conventional microscopy methods can generally not resolve the dynamics of cellular processes and, most importantly, it has been very difficult to generate quantitative data using conventional microscopy.

The discovery of genetically encoded fluorescent tags has revolutionized the way microscopy is used in biology. It is now possible to analyse the dynamics of proteins or organelles in living cells[1] and to probe interactions between molecules *in vivo*[2,3]. More relevant to the topic of this discussion, by combining *in vivo* microscopy with computational approaches, it is now possible, for the first time, to extract quantitative information about the biophysical properties of proteins within living cells. We discuss here some of the kinetic microscopy methods that provide the basis of quantitative *in vivo* imaging and we outline computational approaches to extract biophysical information from *in vivo* imaging data.

CONFOCAL MICROSCOPY
A microscopy method used to obtain a thin optical section through a specimen.

MULTI-PHOTON MICROSCOPY
A microscopy method that uses the simultaneous absorbance of several low-energy electrons to generate an optical section through a specimen.

FLUOROPHORE
A small molecule or a part of a larger molecule that can be excited by light to emit fluorescence.

**BioInformatics Services, Rockville, Maryland 20854, USA.*
‡National Cancer Institute, National Institutes of Health, Bethesda, Maryland 20892, USA.
emails: rphair@bioinformaticsservices.com, mistelit@mail.nih.gov

Kinetic microscopy

Recent advances in microscopy methods have made it possible to visualize the dynamics of proteins and organelles in living cells. To do so, proteins can either be covalently labelled with a FLUOROPHORE and injected into cells, or fluorescent tags can be genetically encoded[1,4–6]. By far the most popular fluorescent label is the autofluorescent green fluorescent protein (GFP) from the jellyfish *Aequorea victoria*. GFP can be fused to any complementary DNA using standard cloning methods, and, as several spectrally distinct derivatives are available, multicolour observations are possible on several proteins simultaneously[7,8]. An alternative genetically encoded tag is the FLASH system (fluorescein arsenic helix binder), which consists of a short peptide that is engineered onto a protein of interest[9]. The protein is then expressed and the cells treated with a peptide-binding ligand, which diffuses into the cell and fluoresces once it is bound to the tag. This system has not been widely used, but is

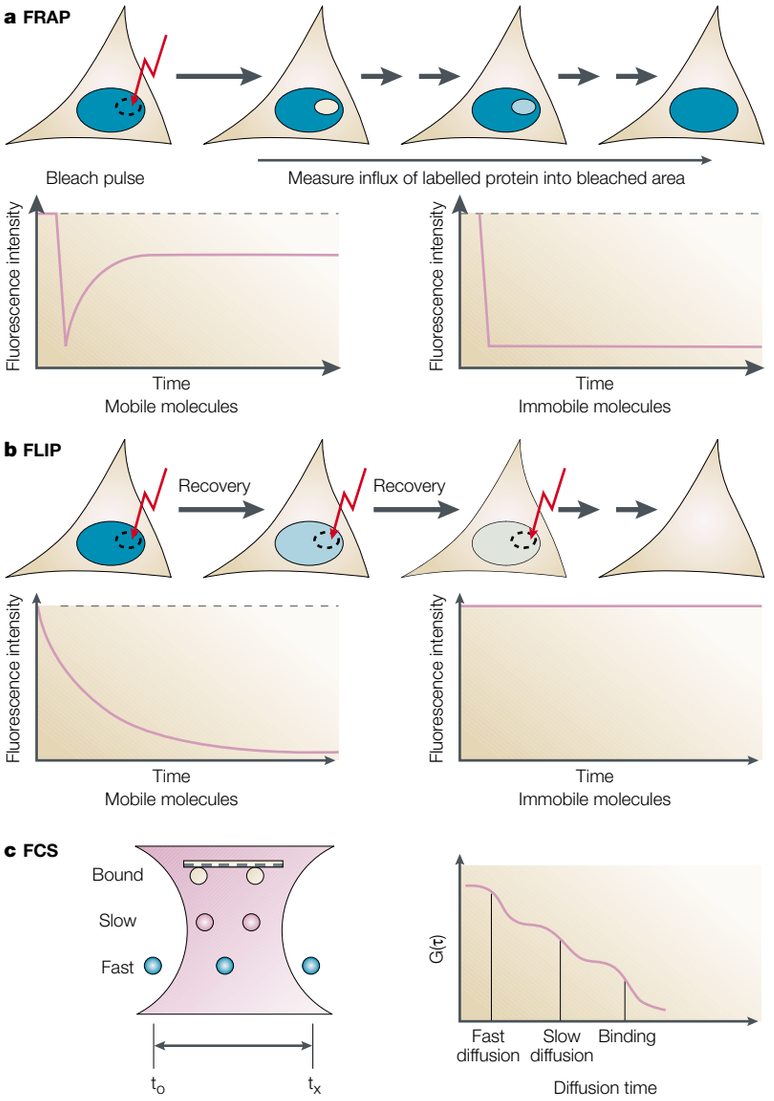

Figure 1 | **Kinetic microscopy methods. a** | In fluorescence recovery after photobleaching (FRAP), the fluorescence intensity in a small area after bleaching by a short laser pulse is measured using time-lapse microscopy. The recovery kinetics of mobile molecules are dependent on the mobility of a protein. Immobile proteins show no recovery. **b** | In fluorescence loss in photobleaching (FLIP), the fluorescence intensity is measured in a small area after repeated bleaching of a region that is distant from this area. The rate of loss of fluorescence signal is dependent on the mobility of the protein. Immobile proteins show no loss. **c** | In fluorescence correlation spectroscopy (FCS), the movement of molecules through a small volume is observed. During an observation period (t_x) rapidly moving molecules traverse the sample volume, whereas slowly moving molecules or bound molecules remain in the sample volume. Fractions of a protein with distinct mobilities are resolved by autocorrelation curves.

STEADY STATE
An open system, the content of which is held constant by a continuous input. Here, the output equals the input.

DIFFUSION COEFFICIENT
A measure to characterize the speed with which a particular molecule moves in a particular medium when driven by random thermal agitation.

attractive, as the small tag is unlikely to interfere with the function of the protein.

Genetically encoded tags are routinely used in time-lapse microscopy experiments to probe the dynamic behaviour of proteins and cellular compartments. For example, tracking the progress of GFP-fusion proteins through the exocytic and endocytic pathway has provided fundamentally new insights into protein transport and the architecture of the endomembrane system[10–12]. Similarly, time-lapse observations of the nuclear envelope[13,14], intranuclear structures[15–18], and genes and chromatin[19–23] have given the first insights into the dynamics of the cell nucleus[19–23]. Whereas many of the early *in vivo* microscopy studies were limited to observations of single focal planes at each time point, recently developed rapid sampling methods combined with the increased stability of fluorescent probes, now make it possible to routinely acquire three-dimensional data sets over time — a method commonly referred to as four-dimensional (4D) microscopy[24,25]. These types of experiments generate large data sets, which often cannot be intuitively and quantitatively interpreted. Visualization tools that facilitate the qualitative and quantitative analysis of 4D-data sets have recently been reported[26–28].

F words of kinetic microscopy: FRAP, FLIP, FCS

FRAP. Observations from studies with fluorescently tagged proteins typically show the STEADY-STATE distribution of a protein, but they do not directly provide information about the kinetic properties of molecules. To determine the kinetic properties of proteins *in vivo*, the movement of the protein of interest must be made visible. The most commonly used technique for this is FRAP (fluorescence recovery after photobleaching)[1,29–31] (FIG. 1). In this method, a small area of a cell is rapidly bleached using a high-intensity laser pulse. The movement of unbleached molecules from the neighbouring areas is then recorded by time-lapse microscopy as the recovery of fluorescence in the bleached area. This method is minimally invasive and the dynamics of the observed protein closely reflect its behaviour *in vivo* as FRAP does not generate protein gradients, but merely makes a fraction of the fluorescently labelled molecules invisible. FRAP experiments often give a qualitative impression of the mobility of a protein, but more importantly, they contain much quantitative information. For example, the apparent DIFFUSION COEFFICIENT and the size of the mobile fraction of a protein can be directly determined from the primary data[1,31].

FLIP. A related method to FRAP is FLIP (fluorescence loss in photobleaching). In this technique, an area within the cell is repeatedly bleached and the loss of fluorescence in areas that are distant from the bleach area is monitored[1] (FIG. 1). FLIP largely eliminates the concern that the recovery properties are due to damage at the bleach spot, as all measurements are made in areas that are never bleached. FLIP is often used to probe the mobility of a protein, but is also a useful tool to study the continuity of cellular compartments[32].

FCS. FCS (fluorescence correlation spectroscopy) provides an alternative method for measurements of protein dynamics *in vivo*[33,34] (FIG. 1). In FCS, a laser beam is focused on a microvolume, typically in the femtolitre range, and fluctuation of the fluorescence signal is measured over a short period of time. The recorded signals reflect the movement of labelled proteins through the sample volume, which is similar to the situation if we looked straight across a busy road and record the fluctu-

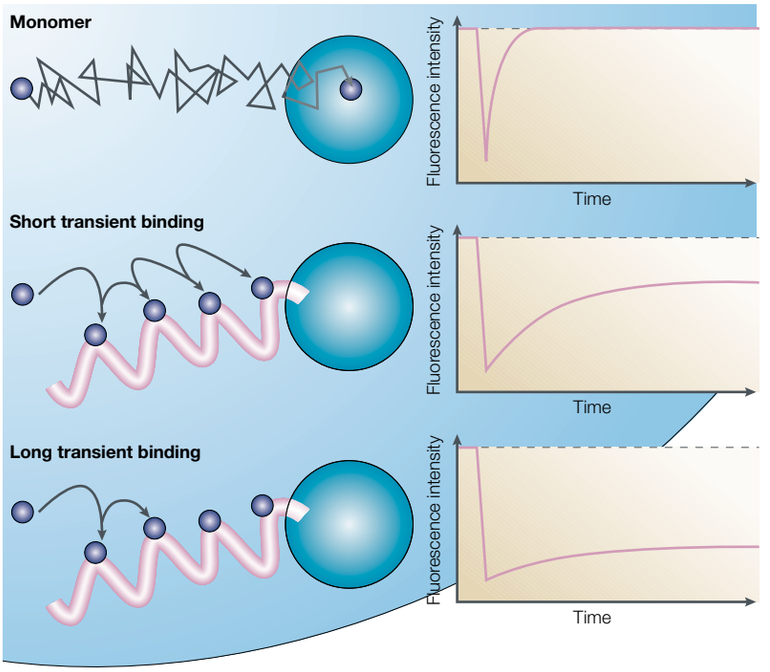

Figure 2 | **FRAP for the measurement of protein binding *in vivo*.** Information about the binding properties of a protein can be obtained from measurements of apparent protein mobility by FRAP. A monomeric protein moves more rapidly than a protein that transiently interacts with relatively more immobile cellular structures, such as the cytoskeleton or chromatin. The FRAP recovery kinetics reflect these transient interactions. A monomeric protein recovers rapidly, a protein with short transient interactions recovers with intermediate kinetics and a protein with long transient interactions recovers slowly. Kinetic modelling allows us to extract information about the binding properties from mobility measurements.

PARAMETER
The numerical constant that determines the absolute speed of a process. A first-order process is characterized by a single parameter, the rate constant. A process that is governed by a Michaelis–Menten equation is characterized by two parameters, V_{max} and K_m.

STOCHASTIC SYSTEMS
A dynamic system, the processes of which are characterized by a probability distribution. The stochastic system theory is particularly important when the abundance of molecules in a particular state falls below the deterministic limit, about 100 molecules per cell.

FRACTALS
These are objects that provide more and more features as the resolution of the observation increases. These finer features show statistical self-similarity as seen in biological branching patterns, ion-channel currents and heart rate.

ations in the passing cars. The time it takes molecules to move through the sample volume depends on their diffusional properties, and the fluctuation patterns give a direct measure of the concentrations of the proteins in the sample volume. FCS can be used to measure diffusion coefficients and binding constants[35–37]. As FCS can simultaneously be done on several fluorophores, it can also be used in cross-correlation spectroscopy to determine whether two proteins physically interact — if they do, they would be predicted to show identical fluctuation patterns. FCS is a single-molecule detection method and it is therefore exquisitely sensitive. However, owing to its great sensitivity, bleaching effects during measurements can generate artefacts. FCS is still in an experimental stage, but it does hold great promise. Early FCS applications include the determination of diffusional mobilities of proteins and RNA[35,36,38], the determination of binding interactions[39,40] and the measurement of ion concentrations[40].

Measuring biophysical properties *in vivo*

Photobleaching methods were initially designed, and are commonly used, to measure the mobility of proteins in living cells. Indeed, in FRAP and FCS, the primary measurement is the diffusion coefficient. However, as all proteins readily interact with many partners *in vivo*, it is virtually impossible to measure pure diffusional mobility of a protein in a living cell (FIG. 2). Furthermore, proteins often form higher-order complexes or associate with relatively immobile cellular structures, such as the cytoskeleton or chromatin. In both cases, the measured mobility is significantly reduced. It is important to realize that all photobleaching methods measure apparent mobilities[41]. This behaviour becomes obvious in the analysis of nuclear proteins. For example, the core histone H3 is virtually immobile, whereas a similarly sized splicing factor is highly mobile[42,43]. A similar situation is found in the analysis of plasma membrane and transmembrane proteins in membranous compartments[32,44,45].

The fact that the interaction properties of a protein are reflected in the mobility measurement complicates the analysis of photobleaching data (FIG. 2). However, the fact that binding to other cellular components affects mobility also indicates that the measured apparent mobility contains information about the behaviour of the protein. Computational approaches, particularly kinetic modelling methods, allow the quantitative testing of hypotheses about why a protein moves slower than would be expected for its size. The strategy in such an approach is to generate a mathematical description — a kinetic model — of the hypothesized biological reality. The model is characterized by biophysical PARAMETERS, such as binding and release constants, residence times and diffusion coefficients. By determining the set of parameters that result in a best fit of the model to the experimental data, the model can be tested and quantitative information about its parameters can be obtained. We outline below step-by-step how, using computational methods, we can extract information regarding biophysical properties of proteins and processes from *in vivo* microscopy data.

Modelling = quantitative hypothesis testing

Techniques for the analysis of dynamic data can usefully be divided into four groups, although the distinctions are not absolute: the statistical tools of time series analysis[46], the analytical and computational tools of differential equations[47–51], the computational tools of STOCHASTIC SYSTEMS[52,53], and the scaling and phase-space tools of FRACTALS and CHAOS[54]. For applications in cell biology, differential equations are often used because they are a natural mathematical language for cellular processes, such as biochemical kinetics, membrane transport and binding events. Alternative approaches to biological modelling and data analysis are described briefly in BOX 1.

The object of any type of data analysis is hypothesis testing. For example, statistical tests, such as the t-test or ANALYSIS OF VARIANCE, ask how probable it is that a particular experimental result occurs by chance. Analysis of quantitative dynamic data, such as those collected in video microscopy, goes one step further — it offers the possibility of quantitative mechanistic hypothesis testing. One way to visualize the role of kinetic modelling in cellular and molecular hypothesis testing is shown in FIG. 3. The difficulty is knowing with precision what is predicted by a complex

Box 1 | **Other types of mathematical models**

There are many approaches to mathematical modelling. Several other types of mathematical descriptions, apart from the dynamic, differential-equation models that are the focus of this review, are compared below.

Curve fitting.
Modern graphics and spreadsheet software typically have various options for fitting experimental data to functions. These tools offer a powerful means of summarizing a data set by fitting it to a SUM OF EXPONENTIALS, a POLYNOMIAL, a SUM OF GAUSSIANS, etc. This is always possible and the coefficients that fit the data can be taken as quantitative parameters, which are derived from the data. Indeed, these parameters are sometimes touted as model independent and therefore desirable. In general, however, these coefficients have no physical meaning. They can quantify patterns and can be useful in diagnosis, but they yield no mechanistic information. By contrast, the parameters of a mechanistic model yield useful information on the biological processes that they quantify. If, for example, the rate constant for a given process is doubled in a given experimental circumstance, then the corresponding process has been fundamentally changed by the experimental protocol.

Statistics.
Statistical models search for patterns in experimental data. Correlation, regression and cluster analysis are all powerful statistical tools that can identify relationships among measured variables that probably are not attributable to chance. Statistics are a powerful tool for supplying us with new and interesting potential mechanisms, mechanisms that need experimental tests and mechanistic analysis.

Phenomenological laws.
Many readers will be familiar with linear phenomenological laws, such as Ohm's law for electric current ($I = g\Delta V$) or the law of bulk flow ($F = (1/R)\Delta P$). These seem to be algebraic, but are really special cases of the general linear differential equations that govern forces and fluxes in irreversible thermodynamics[64]. The current (I) is the rate of charge movement, dQ/dt; and the flow (F) is the rate of volume movement, dV/dt. The 'forces' in these equations (ΔV and ΔP) are gradients in chemical potential and can, when required, be resolved into functions of the state variables whose derivatives are on the left-hand sides of the differential equations.

Enzyme kinetics.
The often-cited form of the Michaelis–Menten equation, $v = V_{max}S/(K_m + S)$, can be taken as a surrogate for all the more complex velocity equations that are derived and documented in REF. 65 and elsewhere. In the context of differential equation models, we can incorporate enzyme kinetics by recognizing that this equation is another differential equation in disguise. Velocity (v) is a symbol for the rate of change of product, dP/dt. This most widely known of biochemical equations is therefore a nonlinear differential equation in which the driving force of chemical potential arises from a concentration of substrate (S), which is greater than its equilibrium value.

Logic models.
An array of modelling tools, which have been developed in theoretical biology, systems biology and biomedical engineering, are beginning to move from qualitative to quantitative simulations. These include electric circuit models[49], logic network models, Petri nets and process algebra.

CHAOS
A deterministic system (for example, some systems of nonlinear differential equations), the output of which seems random, but is not. Such systems show a surprising sensitivity to initial conditions.

ANALYSIS OF VARIANCE
A statistical procedure for testing for differences among the means of several populations. It partitions the total sample variance among several specific sources to carry out the test on means.

SUM OF EXPONENTIALS
An algebraic expression that is made up of exponentials. In a first-order system, the time-course solution for every state can be precisely mimicked by the sum of exponentials that correspond to the number of states in the system.

POLYNOMIAL
Algebraic expressions that are made up of more than one term — for example, mx + b.

SUM OF GAUSSIANS
An approximation by weighted sums of normal distributions, or Gaussians, each characterized by two parameters — a mean and a variance — to describe a data set.

STATE
The generic name used here to identify those variables that change with time and for which differential equations are written.

hypothesis that contains many interacting processes in a given experimental situation. It is here that kinetic modelling and simulation of complex systems have proved valuable.

Molecular and cell-biological hypotheses or theories are often represented as diagrams. The final slide in nearly every scientific seminar and a key figure in every biological review is a diagram that represents the author's current working hypothesis. Typically, these diagrams comprise a collection of molecules represented as symbols, their biochemical transformations and translocations represented as arrows, and some graphic notation, such as lines that are terminated with plus or minus, to indicate regulatory controls. Diagrams offer a language for description of cell-biological systems that is somewhat more precise than printed paragraphs, but it often remains difficult to make quantitative predictions for a given experimental protocol with the use of diagrams alone. Scientific intuition has been successful when systems are limited to a few molecules and processes, but today's summary diagrams generally have many more molecules and arrows than this, and even simple systems often behave in surprising ways. What is needed is a way to know what the diagram predicts in a given experiment.

Translating diagrams to kinetic models

Kinetic modelling supports quantitative hypothesis testing by first translating a diagram into a mechanistic kinetic model (see BOX 2). Diagrams typically consist of molecules, complexes, cellular locations and processes. As molecules and complexes can exist in several locations, it is often necessary to define several STATES for a single molecule — each state is 'a chemical species in a physical place.' For example, phosphorylation of a protein at a single amino acid results in at least two states: the phosphorylated one and the unphosphorylated one. However, if both are present in both cytoplasm and nucleoplasm, then four states are required.

Arrows in a diagram usually represent various types of processes. Three fundamental biological processes can describe virtually any biological diagram: transformations, translocations and binding.

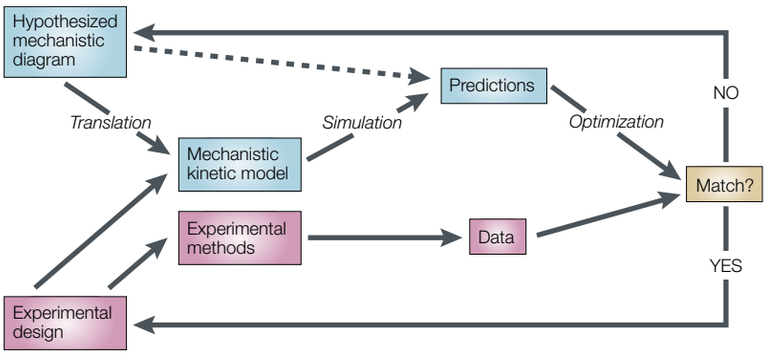

Figure 3 | **Role of kinetic models in quantitative hypothesis testing.** The lower (purple) half of this figure represents experimental design and experimental methods, which combine to produce quantitative experimental data on a biological system of interest. Hypothesis testing is then carried out by comparison of the data to that expected based on the current hypothesis. Arrows in the upper (blue) half of the diagram represent the steps in kinetic analysis that are detailed in this review: translation of diagrams into kinetic models, simulation to obtain the predictions of the model for a given experimental design and optimization of model parameters to ensure an unbiased comparison of model predictions and experimental data. These three steps differ from scientific intuition (dashed arrow) by being quantitative and robust to complexity.

Transformations include everything that makes or breaks covalent bonds, such as the biochemical pathways of intermediary metabolism, the synthesis and splicing of RNA transcripts, the actions of kinases and phosphatases, and the proteolytic activities of proteasomes or caspases. Translocations include all active and facilitated transport mechanisms, currents in ion channels, diffusion and bulk-flow processes that move molecules or complexes from one place to another. Binding comprises all those intermolecular interactions, such as hormones that activate receptors, ALLOSTERIC REGULATION of enzymes or transporters and formation of multimeric protein complexes, that involve bonds whose energy is much less than the energy of a covalent bond.

A biological diagram is therefore a collection of processes that link states. To express the diagram in mathematical form requires two steps. First, a RATE LAW is written for each PROCESS, and second, these rate laws are combined to construct the differential equations for each state. A rate law is an algebraic expression that gives the flux (molecules per second) through a particular process as a function of the relevant molecular abundances or other state variables in the biological system. Rate laws tell us how many molecules are traversing a particular pathway, but to keep track of how many molecules there are in any state at any time, it is necessary to sum up or integrate all the inputs and outputs. To do this, differential equations are constructed for each state (molecule or molecular complex in a cellular location) by setting its rate of change to be equal to the sum of the processes or rate laws that produce this molecular species minus those processes or rate laws that consume it. In other words, we write down the differential equations that represent mass conservation for each state[55]. BOX 2 gives an example of the diagram translation process.

Because most biological diagrams concern themselves with changes in more than a single molecular species, the corresponding kinetic models comprise 'systems' of differential equations. For example, if the diagram contains 17 molecular species, the corresponding model will, in general, consist of 17 differential equations. The form of these equations is perhaps most easily understood by examining the dimensions or units of the various terms. Traditionally, the derivatives are written on the left-hand side of these equations. These derivatives with respect to time represent the instantaneous change in molecular abundance, or the rate of change of the number of molecules of this species in a particular cellular location at a particular moment in time, measured in, for example, molecules per second. As the units on the right-hand side must be the same as those on the left, it is clear that the derivatives must have the same units as the fluxes. Processes or fluxes that produce or deliver the molecular species will have a positive sign; those that consume it or remove it will have a negative one.

By writing rate laws, diagrams are translated into a precise physical–chemical language. The reason for using differential equations rather than algebraic equations is that differential equations are able to describe mechanisms and cause-and-effect relationships. The change on the left-hand side of a differential equation (the derivative) can be seen as the effect, and the processes on the right-hand side can be seen as the causes. The complete differential equation therefore expresses the equality of cause and effect.

The rendering of biological diagrams in mathematical form does not mean that cell biologists must know how to solve differential equations using analytical, pencil-and-paper methods. Indeed, for many nonlinear differential equations, no such solution is even possible. Fortunately, there are many software tools (see online links box) available to solve any system of differential equations, from very simple to very complex. Although the typeset form of a system of differential equations is fairly standardized, it is remarkable how many differential equation-solver software packages with different input formats are currently available. Attempts to construct an 'Esperanto' for biological kinetic models are under way, and are based on the popular EXTENSIBLE MARKUP LANGUAGE (XML). This means that a model file not only encodes the model-definition information, but also encodes how to interpret it. This new language could substantially facilitate the communication of models between software packages and among laboratories. Further details are available in the published descriptions of CellML[56] and SBML[57], as well as in the links included at the end of this review.

Simulation: what does a diagram predict?

Once a biological diagram has been formulated as a quantitative kinetic model, simulation is used to discover what that model predicts for a particular experimental situation. In other words, simulation applies a particular experimental protocol to the kinetic model and displays the model's predictions in a way that can be compared directly to the experimental data (FIG. 3).

ALLOSTERIC REGULATION
A modification of a process by a molecule that binds to an enzyme or a transporter or another protein at a site other than its active, or catalytic, site.

RATE LAWS
Algebraic expressions for the flux through a given pathway.

PROCESS
The generic name for events that bring about changes in one or more states.

EXTENSIBLE MARKUP LANGUAGE
A method for putting structured data in a text file so that applications receive not only unambiguous data but also unambiguous context. XML documents are not meant to be read, except by software.

Simulation provides answers to key questions that cannot be answered with confidence in any other way. You can discover whether a diagram really is consistent with experimental data. You can also learn whether a diagram is consistent with experiments that have been reported by other laboratories and, just as importantly, you can carry out the same tests for diagrams that have been proposed by other investigators. Simulation requires a quantitative language for laboratory procedures so that these can be imposed on the kinetic model just as they are imposed on the cells in the laboratory. Some modelling software packages (for example, SAAM II) have an experiment toolbox to facilitate quantifying your protocol and defining your measurements. Others (for example, Berkeley Madonna, MATLAB, Virtual Cell) provide a flexible set of programming constructs that can be used to specify the sequence of events that defines a protocol.

A protocol is a timeline of pre-planned experimental perturbations. Nearly always, it consists of experimenter-induced changes in state variables or processes that are taking place at known times. In practice, this translates to specifying a set of initial and boundary conditions to be imposed on the solution of the differential equations. For example, FRAP experiments are often assumed to begin in a steady state. This means that the steady-state solution of the differential-equation system can be calculated and used to set the initial condition for each molecular abundance before initiating the bleach pulse. The same applies to other types of experiments. If a growth factor or a hormone is added to the medium, then the corresponding state variable is increased stepwise at the appropriate time.

Box 2 | **Translation**

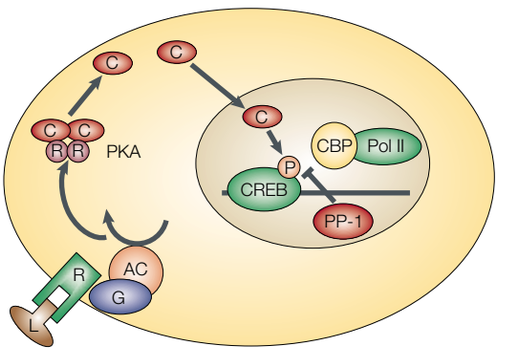

A diagram[66] that contains all three main classes of biological processes — transformation, translocation and binding — is reproduced here to illustrate the translation process. When a ligand (L) binds to its receptor (RGAC), adenylyl cyclase is activated and cyclic AMP (not shown) is synthesized from ATP. The first differential equation represents binding. The derivative (*dLRGAC/dt*) on the left-hand side represents the rate of change of ligand–receptor–G-protein–cyclase complex, and the terms on the right-hand side represent the binding and release of ligand. The second equation represents the rate of change of cAMP, and the two processes are both transformations — the first term represents the flux (molecules per second) of cAMP that is produced by adenylyl cyclase and the second represents the flux of cAMP degradation by phosphodiesterase. Either or both of these simple enzymatic rate laws could be replaced with more complex ones if, for example, saturation or allosteric regulation of the enzymes was thought to be important.

$$dLRGAC/dt = k_f \cdot L \cdot RGAC - k_r \cdot LRGAC$$
$$dcAMP/dt = k_{AC} \cdot LRGAC \cdot ATP - k_{PDE} \cdot cAMP$$

The mechanism of control of protein kinase A (PKA) is summarized in the diagram without kinetic detail both because it is well known and because it is not the focus of the review. For our purposes, the catalytic subunit of PKA can be considered to exist free or bound to its regulatory subunit.

$$dCR/dt = k_{bind} \cdot R \cdot C - k_{unbind} \cdot CR$$
$$dR/dt = k_{unbind} \cdot CR - k_{bind} \cdot R \cdot C - k_{cAMP} \cdot R \cdot cAMP + k_1 \cdot RcAMP$$
$$dC/dt = k_{unbind} \cdot CR - k_{bind} \cdot R \cdot C - k_{InNuc} \cdot C + k_{OutNuc} \cdot C_{Nuc}$$

If the abundance of R is very small compared to cAMP, then the last two terms in *dR/dt* can safely be omitted from the right-hand side of *dcAMP/dt*. Otherwise, we must add these terms. The equation for *dC/dt* emphasizes that C can exist in two places, and therefore includes the first translocation processes in this example. Note that the simple first-order rate laws for nuclear import and export could readily be replaced by more mechanistically detailed ones if desired.

$$dC_{Nuc}/dt = k_{InNuc} \cdot C - k_{OutNuc} \cdot C_{Nuc}$$
$$dCREB/dt = -k_{PKA} \cdot C_{Nuc} \cdot CREB + k_{PP-1} \cdot PP1 \cdot CREBP$$

Once in the nucleus, the catalytic subunit mediates phosphorylation of the cAMP response element binding protein (CREB). Then, CREBP recruits the CREB-binding protein (CBP), which, in turn, recruits RNA polymerase II. Recruitment is easily modelled as binding and the transcription rate can be seen as proportional to the abundance of this heteromeric complex.

$$dCREBP/dt = k_{PKA} \cdot C_{Nuc} \cdot CREB - k_{PP-1} \cdot PP1 \cdot CREBP - k_{recruit} \cdot CREBP \cdot CBPPPolII + k_{dis} \cdot CREBPCBPPolII$$
$$dCREBPCBPPolII/dt = k_{recruit} \cdot CREBP \cdot CBPPolII - k_{dis} \cdot CREBPCBPPolII$$
$$Transcription\ Rate = k_{elong} \cdot CERBPCBPPolII$$

And if an enzyme inhibitor or receptor antagonist is added, a specific rate constant could be altered at the right time to initiate the response of the model. Imposing these boundary conditions on a kinetic model leads to the definition of the boundary of a model as those molecular species or physical quantities that impinge on the model, but for which no differential equation is written. Variables on the boundary must be completely specified in the protocol because they affect the outcome but are not explicitly modelled.

FRAP protocols are initiated by defining a region of cellular space to be bleached and then changing a bleaching rate constant to a non-zero value for the duration of the experimental laser pulse. FLIP experiments are imposed on a model by bleaching as is the case for FRAP, but with an average effective bleach constant, or by a more precise replication of the repeated laser pulses with intervening periods of image collection.

Simulation can also be used to show what a particular biological diagram predicts for every defined region

Box 3 | **Simulation**

When both time and space are variables, mathematicians refer to the resulting differential equations as partial differential equations. To solve these, the space is partitioned into a large number of small, but finite, volumes. This amounts to compartmentalizing the space and then solving ordinary (only time is an independent variable) differential equations for every volume simultaneously. Shown here is such a simulation for Ca^{2+} and inositol-1,4,5-trisphosphate ($Ins(1,4,5)P_3$) dynamics in a neuroblastoma cell[59]. Note that the computing times are vastly different for partial differential equations versus ordinary differential equations. These simulations each required about 25 minutes on an SGI workstation; if diffusion could have been neglected and the Ca^{2+} and $Ins(1,4,5)P_3$ compartments treated as well mixed, these simulations could reasonably have been done in a few seconds. The pseudocolour images graphically depict the evolving solutions of this model for Ca^{2+} and $Ins(1,4,5)P_3$ at more than 7,000 locations, each 1.2 μm on a side, in the simulated neuroblastoma cell. Graphs at the right of this figure show the simulated time courses in two selected locations, one in the soma (red) and one in the neurite (green). The original paper and the online supplementary material should be consulted for details of model structure and equations, but it is instructive to realize that this kinetic model makes predictions for a system with at least ten interacting processes: (1) dynamics of $Ins(1,4,5)P_3$ synthesis, (2) the spatial distribution of bradykinin (BK) receptors on the cell surface, (3) the spatial distribution of SERCA (SR–ER calcium) pumps, (4) $Ins(1,4,5)P_3$ receptors and (5) leak channels in the endoplasmic reticulum, (6) the spatial distribution of Ca^{2+} channels and (7) pumps in the plasma membrane, and Ca^{2+} buffering by both (8) fixed endogenous buffers and (9) mobile exogenous ones (Fura-2 in this case), as well as (10) diffusion of the mobile species. Applications such as this one illustrate the profound usefulness of simulation as the best tool for discovering what your diagram predicts. Figure courtesy of L. Loew.

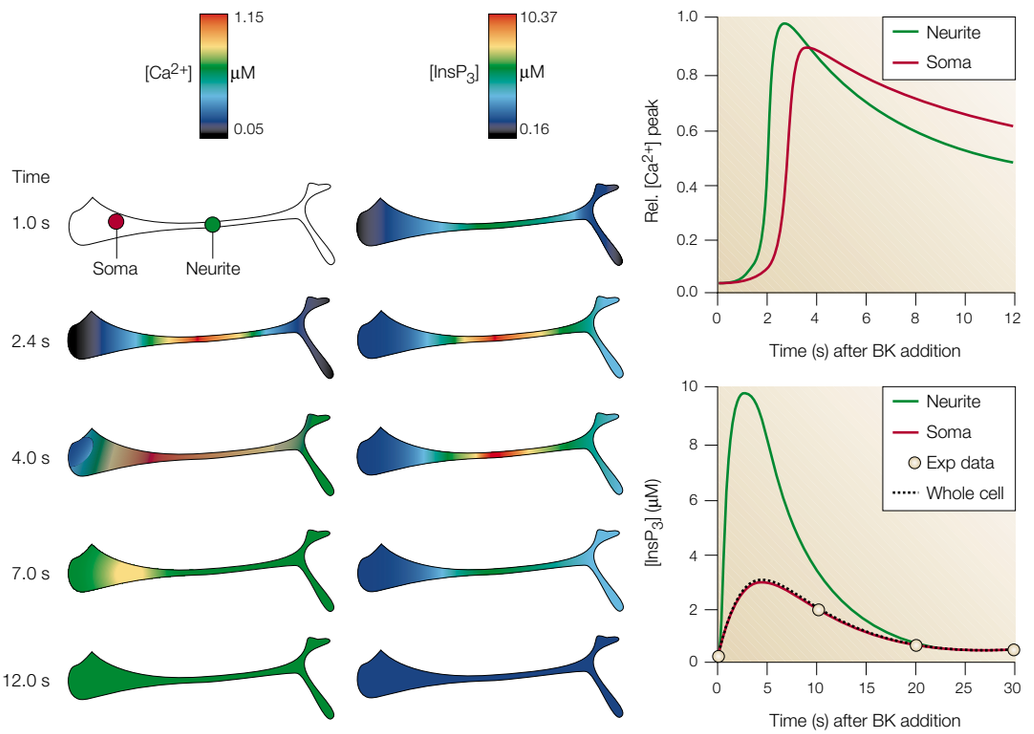

of a spatially complex cell. This is essential whenever diffusion cannot be assumed to be fast on the timescale of the experimental measurements, as is often the case for FRAP experiments, or for experiments in large cells or nerve cells with long projections. One of the most interesting tools for such 'four-dimensional' simulations is the Virtual Cell software[58]; an excellent example of its use in simulating whole-cell calcium dynamics imaged with a fluorescent dye (Fura-2) has recently been published[59] (see BOX 3 for details).

Simulation versus modelling

The terms 'simulation' and 'modelling' are often used interchangeably, but it is useful to make a distinction. Simulation typically makes no explicit reference to experimental data, whereas modelling generally links each experimental measurement to some function of the state variables of the model and then assesses the model's ability to reproduce the data when the corresponding experimental protocol is applied.

Simulation is therefore the first step in modelling. Once a model of the biological system has been proposed and a model of the experiment has been superimposed on it, simulation permits us to know with precision what the model predicts. But in practice we need to know precisely how to decide whether a model fits the data or not. How do we find the best combination of parameters? The answer is optimization. Optimization theory[60] is therefore an essential element of kinetic analysis and modelling (FIG. 3).

Box 4 | **Optimization**

The figure shows the classic model of the secretory pathway with proteins transported from the endoplasmic reticulum to the Golgi complex and to the plasma membrane. Data points in the graphs represent the transport of VSVG–GFP (vesicular stomatitis virus G protein–GFP) through the Golgi apparatus in a single cell[61]. Solid lines in the upper panel represent a solution of the secretory pathway model for the values of the rate constants below the graph. Clearly, this model fails to fit the experimental data for total cellular fluorescence (yellow) and Golgi fluorescence (pink). We would not, however, want to rule out the classical ER–Golgi–plasma-membrane model on these grounds because the poor fit is only a consequence of wrong parameter values. In the lower panel, the optimizer in the SAAM II software (see online links box) has minimized an appropriate objective function and found a point in parameter space that gives excellent fits (brown, blue)of the experimental data. Moreover, the coefficients of variation (CV) for the parameter estimates are all less than 2%, as shown below the graph.

This example emphasizes the usefulness of an optimizer in giving any theory its best chance to fit the available experimental data, as well as simultaneously supplying the very useful statistical information on the confidence that we should place in these parameter estimates. Again, it should be emphasized that these confidence limits hold for the given model structure. Residence times and fluxes that are calculated from these rate constants also hold for this structure and could well change if a new model, which fits the experimental data just as well, is discovered. Original data courtesy of K. Hirschberg, J. Lippincott-Schwartz).

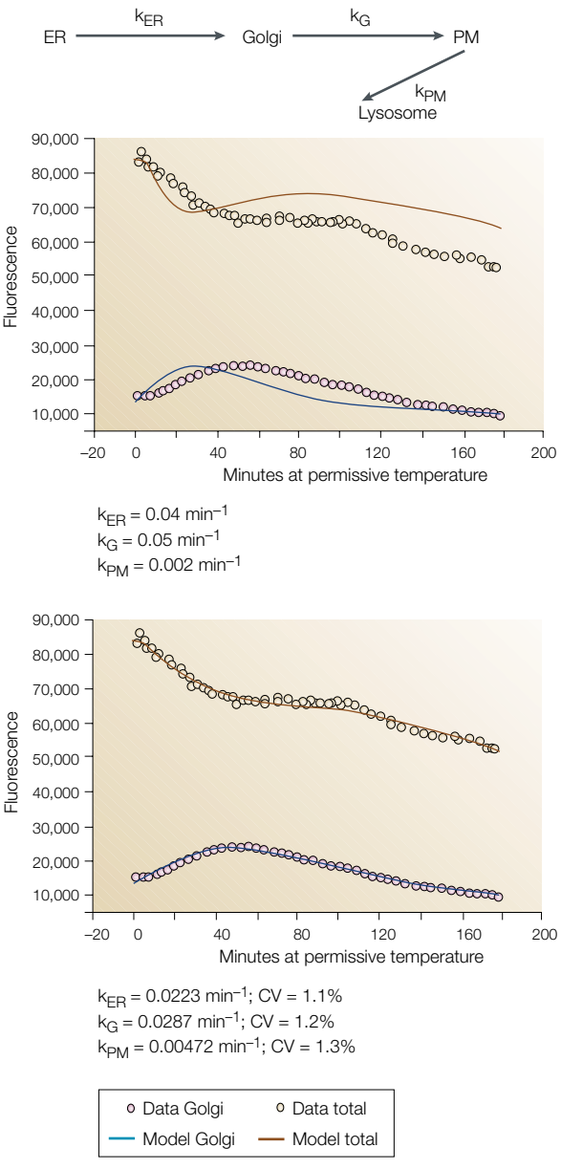

INTEGRATIVE BIOINFORMATICS
The intersection of kinetic modelling and database technology, a combination that becomes essential as cell biologists move to analyse larger and more complex molecular genetic control systems.

Optimization

From the perspective of quantitative hypothesis testing, the purpose of optimization is to give each hypothesis its best chance to account for the available experimental data. Optimization is the exploration of the parameter space of a model in search of numerical values for each parameter that optimize a specific quantitative measure of goodness of fit. You can think of parameter space by imagining an origin with as many axes emerging from it as you have parameters in your model. Every point in this space represents a unique set of numerical values, one for each parameter. Now we add one more axis to this space, one that represents the measure of fit. One intuitively clear measure of fit is the weighted sum of the squares of the errors between the model solution and the experimental data. Every set of parameter values will correspond to a numerical value of the weighted sum of squares. For a perfect fit, the sum of squares would be zero. The task of optimization is to determine the set of parameter values that yields the best or optimal fit. For large models this is not easy, and improvement of methods for efficiently searching a high-dimensional parameter space represent an important research area in numerical analysis. BOX 4 gives an illustration of the optimization process that is applied to the kinetics of protein transport in the secretory pathway[61].

If a set of parameters has been found that fit the experimental data reasonably well, we can say that the theory is quantitatively consistent with the experimental data. This, in itself, is a stronger assertion than the paragraph of a discussion section that begins, 'Taken together, these data indicate…'. If the model is correct, then the parameter values of the mechanistic model can be used to calculate extra features of the system, including residence times, steady-state molecular abundance, steady-state fluxes (molecules per second) or fractional distribution of a given molecule among its various cellular locations. Moreover, if the parameters are evaluated in two or more physiological or pharmacological situations, it becomes possible to discern which cellular processes were affected and by how much. This is new information, much of it unavailable by any other means. All of these motivate the application of kinetic analysis to complex molecular and cellular problems.

Often, however, a model fails to account for all the experimental data. No set of parameter values can be found that eliminates systematic deviations between model solution and experimental data. This means either that the kinetic model is flawed and needs to be improved by ensuring that the biological diagram has been accurately translated, or that the biological diagram itself — that is, the theory — is incorrect. Computational tools are not yet used routinely to discover new theories, but this will probably become essential as complexity grows. A provocative example of a relatively simple computational search for an appropriate model recently appeared[62], and this general goal is a current objective of several research groups.

Optimization also provides tools to evaluate how well our analysis performs. Parameter estimation is able to provide confidence intervals for each parameter because the greater the noise in the experimental data, the greater is the uncertainty or variance that is associated with the optimized parameter values. The standard statistical measure of confidence in a parameter estimate is its coefficient of variation (CV). This number is calculated as the estimated parameter standard deviation divided by the parameter value, and is generally reported as a percentage. Some software packages report this information as the fractional standard deviation (FSD) of the parameter estimate, and other packages, even some that include optimizers, do not report this vital information at all. Another measure of confidence in a model is sensitivity analysis. In its most common form, this procedure involves solving the model again with one of its parameter values increased or decreased to show that this new value no longer fits the experimental data. Although qualitatively useful, this one-at-a-time variation fails to ask whether the fit, once destroyed by a change in the tested parameter, could be recovered by making changes in the other parameters of the model. For this reason, formal parameter estimation and its extensive statistical methods, which lead to coefficients of variation, are preferred.

Conclusions and prospects

Recent advances in applications of fluorescent tracers and indicators have permitted microscopy to move from static images to dynamic recording in live cells. The combination of these powerful imaging methods with mechanistic computational modelling allows us, for the first time, to extract information about biophysical properties of proteins and processes in living cells. Kinetic analysis and modelling aim to help investigators deal with cellular complexity by allowing them to know with precision what their complex diagrams predict. Quantitative predictions can then be compared directly with quantitative experimental data as a means of testing the hypotheses that are represented by the diagrams. Just as database tools have become vital to the field of bioinformatics for the management and statistical analysis of complex data sets, the management and analysis of large numbers of complex biological models is being facilitated by database technology and defines the nascent fields of INTEGRATIVE BIOINFORMATICS or pathway databases[63].

Biology knows, perhaps better than other scientific disciplines, the difficulty of analysing and understanding intact complex systems. It is not surprising that disciplines that routinely deal with complex systems, such as developmental biology or physiology, are strongly represented among the pioneers of computational biology. Kinetic analysis is now also beginning to find a place in the technical repertoire of cell biologists. In the coming years, computational cell biology and systems biology will be powerful tools to help us comprehend the enormous complexity of cell biology.

1. Lippincott-Schwartz, J., Snapp, E. & Kenworthy, A. Studying protein dynamics in living cells. *Nature Rev. Mol. Cell Biol.* **2**, 444–456 (2001).
A comprehensive review on kinetic imaging methods.
2. Periasamy, A. & Day, R. N. Visualizing protein interactions in living cells using digitized GFP imaging and FRET microscopy. *Methods Cell Biol.* **58**, 293–314 (1999).
3. Wouters, F. S., Verveer, P. J. & Bastiaens, P. I. Imaging biochemistry inside cells. *Trends Cell Biol.* **11**, 203–211 (2001).
4. Misteli, T. & Spector, D. L. Applications of the green fluorescent protein in cell biology and biotechnology. *Nature Biotechnol.* **15**, 961–964 (1997).
5. Taylor, D. L. & Wang, Y. L. Molecular cytochemistry: incorporation of fluorescently labeled actin into living cells. *Proc. Natl Acad. Sci. USA* **75**, 857–861 (1978).
6. Tsien, R. Y. The green fluorescent protein. *Annu. Rev. Biochem.* **67**, 509–544 (1998).
7. Patterson, G., Day, R. N. & Piston, D. Fluorescent protein spectra. *J. Cell Sci.* **114**, 837–838 (2001).
8. Verkhusha, V. V. *et al.* An enhanced mutant of red fluorescent protein DsRed for double labeling and developmental timer of neural fiber bundle formation. *J. Biol. Chem.* **276**, 29621–29624 (2001).
9. Griffin, B. A., Adams, S. R. & Tsien, R. Y. Specific covalent labeling of recombinant protein molecules inside live cells. *Science* **281**, 269–272 (1998).
10. Lippincott-Schwartz, J., Roberts, T. & Hirschberg, K. Secretory protein trafficking and organelle dynamics in living cells. *Annu. Rev. Cell Dev. Biol.* **16**, 557–589 (2000).
11. Shima, D. T., Haldar, K., Pepperkok, R., Watson, R. & Warren, G. Partitioning of the Golgi apparatus during mitosis in living HeLa cells. *J. Cell Biol.* **137**, 1211–1228 (1997).
12. Rudolf, R., Salm, T., Rustom, A. & Gerdes, H. H. Dynamics of immature secretory granules: role of cytoskeletal elements during transport, cortical restriction, and f-actin-dependent tethering. *Mol. Biol. Cell* **12**, 1353–1365 (2001).
13. Ellenberg, J. *et al.* Nuclear membrane dynamics and reassembly in living cells: targeting of an inner nuclear membrane protein in interphase and mitosis. *J. Cell Biol.* **138**, 1193–1206 (1997).
14. Moir, R. D., Yoon, M., Khuon, S. & Goldman, R. D. Nuclear lamins A and B1: different pathways of assembly during nuclear envelope formation in living cells. *J. Cell Biol.* **151**, 1155–1168 (2000).
15. Dundr, M., Misteli, T. & Olson, M. O. J. The dynamics of postmitotic reassembly of the nucleolus. *J. Cell Biol.* **150**, 433–446 (2000).
16. Misteli, T., Cáceres, J. F. & Spector, D. L. The dynamics of a pre-mRNA splicing factor in living cells. *Nature* **387**, 523–527 (1997).
17. Platani, M., Goldberg, I., Swedlow, J. & Lamond, A. I. *In vivo* analysis of cajal body movement, separation, and joining in live human cells. *J. Cell Biol.* **151**, 1561–1574 (2000).
18. Savino, T. M., Gebrane-Younes, J., De Mey, J., Sibarita, J. B. & Hernandez-Verdun, D. Nucleolar assembly of the rRNA processing machinery in living cells. *J. Cell Biol.* **153**, 1097–1110 (2001).
19. Manders, E. M., Kimura, H. & Cook, P. R. Direct imaging of DNA in living cells reveals the dynamics of chromosome formation. *J. Cell Biol.* **144**, 813–821 (1999).
20. McNally, J. G., Muller, W. G., Walker, D., Wolford, R. & Hager, G. L. The glucocorticoid receptor: rapid exchange with regulatory sites in living cells. *Science* **287**, 1262–1265 (2000).
21. Robinett, C. *et al. In vivo* localization of DNA sequences and visualisation of large-scale chromatin organisation using lac operator/repressor recognition. *J. Cell Biol.* **135**, 1685–1700 (1996).
The first description of an experimental system to study a chromatin region in living cells.
22. Zink, D. *et al.* Structure and dynamics of human interphase chromosome territories *in vivo*. *Hum. Genet.* **102**, 241–251 (1998).
23. Tsukamoto, T. *et al.* Visualisation of gene activity in living cells. *Nature Cell Biol.* **2**, 871–878 (2000).
24. Thomas, C. F. & White, J. G. Four-dimensional imaging: the exploration of space and time. *Trends Biotechnol.* **16**, 175–182 (1998).
25. Bornfleth, H., Edelmann, P., Zink, D., Cremer, T. & Cremer, C. Quantitative motion analysis of subchromosomal foci in living cells using four-dimensional microscopy. *Biophys. J.* **77**, 2871–2886 (1999).
26. Bergsma, C. B., Streekstra, G. J., Smeulders, A. W. & Manders, E. M. Velocity estimation of spots in three-dimensional confocal image sequences of living cells. *Cytometry* **43**, 261–272 (2001).
27. Tvarusko, W. *et al.* Time-resolved analysis and visualisation of dynamic processes in living cells. *Proc. Natl Acad. Sci. USA* **96**, 7950–7955 (1999).
28. Gehrlich, D., Beaudouin, J., Gebhard, M., Ellenberg, J. & Eils, R. Four-dimensional imaging and quantitative reconstruction to analyse complex spatiotemporal processes in live cells. *Nature Cell Biol.* **3**, 852–855 (2001).
29. Edidin, M., Zagyansky, Y. & Lardner, T. J. Measurement of membrane protein lateral diffusion in single cells. *Science* **191**, 466–468 (1976).
30. Axelrod, D., Koppel, D. E., Schlessinger, J., Elson, E. & Webb, W. W. Mobility measurement by analysis of fluorescence photobleaching recovery kinetics. *Biophys. J.* **16**, 1055–1069 (1976).
This is the classic paper on the quantitative analysis of FRAP data for cases in which the recovery is dominated by diffusion.
31. Reits, E. A. & Neefjes, J. J. From fixed to FRAP: measuring protein mobility and activity in living cells. *Nature Cell Biol.* **3**, 145–147 (2001).
32. Cole, N. B. *et al.* Diffusion mobility of Golgi proteins in membranes of living cells. *Science* **273**, 797–801 (1996).
33. Dittrich, P., Malvezzi-Campeggi, F., Jahnz, M. & Schwille, P. Accessing molecular dynamics in cells by fluorescence correlation spectroscopy. *Biol. Chem.* **382**, 491–494 (2001).
34. Schwille, P., Haupts, U., Maiti, S. & Webb, W. W. Molecular dynamics in living cells observed by fluorescence correlation spectroscopy with one- and two-photon excitation. *Biophys. J.* **77**, 2251–2265 (1999).
35. Wachsmuth, M., Waldeck, W. & Langowski, J. Anomalous diffusion of fluorescent probes inside living cell nuclei investigated by spatially-resolved fluorescence correlation spectroscopy. *J. Mol. Biol.* **298**, 677–689 (2000).
36. Brock, R., Vamosi, G., Vereb, G. & Jovin, T. M. Rapid characterization of green fluorescent protein fusion proteins on the molecular and cellular level by fluorescence correlation microscopy. *Proc. Natl Acad. Sci. USA* **96**, 10123–10128 (1999).
37. Rigler, R. *et al.* Specific binding of proinsulin C-peptide to human cell membranes. *Proc. Natl Acad. Sci. USA* **96**, 13318–13323 (1999).
38. Politz, J. C., Browne, E. S., Wolf, D. E. & Pederson, T. Intranuclear diffusion and hybridization state of oligonucleotides measured by fluorescence correlation spectroscopy in living cells. *Proc. Natl Acad. Sci. USA* **95**, 6043–6048 (1998).
39. Pramanik, A., Olsson, M., Langel, U., Bartfai, T. & Rigler, R. Fluorescence correlation spectroscopy detects galanin receptor diversity on insulinoma cells. *Biochemistry* **40**, 10839–10845 (2001).
40. Widengren, J. & Rigler, R. Fluorescence correlation spectroscopy as a tool to investigate chemical reactions in solutions and on cell surfaces. *Cell. Mol. Biol. (Noisy-le-grand)* **44**, 857–879 (1998).
41. Misteli, T. Protein dynamics: implications for nuclear architecture and gene expression. *Science* **291**, 843–847 (2001).
42. Kimura, H. & Cook, P. R. Kinetics of core histones in living human cells: little exchange of H3 and H4 and some rapid exchange of H2B. *J. Cell Biol.* **153**, 1341–1353 (2001).
43. Phair, R. D. & Misteli, T. High mobility of proteins in the mammalian cell nucleus. *Nature* **404**, 604–60 (2000).
An application of FRAP, FLIP and kinetic modelling to obtain quantitative measures of the mobility of several functionally distinct nuclear proteins.
44. Nehls, S. *et al.* Dynamics and retention of misfolded proteins in native ER membranes. *Nature Cell Biol.* **2**, 288–295 (2000).
45. Adams, C. L., Chen, Y. T., Smith, S. J. & Nelson, W. J. Mechanisms of epithelial cell–cell adhesion and cell compaction revealed by high-resolution tracking of E-cadherin–green fluorescent protein. *J. Cell Biol.* **142**, 1105–1119 (1998).
46. Pena, D., Tiao, G. C. & Tsay, R. S. *A Course in Time Series Analysis* (Wiley, New York, 2000).
47. Eriksson, K., Estep, D., Hansbro, P. & Johnson, C. *Computational Differential Equations* (Cambridge University, Cambridge, 1996).
48. Newton, I. *The Method of Fluxions and Infinite Series.* (Henry Woodfall, London, 1736).
49. McAdams, H. H. & Shapiro, L. Circuit simulation of genetic networks. *Science* **269**, 650–656 (1995).
50. Brenan, K. E., Campbell, S. L. & Petzold, L. R. *Numerical Solution of Initial-value Problems in Differential Algebraic Equations* (Society for Industrial and Applied Mathematics, 1996).
51. Bhalla, U. S. & Iyengar, R. Emergent properties of networks of biological signaling pathways. *Science* **283**, 381–387 (1999).
52. Firth, C. A. J. M. & Bray, D. *Computational Modeling of Genetic and Biochemical Networks* (eds Bower, J. M. & Bolouri, H.) 263–286 (MIT Press, Cambridge, 2001).
53. Gillespie, D. T. Exact stochastic simulation of coupled chemical reactions. *J. Phys. Chem.* **81**, 2340–2361 (1977).
54. Bassingthwaighte, J. B., Liebovitch, L. S. & West, B. J. *Fractal physiology* (Oxford University Press, New York, 1994).
55. Phair, R. D. Development of kinetic models in the non-linear world of molecular cell biology. *Metabolism* **46**, 1489–1495 (1997).
56. Hedley, W. J., Nelson, M. R., Bullivant, D. P. & Nielsen, P. F. A short introduction to CellML. *Phil. Trans. R. Soc. Lond. A* **359**, 1073–1089 (2001).
57. Hucka, M. *et al. Foundations of Systems Biology* (ed. Kitano, H.) (MIT Press, Cambridge, 2001).
58. Schaff, J. C., Slepchenko, B. M. & Loew, L. M. Physiological modeling with virtual cell framework. *Methods Enzymol.* **321**, 1–23 (2000).
59. Fink, C. C. *et al.* Morphological control of inositol-1,4,5-trisphosphate-dependent signals. *J. Cell Biol.* **147**, 929–936 (1999).
A clear and compelling examination of the importance of partial differential equation models when studying large cells or cells with long processes in which one must account for simultaneous diffusion and spatially distributed chemical reactions.
60. Nocedal, J. & Wright, S. J. *Numerical Optimisation* (Springer, New York, 1999).
61. Hirschberg, K. *et al.* Kinetic analysis of secretory protein traffic and characterization of golgi to plasma membrane transport intermediates in living cells. *J. Cell Biol.* **143**, 1485–1503 (1998).
This was among the first studies to combine the power of green fluorescent protein chimaeras, photobleaching techniques and kinetic analysis to answer questions about protein transport in living cells.
62. Bagowski, C. P. & Ferrell, J. E. Jr Bistability in the JNK cascade. *Curr. Biol.* **11**, 1–20 (2001).
63. Karp, P. D. Pathway databases: a case study in computational symbolic theories. *Science* **293**, 2040–2044 (2001).
64. Onsager, L., Hemmer, P. C., Holden, H. & Ratkje, S. K. *The Collected Works of Lars Onsager with Commentary* (World Scientific, Singapore, 1996).
65. Segel, I. H. *Enzyme Kinetics Behavior and Analysis of Rapid Equilibrium and Steady State Enzyme Systems* (Wiley, New York, 1975).
66. Mayr, B. & Montminy, M. Transcriptional regulation by the phosphorylation–dependent factor CREB. *Nature Rev. Mol. Cell Biol.* **2**, 599–609 (2001).

Online links

DATABASES

The following terms in this article are linked online to:

Swiss-Prot: http://www.expasy.ch/
GFP

FURTHER READING

Simulation and Modelling Software

SAAM Institute: http://www.saam.com/
Berkeley Madonna: http://www.berkeleymadonna.com/
Gepasi: http://www.gepasi.org/gepasi.html
StochSim: http://www.zoo.cam.ac.uk/comp-cell/StochSim.html
MATLAB: http://www.mathworks.com/index.shtml
Virtual Cell: http://www.nrcam.uchc.edu/
WinSAAM: http://www-saam.nci.nih.gov/
XPPAut: http://www.math.pitt.edu/~bard/xpp/xpp.html
E-Cell: http://www.e-cell.org/

Online Textbook

Integrative Bioinformatics: http://www.bioinformatics services.com/bis/resources/cybertext/IBcont.html

Databases

PathDB: http://www.ncgr.org/pathdb/index.html
KEGG: http://www.genome.ad.jp/kegg/
BIND: http://www.bind.ca/cgi-bin/bind/dataman
WIT: http://wit.mcs.anl.gov/WIT2/
EMP: http://emp.mcs.anl.gov/
EcoCyc:http://ecocyc.pangeasystems.com/ecocyc/ecocyc.html
Klotho: http://www.ibc.wustl.edu/klotho/

Standards

CellML: http://www.cellml.org/
SBML: http://www.cds.caltech.edu/erato/sbml/docs/index.html

Access to this interactive links box is free online.